NUCLEAR TANKER PRODUCING LIQUID FUELS FROM AIR AND WATER

By

JOHN MICHAEL GALLE-BISHOP
B.S. English (Honors) United States Naval Academy 2002
M.A. English George Mason University 2003
M.E.M. Old Dominion University 2008

Submitted to the
DEPARTMENT OF NUCLEAR SCIENCE AND ENGINEERING
And the
DEPARTMENT OF MECHANICAL ENGINEERING
In Partial Fulfillment of the Degrees of
MASTER OF SCIENCE IN NUCLEAR SCIENCE AND ENGINEERING
And
MASTER OF SCIENCE IN NAVAL ARCHITECTURE AND MARINE ENGINEERING
At the
MASSACHUSETTS INSTITUTE OF TECHNOLOGY
June 2011

Signature of Author:

_____
Department of Nuclear Science and Engineering
Department of Mechanical Engineering
March 31, 2011

Certified by:

_____
Michael J. Driscoll
Professor Emeritus of Nuclear Science and Engineering
Thesis Co-Supervisor

Certified by:

_____
Charles W. Forsberg
Executive Director, MIT Nuclear Fuel Cycle Project
Thesis Co-Supervisor

Certified by:

_____
Mark S. Welsh
Professor of Practice of Naval Construction and Engineering
Thesis Reader

Accepted by:

_____
David E. Hardt
Ralph E. and Eloise F. Cross Professor of Mechanical Engineering
Chairman, Department Committee on Graduate Studies

Accepted by:

_____
Mujid S. Kazimi
TEPCO Professor of Nuclear Science and Engineering
Chair, Department Committee on Graduate Students

(This Page Intentionally Blank)

Nuclear Tanker Producing Liquid Fuels from Air and Water
By
Lieutenant John M. Galle-Bishop, United States Navy

Submitted to the Department of Nuclear Science and Engineering and
the Department of Mechanical Engineering in partial fulfillment for the requirements for the
degrees of Master of Science in Nuclear Science and Engineering and
Master of Science in Naval Architecture/Marine Engineering

Abstract

Emerging technologies in CO_2 air capture, high temperature electrolysis, microchannel catalytic conversion, and Generation IV reactor plant systems have the potential to create a shipboard liquid fuel production system that will ease the burdened cost of supplying fuel to deployed naval ships and aircraft. Based upon historical data provided by the US Navy (USN), the tanker ship must supply 6,400 BBL/Day of fuel (JP-5) to accommodate the highest anticipated demand of a carrier strike group (CSG).

Previous investigation suggested implementing shipboard a liquid fuel production system using commercially mature processes such as alkaline electrolysis, pressurized water reactors (PWRs), and methanol synthesis; however, more detailed analysis shows that such an approach is not practical. Although Fischer-Tropsch (FT) synthetic fuel production technology has traditionally been designed to accommodate large economies of scale, recent advances in modular, microchannel reactor (MCR) technology have to potential to facilitate a shipboard solution. Recent advances in high temperature co-electrolysis (HTCE) and high temperature steam electrolysis (HTSE) from solid oxide electrolytic cells (SOECs) have been even more promising. In addition to dramatically reducing the required equipment footprint, HTCE/HTSE produces the desired synthesis gas (syngas) feed at 75% of the power level required by conventional alkaline electrolysis (590 MW_e vs. 789 MW_e). After performing an assessment of various CO_2 feedstock sources, atmospheric CO_2 extraction using an air capture system appears the most promising option. However, it was determined that the current air capture system design requires improvement. In order to be feasible for shipboard use, it must be able to capture CO_2 in a system only ¼ of the present size; and the current design must be modified to permit more effective operation in a humid, offshore environment.

Although a PWR power plant is not the recommended option, it is feasible. Operating with a Rankine cycle, a PWR could power the recommended liquid fuel production plant with a 2,082 MW_{th} reactor and 33% cycle efficiency. The recommended option uses a molten salt-cooled advanced high temperature reactor (AHTR) coupled to a supercritical carbon dioxide (S-CO_2) recompression cycle operating at 25.0 MPa and 670 ^oC. This more advanced 1,456 MW_{th} option has a 45% cycle efficiency, a 42% improvement over the PWR option. In terms of reactor power heat input to JP-5 combustion heat output, the AHTR is clearly superior to the PWR (31% vs. 22%).

In order to be a viable concept, additional research and development is necessary to develop more compact CO_2 capture systems, resolve SOEC degradation issues, and determine a suitable material for the molten salt/S-CO_2 heat exchanger interface.

Thesis Supervisors: Dr. Charles Forsberg, Prof. Michael Driscoll, Prof. Mark Welsh
Thesis Title: Nuclear Tanker Producing Liquid Fuels from Air and Water

(This Page Intentionally Blank)

Acknowledgements

(This Page Intentionally Blank)

Table of Contents

Tables

Figures

(This Page Intentionally Blank)

1 Introduction

1.1 The Logistical Burden of Delivering Fuel

This thesis evaluates the potential impact of recently emerging technologies to the application of using shipboard nuclear energy to produce synthetic liquid fuel (synfuel) for consumption by the US naval fleet. Such capability has the potential to greatly ease the logistical burden of supplying fuel to deployed naval ships and aircraft; it also would enhance the operationally flexibility of combatant and operational commanders, allow for greater on-station time, and potentially obviate the need for coordinating refueling in remote and inhospitable regions. Synfuel technology also promises to enhance US national security by providing a marked first step toward US energy independence. Figure 1-1 shows that while the US Government (USG) has a diverse portfolio of petroleum suppliers, 2/3 of its supply is from abroad [1]; and it highlights the security risk even more by showing that US petroleum consumption continues to rise even as domestic production declines[2].
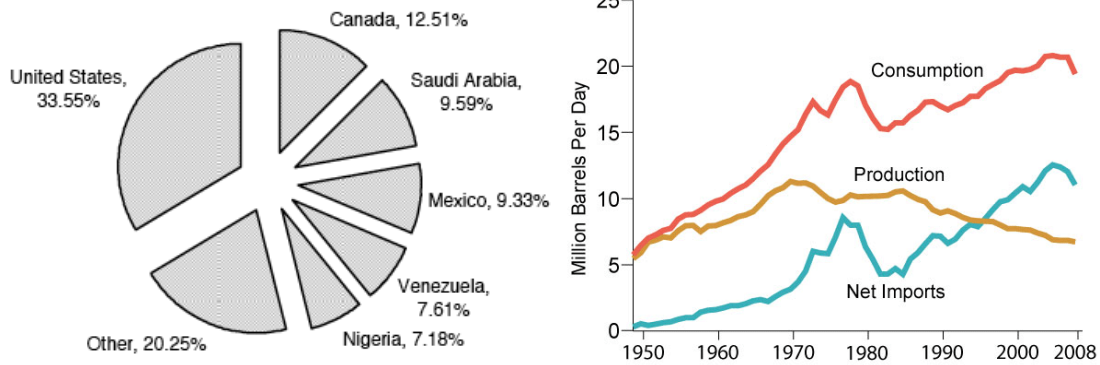
Figure 1-1 – US Government Supply Sources vs Consumption Trends

The US military certainly feels the impact of constrained petroleum resources and its impact on market prices. Figure 1-2 shows an ever increasing trend for the military's fuel costs [1]:

	FY2000	FY2001	FY2002	FY2003	FY2004	FY2005	FY2006	FY2007	FY2008
$/barrel	$34.62	$37.64	$30.78	$38.36	$47.98	$67.66	$84.24	$84.26	$133.04
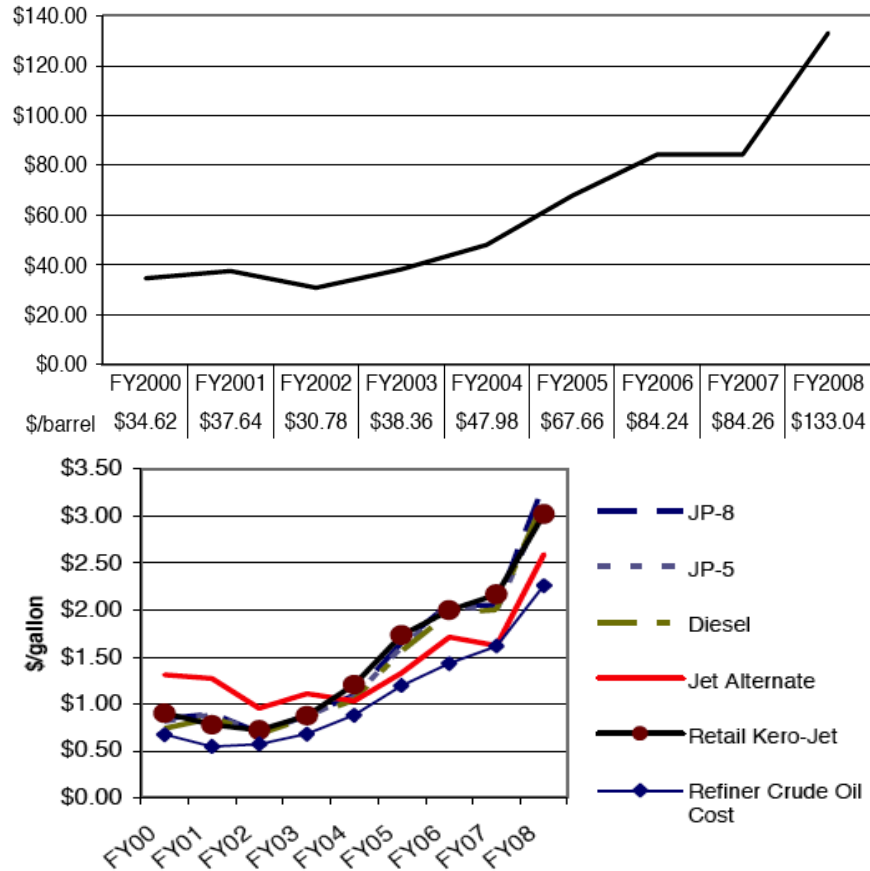
Figure 1-2 - Average Defense Department Fuel Costs

The US Navy (USN) is feeling the budgetary pressure of these rising fuel costs and is actively pursuing comprehensive measures not only to mitigate the effect of rising fuel costs, but also to determine which fuel saving methods are of greatest impact. Its approach includes the following:

- Providing energy conservation awards and incentives to naval units [3]
- Saving fuel through low-risk changes to tactical procedures [4]
- Evaluating how it can quickly upgrade existing platforms with more energy efficient technology, and how it can implement promising new fuel efficient propulsion systems (such as fuel cells and integrated electric drive propulsion) onto naval platforms [5]
- Designing future naval platforms so that the life cycle cost of the platform accounts for the fully burdened cost of fuel (FBCF)[1] [6]

Appendix A provides USN fuel consumption statistics.

---

[1] The FBCF concept provides a measure to assess changes in vulnerabilities to the new system and its supporting assets, as a function of the new capability's fuel requirements. As the energy demands for a system increase, so do the demands (burdens) on the supporting logistics tail. Use of the FBCF ensures these burdens are taken into consideration and enables a more realistic assessment of the trades under review before major production and fielding a new capability.

Despite the mitigation measures above, the trends shown by Figure 1-2 are still likely to exacerbate due to an ever increasing global petroleum demand. Figure 1-3 shows that global petroleum demand volume exceeds the rate of discovery and has an increasing trend, while Figure 1-4 predicts an ever decreasing global petroleum supply in the coming years [7]:
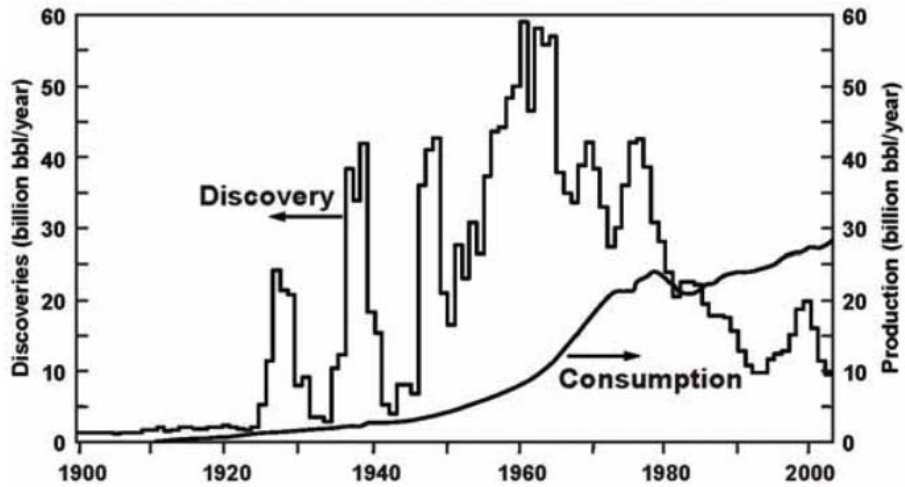
Figure 1-3 - Global Petroleum Discovery vs Consumption
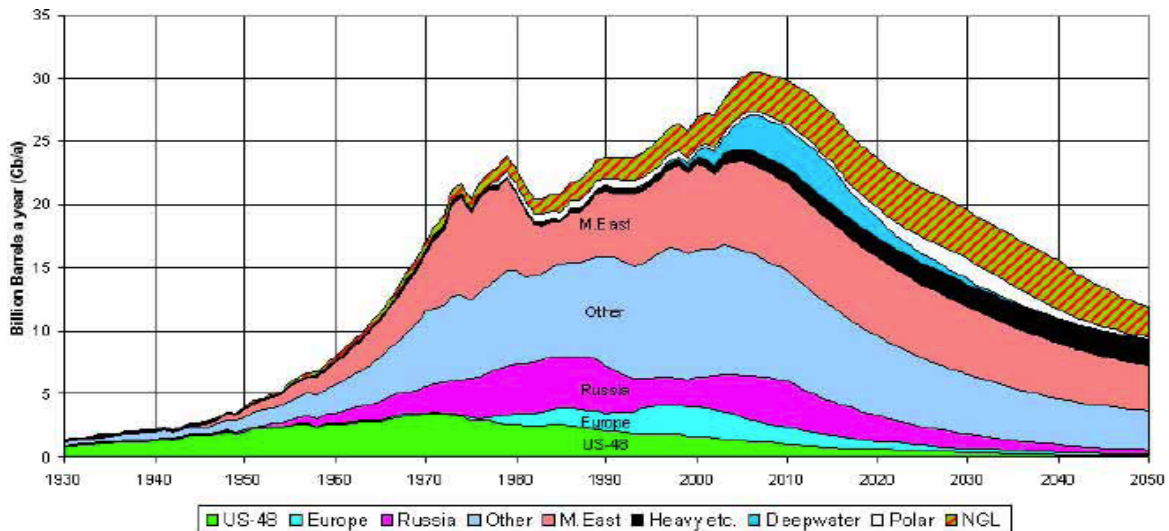
Figure 1-4 - Forecast of Global Petroleum Supply

 Increased competition for dwindling petroleum sources by rapidly growing, population-dense nations such as India and China will undoubtedly place even more strain on global supplies. Although the fuel consumption reduction measures above must certainly be part of the navy's solution, the navy must also eventually move beyond measures that merely address commodity prices and complement them with a strategy that (1) reduces (or even eliminates) dependence on foreign sources and (2) reduces all

19

of the costly infrastructure and logistics associated with actually getting fuel to deployed combatant units.

A 2008 report, *More Fight-Less Fuel*, by the Defense Department's (DOD) Defense Science Board Task Force specifically advocates the following actions:

- Invest in basic research to develop new fuels technologies … too risky for private investments.
- Conduct full "well-to-wheel" life cycle assessments of each synthetic fuel technology.

The report specifically notes that "synfuel technology that can be adapted to forward deployed[2] locations … would be valuable because it would directly reduce the amount of fuel that would have to be moved and protected in theater" [8]. One can indeed learn through unclassified, open-source channels that the DOD is currently researching the viability of synfuel technology. The Naval Research Laboratory (NRL) is performing extensive research on the Fischer-Tropsch (FP) synthetic fuel generation process. The Defense Advanced Research Projects Agency (DARPA) solicited a request for information (RFI) for "deployable reactor technologies for generating power and logistic fuels" (RFI SN10-37) [9]. The DOD has such a keen interest in forward deployed synfuel technology because it attacks the "hidden" but ultimately much more expensive costs of the fuel supply chain, illustrated in Figure 1-5:
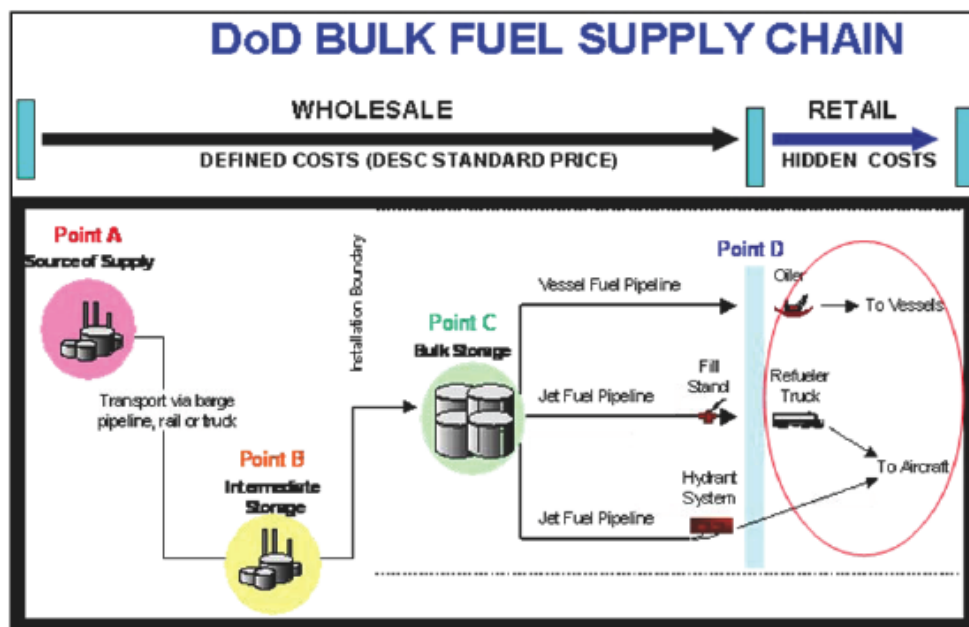
Figure 1-5 - Fuel Supply Chain

---

[2] In close proximity to a conflict, or potential conflict, and has not been introduced to hostilities.

As the *More Fight-Less Fuel* report notes, transporting fuel to deployed combatants not only consumes "significant resources," but also constrains the combatants' "freedom of movement." Military commanders must divert assets from combat operations in order to protect supply lines, and such assignments make them "vulnerable to attack." Thus, the "hidden costs" of Figure 1-6 below[10] illustrate not only include the additional infrastructure and operations necessary to complete the tail end of the supply chain, but also the more significant, intangible cost of "diverting and endangering in-theater force capability"[8].

Fuel for DoD *Operations*

Direct Cost
~$12.6B in FY07 purchases

Indirect Costs
Huge "tail" to deliver
  – Airborne tanking
  – Refueling trucks & helos
  – Navy oilers
  – Personnel
  – Force Protection
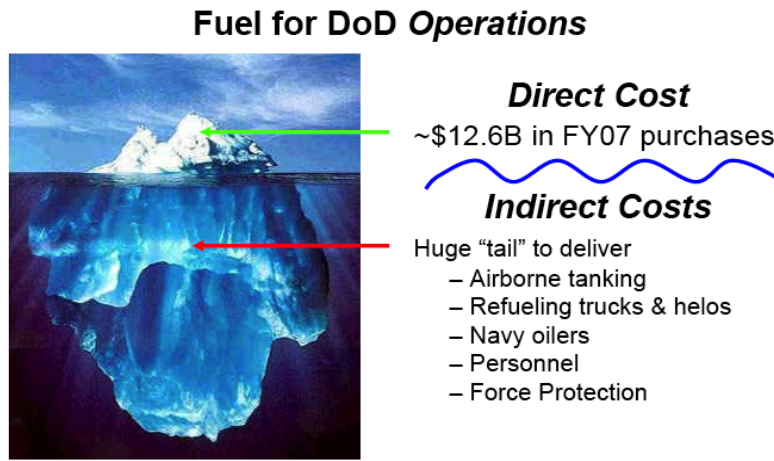
Figure 1-6 - Hidden Fuel Cost

The October 12, 2000 attack on the USS Cole (DDG-67) in Yemen during a routine fuel stop provide a relatively recent and stark example of the indirect costs associated with the risks involved in getting fuel to naval combatants, and the conflicts Operation Iraqi Freedom (OIF) and Operation Enduring Freedom (OEF) have heightened the DOD's attention to the issue even more.

Figure 1-7 - Consequences of USS Cole (DDG-67) Refueling in Yemen

A nuclear powered tanker ship capable of generating synthetic fuel for consumption by USN and US Marine Corps (USMC) platforms would directly attack the difficulties caused by hidden, indirect costs, and would do much to obviate the challenges military logisticians face when naval forces are operating in remote regions.

1.2   Synfuel Production Plant

Publicly available information regarding the use of synfuel to enhance military capability is scarce even though synfuel production is a mature technology. Synfuel is not common in the United States because synfuel production technology is an expensive, capital intensive endeavor [11]. The main proponents are large coal and natural gas companies. A cursory survey at the marketing literature will highlight the benefit of using coal for energy independence. Unfortunately, conventional synfuel technology produces even more green-house gas emissions than conventional petroleum sources. Consequently, more recent research regarding synfuel production relates to finding a carbon neutral technology capable of adequately addressing current and projected energy demands. For this reason, coal and natural gas are often eschewed as an energy source or a feedstock by environmental advocates, while favored CO_2 feedstock sources include biomass or CO_2 extracted directly from the surrounding environment along with renewable or nuclear energy sources. Figure 1-8 below compares CO_2 release from synfuel produced from alternate sources, demonstrating the environmental benefit of synfuel produced from non-carbon emitting energy sources [7]:
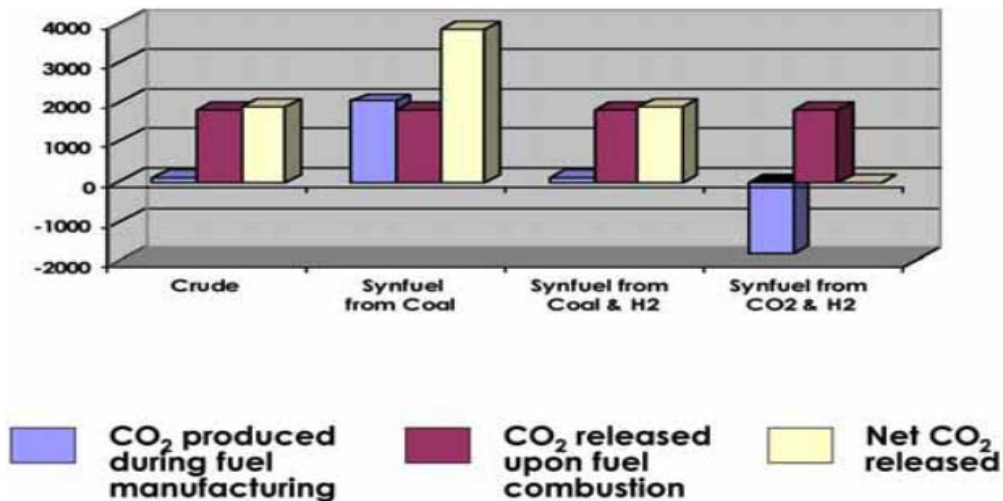
Figure 1-8 - CO2 Release Comparison

One of the primary architects, some would claim the original driving force of using nuclear power to produce synfuel, is Meyer Steinberg, who produced numerous technical papers on synfuel production spanning from the 1960s to the 1980s. A notable report is *Nuclear power for the Production of Synthetic Fuels and Feedstocks* (1977), where Steinberg encourages the use of aquatic or atmospheric sources of CO_2, as they "eliminate the need for fossil fuel" and its associated "environmental hazards … and pollution"[12]. From a military perspective, a notable disadvantage for using fossil fuels such as coal to produce synfuel is that they alleviate none of the logistical burdens; military logisticians essentially trade one problem for another. Essentially the only practical carbon feedstock that can provide naval platforms adequate logistical freedom is CO_2 extraction from the surrounding sea or atmosphere. Additionally, the only reliable energy source capable of satisfying the energy demands of a naval platform, while also providing logistical freedom, is a nuclear power plant. Figure 1-9 provides an example of a synfuel production system using nuclear energy [7]:
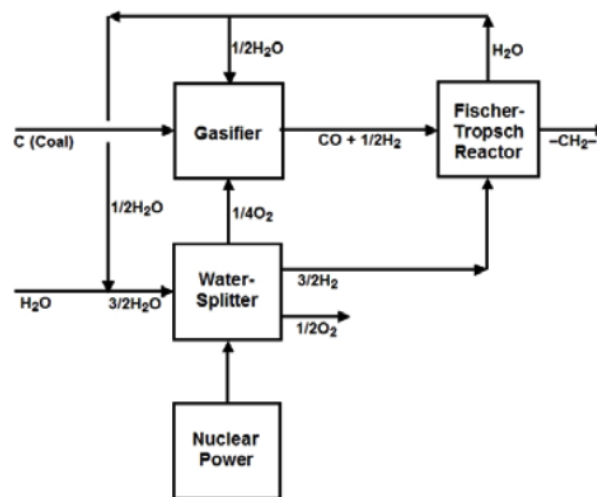
Figure 1-9 - Example Synfuel Production System

The purpose of the nuclear energy is to supply the energy required to produce syngas (a combination of H_2 from H_2O and CO from CO_2), which is the input to either a FT or a Mobil process.[3] With H_2 generated via nuclear energy, the process is essentially as follows [13]:

$$Carbon feedstock + Water + Energy \rightarrow Liquid fuels$$

---
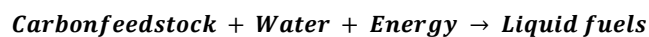
[3] Chapter 3 explains Fischer-Tropsch and Mobil Processes in detail.

1.3 Previous Investigation

The concept of using nuclear energy to produce synfuel is not new, nor is placing a nuclear-powered synfuel plant onboard a tanker ship.   Two Massachusetts Institute of Technology (MIT) theses from the Department of Nuclear Science and Engineering (NSE) [4] explore the application of Steinberg's concept on naval platforms using early to mid 1970s technology [14]; a more recent work is LT K. Terry's 1995 MIT thesis, *Synthetic Fuels for Naval Applications Produced Using Shipboard Nuclear Power*. LT Terry's thesis, like this one, evaluates the application of nuclear generated synfuel technology by USN platforms. The synfuel plant design concept in Terry's thesis has the following parameters [14]:

- A pressurized water reactor (PWR) plant system to supply all load requirements
- CO_2 extraction from seawater via single effect evaporator, conventional vapor compression, or modified vapor compression
- H_2 generation via conventional, low temperature alkaline water electrolysis
- Methanol synthesis of CO_2 and H_2 followed by liquid fuel production of JP-5 via the Mobil methanol to gasoline (MTG) process
- Net overall thermal energy requirement of 10.5 $MW_{th}hr$/Barrel of $(CH_2)_n$ based on the process energy requirements of Table 1-1 below:

Process Step	Predicted Process Energy Requirement (kW-hr/ kg $(CH_2)_n$)
Electrolysis for H_2 Generation	17.7
CO_2 Separation from Seawater	1.9
H_2 Compression to 100 bar	1.8
CO_2 Compression to 100 bar	0.45
H_2 Heatup to 270 ^{0}C	0.37
CO_2 Heatup to 270 ^{0}C	0.24
Methanol Sythesis	-1.7
MTG	-0.9
Total Required (25% Rx Plant efficiency)	87.6

Table 1-1 - PWR Synfuel Plant Energy Requirements

After establishing the Table 1-1 energy requirements above, LT Terry evaluates the application of his concept for use on an aircraft carrier (CVN), a barge, and a tanker ship. The CVN conceived in his thesis would only supply synfuel to the embarked air wing. By adopting conservative approximations, his

---

[4] The theses are (1) Robin P. Bushore's *Synthetic Fuel Generation Capabilities of Nuclear Power Plants with Application to Ship Technology* (1977) and (2) Christian Schmidt's *Nuclear Generated Synthetic Fuel Systems for Ship Propulsion* (1976).

thesis establishes the demand required by a CVN-based synfuel plant to supply JP-5 to its embarked air wing [14]:

Barrels of JP-5 per Day (Sorties per Day)	Days until 40% of Onboard JP-5 Capacity Reached
1,785 (30)	125
2,530 (43)	40
5,060 (85)	12
10,120 (170)	5

Table 1-2 - Estimated CVN JP-5 Consumption

LT Terry incorporates the synfuel demand from Table 1-2 with additional assumptions regarding the CVN's propulsion and electrical power generation requirements and thermal efficiency to conclude that to merely sustain peacetime operations (~ 2500 BBL/Day) would require nearly doubling the current power rating of a Nimitz class A4W design (~ 500 MW$_{th}$), along with refueling every 5 vice 20 years [14]. Taken together with the space and energy requirements of the primary and ancillary systems required to support the synfuel plant (especially the CO_2 extraction systems), one could concur with LT Terry's recommendation against using a CVN based synfuel plant. Chapter 2 of this thesis shows that the estimated fuel consumption data in Table 1-2 exceeds the postulated peacetime requirement by only about 500 BBL/Day, which is close enough to conclude that the PWR based synfuel plant design used in LT Terry's thesis is not adequate to provide the desired military capability.

Another option is basing the synfuel plant on a barge; however, this option is unattractive for several reasons:

- Since a barge has no propulsion, it would have to be transported by other military assets to the theater of operations.
- A barge would not be able to operate at sea without dedicated assistance from another vessel.
- The USG would face enormous challenges in obtaining host nation (HN) permission to berth a barge with an operating nuclear synfuel plant, if such an option is even possible.
- The military would still have to provide much of the logistical support to get fuel from the barge to combat assets, including force protection, oilers, military convoys, and associated infrastructure.

Since the shortcomings associated with the barge result in many logistical and operational hindrances, this thesis will not consider it.

The application that LT Terry's thesis implicitly endorses is a nuclear powered tanker ship. The advantages of basing the capability on a tanker ship are that (1) having a dedicated tanker ship allows

the combatant units to operationally focus on combat objectives; (2) locating the synfuel plant on a tanker ship instead of combatant units frees up space for weapon systems or other capabilities; and (3) a tanker ship is self sufficient and requires no additional assets to keep it on station with the other combatant units. LT Terry's thesis estimates an 8,200 BBL/Day demand requirement that the tanker's synfuel plant must satisfy, which corresponds to a 3,600 MW_{th} power rating for his tanker's PWR reactor plant and liquid fuels production plant systems (roughly equivalent to 7 Nimitz-sized A4W reactor plants). Utilizing the size scaling "2/3 rule"[5], LT Terry estimates that an adequate tanker would be on the order of ~ 160,000 Ltons (~ 162,500 Mtons), which is a tanker on the order of a Medium Sized Crude Carrier (MCC) [14].

1.4 A New Look

The implied point in LT Terry's thesis is that while liquid fuels production on a naval tanker might be feasible, it would be costly if constrained by the parameters of his design. Stated more bluntly, the requirements for the nuclear and synfuel generation systems of the proposed tanker design in LT Terry's thesis are too burdensome to be realistically implemented. More accurate demand estimates that would serendipitously reduce capacity requirements, while helpful, are not enough. Improvements in shipboard propulsion system economy, although desirable, are also unlikely to reduce capacity requirements to a level manageable to LT Terry's synfuel production system. However, recent advances in H_2 electrolysis and reactor technology might result in a more desirable solution, and the primary goal of this thesis is to specifically evaluate the impact of these newly emerging technologies on a naval synfuel production system. Specific examples of promising technological developments include the following:

- **The salt-cooled Advanced High Temperature Reactor (AHTR).** AHTRs have much higher outlet temperatures than PWRs, and they have greater power densities than gas cooled reactors. This facilitates not only a more compact power plant, but also the potential for more efficient, less energy intensive methods of H_2 generation [15], [16].
- **Developments in modular CO_2 capture and synfuel technology systems.** Conventional synfuel production and refinery facilities contain some of the largest pieces of industrial equipment in existence. Modular, compact, and efficient syngas and synfuel production systems are essential in order to realize synfuel capabilities on a naval platform. Advances in modular carbon capture

---

[5] Refer to Popper, H.; Modern Cost Engineering Techniques. McGraw-Hill, New York, 1970 for details.

technology and micro channel reactors (MCRs) have the potential to make the synfuel tanker concept feasible.

- **High Temperature Electrolysis of H_2 and CO_2.** Table 1-1 above clearly shows that H_2 generation by traditional water electrolysis is the primary energy consumption step; significant dividends could be realized for any improvement. High-temperature electrolytic water-splitting supported by nuclear process heat and electricity has the potential to produce hydrogen with overall thermal-to-hydrogen efficiencies of 50% or higher [17]. Coelectrolysis, developed by Idaho National Laboratory (INL), is a technique in which solid-oxide cells operating at high temperature simultaneously produce syngas (vice using a water-shift reaction to produce syngas from conventional electrolysis), which could improve process efficiency even more [18].

1.5 Thesis Outline

As mentioned above, the objective of this thesis is to evaluate the impact of newly emerging technologies on a naval synfuel production system. Chapter 2 discusses the type and quality of fuel the synfuel plant must produce, essentially driving the remaining parameters of the synfuel production system. With demand established, chapter 3 discusses liquid fuels production from syngas in detail; this process includes the extraction of CO_2 feedstock from the environment and H_2 generation from electrolysis. Chapter 4 provides an overview of the AHTR, contrasts the ATHR with a PWR, and proposes a thermodynamic power cycle. Chapter 5 evaluates the feasibility of integrating a liquid fuels production module within an existing naval platform, and estimates the cost of developing a new ship with liquid fuels production capability. Finally, chapter 6 summarizes the results, and makes conclusions and recommendations.

1.6   Chapter 1 References

[1] Andrews, A., 2009, "Department of Defense Fuel Spending, Supply, Acquisition, and Policy," Congressional Research Service, R40459, Washington, DC.

[2] US Energy Information Administration, 2008, "Annual Energy Review, Table 5.1," **2010**(6/27) pp. 1.

[3] Loose, VADM N. K. (N4), 2010, "NAVADMIN 66-10, Energy Conservation Award," **2010**(6/27) pp. 1.

[4] Fonte, S., 2009, "M.S. Thesis: A Cost Estimation Analysis of US Navy Ship Fuel-Saving Techniques and Technologies," Naval Postgraduate School, http://handle.dtic.mil/100.2/ADA510113, Monterey, CA.

[5] O'Rourke, R., 2006, "Navy Ship Propulsion Technologies: Options for Reducing Oil Use — Background for Congress," Congressional Research Service, RL33360, Washington, DC.

[6] Corley, R., 2009, "M.S. Thesis: Evaluating the Impact of the Fully Burdened Cost of Fuel," Naval Postgraduate School, http://handle.dtic.mil/100.2/ADA508983, Monterey, CA.

[7] Schultz, K., Bogart, L., Besenbruch, G., 2006, "Hydrogen and Synthetic Hydrocarbon Fuels-A Natural Synergy," National Annual Hydrogen Conference 2006, A. Cutair, ed. NHA, Washington, DC, pp. 1-10.

[8] Schneider, W., 2008, ""More Fight – Less Fuel"," Office of the Under Secretary of Defense For Acquisition, Technology, and Logistics, Defense Science Board Task Force on DoD Energy Strategy, Washington, DC.

[9] Lazarus, A., 2010, "Request for Information (RFI) on Deployable Reactor Technologies for Generating Power and Logistic Fuels (SN10-37)," **2010**(6/25) pp. 1.

[10] DiPetto, C., 2008, "DoD Energy Demand-Addressing the Unintended Consequences," Office of the Director, Defense Research and Engineering, http://www.acq.osd.mil/se/briefs/20080912-ODUSD-AT-Energy-Demand-Brief-DiPetto.pdf, Arlington, VA.

[11] Andrews, A., 2007, "Liquid Fuels from Coal, Natural Gas, and Biomass: Background and Policy," Congressional Research Service, RL34133, Washington, DC.

[12] Steinberg, M., 1977, "Nuclear Power for the Production of Synthetic Fuels and Feedstocks," Energy Policy, **5**(1) pp. 12-24.

[13] Forsberg, C., 2005, "Nuclear Hydrogen for Production of Liquid Hydrocarbon Transport Fuels," 2005 American Institute of Chemical Engineers Fall Meeting, K. Schnelle, ed. Oak Ridge National Laboratory, Oak Ridge, TN, pp. 1-10.

[14] Terry, K., 1995, "NEng Thesis: Synthetic Fuels for Naval Applications Produced Using Shipboard Nuclear Power," Massachusetts Institute of Technology (DSpace@mit), http://hdl.handle.net/1721.1/11590, Cambridge, MA.

[15] Forsberg, C., and Peterson, P., 2010, "Advanced High Temperature Reactor for Electricity and Fuels Production using High-Temperature Electrolysis and Fischer-Tropsch Synthesis," **Reply to Request for Information (RFI): Defense Advanced Research Projects Agency SN10-37**pp. 1-3.

[16] Yildiz, B., and Kazimi, M., 2006, "Efficiency of Hydrogen Production Systems using Alternative Nuclear Energy Technologies," International Journal of Hydrogen Energy, **31**pp. 77-92.

[17] O'Brien, J., McKellar, M., Harvego, E., 2009, "High-Temperature Electrolysis for Large-Scale Hydrogen and Syngas Production from Nuclear Energy – System Simulation and Economics," Idaho National Laboratory, INL/CON-09-15563, Idaho Falls, ID.

[18] Stoots, C., 2010, "Production of Synthesis Gas by High-Temperature Electrolysis of H_2O and CO_2 (Coelectrolysis)," Sustainable Fuels from CO_2, H_2O, and Carbon-Free Energy, C. Stoots, ed. Idaho National Laboratory, Idaho Falls, ID, pp. 6-7.

2 Fuel Requirements

2.1 The Case for a Single Fuel at Sea

The two fuels used by the US Navy (USN) are (1) Turbine Fuel, Aviation JP-5 (MIL-DTL-5624U) and (2) Fuel Oil, Naval Distillate (MIL-DTL-16884L), more commonly known as Diesel Fuel Maritime (DFM) or F-76. For safety reasons, military specification JP-5 is the only fuel allowed for naval aircraft while operating at sea, due to its higher flashpoint (>140 ^{o}F, >60 ^{o}C) [1]. F-76 and JP-5 are both military grade fuels, with specifications delineated by [2] and [3], respectively. No substitute exists for JP-5; however, JP-5 can be substituted for F-76 [4]. Appendix B provides the specification details for F-76 and JP-5.

Two reasons cited by Sermarini in his thesis, *The Universal Fuel at Sea: Replacing F-76 with JP-5*, as to why a single naval fuel does not exist are availability and cost. He claims that not all refineries are willing or able to produce JP-5, and JP-5 costs more than F-76 [1]. According to the Defense Energy Support Center (DESC), which is the agency responsible for Department of Defense (DoD) fuel logistics, fiscal year (FY) 2010 prices shows the per gallon cost of JP-5 at $2.84, compared to $2.81 for F-76 (the same price ten years ago) [5]. A 1992 *Navy Fuel Specification Standardization Study* by the Belvoir Fuels and Lubricants Facility stated that "major penalties" included "higher fuel cost" and "difficulty in procuring adequate supplies of JP-5 to meet … fuel requirements" [4]. According to the *DESC FY09 Fact Book*, approximately 21,159,000 barrels of distillates and diesels were purchased, which amounts to a cost increase of $26,660,340 [6]. Furthermore, the study concluded that although using solely JP-5 would not harm operational readiness, the "benefits would be difficult to quantify" and it would be "at least initially, very costly to the Navy" [4].

Sermarini and Tosh also note that JP-5 has been infrequently, but routinely "downgraded" to F-76 when it no longer meets aviation specifications, and JP-5 has been used as a substitute when F-76 is not available. However, not all JP-5 specifications meet or exceed F-76 specifications (e.g., "cloud point"). Furthermore, JP-5 has a lower heat value, lower cetane number, and lower viscosity and lubricity than F-76 [1]. Despite these potential undesirable characteristics, navy ships have not reported abnormal operating conditions from JP-5 use. General Electric (GE) specifically approves of using JP-5 on its GE-LM2500 gas turbine engines, which are used on most US Navy warships, including Arleigh Burke class destroyers and Ticonderoga class cruisers. While an analysis of JP-5 performance characteristics is

beyond the scope of this thesis, Table 2-0-1 summarizes the postulated technical/maintenance advantages and disadvantages of using JP-5 as a shipboard fuel [1]:

Potential Advantages	Potential Disadvantages
• **Reduced engine combustion-related wear** • **Reduced nozzle fouling and deposit problems** • **Reduced potential for fuel system corrosion problems** • **Longer fuel filter replacement intervals** • **Reduced exhaust emissions and signature** • **Extended oil change and filter replacement intervals** • **Reduced low temperature operability problems due to fuel waxing** • **Reduced potential for microbiological growth problems in fuel tanks** • **Reduced entrainment and emulsification problems in fuel tanks** • **Increased storage stability** • **Improved fuel and lubricant related cold starting**	• **Reduced power and slower acceleration in some systems** • **Increased wear in some fuel lubricated pumps and injectors** • **Marginally increased fuel consumption and decreased range** • **Hot starting problems in some diesel engines with rotary fuel pumps** • **Initially increased fuel filter replacement after mixing JP-5 with diesel fuels**

Table 2-1 - Potential Technical Advantages and Disadvantages of JP-5 as Single Use Navy Fuel

A study commissioned by Energy Plans and Policy Branch for the Deputy Chief of Naval Operations (OPNAV N420) concluded that potential technical/maintenance shortcomings of making JP-5 the primary shipboard fuel "should be manageable although … more thorough research may be required to verify this assumption" [7].   D. M. Korres et al. evaluated the use of JP-5, biodiesel, and traditional diesel on a diesel engine and concluded that traditional diesel and JP-5 had equivalent fuel consumption, except at high loading, where traditional diesel fuel consumption was higher. Additionally, JP-5 had lower nitrogen oxides (NO_x) and particulate (SO_x) emissions [8]. Although the OPNAV N420 study did not include a detailed cost benefit analysis of using JP-5, its conclusions were also favorable for using JP-5 as a single at-sea fuel [7]:

- An adequate supply base exists to supply USN and USMC sea, air, and ground equipment. Most suppliers not producing JP-5 could produce it.

- Additional costs from the fuel conversion would at least be partially offset by reduced maintenance and infrastructure costs, economies of scale, and fewer fuel rotation requirements.

- Exclusive use of JP-5 would reduce fuel supply and transportation risk, provide greater flexibility with underway replenishment (UNREP), and enhance readiness and capability.

The tanker's synthetic fuel production plant would probably have a simpler design and operational schedule if it generated only one fuel, suitable for all USN and USMC platforms. The DOD has yet to reach a decision on using JP-5 as a universal at-sea fuel. However, there is demonstrated precedent of using JP-5 as DFM substitute, and it is certainly safe to use in nearly all USN propulsion systems. LT Terry's 1995 thesis on synthetic fuel plants only considered JP-5 as the universal product since its properties are so similar to F-76. Multiple independent references corroborate the similarity between the two fuels, and even advocate the gradual implementation of JP-5 as the universal at-sea fuel. The primary reason for even considering a nuclear powered tanker ship with synthetic fuel generation capability is to provide operational and logistical freedom to operational commanders and combatants. Having such a tanker able to produce a single fuel for consumption by USN and USMC platforms enhances such freedom even more. Thus, this thesis will assume that JP-5 will be the sole fuel generated by the tanker, and that it will be permitted to use JP-5 as a DFM substitute for USN/USMC platforms. Even if a future analysis determines that JP-5 should not be substituted for F-76, the two fuel types are similar enough that the configuration and power requirements of the liquid fuels production plant would not change appreciably as far as this analysis is concerned.

2.2   Fuel Demand

A significant aspect of the tanker's synthetic power plant design is its anticipated demand. The anticipated fuel demand from a Carrier Strike Group (CSG) or an Amphibious Readiness Group (ARG) is the synthetic production plant's desired capacity. Fuel demand drives the quantity of feedstock required for liquid fuel generation. The amount of feedstock required determines the amount of CO_2 that must be extracted for electrolysis as well as the power rating of the reactor plant system. Integrated together, these parameters ultimately drive the overall size, power rating, and operating characteristics of the entire onboard fuel production facility and the tanker vessel.

LT Terry's thesis determined the required fuel generation capacity from computer model simulations predicting fuel consumption in LT Christopher Reeger's 1993 Thesis, *Optimal Cargo Volume Mix for a Kaiser Class Oiler* [9], and the model inputs for individual ship fuel consumption used in Reeger's thesis came from an previous, 1990 version of David Schrady's technical report, *Predicting Ship Fuel Consumption* [10]. The underlying premise of this methodology is that by knowing the complement of ships and aircraft in a CSG, one can calculate fuel consumption for a given scenario by using a non-linear regression model that fits an analytical function of the ship's hydrodynamic resistance and

powering requirements to fuel consumption data for a given class of ship taken during sea trials. The data issues regarding this approach include (1) the amount of speed vs. fuel use data available, (2) the range of the data available, and (3) data consistency for different ships of the same class. Reference [11] provides a concise explanation of the methodology relating ship's resistance to fuel consumption. The baseline fuel consumption scenario chosen by LT Terry, was originally postulated in LT Reeger's thesis:

- 1 nuclear-powered aircraft carrier (CVN) with embarked airwing
- 6 gas turbine-powered destroyer and cruiser escort ships
- 1 auxiliary oiler (AOE)
- A "scenario" of 10 days "transit" at 20 knots (kts), 20 days at 12 kts "presence", and 50 days at 16 kts "combat"

Calculations using the above parameters yielded an average consumption rate of 4,200 barrels per day (BBL/day) of JP-5 and 4,000 BBL/day of F-76 [9],[10].

The tanker conceptualized for this thesis will also support traditional "blue water" CSG or ARG operations, as opposed to littoral operations envisioned for platforms such as the Littoral Combat Ship (LCC) or Naval Expeditionary Combat Command (NECC) riverine squadrons (although a tanker ship could in theory serve as a fuel supply source for these platforms, their required fuel demand is not on the same order of magnitude as a CSG or ARG). This thesis uses, however, a different approach to estimate the required fuel demand: NAVSEA provided fuel consumption data for this thesis based on a historical three year (FY07/08/09) class average. As shown below, the fuel consumption figures are consistent with the semi-empirical approach utilized by Reeger and Terry after accounting for the fact that CSGs today typically comprise of 5 (not 6) gas turbine ships (3 guided missile destroyers (DDG) and 2 guided missile cruisers (CG)).

2.2.1 F-76 Fuel Consumption

Since west-coast based ships must travel farther to reach station, they have a higher average comsumption. Table 2-0-2 shows the west-coast based underway BBL/day fuel consumption requirements of CSGs and ARGs [12]:

Carrier Strike Group				Amphibious Readiness Group			
Platform	#/ CSG	BBL/Day	Total (BBL/Day)	Platform	#/ARG	BBL/Day	Total (BBL/Day)
CVN	1	3	3	LHA/D	1/1	1,375/1,243	1,375/1,243
CG	2	714	1,428	LPD	1	548	548
DDG	3	583	1,749	LSD	2	326	652
SSN	2	0	0				
CSG F-76 Consumption		3,177		ARG F-76 Consumption			2,575 / 2,443

Table 2-2 – Deployed CSG & ARG F-76 Consumption

Thus, the most demanding case is a west-coast based CSG, with an F-76 consumption rate of 3,177 BBL/Day. For comparison, the average F-76 consumption rate is 4,200 BBL/Day for an east-coast based CSG and 4,450 BBL/Day for a west-coast based CSG if the CSG composition includes the additional gas turbine and oiler platform that LT Terry's thesis uses. Both figures are within 10% of the 4,000 BBL/Day value independently determined through a postulated speed-power relationship, thereby engendering considerable confidence.   Hence, the deployed fuel consumption figure of 3,177 BBL/Day in Table 2-0-2 is a good value to input for tanker fuel generation capacity. The majority of the deviation between the model results in Terry's thesis and the historical data is due to the constraints imposed by the postulated scenario. Ship maneuver scenarios that better approximate deployed operations will facilitate better results.

2.2.2   JP-5 Fuel Consumption

For JP-5 consumption, NAVSEA provided data for fuel consumed in FY03 and for FY09 in Table 2-0-3 below in order to show the increased demand caused by the "Shock and Awe" campaign of Operation Iraqi Freedom (OIF) in FY03 [13]:

Carrier Strike Group		Amphibious Readiness Group	
Aircraft Composition	5x EA-6b	Aircraft Composition	4x AH-1W/Z
	2x C-2A		3x UH-1N/Y
	5x E-2C		12x CH-46/MV-22
	12x FA-18F		4x CH-53E/D
	12x FA-18E		6x AV-8B
	20x FA-18C		3x KC-130
	8x SH-60F		12x FA-18C
	11x SH-60B		
CSG FY09 JP-5 Consumption	2,005 (BBL/Day)	ARG FY09 JP-5 Consumption	827 (BBL/Day)
CSG FY03 JP-5 Consumption	3,214 (BBL/Day)	CSG FY03 JP-5 Consumption	1,424 (BBL/Day)

Table 2-3 - Deployed CSG & ARG JP-5 Consumption

Since the OIF campaign was an impressive and representative display of USN and USMC air power, the FY03 deployed JP-5 consumption data is useful estimate for required capacity to support wartime combat operations. Conveniently rounding both of the JP-5 and F-76 figures to 3,200 BBL/Day results in a total estimated required tanker capacity of 6,400 BBL/Day. Appendix A contains the fuel consumption data provided by NAVSEA.

2.3 Conclusions and Recommendations

The USN uses two fuels, F-76 for maritime platforms and JP-5 for aircraft. If necessary, the DOD should perform more analysis to determine if JP-5 could serve as the sole "battlefield" fuel for deployed assets. Several studies show that the technical issues involved with using JP-5 for marine platforms appear manageable. The initial changeover to a single fuel would have costs, but the simplified fuel logistics could pay back the cost over time. The DOD should commission a study to specifically examine the cost benefit of this proposal. In any event, the detailed specifications of these two fuels show that they are very similar, and for the purposes of a liquid fuels production plant, they can be considered the same fuel.

The data analysis approach used in Terry's thesis to predict fleet fuel consumption has good agreement with the fuel consumption statistics provided by NAVSEA. The accuracy of the data analysis approach depends upon the agreement of actual ship operations with a postulated scenario. Provided the propulsion characteristics of a new marine platform are known, such a tool would be invaluable in predicting fuel consumption for fleet composition with limited historical basis. This thesis, however, shall use the NAVSEA provided fuel consumption statistics because they provide the best obtainable estimate of required fuel demand for any fleet composition currently utilized by the USN.

2.4 Chapter 2 References

[1] Sermarini, J., 2000, "M.S. Thesis: The Universal Fuel at Sea: Replacing F-76 with JP-5," Naval Postgraduate School, http://handle.dtic.mil/100.2/ADA378613, Monterey, CA.

[2] Department of Defense, 2006, "Detail Specification: Fuel, Naval Distillate," Department of Defense, MIL-DTL-16884L, Arlington, VA.

[3] Department of Defense, 2004, "Detail Specification Turbine Fuel, Aviation Grades JP-4 and JP-5," Department of Defense, MIL-DTL-5624U, Alexandria, VA.

[4] Tosh, J., Moulton, D., and Moses, C., 1992, "Navy Fuel Specification Standardization," Southwest Research Institute, BFLRF No. 225, San Antonio, TX.

[5] DESC, 2010, "FY 2010 Prices," DESC, http://www.desc.dla.mil/DCM/DCMPage.asp?pageid=722, Fort Belvoir, VA.

[6] DESC, 2009, "DESC FY09 Fact Book," DESC, Fort Belvoir, VA, pp. 93.

[7] Giannini, R., Martin, C., Strucke, R., 2002, "Single Fuel at-Sea Feasibility Study - Part One," NAVAIRSYSCOM, 445/002-004, Patuxent River, MD.

[8] Korres, D., Karonis, D., Evripidis Lois, E., 2008, "Aviation Fuel JP-5 and Biodiesel on a Diesel Engine," Fuel, **87** pp. 70-78.

[9] Terry, K., 1995, "NEng Thesis: Synthetic Fuels for Naval Applications Produced Using Shipboard Nuclear Power," Massachusetts Institute of Technology (DSpace@mit), http://hdl.handle.net/1721.1/11590, Cambridge, MA.

[10] Reeger, C., 1993, "M.S. Thesis: Optimal Cargo Volume Mix for a Kaiser Class Oiler," Naval Postgraduate School, AD-B178 592, Monterey, CA.

[11] Schrady, D., Smyth, G., and Vassian, R., 1996, "Predicting Ship Fuel Consumption: Update," Naval Postgraduate School, NPS-OR-96-007, Monterey, CA.

[12] Dimirack, S., 2010, "RE: Fuel Consumption Data," **Email to Author of Historical Three Year Average of F76 Consumption in BBLs/day (.xls format)**pp. 1.

[13] Greg, R., 2010, "RE: Fuel Consumption Data," **Email to Author of JP5 Fuel Consumption Data (.xls format), FY03 and FY09**pp. 1.

3   Synthetic Fuel Production Plant

3.1   Introduction

3.1.1   General Overview

Chapter 2 establishes that (1) US Navy jet fuel (JP-5) could probably serve as an alternative fuel to maritime distillate (F-76), and (2) that a naval synthetic fuel (synfuel) tanker ship must be able to produce 6,400 BPD (268,800 GPD) in order to satisfy the wartime fuel demand of a deployed carrier strike group (CSG).   The next step is determining the synfuel generation process. Several options exist, and the goal of this chapter is to identify the most suitable option for a military tanker. The basic process is using energy to convert feedstock materials to synthesis gas (syngas), send the syngas through a chemical reactor plant, and refine the distillate product into the desired hydrocarbon product (JP-5):

Convert Feedstock to Syngas	→	Convert Syngas to Synfuel	→	Refine Synfuel	→	JP-5 Product
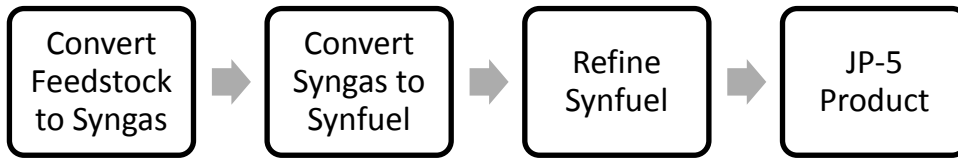
Figure 3-1 - Overall Synfuel Process Diagram

Essentially, the process is the reversal of jet fuel combustion, where **oxygen + jet fuel = water + carbon dioxide + energy**. Hence, the goal of this chapter is to find a feasible solution to implement such a process on an at-sea tanker.

3.1.2   Introducing a Baseline Synfuel Production System

Creating liquid fuel from syngas is a well-established, mature technology. South Africa's SASOL facility can produce an entire range of hydrocarbon products using the process illustrated in Figure 3-1 [1]. The reason synfuel production is not ubiquitous technology is that generating syngas requires significant amounts of energy.   In general, traditional petroleum is less expensive and more convenient. To create syngas, a carbon based feedstock must be converted into a CO_2, CO, and H_2 mixture, which is normally done using coal or natural gas. In a traditional coal-to-liquids (CTL) production, coal is converted to syngas that is then converted into liquid fuel. In a gas-to-liquid (GTL) production scheme, steam is combined with natural gas over a catalyst bed to produce the carbon-hydrogen syngas mixture. Although the reaction is endothermic, GTL provides a better hydrogen-to-carbon ration, has far fewer

emissions, and requires less elaborate and less expensive syngas cleanup operations. There has been a significant amount of research on carbon capture, as well as the use of biomass or municipal solid waste (MSW) as carbon feedstock sources; however, they are not mainstream technologies.

The hydrogen/carbon syngas feed is then purified and sent to a chemical reactor, in a precise chemical proportion, under a prescribed temperature and pressure. The actual ratio of H_2 to CO_2 and CO depends on the synfuel process used and the desired product slate. The two primary options to convert syngas to synfuel are Fischer-Tropsch or a Mobil methanol conversion, both of which are mature, commercially established processes. They are similar in that the syngas undergoes an exothermic reaction over a catalyst bed under prescribed reaction conditions. The reaction conditions and the type of catalyst used ultimately determine the product slate. The synfuel product is then sent to a refinery, which uses a range of chemical processes (hydrocrackers, aromatizers, etc.) that essentially shorten or lengthen the product hydrocarbon chains as necessary to produce the desired product. The refinery techniques for synfuel are similar to conventional petroleum refineries, and one can configure a refinery in any number of ways to optimally produce a desired hydrocarbon product.

The entire synfuel generation process is quite versatile. Table 3-1 provides a partial listing of the available synfuel production options, some of which are explored in-depth later in the chapter:

Feedstock Source for CO_2/CO Syngas Feed	**Coal (CTL)**
	Municipal Solid Waste (MSW)
	Natural Gas (GTL)
	Biomass
	Environment (Sea or Atmosphere)
Hydrogen Production for Syngas Feed	**Alkaline Electrolysis**
	High Temperature Steam Electrolysis (HTSE)
	High Temperature Coelectrolysis (HTCE)
	Steam Methane Reforming (SMR)
	Thermochemcial Water Splitting
Synfuel Production	**CAMERE Process followed by MTO/ODG^{TM}**
	Fischer-Tropsch

Table 3-1 - Summary of Synfuel Production System Options

Figure 3-2, developed by Idaho National Labs (INL), emphasizes the versatility of a synfuel production scheme by showing how even nuclear energy could be used to make H_2 in a CTL scheme to produce synthetic fuel (it provides a good illustration of the general process steps) [2]:
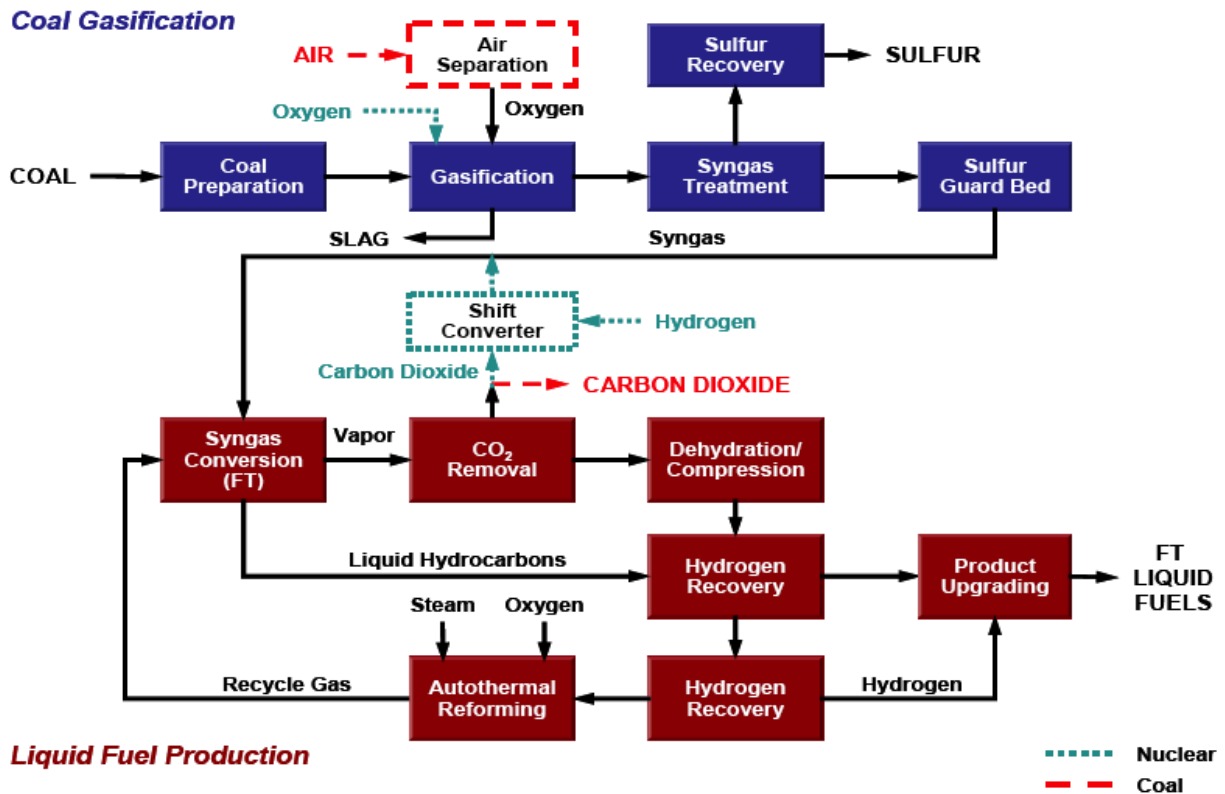
Figure 3-2 - Nuclear Coal Liquefaction and Coal Liquefaction by Indirect Coal-Gasification

The goal of the above process flow diagram is merely provide an example of the versatility of a synfuel production process. The process above is merely a more detailed representation of the following basic concept:
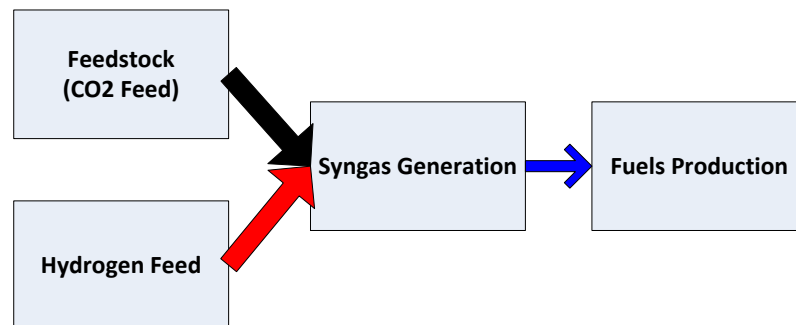
Figure 3-3 - Basic Synfuel Generation Concept

Referring back to the previous assertion that the synfuel generation process is essentially the reversal of jet fuel combustion (**oxygen + jet fuel = water + carbon dioxide + energy**), the tanker ship operating at-sea should ideally be able to use water and carbon dioxide (both locally available) and nuclear energy to provide the heat and electricity to reverse the process. Conveniently, water and CO2 are both readily available from the sea and the atmosphere, and a baseline design that produces jet fuel from water and air could have the following conceptual design:
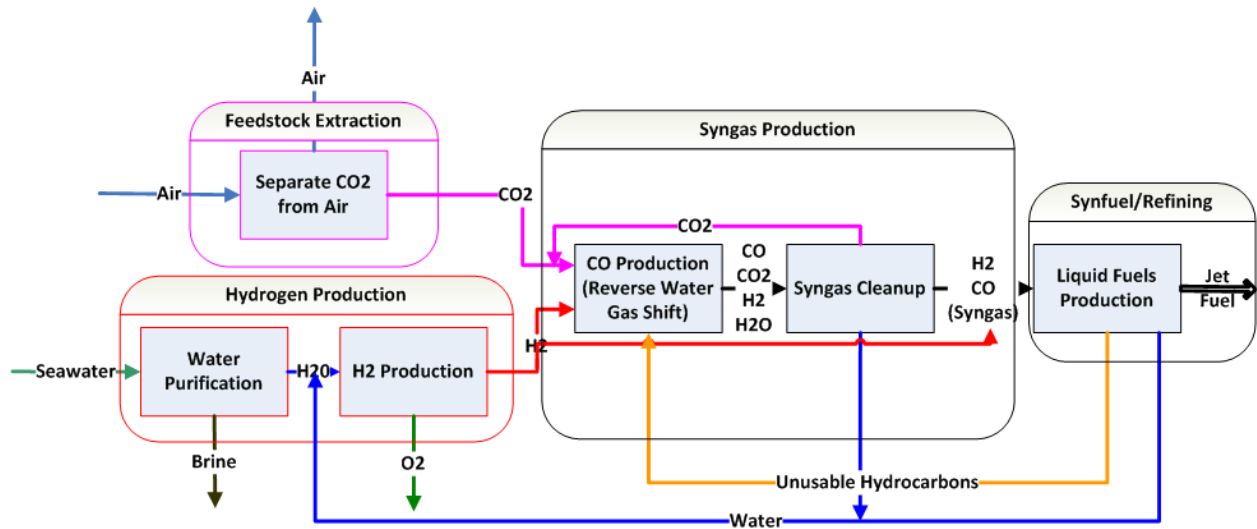
Figure 3-4 – Simplified Flowsheet of Jet Fuel from Air and Water

3.1.3   Exploring the Available Options

Despite the number of "options" contained above in Table 3-1, the inherent constraints of designing the synfuel plant to operate on an at-sea platform make several of the choices impractical. The aim of the following sections is to identify and eliminate the processes that are not suitable so that the remainder of the chapter can perform a more detailed analysis on more promising alternatives.

3.1.3.1   Carbon Feedstock Selection

Generating syngas feed is the most energy intensive process in the entire synfuel production plant. In a conventional Fischer-Tropsch complex, the production of purified syngas typically accounts for 60-70% of the capital and running costs of the entire plant [3]. Unless relatively cheap energy sources are available, synfuel production is simply not an economically viable option compared to traditional petroleum. The most extensively used industrial processes to obtain syngas are steam

methane reforming (SMR) and coal gasification, as respectively shown by the overall reaction stoichiometries in (3-1) and (3-2) below:

$$1.11CH_4 + 0.72O_2 \rightarrow 2H_2 + CO + 0.11CO_2 + 0.22H_2O, SMR \tag{3-1}$$

$$1.78\ CH_{0.5}(coal) + 0.5\ O_2 + 1.56\ H_2O \tag{3-2}$$
$$\rightarrow 2\ H_2 + CO + 0.78\ CO_2, Coal\ Gasification$$
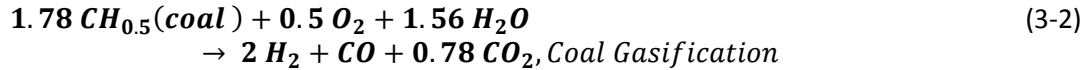
Equations (3-1) and (3-2) show that natural gas is superior to coal in that (1) less feedstock is necessary to produce an equivalent amount of syngas, and (2) there is much less CO_2 emission [4]. However, coal is more abundant and less expensive.

The development of shore-based CTL/GTL facilities certainly provides an attractive option to decouple the military fuel infrastructure to imported petroleum. Economic sanctions during the Apartheid period, the desire for energy independence, and a combination of large coal but low hydrocarbon reserves resulted in South Africa's development of the Sasol synthetic fuel plants that supply South Africa's energy supply needs [5]. Although comparable shore-based facilities would require enormous capital investment outlays, such infrastructure would insulate the Department of Defense (DOD) from perturbations in the global petroleum market. The US Air Force and US Army have research endeavors through the Defense Advanced Projects Research Agency (DARPA) that focus on using synfuel production to enhance energy security [6-8]. As Min Leung shows in his MIT thesis, such facilities could certainly produce sufficient quantities of synthetic fuel, and they can do so even more effectively if they leverage the innovative capabilities offered by CO_2 capture and sequestration (CCS), nuclear power, and a new, innovative hydrogen production technology known as high temperature steam electrolysis (HTSE) [9].

A consequence of using CTL, GTL, and even MSW gasification is the excess CO_2 emission resulting from the syngas generation process. The excess CO_2 emission is most severe for the direct liquification of coal, which is unfortunately the most convenient process due to coal's abundance [10]:
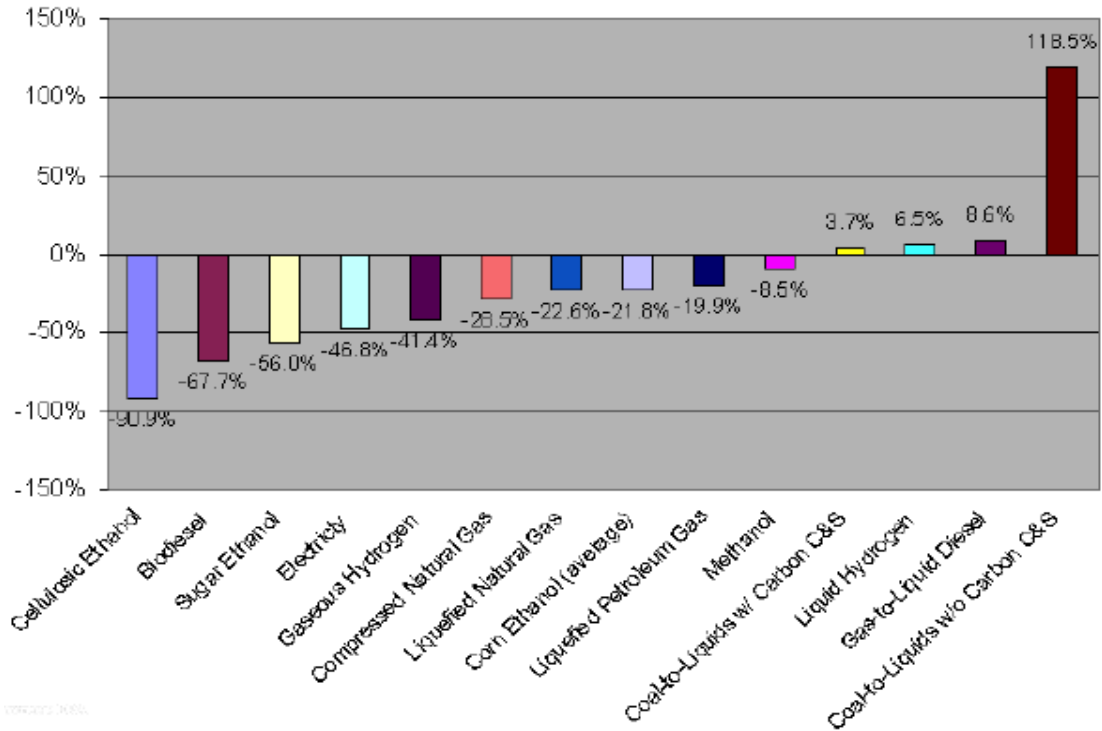
Figure 3-5 – Percent Change in CO$_2$ Emissions from Alternative Fuel Use (Relative to Petroleum-Based Fuels)

As shown in Figure 3-5, even using CTL fuel with carbon capture and storage (CCS) nevertheless increases greenhouse gas (GHG) emissions 3.7% over petroleum-based fuels; without CCS, there is a staggering 118.8% increase. GTL, while not as severe, still increases GHG emissions by 8.6% over a carbon neutral technology.

Shore based CTL/GTL facilities could potentially provide a solution for the military's energy security concerns, regardless of their CO$_2$ emissions. However, a significant shortcoming of their use is that they do little to alleviate the difficulty of providing fuel to deployed military assets, especially forces that are operating in remote or hostile environments. While it would be convenient to leverage mature, existing technology such as CTL and GTL for a synfuel platform, there would obviously be no practical way to deliver adequate quantities of coal or natural gas to a deployed CTL or GTL platform. As discussed in chapter 2, the major fuel costs for the DOD are not necessarily commodity costs, but rather the onerous logistics associated with fuel transport into theater. The same logistics constraint exists for integrating MSW and biomass feedstocks. However, extracting CO$_2$ directly from the atmosphere or sea decouples the synfuel production platform from the supply chain. If technically feasible, this option provides not only energy security, but also logistical freedom for deployed military assets. Furthermore, such an option is also carbon neutral [11, 12]. In Figure 3-4 above, air is the source of the CO$_2$ feedstock.

Some researchers have noted that seawater contains a more abundant concentration of dissolved CO_2 than air [13]; however, as later explained in this chapter, the technology does not yet exist to extract CO_2 from seawater efficiently.

3.1.3.2 *Hydrogen and Syngas Production*

The two general approaches to generate hydrogen are thermochemical and electrochemical. The two possible thermochemical processes are Steam Methane Reforming (SMR) and thermochemical water splitting. SMR, which requires natural gas, is not desirable for reasons previously discussed above. Thermochemical water splitting only exists on a laboratory scale and requires aggressive chemistry controls [14]. The high temperature (> 800 ^{o}C) thermolysis reaction decomposes H_2SO_4 (sulfuric acid) into SO_2 (sulfur dioxide), which is used in a lower temperature reaction to split H_2 from H_2O. Obviously, even if perfected, the use of such highly corrosive and noxious chemicals would in all likelihood preclude the process from ever being considered for shipboard use.

The electrochemical approaches include alkaline electrolysis, proton exchange membrane cells (PEM), and solid oxide electrolysis cells (SOEC); of these, only alkaline electrolysis is commercially mature. Two processes that utilize SOECs are high temperature steam electrolysis (HTSE) and high temperature co-electrolysis (HTCE). The Figure below summarizes their respective capabilities and stage of development [12]:
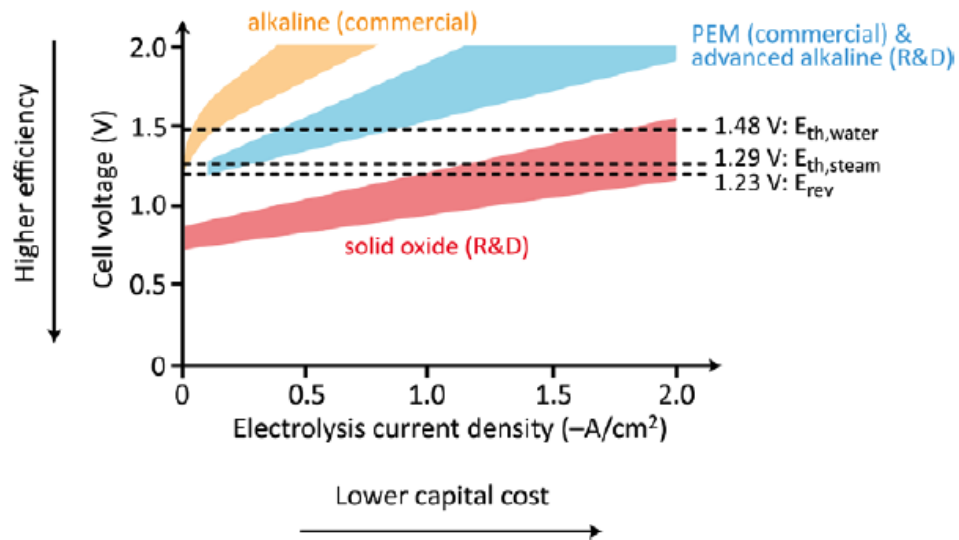
Figure 3-6 - Electrolyzer Capability Summary

PEM cells are commercially available and have better performance than traditional alkaline electrolysis cells, but they are very expensive because of their noble metal electrocatalysts (usually platinum) and exotic membrane materials. If three times higher current density could be achieved at a given efficiency, with the capital cost of a cell stack less than three times larger, the PEM cell hydrogen production price would ultimately be lower than for alkaline cells. However, the higher capital cost appears to be an obstacle to affordable PEM-based electrolysis. Less expensive materials are needed [12]. The conventional choice for electrochemical electrolysis is alkaline electrolyzers. Alkaline electrolyzers typically utilize a potassium hydroxide solution (KOH) to create the cathode-anode potential for the following well known half-reactions:

$$Cathode: \mathbf{2H_2O(l) + 2e^- \rightarrow H_2(g) + 2OH^-(aq)} \tag{3-3}$$

$$Anode: \mathbf{2OH^-(aq) \rightarrow 2e^- + \frac{1}{2}O_2(g) + H_2O(l)}$$
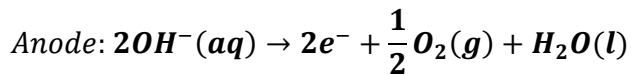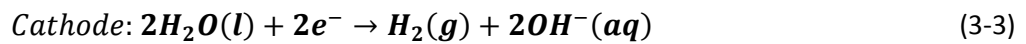
More conveniently, the electrolysis stoichiometry is represented as follows:

$$\mathbf{H_2O \rightarrow \frac{1}{2}O_2 + H_2} \tag{3-4}$$

The more advanced hydrogen production options (HTSE and HTCE) use SOECs to produce hydrogen at high temperature, which reduces the electrical power needed. HTSE and HTCE are both being investigated by Idaho National Laboratory (INL) with sponsoring from the US Department of Energy (DOE). The SOEC is a solid-state electrochemical device consisting of an oxygen-ion-conducting electrolyte (e.g., yttria- or scandia-stabilized zirconia) with porous electrically conducting electrodes deposited on either side of the electrolyte. A cross-section of a planar design is shown below [15]:
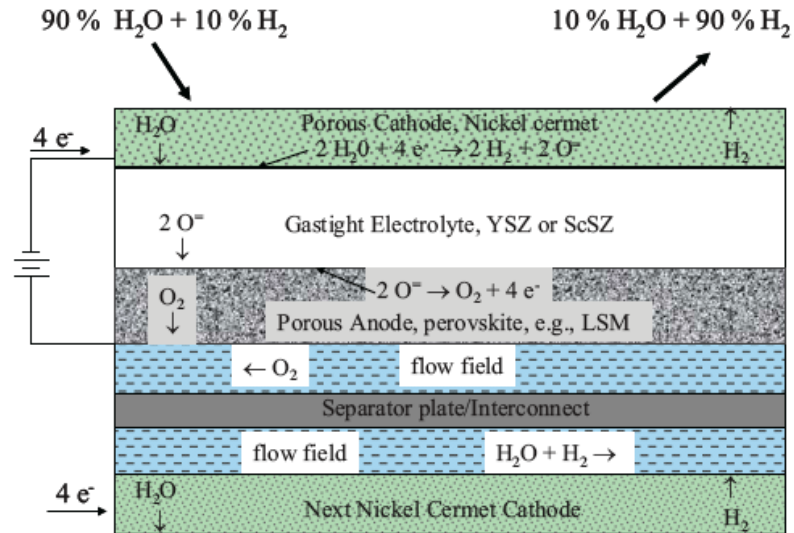
Figure 3-7 - Cross Section of SOEC

The flow fields conduct electrical current through the stack and provide flow passages for the process gas streams. The process gas streams are separated by the separator plate or bipolar plate [16]. HTCE differs from HTSE in that HTCE simultaneously converts CO_2 to CO while electrolyzing steam to H_2 and O_2. If perfected, SOECs have the potential to significantly reduce the power required for syngas consumption (they are discussed in more detail later in the chapter). Detailed information on materials, configurations, and designs of SOEC systems is available in reference [17].

Of the hydrogen production technologies available today, alkaline electrolysis is, considering cost, the best option. However, as demonstrated later, the potential energy savings offered by HTSE and HTCE are too promising to ignore. The three hydrogen production variants this thesis will examine are (1) alkaline electrolysis, (2) HTSE, and (3) HTSE and HTCE. Between HTSE and HTSE with HTCE, the option with HTCE is superior because it eliminates the need to generate hydrogen for the Reverse-Water-Gas-Shift (RWGS) reaction (explained in more detail later). Thus, the baseline hydrogen production process will use alkaline electrolysis while HTSE and HTCE will serve as advanced, future variants.

Regardless of the method used, the syngas feed must be adjusted to the proper $H_2/CO_2/CO$ ratio, depending on the process and catalyst used. A reverse water gas shift reaction (RWGS) reactor may be necessary to adjust the syngas feed prior to entering the Fischer-Tropsch reactor if the feedstock has little or no CO (such as biomass or atmospheric CO_2). As mentioned previously, the advanced HTCE option has the capability to reduce CO_2 to CO, thereby eliminating the need for the RWGS process.

Additionally, membrane and gas separation systems are required to ensure that only the desired reactants in the syngas enter the synfuel plant. Systems such as CTL and GTL require process steps to remove impurities such as NO_x and SO_x, which can poison the chemical reactor catalysts; however, since the tanker ship will utilize atmospheric CO_2, this thesis shall assume that the contaminant concentration is negligible and it shall not be discussed further.

3.1.3.3 Synfuel Production and Refining

The two principle options of producing synfuel from syngas are the Fischer-Tropsch process or a Mobil process. Essentially, Fischer-Tropsch is a brute force process that can process any carbon stream [18]. If using Fischer-Tropsch to produce liquid fuels, the syngas must first be refined to a 2:1 H_2/CO molar ratio before the syngas feed is sent through a catalyst bed reactor. Although the process chemistry is quite complex, one can summarize the entire process using two stoichiometric reactions [19]:

$$(2n + 1)H_2 + nCO \rightarrow C_nH_{2n+2} + nH_2O, paraffins\ production \qquad (3\text{-}5)$$

$$2nH_2 + nCO \rightarrow C_nH_{2n} + nH_2O, Olefins\ production, \Delta H \qquad (3\text{-}6)$$
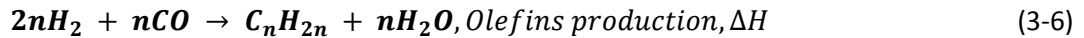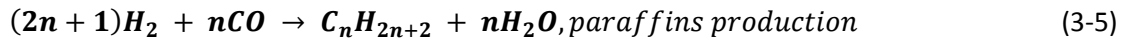
$$= -165 \frac{kJ}{mol}(exothermic)$$

When compared to Mobil processes, the inherent drawback of using Fischer-Tropsch is poor product selectivity. Due to the polymerization nature of Fischer-Tropsch, even specifically designed catalysts usually produce a range of hydrocarbon products. Typical Fischer-Tropsch distributions are usually estimated using the Anderson-Schultz-Flory (ASF) model shown in Figure 3-8 (the ASF model is explained in more detail later in the chapter) [20]:
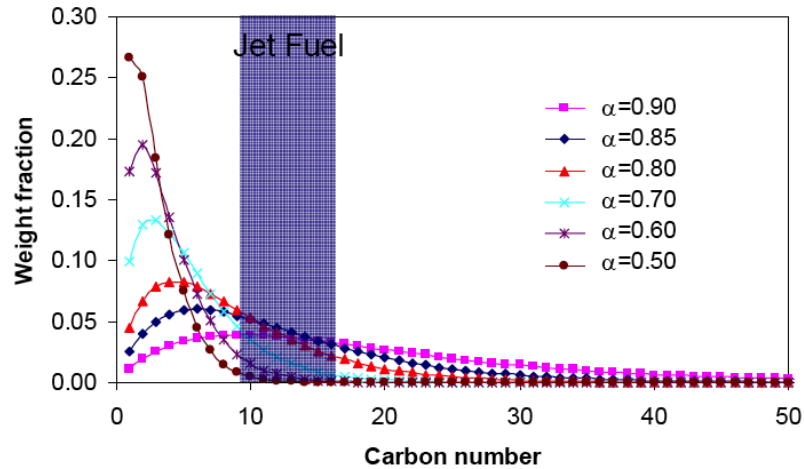
Figure 3-8- Example Fischer-Tropsch Distributions

Fortunately, substantial research and design effort has mitigated this inherent drawback of the FT process.

The other method to produce synfuel, a Mobil process, is multistep. First, the syngas passes through a RWGS reactor to obtain the optimum $CO_2/CO/H_2$ ratio before being converted to methanol. Mobil's patented Methanol-to-Olefins (MTO) process followed by the Mobil Olefins to Gasoline/Diesel (MOGD or ODG^{TM}) process then converts the methanol to the desired hydrocarbon product. Mobile's more commonly known methanol to gasoline (MTG) process does not produce a hydrocarbon distribution in the kerosene (jet fuel) range. Although Mobil processes have the advantage in that they have been tailored to produce a more precise range of hydrocarbons, the chapter will show later that the Mobil process is much more energy intensive. Hence, Fischer-Tropsch is the desired synfuel production process.

The hydrocarbon products produced by the synfuel system are sent through a distillation column. Although the syngas ratio, the reactor's catalyst, and the system's temperature and pressure are usually set to generate a specific type of hydrocarbon (e.g., diesel, gasoline, etc), the process generally produces a range of hydrocarbon products. The desired products are extracted from the product stream, while the remainder is recycled back into the system, refined, or discarded. In any event, the extracted final product will require additives and inspection to ensure conformance with US Navy JP-5 specifications. Sasol has developed a refinery flow scheme specifically designed to optimize jet fuel production, which is explained in following sections in more detail [21, 22, 22].

A key component in the refining process is the autothermal reformer (ATR). An ATR uses high temperature steam and oxygen over a catalyst bed to convert hydrocarbon products back to H_2 and CO. Since most refineries produce a range of hydrocarbon products, such a device has limited commercial utility. However, the tanker ship will solely produce JP-5, effectively limiting the desired hydrocarbon range to C_9-C_{16}. Since the electrolysis process produces more than enough by-product O_2 for ATR, the tanker ship can take advantage of this valuable, energy saving process to recycle undesired hydrocarbon products. Being able to recycle unused hydrocarbons back to raw syngas feed reduces the amount of carbon and hydrogen feed that the syngas production system must generate, resulting in large savings in energy and equipment. In fact, the reason that the Fischer-Tropsch process is much more preferable to the Mobil process for the tanker ship application is that it is possible to take advantage of the ATR's capability of using Fischer-Tropsch.

3.1.4 Baseline Variant, Advanced Option Variant, and Assumptions

The variants shown below essentially acknowledge the following assumptions:

- The synfuel system must use a carbon feedstock that is available without logistics. Without such a constraint, there is little incentive to develop an at-sea synfuel production platform.
- The only product that will be developed by the synfuel plant is jet fuel. All other hydrocarbon products are considered undesirable and shall be recycled back into syngas via ATR. Although the synfuel plant could in theory produce JP-5 and F-76, the analysis performed in chapter 2 shows that they are very similar; hence, they shall be treated as the same fuel for this thesis.
- Several of the refining processes as well as HTSE and HTCE require temperatures well above the capabilities of a light water reactor (LWR). This chapter shall assume that either an advanced high temperature reactor (i.e., the AHTR) or a LWR heat supplemented by recuperation and electric heaters can adequately provide the required heat load.
- Complicated chemical processes such as RWGS, Fischer-Tropsch, and the refining processes (e.g., ATR) shall be approximated by simplified formulas in order to facilitate analysis and limit the scope of this thesis.

As explained above, the baseline option will use CO_2 extracted from the atmosphere as a carbon feedstock and produce H_2 using commercially available alkaline electrolysis. After CO_2 conversion to CO via the RWGS reaction, the H_2/CO syngas mixture will undergo synfuel production via Fischer-Tropsch. After refining, the unused hydrocarbon products are recycled back into the syngas production system via an ATR. The advanced option differs from the baseline option in that it uses the more energy efficient HTSE and HTCE processes. Since HTCE produces CO, the RWGS step is not necessary; however, a H_2 separation membrane is necessary to remove excess steam from the syngas mixture. The two options are illustrated in Figure 3-9 and Figure 3-10:
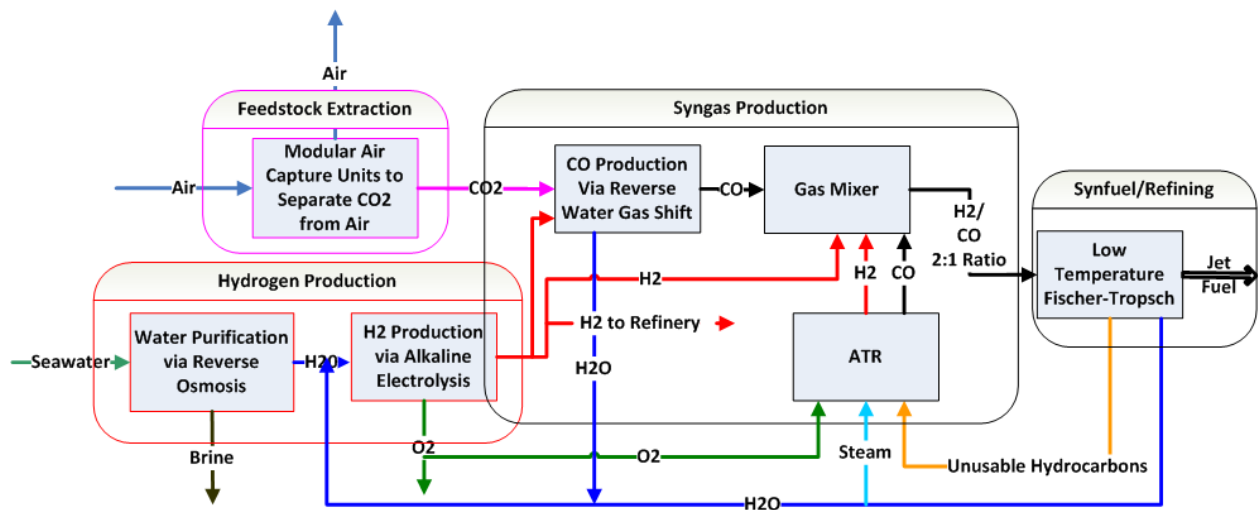
Figure 3-9 - Synfuel Production System: Baseline Option

Figure 3-10 - Synfuel Production System: Advanced Option

51
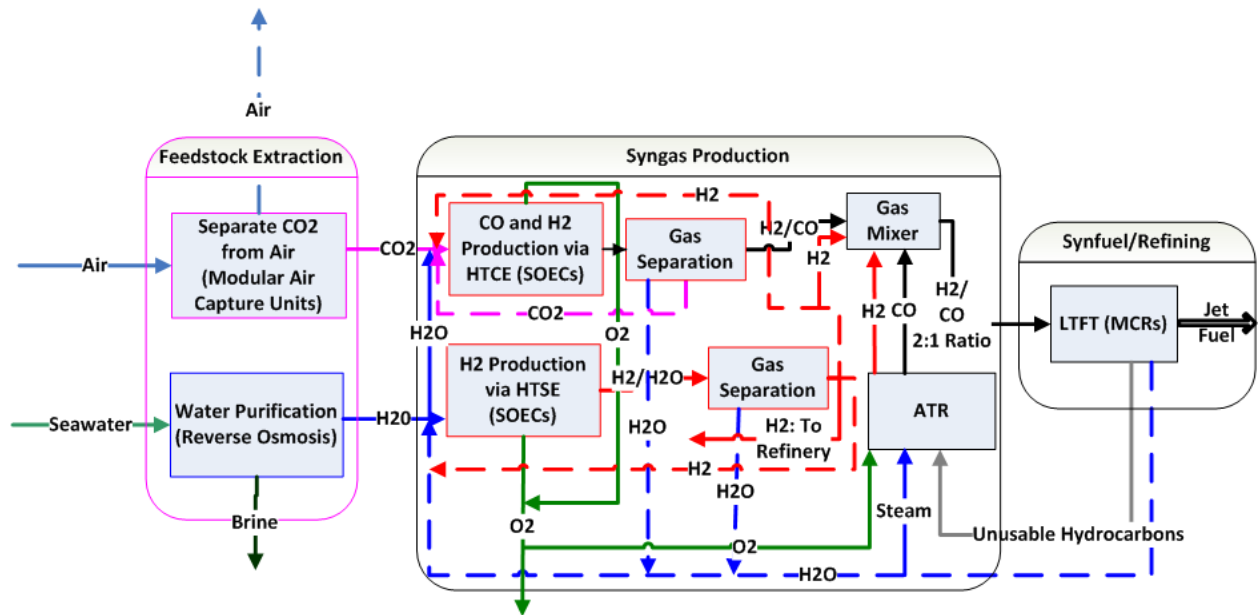
3.2 Syngas Production

3.2.1 Feedstock Selection and Production

3.2.1.1 CO₂ Extraction from the Sea

3.2.1.1.1 CO₂ Concentration in Seawater

Although the global warming debate attracts attention to the magnitude of atmospheric CO_2, the ocean serves as another promising CO_2 feedstock source; a source that conveniently suits an ocean-going synfuel tanker. The total carbon dioxide concentration, $[CO_2]_T$, is represented by equation (3-7) as the combined sum of gaseous, bicarbonate, and carbonate CO_2 concentrations, and it has an approximate value of 100 mg/L [23]:

$$\sum [CO_2]_T = [CO_2(g)] + [HCO_3^-] + [CO_3^{2-}] \tag{3-7}$$

The typical atmospheric CO_2 concentration is 370 ppm (v/v), which corresponds to a value of 0.7 mg/L. Thus, seawater has 140 times the CO_2 concentration as the atmosphere [24].

3.2.1.1.2 Vacuum Degassing/Evaporation

Because of seawater's higher CO_2 concentration, and because of the higher achievable system mass flow rate of water over air due to increased density, LT Terry's thesis proposed extracting CO_2 utilizing one of three variants of vacuum degassing/evaporation systems. Assuming ideal equipment and 100% CO_2 extraction, his modified vacuum degassing technique required 0.543 kWhr/kg CO_2. However, he later remarks that the gaseous CO_2 concentration really comprises a tiny fraction of the total CO_2 content in seawater, and therefore caveats his calculation with the remark that "CO_2 seawater extraction experiments must be conducted to determine the actual CO_2 extraction percentage" [25]. (3-8) below shows the complicated relationship of CO_2 in seawater:

$$CO_{2(g)} + H_2O_{(l)} \leftrightarrow H^+ + HCO_3^- \leftrightarrow 2H^+ + CO_3^{2-} \tag{3-8}$$
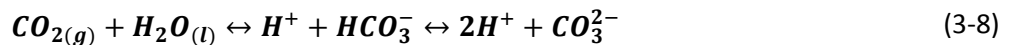
Any reduction in the gas phase partial pressure forces equilibrium of (3-8) to shift left; however, this is a very slow and not well understood process in such a complex system as seawater. Furthermore, the

dissolved CO_2 content is only 2-3% of the total concentration (with carbonate ~ 1% and the remaining fraction bicarbonate). Removing all of the carbonate species in the form of CO_2 gas in one liter of seawater by applying a vacuum of 15 mm Hg to the seawater spread in a thin film requires 2.8 hours [26]. Obviously, such a rate of carbon recovery is far too slow for a synfuel feedstock application. Vacuum degassing the 2-3% of the gaseous CO_2 yields only about 0.1 kg/sec (8.64 MT/day) CO_2 production under the maximum pumping rates available to a very large vessel, which is, again, not nearly adequate enough to satisfy demand [23].

3.2.1.1.3 Strong Base Anion Exchange

Since vacuum degassing is not a feasible approach, the Naval Research Laboratory (NRL) attempted to use strong base anion exchange resins to sequester CO_2 from seawater. Although the NRL was able to accelerate the rate of CO_2 capture, the CO_2 had a limited loading of 0.07 mg/g of resin. Producing 100,000 gal/day (2,300 BBL/day) of JP-5 requires 8,700 MT/min of resin and a 60 second extraction and regeneration time for the resin. The resin, however, is difficult to regenerate in the presence of chlorides without the use of a strong base such as sodium hydroxide. Although a shore based facility could adapt the technique, it is clearly inappropriate for ship board use [27].

3.2.1.1.4 Gas Permeable Membranes

Because the resin approach is impractical, NRL is investigating the use of gas permeable membranes for seawater CO_2 extraction. Willauer et al. successfully demonstrated the feasibility using gas permeable membranes to extract bound CO_2 in the bicarbonate and carbonate ionic forms in addition to the dissolved gas in solution on a laboratory scale [23, 23]. They also realized that bound CO_2 could not be extracted at pressures below 100 psi (0.69 MPa) because the equilibrium of the buffer anions is an opposing force that limits the amount of released CO_2. Willauer et al. performed an additional experiment to determine and establish a relationship between pressure, CO_2 selectivity, and CO_2 flux across the membrane. By increasing pressure to 250 psi (1.7 MPa), they were able to extract 15%, vice the typical 2-3% of dissolved CO_2, in a 5 hour period under experimental conditions [28]. While these results are encouraging, the use of gas permeable membranes to extract CO_2 is still in the experimental stage and requires much more investigation. Furthermore, the system will need to extract an order of magnitude more CO_2 in order be a competitive option with air capture technology.

3.2.1.2   CO$_2$ Extraction from Air

3.2.1.2.1   Overview of Air Capture System

An assessment from Pacific Northwest National Laboratory (PNNL), performed on behalf of the Department of Energy (DOE), asserts that with respect to carbon dioxide capture and storage (CCS) "the core technologies required to address capture, transport, injection, monitoring, management and verification for most large CO2 source types and in most CO2 storage formation types, exist" [29]. While the report strikes the balance between noting that substantial, industrial scale CCS technology already exists as well as encouraging additional CCS research, the technology described in the report is for flue gas capture systems that satisfy the needs of fossil fuel power plants. A tanker ship, however, would need to use an *air capture system* rather than a *flue gas system*. Flue gas concentrations range from 3% to 5% CO$_2$ for natural gas plants and 10-15% for coal plant, which is ~ 100-300 times the typical atmospheric CO$_2$ concentration. Because of the higher CO$_2$ concentration, the sorbents used in a flue gas system do not have to be as strong as in an air capture system, and flue gas systems can be smaller with similar collection capacity. The only real advantage of an air capture system is that it does not have to achieve 100% CO$_2$ capture [30]. By examining the absorption process, one can understand why air capture systems are more expensive than flue gas capture systems. The capture rate of CO$_2$ is:

$$\Delta CO_2 = C_{CO_2} * f * A * v \tag{3-9}$$

$$Where\ \Delta CO_2 = Rate\ of\ CO_2\ captured, \frac{mol}{s}$$

$$C_{CO_2} = Inlet\ Concentration\ of\ CO_2, \frac{mol}{m^3}$$

$$f = fraction\ of\ inlet\ CO_2\ captured$$

$$A = Cross\ sectional\ area\ of\ the\ column, m^2$$

$$v = linear\ velocity\ of\ vapor\ in\ column, \frac{m}{s}$$

Assuming a fixed CO$_2$ rate and a fixed linear gas velocity (common in absorber design) and rearranging equation (3-9) to solve for area:

$$A = \frac{C_1}{(C_{CO_2} * f)} \tag{3-10}$$

$$Where\ C_1 = A\ constant\ term$$

Equation (3-10) shows that the cross sectional area of a column is inversely proportional to the inlet CO_2 concentration and the fraction of CO_2 captured. As Ranjan astutely recognizes in his thesis, <u>for the same rate of CO_2 capture</u>, if air capture percentage is reduced from 90% to 25%, the required cross sectional area goes up by a factor of 3.6. Additionally, such a system would also have to process over 1000 times as much air for the same capture rate as a flue gas system. Thus, an air capture system will have higher capital costs as well as higher energy consumption [31].

The analysis above explains why much of the existing CCS research and technology pertains to flue gas vice air capture systems. Despite the more limited research and design effort, air capture systems exist that could be feasible options for the synfuel tanker. The technology for direct air capture is as follows [31]:
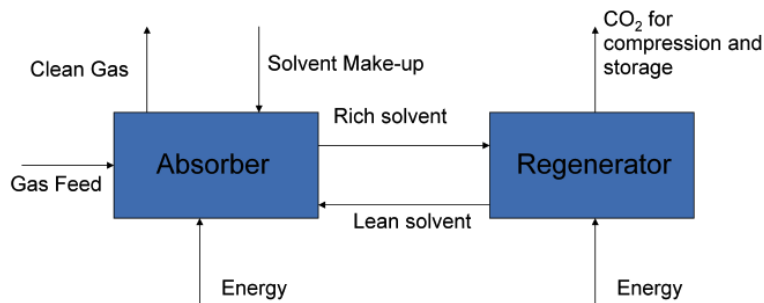
Figure 3-11 - Air Capture System Process Flow

The absorber contains the contacting agent between the sorbent and CO_2; the gas feed is ambient air; and clean gas is air with a lower CO_2 concentration. The rich, CO_2 loaded solvent is sent to the regenerator, where it is stripped of CO_2, and then compressed for downstream use. The lean solvent returns to the absorber for contacting with fresh air.

Reference [31] provides an excellent overview of proposed air capture schemes. The most common air capture system types found in literature use monoethanolamine (MEA) or some other type of amine (e.g., KS-1) as an absorber and sodium hydroxide (NaOH) as the regeneration solvent. However, amine and NaOH are caustic chemicals that are poorly suited for shipboard use on a large scale. Biomass can also absorb CO_2, but such an approach provides obvious complications for shipboard use. Global Research Technologies (GRT), Columbia University, and Los Alamos National Laboratory (LANL) have developed a novel portable, modular air capture system prototype that uses a non-caustic resin compound. The marketing of GRT's prototype stresses that it can produce a modular, cargo shipping container sized unit that it can easily transport, thereby obviating the need to transport CO_2 to

the site of use or disposal site [30]. Although this thesis does not necessarily endorse GRT or its ACCESS™ air capture system, the fact that GRT has developed and demonstrated the use of a modular, commercial scale prototype platform justifies evaluating its air capture system as a baseline technology for use onboard a tanker ship. It is the only air capture technology developed to date that proposes a method to safely extract CO_2 without reliance on hazardous chemicals. If the DOD decided to create a nuclear powered synfuel tanker ship program, the acquisition process would provide ample opportunity for other potential vendors to develop and showcase their designs.

The air capture system developed by K.S. Lackner and GRT utilizes an ion exchange resin composed of a polystyrene backbone with quarternary amine ligands attached to the polymer. The resin acts like a strong base, analogous to NH_4^+, where each hydrogen has been replaced by an organic carbon chain attached to the polymer matrix. The solvent has a very low binding energy but the uptake rate is reported to be greater than 1M NaOH solution. The sorbent can exist in three states, (1) a bi-carbonate state, (2) a carbonate state and (3) a hydroxide state. The fundamental reactions are as follows:

$$OH^- + CO_2 \rightarrow HCO_3^- \ (direct\ bicarbonate\ formation\ on\ resin) \qquad (3\text{-}11)$$

$$2OH^- + CO_2 \rightarrow CO_3^{2-} + H_2O \ (formation\ of\ carbonate) \qquad (3\text{-}12)$$

$$CO_3^{2-} + CO_2 + H_2O \rightarrow 2HCO_3^- \ (formation\ of\ bicarbonate\ from\ carbonate) \qquad (3\text{-}13)$$
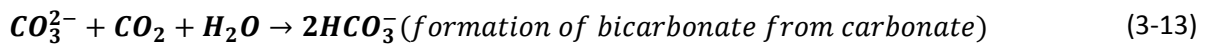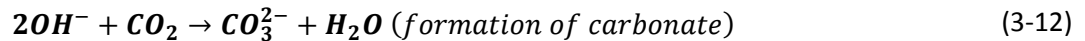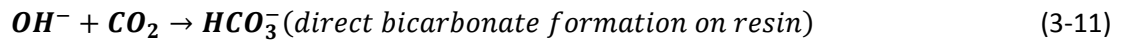
Although fresh resin is in a hydroxide state, the reactions change between the carbonate and bicarbonate to absorb CO_2 and the sorbent is never allowed to go back to the original hydroxide state. The device uses water vapor at 45^oC to regenerate the resin. The notable advantages of this system are that (1) it completely eliminates the use of the extremely caustic NaOH resin regeneration solvent; and (2) the water regeneration system actually boosts the CO_2 partial pressure, effectively creating a "CO_2 pump" [30]. Figure 3-12 and Figure 3-13 provide an illustration of the GRT air capture system [32]:
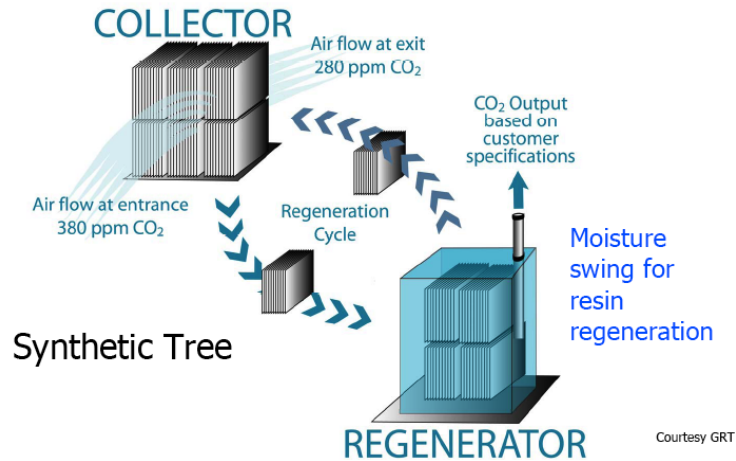
Figure 3-12 - GRT Air Capture System Overview
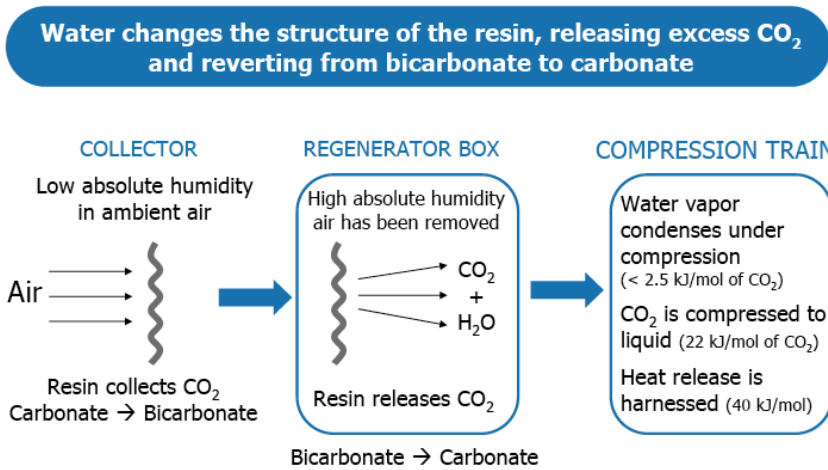
Figure 3-13 - GRT Air Capture System Regeneration Process

3.2.1.2.2 Mass and Energy Requirements of Air Capture System

The air capture system must have the capacity to supply an adequate amount of CO_2 feedstock to the 6,400 BBL/Day synfuel production system while meeting size and energy constraints appropriate for an ocean going vessel. Accurately modeling the CO_2 production rate from the GTL air capture system requires fluid dynamic simulations that incorporate the physical properties and geometric arrangement of the system's resin filters size. However, the modeling information is proprietary and developing such a simulation is beyond the scope of this thesis (the goal is only to obtain baseline operating characteristics).

Conveniently, Lackner has provided enough information to provide baseline production and energy consumption estimates for a proposed air capture system. Equation (3-9) above provides a general overview of the system's reference parameters: CO_2 concentration is 400 ppm, surface uptake rates range from 10-100 μ mol m^{-2} s^{-1}, and 2,500-25,000 m^2 required surface area assuming a (metric) ton per day device producing 0.263 mol s^{-1} CO_2. The specific uptake rate is proportional to CO_2 concentration, and the proportionality constant is dependent on the physical properties of the resin. The total amount of required sorbent material depends on the amount of surface created per unit mass as well as the material's absorption effectiveness. An example system proposed by Lackner has a specific surface area of 4.0 m^2/kg and an uptake rate of 25.0 μ mol m^{-2} s^{-1}; such a collector can absorb 100 μ mol m^{-2} s^{-1} and requires 2,500 kg of resin to produce 0.25 mol/s (~ 1 MT/day). Assuming 10% volume occupancy and a resin density of 1.0 g/cm^3, this requires 25.0 m^3 of filter boxes. GRT's 1 MT/day prototype design consists of a modular set of 60 filters, each 2.5 m tall, 1.0 m wide, and 30-40 cm thick with a design flow rate of ~ 1.0 m/sec. Since the recovery and partial drying time is equally long as the collection time (2,500 sec), half the units (30) are in collection mode while the other half are in recovery mode. The entire filter system set can "easily" fit inside a standard shipping container (12m x 2.5m x 3m) [30]. Assuming that the system fits in the standard shipping container, roughly 90 m^3 of space per MT CO_2 produced is required. Since the system Lackner proposes is a baseline model, perhaps the air capture system described above can be improved and optimized to produce an equivalent amount of CO_2 within an even smaller volume. As chapter 5 shows, reducing the operational footprint of these air capture units is necessary to make them a viable option for an at-sea tanker.

The three major energy consumption components of the air capture system are (1) mechanical operation of the air collector (this includes inefficiencies of the system's pumps and compressors), (2) the removal of air from the regeneration chamber, and (3) CO_2 compression for downstream use. Evacuating a 1.0 m^3 volume, with 100 kg of resin and roughly 25.0 mol of CO_2, requires about 100 kJ (this assumes 10% volume fill and CO_2 loading of 0.25 mol/kg). Thus, CO_2 evacuation requires 4.0 kJ/mol CO_2. Lackner's system compresses the extracted CO_2 from 5.0 kPa to 6.7 MPa; however, the Fischer-Tropsch reactor typically operates at ~ 3.0 MPa [19], and the reverse water gas-shift (RWGS) reactor is at ~ 1.0 MPa. Furthermore, Lackner assumes compression at 300 K, even though the system actually operates well above room temperature at 45°C (318 K). Since the 19 kJ/mol compression energy value Lackner provides is not suitable, equation (3-14) below is necessary to determine the system's compression energy requirement:

$$W_{CP} = c_p T_1 \left[(r_p)^{\frac{\gamma-1}{\gamma}} - 1 \right]$$

<div align="right">(3-14)</div>

$Where\ W_{CP} = ideal\ specific\ work\ of\ compression$

$C_p = Specific\ heat, constant\ pressure$

$T_1 = Initial\ temperature$

$r_p = compression\ ratio\ \left(= \dfrac{P_2}{P_1} \right)$

$\gamma = \dfrac{C_p}{C_v}, where\ C_v = specific\ heat, constant\ volume$

The given system parameters are T_1=45°C (318 K), P_1=116 kPa, P_2=3.0 MPa, r_p=29.6, c_p=0.865 kJ/kg-K, c_v=0.676 kJ/kg-k, γ=1.28. Thus, $w_{cp,i}$=302 kJ/kg, or 13.3 kJ/mol CO_2. Assuming the compressor is 90% efficient, $w_{cp,r}$=14.8 kJ/mol CO_2. Lackner notes that during the initial compression stage, water is compressed against a constant partial pressure, a condensation that requires ~ 2.5 kJ/mol CO_2. To account for the mechanical energy required to for all of the system's ancillary components and inefficiencies, Lackner estimates the system's energy consumption as 50 kJ/mol CO_2 (1.1 MJ/kg CO_2) [30]. However, the calculated value of the device, assuming a real compressor, from evacuation, compression, and condensation is 21.3 kJ/mol, a value that is 57% lower. Since the energy requirements of the remaining ancillary components of the system are not detailed anywhere in open literature, Lackner's 50 kJ/mol energy consumption figure is difficult to verify. Reference [31] doubts the figure's credibility because of its higher second law thermodynamic efficiency compared to other air capture systems. In any event, subsequent sections in this chapter show that the energy requirements of the air capture system are relatively insignificant compared to electrolysis. Future analysis and detailed design of the air capture system will be able to clearly articulate the true energy and volume requirements. This thesis, however, shall assume a convenient 30 kJ/mol CO_2 compression energy requirement because of the lower pressure required of the CO_2 product.

In addition to its relatively large size, another shortcoming of the GRT ACCESS™ air capture system is that its process has been engineered for a desert climate. Extremely cold temperatures and a tropical climate, with a high relative humidity, both limit the operation of the device. The reaction kinetics are too slow for the current design if the temperature drops below -5°C. Hot and humid temperatures limit the load capacity of the resin. However, design changes and engineering improvements should be able to overcome these limitations so that the system can operate to full or nearly full capacity in all but the most extreme operational environments [30].

3.2.1.3 Feedstock Selection Summary

After performing an assessment of various CO_2 feedstock sources (including section 3.1.3.1 above), atmospheric CO_2 extraction using an air capture system appears the most viable option. Traditional synfuel feedstocks (i.e., coal and natural gas) have potential for shore based facilities, but are of limited utility for a naval platform. In addition to not being carbon neutral, their use would complicate military logistics even more, while not addressing the problem of supplying fuel to deployed forces. Similar problems exist with using MSW and biomass, thus leaving CO_2 extraction from the air or sea as the only viable alternatives. Seawater is an attractive feedstock source since it contains 140 times the CO_2 concentration as the equivalent air volume. Unfortunately, the majority of seawater CO_2 is in a bicarbonate form, which makes using vacuum degassing/evaporation impractical. Using a strong anion based resin is impractical because of (1) the extremely large amounts of resin required to accommodate the low CO_2 capacity and (2) the need to use large amounts of a strong base chemical such as sodium hydroxide aboard ship. Laboratory scale results of CO_2 extraction using gas permeable membranes are trending in the right direction; however, much more progress is required before they can be considered as an option. This leaves atmospheric air capture as the most promising approach. Modular and transportable 1 MT/day CO_2 air capture prototypes exist, indicating that such technology could be optimized for use on a naval vessel with research and design investment.

3.2.2 Hydrogen Production

3.2.2.1 Seawater Desalination

Hydrogen is the other important syngas component. Conveniently, water is an abundant, ubiquitous resource for an ocean going vessel. Raw seawater must undergo desalination prior to use. Fortunately, processes and technologies to desalinate water on marine platforms are quite mature. Two well known methods are evaporation and reverse osmosis (RO), with RO clearly being the superior, less energy intensive choice [33]. One company, Village Marine, specializes in outfitting US Navy and US Coast Guard vessels with RO units designed to military specifications (MILSPEC) [34].

An important caveat is that the installed RO units must also supply fresh water for numerous other onboard systems (e.g., potable water for drinking and cleaning, propulsion plant consumption, chill water for air conditioning, etc.); however the synfuel plant will probably dominate the RO system's demand. Despite the synfuel plant's relatively large consumption, Village Marine could outfit the tanker

with its MILSPEC Generation 2 Expeditionary Unit Water Purification System (EUWP Gen 2) units. Each EUWP Gen 2 unit can produce over 250,000 gpd (947,500 lpd) of deionized water and over 320,000 gpd (1.2 million lpd) of potable water. Three EUWP Gen 2 units could probably accommodate all tanker loads and four units would be more than adequate; additionally, having four units facilitates 100% capacity in the event of failure of one unit. The EUWP Gen 2 RO units require only a modest amount of power (325 kW each at full load), and four units operating at full power would only consume 1.30 MWe, and occupy 342 m^3 [35].

3.2.2.2 Alkaline Electrolyzer

As mentioned in section 3.1.3.2, the alkaline electrolyzer is the most affordable and commercially mature option for hydrogen production. To reiterate the fundamentals of alkaline electrolysis, the electrolyzers typically use a potassium hydroxide solution (KOH) to create the cathode-anode potential for the following half-reactions, as previously shown in (3-3) and (3-4) above. The ideal theoretical energy required to electrolyze water, $\Delta G_{electrolysis}$, is 237.3 kJ/mol H_2. Knowing that ΔG is referenced to STP, and that there are 0.0224 m^3/mol gas at STP, results in 2.94 kWhr/m^3 [25]. Only a large number of the largest of the commercially available electrolyzers (Statoil's Norsk Hydrotech 5040), shown in Figure 3-14, could generate the required H_2 for 6,400 BBL/day JP-5:

Figure 3-14 - Commercially Available Alkaline Electrolyzer

According to vendor data, the most capable Norsk 5040 electrolyzer has 230 cells, a maximum H_2 production capacity of 2.11 Nm^3 H_2/hr-cell, and a power consumption of 4.3 kWhr/Nm^3 H_2 [36]. Compared to the theoretical energy, ΔG, this results in a 68.4% electrolyzer efficiency, which is typical

for a high current density alkaline electrolyzer [12]. The maximum H_2 production of a single unit is 485 Nm^3 H_2/hr at about 2.1 MW_e.

3.2.2.3 *Solid Oxide Electrolytic Cells (SOECs)*

Recalling section 3.1.3.2, a SOEC is a solid-state electrochemical device consisting of an oxygen-ion-conducting electrolyte (e.g., yttria- or scandia-stabilized zirconia) with porous electrically conducting electrodes deposited on either side of the electrolyte. The flow fields conduct electrical current through the stack and provide flow passages for the process gas streams. The process gas streams are separated by the separator plate or bipolar plate. Figure 3-7, shown again here for convenience, provides a graphic depiction of the process:
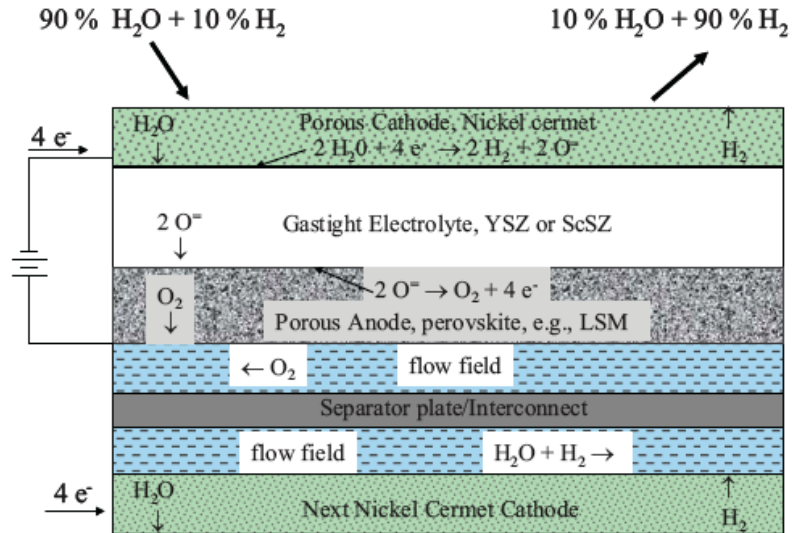
Figure 3-15 demonstrates the motivation to attempt HTSE vice traditional electrolysis. It shows that the Gibbs free energy change, ΔG_R, for the system decreases as temperature increases, while the product of temperature and the entropy change, $T\Delta S_R$, increases. Thus, for a reversible operation, the amount of electrical work required decreases with temperature, and a larger fraction of the total energy required for electrolysis, ΔH_R, can be supplied in the form of heat, represented by $T\Delta S_R$. Since heat-engine-based electrical work is limited to a production thermal efficiency of 50% or less, decreasing the work requirement results in higher overall thermal-to-hydrogen production efficiencies [15]:
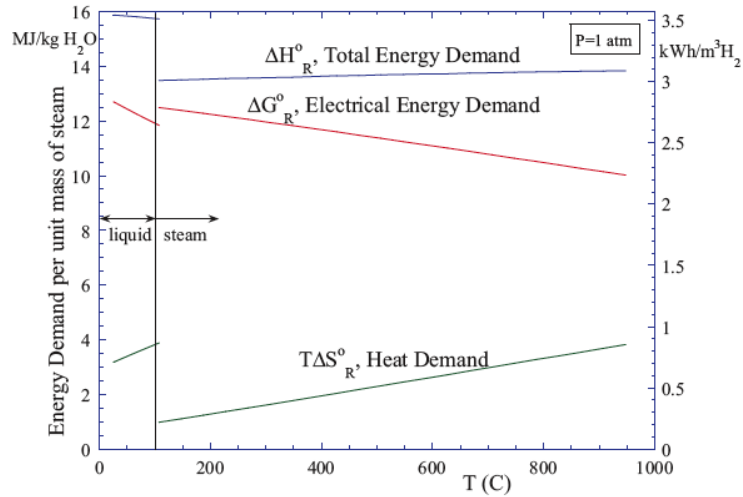
Figure 3-15 - Ideal Energy Requirements as a Function of Temperature

HTCE is a process closely related to HTSE. As with HTSE, it uses the same SOEC design described above. The attractive feature of HTCE is that it simultaneously reduces H_2O and CO_2 to produce syngas, as equation (3-15) shows [37]:

$$H_2O + CO_2 + heat, electricity \rightarrow H_2 + CO + O_2 \qquad (3\text{-}15)$$
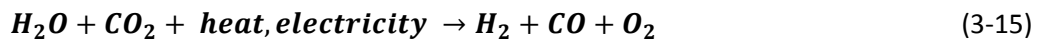
The process diagram below succinctly summarizes the differences between the two processes. A noticeable HTCE advantage is that it obviates the need for a RWGS reactor:
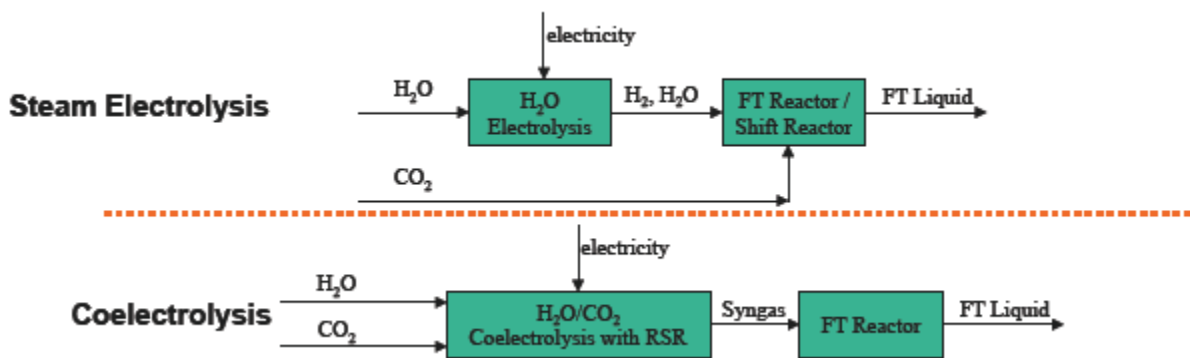
Figure 3-16 - Comparison of HTSE and HTCE

Because of the simultaneous occurrence of multiple, complicated reactions, HTCE theory is not completely understood. The prevailing theory is that H_2 production via HTSE and CO production via the RWGS reaction occur simultaneously. Empirical evidence from INL argues against CO_2 electrolysis, as Figure 3-17 shows [37]:
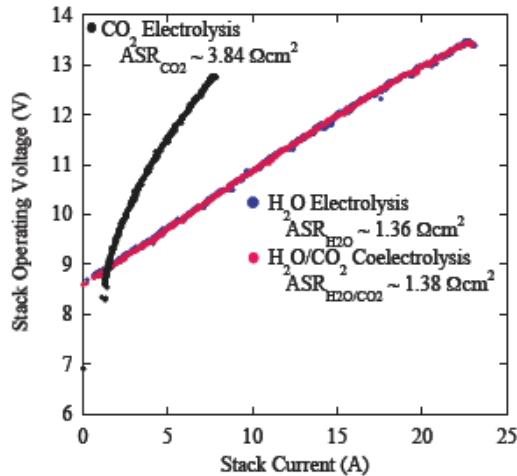
Figure 3-17 - Comparison of CO2 Electrolysis with HTSE and HTCE

3.2.2.3.1 Model of HTSE Performance

Since commercial HTSE electrolyzers do not exist, convenient vendor data similar to that provided for alkaline electrolysis is not available. INL is coordinating a series of electrolysis cell and stack testing activities, at increasing scales, along with a continuation of supporting research activities in the areas of materials development, single-cell testing, detailed computational fluid dynamics (CFD) analysis and system modeling using HYSYS, FLUENT, and UniSim [38]. A survey of INL's HTSE literature conveniently provides all the key information necessary to model the process, such as current density, molar flow rate, H_2 recycle fraction, cell area, and cell resistance values. To model the theoretical power requirements and hydrogen production rate of HTSE cells, thermodynamic mass and energy conservation equations must be applied to an electrolysis cell control volume and solved iteratively using a convergence algorithm. References [15, 39, 40] provide the cell parameters and thermodynamic equations used to develop and validate an in-house 1D HTSE model using MATLAB [41]. Appendix C contains a detailed description of the model used to calculate the hydrogen generation rate and power requirements of a HTSE cell, as well as table for the nomenclature used in the following discussion.

To determine the HTSE cell's hydrogen production rate and power consumption, the HTSE model described in Appendix C assumes a cell area size (A) of 225 cm^2, an area specific resistance (ASR) of 0.25 Ω-cm^2, and a current density (i) of 1 A/cm^2. Although these cell design and performance attributes are optimistic, they should be achievable in the near term [40]. The combined molar flow rate, $(\dot{N})_{in}$, of 0.0013 mol/s was obtained by first linearly scaling the molar flow rates used in INL's 64 cm^2 10 cell stack test described in reference [42] as an initial guess, and then adjusted iteratively until a

64

desirable conversion rate was obtained. For the case where the output H_2 must enter a RWGS reactor to support CO_2 to CO conversion, the HTSE model uses the RWGS reactor pressure (P) of 1.0 MPa. Otherwise, the pressure is the Fischer-Tropsch reaction pressure of 3.0 MPa. The steam side electrolyzer inlet requires at least 5% recycled H_2 ($y_{H2,0}$) (molar or volume basis) to maintain reducing conditions at the electrolysis stack cathode, which prevents oxidation of the nickel cermet material [39]. The inlet temperature (T_{in}) of the steam/H_2 mixture is 1,073 K (800 $^{\circ}$C), which accommodates projected capabilities of an advanced high temperature reactor (AHTR) heat source while still receiving an appreciable advantage from performing electrolysis at high temperature [43]. An outlet temperature (T_{out}) must be assumed, and then the model converges on an iteratively calculated value. Table 3-2 and Table 3-3 provide a summary of the HTSE simulation results, including cell voltage (v), power (w), and outlet flow rates and molar fractions for simulations performed at 1.0 MPa and 3.0 MPa respectively:

Input Parameters	
T_{in} (K)	1073
T_{out} (guess) (K)	1073
A (cm^2)	225
ASR (Ω-cm^2)	0.25
i (A/cm^2)	1.0
P (MPa)	1.0
$(\dot{N})_{in}$ (mol/s)	0.0013
$y_{H2O,0}$ (molar fraction)	0.95
$y_{H2,0}$	0.50
$(\dot{N})_{in, sweep}$ (mol/s)	0.0
$Y_{O2,0}$	0.0
Output Parameters	
T_{out} (converged) (K)	1095.5
V (volts)	1.2983
W (watts)	292.1236
$(\dot{N})_{out}$ (mol/s)	0.0013
$y_{H2O,1}$ (molar fraction)	0.053092
$y_{H2,1}$	0.94691
$(\dot{N})_{out, sweep}$ (mol/s)	0.00058299
$Y_{O2,1}$	1.0

Table 3-2 - HTSE Simulation Results, 1.0 MPa

Input Parameters	
T_{in} (K)	1073
T_{out} (guess) (K)	1073
A (cm^2)	225
ASR (Ω-cm^2)	0.25
i (A/cm^2)	1.0
P (MPa)	1.0
$(\dot{N})_{in}$ (mol/s)	0.0013
$y_{H2O,0}$ (molar fraction)	0.95
$y_{H2,0}$	0.50
$(\dot{N})_{in, sweep}$ (mol/s)	0.0
$Y_{O2,0}$	0.0
Output Parameters	
T_{out} (converged) (K)	1105.5
V (volts)	1.3011
W (watts)	292.7486
$(\dot{N})_{out}$ (mol/s)	0.0013
$y_{H2O,1}$ (molar fraction)	0.053092
$y_{H2,1}$	0.94691
$(\dot{N})_{out, sweep}$ (mol/s)	0.00058299
$Y_{O2,1}$	1.0

Table 3-3 - HTSE Simulation Results, 3.0 MPa

3.2.2.3.2 Model of HTCE Performance

Because HTCE and HTSE both utilize the same SOECs, nearly all of the physical characteristics assumed for the HTSE model in section 3.2.2.3.1 (i, ASR, A, inlet/sweep gas flow rate, recycle fractions, etc) apply to HTCE as well. The HTCE model also accounts for (1) different process stream gases, and (2) a chemical equilibrium model to describe co-electrolysis. Since a RWGS reactor is not necessary when using HTCE, the simulation results below are only for 3.0 MPa. As with the HTSE model, an algorithm was developed using MATLAB to calculate the various co-electrolysis parameters using references [15, 42, 44, 45] and validated against INL's predicted and empirically derived results [46]. Appendix C describes the HTCE model in detail, and the simulation results are summarized in Table 3-4:

Input Parameters	
T_{in} (K)	1073
T_{out} (guess) (K)	1073
A (cm^2)	225
ASR (Ω-cm^2)	0.25
i (A/cm^2)	1
P (MPa)	3.0
$(\dot{N})_{in}$ (mol/s)	0.0013
$(\dot{N})_{in, sweep}$ (mol/s)	0.0
$y_{H2O,0}$ (molar fraction)	0.60
$y_{H2,0}$	0.07
$Y_{CO2,0}$	0.30
$Y_{CO,0}{}^6$	0.03
$Y_{O2,0}$	0.0
Output Parameters	
$T_{out\_}$converged (K)	1084.0
V (volts)	1.3614
W (watts)	306.3152
T_{out} (after cool down) (K)[7]	973
$(\dot{N})_{out}$ (mol/s)	0.0013
$y_{H2O,1}$ (molar fraction)	0.0017396
$y_{H2,1}$	0.66826
$Y_{CO2,1}$	0.0013525
$Y_{CO,1}$	0.32865
$(\dot{N})_{out, sweep}$ (mol/s)	0.00058299
$Y_{O2,1}$	0.47273

Table 3-4 - HTCE Simulation Results

Because of the similarity between the HTSE and HTCE input parameters, the mass flow rate and molar fractions of the oxygen sweep gas are identical to the HTSE simulation. The low H_2O and CO_2 outlet fractions and the precise H_2/CO molar ratio are a result of iteratively adjusting the simulation input values. Since the CO feed requirements are met from HTCE before enough H_2 is produced, it is necessary (based on the simulation results) to supplement HTCE with HTSE to prevent generation of excess CO.

---

[6] For the model to converge, a small inlet fraction of CO must be assumed to prevent a singular matrix.
[7] Cool down temperature is empirically derived temperature at which RWGS freezes. All output molar fractions are from cool down temperature value.

3.2.2.3.3 SOEC Technological Challenges

SOECs must operate in extreme temperature and electrochemical conditions, which creates a need for special materials and challenges the longevity of SOEC components. In order to be commercially viable, SOECs need a 40,000-50,000 hour lifetime, which means that the cell components must have a very low degradation rate. Regretfully, SOECs have yet to attain that level of performance. Although the actual metrics for SOEC degradation are more complex, a good indicator of SOEC degradation is an increase in ASR.[8] As Figure 3-18 shows, a recent 25 cell SOEC stack test at INL demonstrated an ASR increase of 40% in only 400 hours [47]:
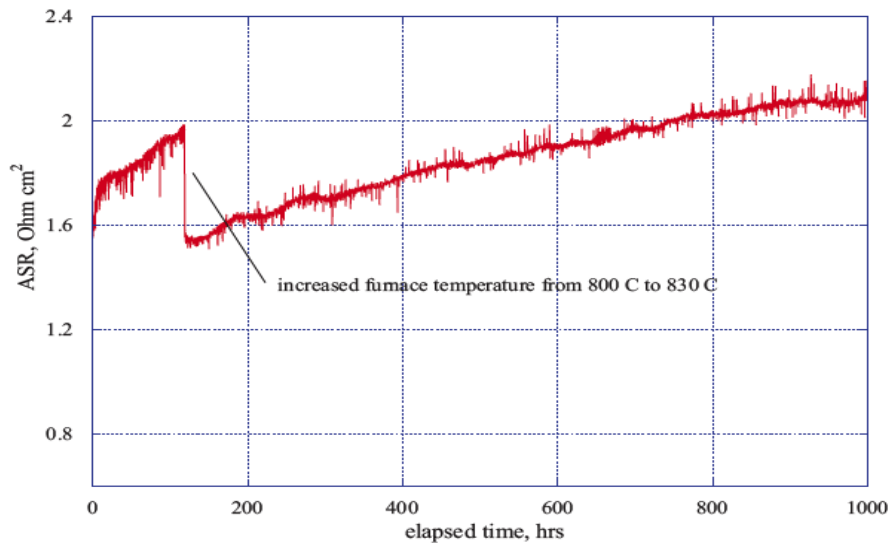
Figure 3-18 - SOEC Degradation

Although INL has published detailed technical reports discussing SOEC degradation in references [47] and [15], the precise mechanism(s) of SOEC degradation is still not completely understood [15]. SOEC degradation is an area of intense, ongoing investigation, and it must be overcome if the capabilities promised by HTSE and HTCE are ever to be realized. Considering the INL's process in SOEC research in the previous decade, one could reasonably believe that INL will be able to resolve the cell degradation issues in the near term. Another issue requiring resolution is the ability to mitigate corrosion resulting from high temperature steam and CO_2. Corrosion inhibitors are generally used to minimize material degradation, but investigation has not yet been performed to evaluate any suitable inhibitor candidates. Inhibitors that prevent piping degradation could adversely impact SOEC

---

[8] As ASR goes up, the reactant products do not transport as easily across the cell, thereby inhibiting the required chemical reactions.

performance. Presently, there is no resolution on this issue, but it must be satisfactorily addressed by future research.

3.2.3   Syngas Refinement

3.2.3.1   Overview

Although producing H_2 and CO_2 are essential processes in the syngas generation scheme, the combination of these gases from the electrolyzer and air capture units does not produce the necessary gas mixture needed for liquid fuels production in a chemical reactor. When considering the Fischer-Tropsch process, CO, not CO_2, is the desired gas; and for a methanol conversion process, the syngas production system must convert some of the CO_2 into CO, as both reactants are necessary. Unless the syngas production system uses HTCE, a Reverse Water Gas Shift (RWGS) system is necessary to convert CO_2 into CO. If using the HTSE process, a small yet not insignificant fraction of steam remains in the H_2/H_2O product. Excessive H_2O can interfere with the liquid fuel and refinery processes as well as the RWGS reaction, so the syngas production system requires a means to purify the hydrogen stream.

3.2.3.2   Reverse Water Gas Shift (RWGS)

A successfully engineered RWGS process is absolutely critical in order to produce synfuel from syngas with a high CO_2 concentration. The process uses H_2 to convert CO_2 to CO and H_2O [48]:

$$CO_2 + H_2 \Leftrightarrow CO + H_2O, \Delta H = +38.9 \frac{kJ}{mol} \ (endothermic) \tag{3-16}$$
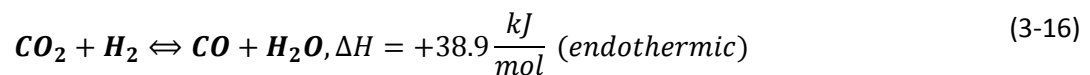
Upon inspection, the RWGS reaction reveals two significant shortcomings: (1) the syngas production system must consume additional power in order to generate extra H_2 for CO_2 conversion to CO; and (2) since the RWGS reaction is endothermic, the process consumes even more energy. Making matters worse is that the temperature dependent equilibrium constant (K_p) exhibits very poor reaction kinetics below 700 K [48-50], which necessitates the use of electric heating power or product gas recuperation to attain reaction conditions if using a pressurized water reactor (PWR) heat source. Another inconvenience is that there is a dearth of available literature regarding RWGS experimental results and process optimization – the RWGS process is not a mature, commercially available technology. A specific RWGS process step is not required if generating syngas via the traditional GTL or CTL processes (refer to equations (3-1) and (3-2) above). The reverse of the RWGS, known as the Water Gas Shift (WGS)

reaction, is a more thoroughly researched process due to its application to hydrogen fuel cell technology; however, the goal of such research is typically to ***minimize*** CO production, as CO deactivates fuel cell electrodes [51]. Successful development of a robust RWGS process is absolutely critical if the goal is to generate synfuel using a CO_2 based feedstock (unless the syngas system uses HTCE).

Another challenge with the RWGS reaction is driving the reaction to completion. Although the RWGS reaction is more responsive at higher temperatures, a significant amount of undesirable methane and coking reactions occur if the reaction temperature exceeds 800 K [48]. One method to obviate this challenge is to recycle a fraction of the RWGS products, as in Joo's CAMERE process, to produce methanol from a CO_2/CO mixture [52]. However, such a method is not practical if using a Fischer-Tropsch process because efficiently separating the desired gases is very expensive. Doty recommends a promising, multi-stage RWGS process in reference [50] that separates out the H_2O between stages. Although Doty suggests three options, the lower temperature option (740 K, 1.0 MPa) using a five-stage, Cu-Alumina catalyst reactor bed is obviously the most appropriate, as it requires the least amount of heat input and is least likely to develop unwanted methane and coke products. In order to effectively remove the water by-product between stages, Doty proposes using a compact, gas-to-gas, compound recuperator with liquid intermediary (CRLI), which reference [53] explains in detail. Reference [50] claims that such a RWGS process has a CO_2-CO conversion efficiency of greater than 95%; however, not enough research and independent experiments have been performed to conclusively corroborate this claim. More investigation is necessary to determine performance characteristics. Since only a very small amount of residual CO_2 remains following the RWGS process, analyses in this thesis assume 100% CO_2 to CO conversion. This assumption can be justified by the fact that the RWGS reaction consumes a relatively small amount of energy compared to other components in the liquid fuel production system.

3.2.3.3   Gas Separation

As shown in Table 3-2, Table 3-3, and Table 3-4, the resultant product gases do not entirely compose the desired syngas composition. In the case of HTSE, roughly 5% of the outlet molar fraction is steam; for HTCE, the simulation shows that over 99% of the product gases are H_2 and CO. Something to consider, however, is that the simulation results represent a theoretically ideal scenario. HTSE and HTCE SOEC stack demonstrations have not produced results as postulated by the simulations performed for this thesis. Higher outlet molar fractions of CO_2 and steam are likely for HTCE. Furthermore, more detailed investigation could conclude that a N_2 or other inert sweep gas is necessary to drive the product

70

gases from the SOEC. At the very least, the syngas production system needs the capability to efficiently separate H_2 from steam if using HTSE. If HTCE produces greater amounts of CO_2 and steam, or if the use of an inert sweep gas is necessary, then the syngas production system also requires the capability to separate CO as well. Although this thesis assumes 100% CO_2 to CO conversion for the RWGS reaction, a CO separation mechanism might also be necessary to ensure no CO_2 or CH_2 exists in the RWGS product stream.

3.2.3.3.1 CO Separation

References [54] and [55] provide excellent system level descriptions of feasible, technologically mature CO separation technologies. The primary processes available today are cryogenic, carbon monoxide sorbent (COSORB), and pressure swing adsorption (PSA), but researchers are also investigating the use of separation membranes [55]. The cryogenic process, which is the most established and mature process, involves liquification of the gas stream, followed by phase separation and distillation of the unwanted components; since this process incurs a massive energy penalty, it is suitable only for very large facilities. Furthermore, cryogenic separation cannot effectively separate N_2 from the product stream because the boiling point between N_2 and CO varies by only 6 $^{\circ}$C. The COSORB process uses a liquid activating agent ($CuAlCl_4$) within an aromatic hydrocarbon solvent to electrochemically separate CO from a gas stream, including streams with low CO or high N_2 content. The COSORB process is less capitally intensive than the cryogenic process, but it is seldom used due to frequent degradation of the COSORB absorbent. PSA provides an option to COSORB if the compression cost for a PSA plant is less than the cost of regenerating and replacing the COSORB absorbent. PSA utilizes an adsorbent material (e.g., al alumina carrier impregnated with $CuCl_2$) to adsorb a high pressure target gas near ambient temperature. The process then "swings" to low pressure (~ ambient) to desorb the adsorbent material, thereby producing a high purity gas stream [55]. Table 3-5 summarizes the key features of each system [54]:

Process	PSA	COSROB	Cryogenic
Principle	Adsorption	Absorption	Distillation
Applicable Scale	Small to Medium	Medium	Large
Product Purity	99%	99%	98%
Product Yield	90%	99%	90%
Operation	Simple	Less simple	Less simple
Disadvantage	Requires cooling gas to ambient temperature. High compression cost.	Requires absorbent regeneration/replacement.	Cannot separate N_2. Extremely energy intensive.

Table 3-5 - Summary of CO Separation Processes

Considering the tradeoffs associated with each option, PSA seems most appropriate choice given the size and operational constraints of a shipboard synfuel production system.

The above discussion of CO separation technologies serves to inform the reader that feasible and mature CO separation technologies exist in industry today, and as well to provide a system level perspective of each available option. Because the HTCE simulation results in Table 3-4 have such a negligible fraction of non-H_2/CO gas, and also because the RWGS reaction has such a high CO_2 to CO conversion rate, this thesis will neglect accounting for CO separation processes by PSA without really affecting the overall mass and power requirements of the synfuel production system.

3.2.3.3.2 Hydrogen Separation

Because of intense research interest in developing a hydrogen economy, a plethora of hydrogen production and purification literature is available. Reference [56] provides an excellent description of available and emerging hydrogen purification technologies, which are summarized as follows:

- Adsorption of gas species other than hydrogen, which produces pure hydrogen as a product.
- Absorption (physical or chemical) of CO2, which produces pure carbon dioxide as a product.
- Polymeric membranes, which offer bulk separation of hydrogen.
- Cryogenic separation, which can provide multiple pure products and is especially used for separation of pure carbon monoxide.

The principles of the above process remain consistent with the adsorption, absorption, and cryogenic processes described above for CO separation. The advantage of membrane separation to PSA is that it provides a near continuous, vice batch process, product stream. The disadvantage of polymeric membranes is that they separate hydrogen from other species based on relative permeability, so they are not capable of providing high-purity hydrogen or absolute separation of species. Furthermore, as with PSA, the hydrogen permeate is produced near ambient pressure, thereby incurring a recompression energy penalty [56].

A significant limitation of all of the above processes is that they require cooling the inlet gas stream to near ambient temperature prior to separation, thus imposing an additional and significant energy penalty if using HTSE. Several high-temperature membrane H_2 separation processes are in various stages of development. References [56] and [57] describe them in detail, but Table 3-6 provides a succinct summary for convenience:

Membrane Type	Dense Polymer	Microporous Ceramic	Dense Metallic	Porous Carbon	Dense Ceramic
Temp Range (K)	< 373	473-873	575-873	773-1173	873-1173
H_2 Selectivity	Low	5-139	>1000	4-20	>1000
H_2 Flux[9]	Low	60-300	60-300	10-200	6-80
Stability Issues	Swelling, compaction	Stability in H_2O	Phase transition	Brittle	Stability in CO_2
Poisoning Issues	HCl, SO_x	-	H_2S, HCl, CO	Strong adsorbing vapors	H_2S
Materials	Polymers	Silica, alumina, zirconia, titania, zeolites	Palladium and its alloys	Carbon	Proton-conducting ceramics
Stage of Development	Commercially available.	Laboratory scale. Need to demonstrate long term stability and durability.	Pilot-scale testing. Requires Demonstration of long term stability in practical applications.	Pilot scale testing for hydrogen permeation. Requires demonstration with practical hydrogen recovery.	Laboratory scale. Need to increase H_2 flux by incorporating hydrogen permeable metals.

Table 3-6 - Hydrogen Membrane Separation Options

An examination of the various options above reveals that every option requires a tradeoff. While a dense metallic membrane is suitable for a HTSE application, it would not be suitable if H_2

---

[9] 10^{-3} mol m^{-2} s^{-1} @ ΔP=1 bar

separation was also required for HTCE. Microporous ceramic membranes are obviously unsuitable since they exhibit stability issues in water. Porous carbon applications have a relatively low H_2 selectivity, thereby requiring a much larger and expensive apparatus. A more advanced option described in reference [56] describes the use of "Group V" elements (niobium, tantalum, and vanadium), which have been successfully used in the nuclear industry to separate hydrogen isotopes from helium in plasmas. They have an order of magnitude more selectivity of H_2 than palladium; but, since they are reactive, they require a very thin protective and catalytic layer film, such as Palladium. Besides the high cost associated with using such exotic materials, a common problem with the Pd-coated metallic membranes is the intermetallic diffusion of the coated Pd with the base metal. This phenomenon reduces the catalytic and protective ability of the coated layer, especially at a high-temperature operation above 500 ^{o}C [56]. This thesis shall assume that a dense metallic hydrogen separation membrane will be available for use in conjunction with HTSE, which seems reasonable given the developmental stages of each technology. Since the HTCE product stream does not require gas separation, the CO poisoning issue associated with dense metallic membranes is not of concern. Furthermore, if HTCE gas separation would be required, using H_2 PSA would make intuitive sense because PSA would already be necessary for CO separation.

3.2.4   Autothermal Reforming (ATR)

Since the goal of the synfuel tanker ship is to produce a single fuel, JP-5, an absolutely critical capability is the recycling of the unwanted hydrocarbon products back into syngas. Since only a fraction (~ 35% at best) of the total hydrocarbons produced are in the C_9-C_{16} kerosene spectrum, the synfuel production system would waste a large amount of energy producing unwanted hydrocarbons if they were not recycled back into syngas. As shown in Chapter 2, fleet requirements dictate the tanker's required JP-5 output; from that required output for a given synfuel production process, one can determine the amount of unwanted hydrocarbon by-product available for recycle. Considering a plant operating at steady-state, the amount of syngas feed that the syngas production system must generate via electrolysis and air capture will be reduced by the amount of H_2 and CO generated by recycling unwanted hydrocarbons. Thus, recycling the unwanted hydrocarbons back into syngas significantly reduces the amount of CO_2 air capture and H_2 electrolysis required to produce the requisite amount of syngas feed. Through conservation of mass, one can readily determine that the syngas production system must only produce the syngas feed required to make-up for the JP-5 product exiting the system. Not only does this translate into significant power consumption savings, but also a much smaller and

74

less costly syngas production system is feasible since not nearly as many electrolysis and air capture units are necessary. The shortcomings of recycling the unwanted hydrocarbons back into syngas are (1) that the recycling process itself is an energy intensive, high-temperature process and (2) the synfuel production will not be able to operate at full capacity until the system generates enough waste hydrocarbon products for conversion back into syngas.

The options for recycling the waste hydrocarbon products back into the system as syngas are steam reforming, partial oxidation (POX), and autothermal reforming (ATR). Table 3-7 provides a succinct comparison of the technologies [58]:

Technology	Advantages	Disadvantages
Steam Reforming	• Most extensive industrial experience • O_2 not required • Lowest process temperature • Best H_2/CO ratio for H_2 production	• Highest waste gas emissions
Autothermal Reforming	• Lower process temperature than POX • Low methane slip	• Limited commercial experience • Requires air or oxygen
Partial Oxidation	• Decreased desulfurization requirement • No catalyst required • Low methane slip	• Low H_2/CO ratio • Very high processing temperatures • Soot formation/handling adds process complexity

Table 3-7 - Hydrocarbon Recycling Options

Although not mentioned in the table above, steam reforming is endothermic while POX is essentially controlled combustion. Although traditionally a disadvantage, a system that requires oxygen is actually desirable for the synfuel system proposed by this thesis due to the significant O_2 by-product resulting from electrolysis. Rather than being completely discarded overboard, the plant can use a significant fraction of the generated O_2 to recycle hydrocarbons back into syngas feed. Unlike steam reforming or POX, ATR is thermally neutral, thereby obviating extensive additional reactor heating or cooling components (respectively). The limited commercial experience with ATR primarily results from (1) the requirement to supply pure O_2 and (2) the desire for synfuel production facilities to provide a broad product slate vice a single hydrocarbon product; however, the process is well-understood and should be

mature enough to implement onboard a tanker ship[10], and the need to supply pure O_2 is not a concern to the synfuel plant described in this thesis.

As with the RWGS and gas separation sections above, this thesis shall make some simplifying assumptions associated with the ATR process in order to provide a convenient, yet realistic estimate. Although the purpose of the ATR is to produce H_2 and CO, other gases might also result in the product stream, thus requiring an additional gas purification step prior re-introduction into the syngas feed. However, as reference [58] indicates, ATR methane slip is low and coking is generally not a concern. Therefore, this thesis shall model ATR according to equation (3-17) [58]:

$$C_mH_n + \frac{1}{2}mH_2O + \frac{1}{4}mO_2 = mCO + \left(\frac{1}{2}m + \frac{1}{2}n\right)H_2; \; \Delta H = 0 \; (thermally \; neutral) \tag{3-17}$$
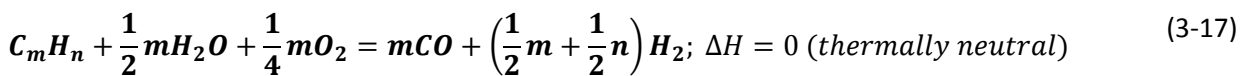
The waste hydrocarbon product feed into the ATR is a rather complicated brew, but the refinery process (described in detail later) breaks the waste product distribution into discretized fractions by carbon number. By making the convenient assumption of two hydrogen atoms per carbon atom in the hydrocarbon molecule, one can readily calculate the resulting H_2 and CO product gas.

Reference [59] provides a good overview on the various catalysts and reactor configurations available for ATR; but reference [60] provides excellent HYSYS simulation results of reforming a complex mixture of high and low weight hydrocarbons. The simulation shows (for a pressure of 0.3 MPa) that the optimum ATR efficiency occurs at 700 ^{o}C (973 K). These results correspond to the operating parameters for ATR described in references [59] and [61] and shall be used as the ATR operating parameters for calculation purposes in this thesis.

3.2.5   Syngas Production Summary

The primary constituents of syngas are H_2 and CO. To produce CO requires a carbon feedstock, which for a self-sustaining tanker ship leaves atmospheric air capture as the most promising approach. Modular and transportable MT/day CO_2 air capture prototypes already exist, indicating that they could be optimized for use on a naval vessel with enough research and design investment. It must first be proven that it can reliably operate in a demanding at sea environment. The syngas production system can readily produce hydrogen by electrolyzing water desalinated by RO units. Although alkaline electrolysis is a mature, readily feasible technology, it is also energy intensive and not the most desirable

---

[10] One of the big trade studies for a real ship would be the size of the recycle autothermal reforming step along with its required ancillary systems.

method. More energy efficient options involve using SOECs for HTSE or HTSE combined with HTCE to obviate the need for the RWGS reaction to convert CO_2 to CO. Although this study largely neglects the computational details associated with gas separation and purification, the syngas system production system will in all likelihood require the use of PSA or membrane separation of H_2 or CO or both to ensure a pure H_2/CO syngas mixture of the correct ratio in to the synfuel system. Finally, a means of recycling the unwanted hydrocarbon products back into syngas is necessary to limit the size, cost, and power consumption of syngas generation equipment. Of the options available, ATR is the most logical because it provides a means to efficiently dispose of the by-product O_2 from electrolysis and it produces a relatively pure H_2/CO syngas product.

3.3   Liquid Fuels Production

3.3.1   Methanol Conversion

3.3.1.1   Methanol to Olefins/Olefins to Gasoline-Distillate Process (MTO/MOGD)

The approach LT Terry uses in his synfuel production thesis is to first convert feedstock CO_2 and H_2 to methanol, and then convert methanol to jet fuel using Mobil's Methanol to Gasoline (MTG) process [25]. Even though synfuel production from methanol is possible, there are two significant problems with LT Terry's approach. The first issue is that LT Terry's analysis assumed over 99% conversion to methanol using CO free feed, but such a conversion rate is not possible. To illustrate why, it is helpful to provide the principal stoichiometric reactions involved in the chemical conversion [52, 62, 63]:

$$\boldsymbol{CO(g) + 2H_2(g) \rightarrow CH_3OH}, \Delta H = -91\frac{kJ}{mol}(exothermic) \tag{3-18}$$

$$\boldsymbol{CO_2(g) + 2H_2(g) \rightarrow CH_3OH + H_2O}, \Delta H = -45.5\frac{kJ}{mol} \tag{3-19}$$
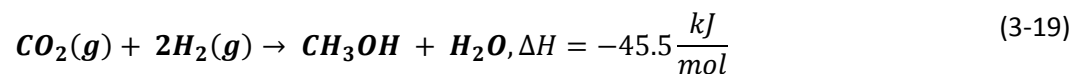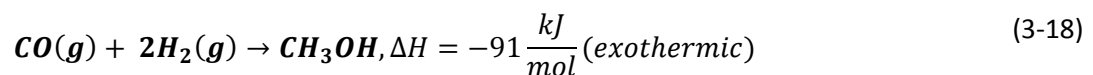
The other reaction of significance is the RWGS reaction, equation (3-16). In an absence of CO, only equations (3-16) and (3-19) apply. Due to the total absence of CO, equation (3-16) reacts in the direction generating more CO. Consequently, two reactions compete with each other for CO_2 consumption. The RWGS reaction, however, is a faster reaction than methanol synthesis, which adversely affects the methanol production rate. Additionally, the RWGS reaction and the methanol synthesis reaction generate H_2O, whose buildup in the system adversely affects the methanol conversion by pushing the chemical system closer to equilibrium. The high water concentration in the catalyst pore also reduces the catalyst's useful lifetime, which further reduces methanol conversion [62].

The main point of this argument is to emphasize that CO_2 and CO feed are both required for methanol conversion.

The second issue with LT Terry's approach is that the MTG process is inappropriate to produce JP-5. Table 3-8, courtesy of ExxonMobil's 2010 CTL conference, demonstrates the point [64]:

Components	Fischer-Tropsch Co Catalyst @ 220 ^{o}C	Fischer-Tropsch Fe Catalyst @ 340 ^{o}C	MTG
Fuel Gas	6	15	1.1
LPG	6	23	10
Naphtha	19	36	
Gasoline			88.8
Distillate/Diesel	22	16	
Fuel Oil/Wax	46	5	
Oxygenates	1	5	

Table 3-8 - Typical FT and MTG Component Yields

The MTG figures in Table 3-8 are in good agreement with S. Tabak's empirically derived results of 83.9% for fixed bed and 91.2% for fluidized bed MTG processes [65]. MTG is an excellent process for producing gasoline, but not distillate and not jet fuel.

Methanol synthesis followed by conversion to hydrocarbon products is nevertheless an option worth considering because other processes are available to convert methanol to JP-5. If using CO free feedstock, the first step is utilizing a RWGS reactor to convert a fraction of the CO_2 feedstock to CO, as explained in section 3.2.3.2 and by (3-16) above. Joo et al. developed the CAMERE process to produce methanol using CO_2 feedstock [52]:
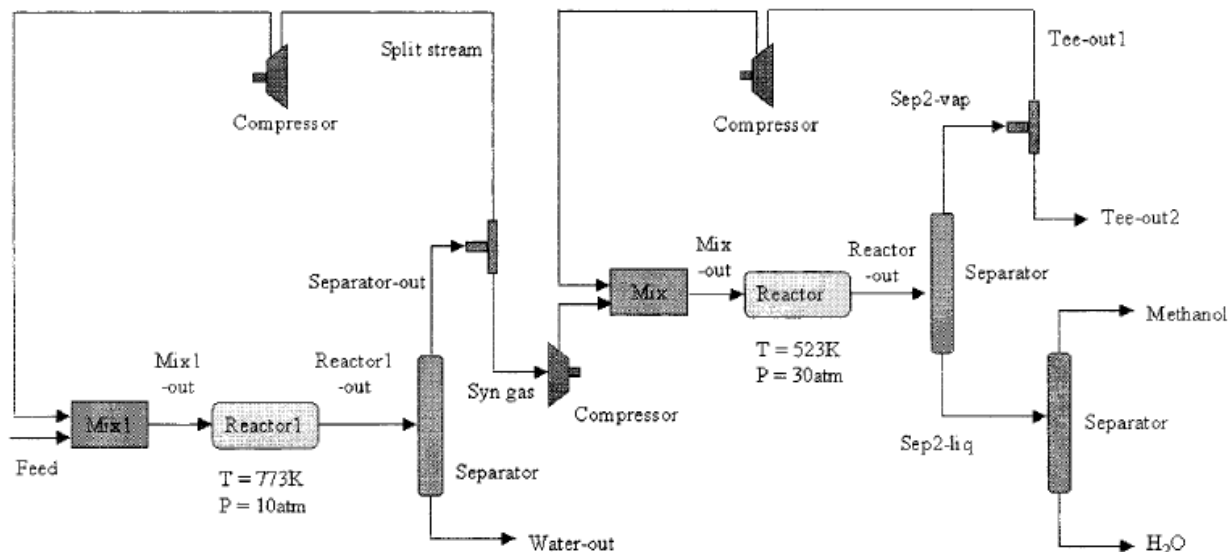
Figure 3-19 - Diagram of the CAMERE Process

In Figure 3-19, reactor 1 is the RWGS reactor while reactor 2 is the methanol synthesis reactor utilizing a

Cu/ZnO/ZrO$_2$/Ga$_2$O$_3$ (5:3:1:1) catalyst. Joo reported 61% CO$_2$ conversion to CO as well as a methanol

conversion yield of 89% when utilizing recycle of the methanol product [52]. Sandia national laboratory

was able to produce an 87% yield using nearly an identical process [66].

After producing methanol, two additional steps are necessary in order to produce a hydrocarbon

that can be refined into JP-5. The first step of the two step process is actually very similar to the MTG

process, which likewise occurs over a ZSM-5 catalyst [67]:

$$\boldsymbol{2CH_3OH + H_2O \leftrightarrow CH_3OCH_3 - H_2O \rightarrow light\ olefins} \tag{3-20}$$
$$\boldsymbol{\rightarrow higher\ olefins + n/iso - paraffins + aromatics}$$
$$\boldsymbol{+ naphthenes}$$
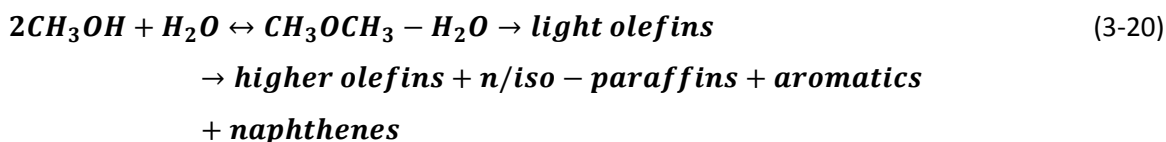
Equation (3-20) shows that dimethylether (DME) is produced by dehydrating methanol, and the

DME/methanol/water equilibrium mixture is then converted to light olefins (C$_2$-C$_4$). The final reaction

step results in the product mixture of higher olefins, n/iso paraffins, aromatics, and naphthenes.

Interrupting the reaction produces light olefins instead of gasoline, which is known as the MTO process

[68]. Mobil also developed a flexible process to convert the light olefin product to either distillate or

gasoline, known as the Mobil Olefins to Gasoline and Distillate (MOGD) process, and integrated it with

the MTO process to invent the MTO/MOGD process [69]. An overall process schematic of the

MTO/MOGD process is shown in Figure 3-20 [67]:
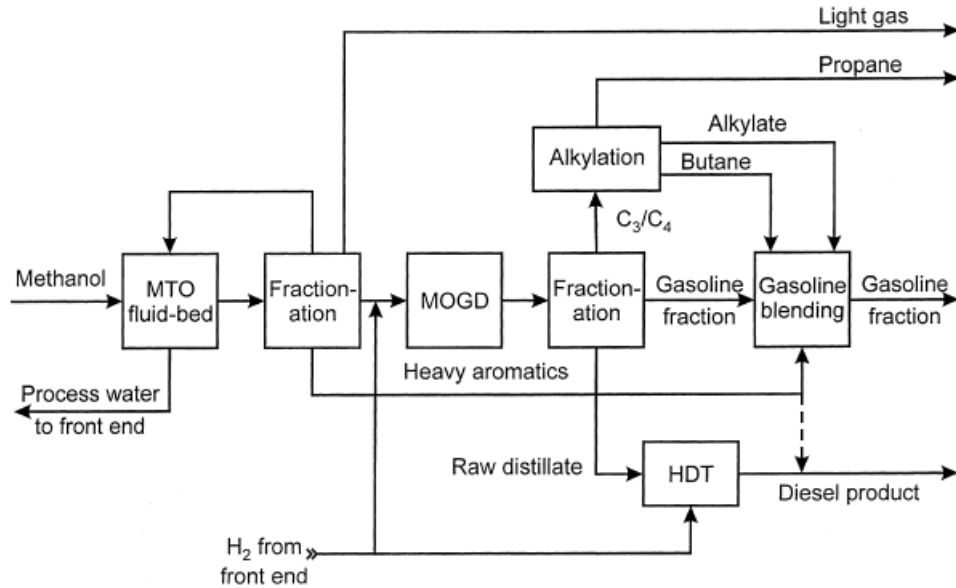
Figure 3-20 - MTO/MOGD Process

When operating in maximum distillate mode, the MOGD process yields about 80% diesel and 20% gasoline. Furthermore, because of its nearly pure iso-paraffinic structure, MOGD makes excellent jet fuel (meeting or exceeding military specifications) as Table 3-9 shows [68]:

	MOGD Product	Industry Standards
Jet Fuel		
Freeze Point, ^{o}C	<-60	-40
Aromatics, Vol %	4	25 max
Smoke Point, mm	28	18 min
JFTOT, ^{o}C	343	260

Table 3-9 - MOGD Product Quality

Mobil has also developed ODG^{TM} (Olefins to Distillate and Gasoline), a related zeolite catalyzed process that is even more effective than MOGD. The ODG^{TM} process shifts the product distribution to high octane gasoline, high centane diesel, and premium jet fuel, and "is a significant advance over the earlier MOGD process in terms of product yield and stability" [70]. In addition to a step change in catalyst lifetime (shown by **Figure 3-21**), Table 3-10 and Figure 3-22 show the product's remarkable conformance to military jet fuel specifications [71, 72]:
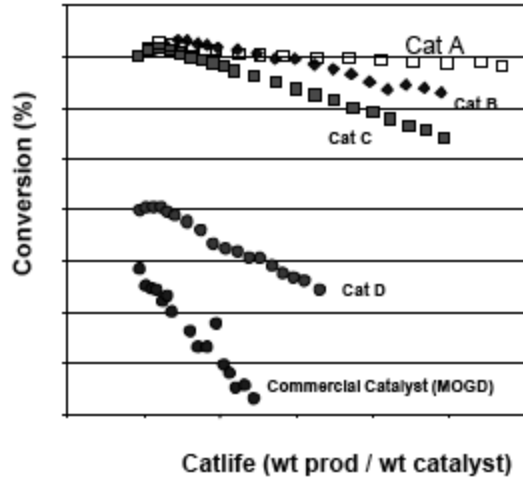
Figure 3-21 - ODG (Cat A) vs MOGD Performance
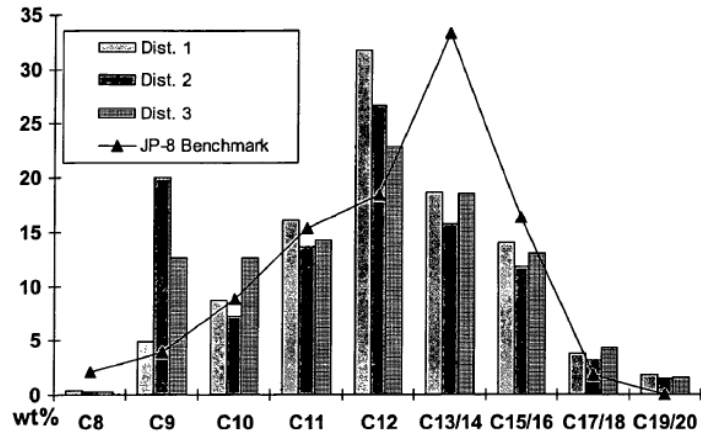
Figure 3-22 - ODG Product Distribution Compared to JP-8

Property	ODG Cat A	JP-8 Specs
Distillation T90, ^{o}C	<260	None
Density (15 ^{o}C)	<0.8	Max 0.84
Freezing Point, ^{o}C	<-50	Max -47
Aromatics (%Vol)	<0.01	Max 25
Sulfur (% Wt)	<0.0001	Max 0.3
Olefins (% Wt)	<0.01	Max 5

Table 3-10 - ODG Product Quality

In addition to the MTO/ODG^{TM} processes' excellent product yields and distributions, they also already exist as commercial or near commercial processes [70-72].

3.3.1.2 Synfuel Production via Methanol Conversion

Despite the attractive hydrocarbon yield within the kerosene spectrum for the methanol conversion processes described above, several significant shortcomings exist using a methanol conversion route that make it unsuitable for shipboard application. Compared to Fischer-Tropsch, producing synfuel via methanol is much more complicated because of the number of systems and process steps in converting syngas to synfuel. The syngas production system must first chemically convert CO free feed into a carefully balanced $CO_2/CO/H_2$ mixture in a RWGS reactor so that a second chemical reactor can convert the mixture into methanol. Then, another chemical reactor must dehydrate the methanol product to DME and convert the methanol/DME/H_2O mixture to light olefins. A series of reactors then upgrades the light olefins to distillate. A Fischer-Tropsch process converts syngas to synfuel in one process step. Another disadvantage is that methanol, which is a very toxic substance, must be produced in bulk in a confined space aboard ship.

However, the primary disadvantage is that a methanol conversion process is not able to take advantage of an autothermal reformer (ATR) to recycle a significant fraction of hydrocarbons back to syngas. In order for the MOGD process to oligomerize the olefin feed into the kerosene/distillate range, it must continuously recycle the lighter olefin hydrocarbons back through the oligomerization reactor. The continuous recycle of lighter weight olefins is necessary for proper oligomerization to higher number hydrocarbons. When operating in steady state at maximum capacity, the mass flow rate of MTO olefin feed into the MOGD system will directly equal the mass flow rate of jet fuel range hydrocarbon product leaving the system. 6,400 BBL/day JP-5 equates to ~ 9.43 kg/s JP-5, which requires 9.43 kg/s of olefin feed into the system. References [73] and [72] provide enough information to model the process, including temperature, pressure, catalyst, reactor configuration, and (most importantly) olefin feed chemical composition. From this information, one can estimate the amount of methanol required for the MTO process to produce an olefin feed of 9.43 kg/s using simple stoichiometric relations. Based on the assumptions used for the olefin feed chemical composition, the MTO system needs an estimated methanol feed of 21.6 kg/s (673.8 mol/s). Utilizing the rather detailed information provided about the CAMERE process in reference [52] shows that 8.55 kg/s (4,274 mol/s) H_2 feed and 55.7 kg/s (1,267 mol/s) CO_2 feed is necessary to produce 21.6 kg/s methanol. Utilizing the assumptions detailed in sections 3.2.1.2.2, 3.2.2.2, and 3.2.2.3.1 shows that 1,482 MWe of power is required for alkaline electrolysis using 711 Norsk 5040 electrolyzers; 4,815 air capture units (consuming a total of

82

38.0 MWe) are necessary to provide the requisite amount of CO_2. These power requirements exceed the capacity of a commercial nuclear reactor power plant. If HTSE is used instead of alkaline electrolysis, only 1,068 MWe is required for electrolysis. For interested readers, Appendix D contains a detailed breakdown of the calculations. Obviously, the power requirements for the methanol conversion route to synfuel production are too onerous to feasibly implement on a ship. Even if an advanced, commercial sized reactor plant was available to accommodate the loading, the size of the air capture and synfuel production systems would be too large to accommodate on even the largest supertankers. Clearly, another approach is necessary.

3.3.2   The Fischer-Tropsch Process

3.3.2.1   *Fischer-Tropsch Overview*

The alternative to using a Mobil process for synthetic fuel production is the Fischer-Tropsch process, which is basically the catalytic conversion of CO and H_2 to heavier hydrocarbons. Fischer-Tropsch is a well known, commercially established technology, which German scientists Franz Fischer and Hanz Tropsch patented in 1925 [21] and Ruhrchemie A.G. commercialized in 1934 [74]. It differs from the Mobil processes described above in two fundamental aspects. First, Fischer-Tropsch uses the reactor bed catalyst to directly convert syngas feed into a hydrocarbon product; no intermediate steps are required. The reaction is initiated by the adsorption of CO on the catalyst surface followed by chain propagation by various routes as illustrated by Figure 3-23 [21]:
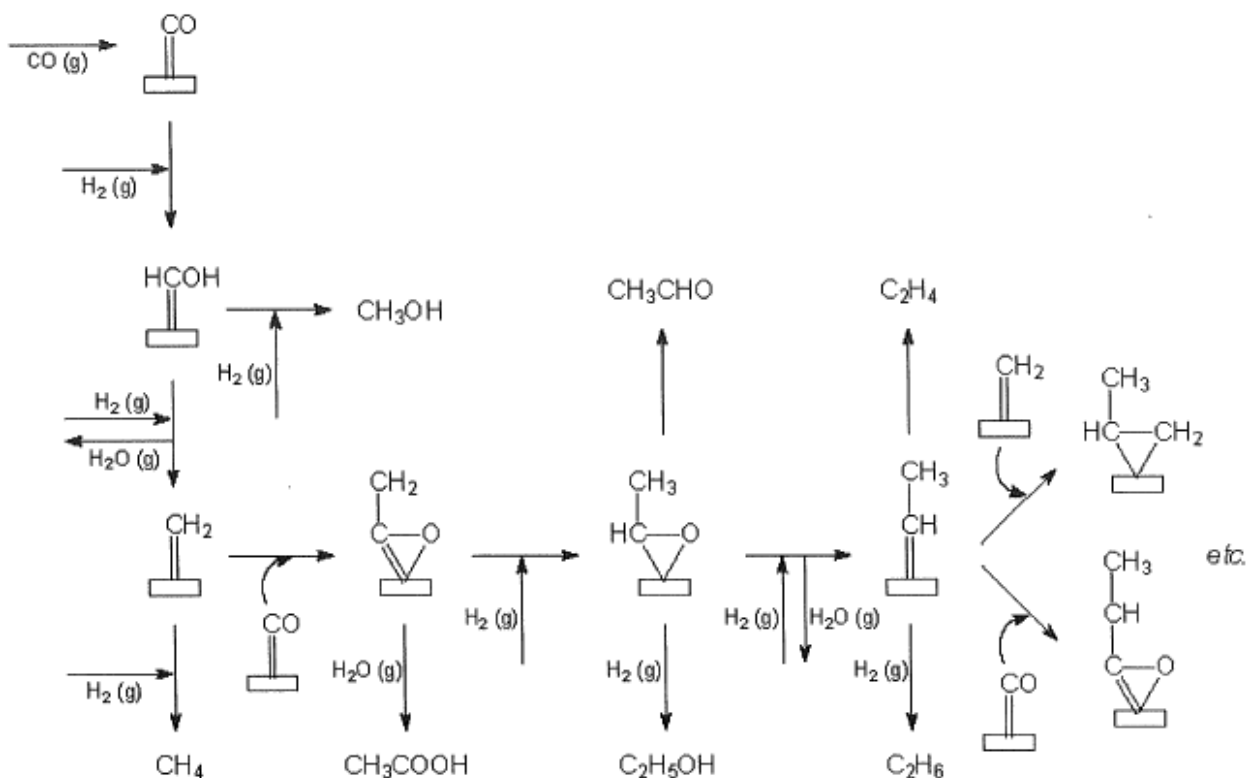
Figure 3-23 - Illustration of Fischer-Tropsch Reaction

The chemistry and reaction kinetics of the Fischer-Tropsch process are quite complicated. For those interested, reference [19] lists over 24 separate reactions used to model the process and reference [75] describes Fischer-Tropsch reaction kinetics in detail. However, equations (3-5) and (3-6), along with the WGS reaction, conveniently summarize the chemistry of the entire Fischer-Tropsch process[11]. The other significant difference from the Mobil processes is that the Fischer-Tropsch reaction produces a wide range of hydrocarbon products. The probability of chain growth on a catalyst, which is also known as the catalysts' "α value", determines the carbon number distribution of the reaction. Besides the catalyst itself, operational parameters of the reaction such as temperature, pressure, reactor type, and feed gas composition are other variables that determine α. Although several methods exist to model the hydrocarbon distribution as a function of α, the Anderson-Schultz-Flory (ASF) distribution is a widely known and convenient method to illustrate the interrelationship [4, 21, 75]:

---

[11] The WGS reaction is merely the reverse of the RWGS reaction, (3-16) above.

$$\frac{w_n}{n} = \frac{(1-\alpha)^2}{\alpha} \alpha^n \qquad \text{(3-21)}$$

$Where\ n = hydrocarbon\ \#$

$\alpha = Chain\ growth\ probability$

$\frac{w_n}{n} = weight\ percent\ (\%Wt)\ of\ a\ particular\ carbon\ number$

A graphical representation of the ASF distribution is as follows:
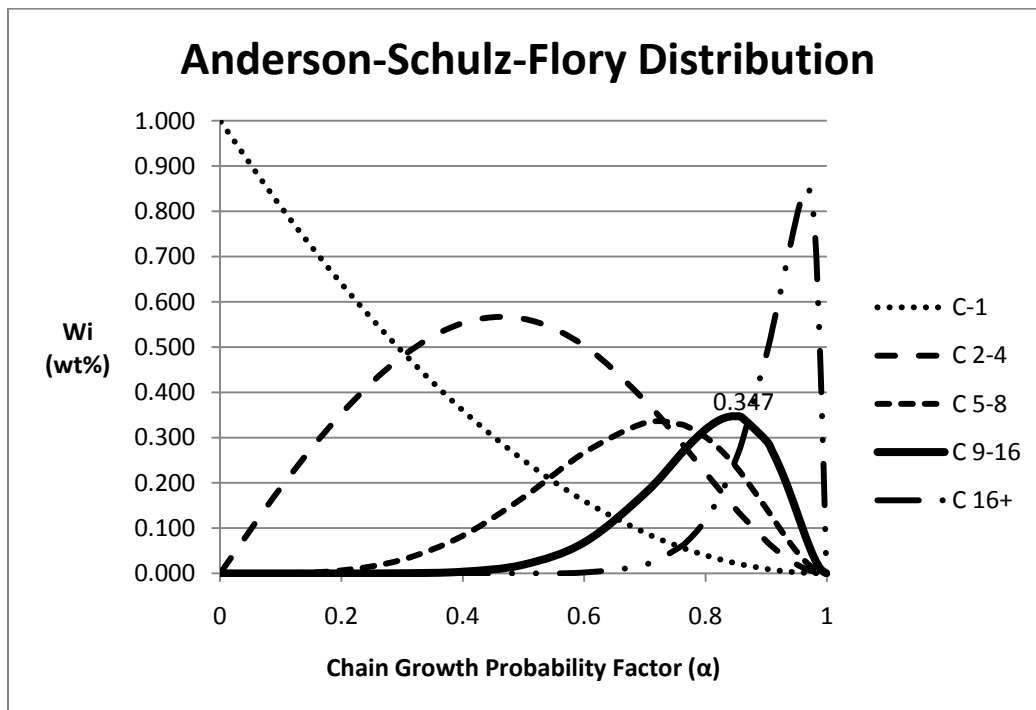
Figure 3-24 - ASF Distribution

The curves are merely the summation of the carbon numbers computed from equation (3-21) plotted as a function of α. The important concepts to realize are (1) that a relatively broad hydrocarbon distribution exists for Fischer-Tropsch regardless of the α value, and (2) that the strategy to optimize production of a particular hydrocarbon range is by tweaking the parameters affecting α.

3.3.2.2   *Desired Fischer-Tropsch Process Conditions for Jet Fuel Production*

Referring back to Figure 3-24, one can readily determine that the desired Fischer-Tropsch process conditions would be those that produce an α value of ~ 0.85, which corresponds to the maximum weight fraction value of the C_9-C_{16} hydrocarbon range. According to reference [22], the α value for maximizing jet fuel production should range between 0.76 and 0.86. Most commercial Fischer-

Tropsch facilities, however, operate outside of this range; and, as De Klerk notes, even with a Fischer-Tropsch process optimized for jet fuel production, the kerosene yield is unlikely to exceed 30% [22]. An important consideration is that commercial Fischer-Tropsch facilities, such as Sasol, endeavor to produce a range of hydrocarbon products and have tailored their operating processes to accomplish that objective. Conversely, the objective of the synfuel tanker is to produce a single hydrocarbon product. However, with relatively modest research and design effort, the chemical engineering industry (as indicated by references [6, 19, 74, 76, 77]) could certainly design a Fischer-Tropsch system and an accompanying refinery scheme to maximize the production of jet fuel.

Since an actual Fischer-Tropsch system optimized for jet fuel production does not exist, this thesis shall use reasonable assumptions obtained from a literature survey to estimate process conditions. Although the parameters used in this thesis might not correspond to the actual ASF α value actually attained by research and development for jet fuel production (assumed to be 0.85 for this thesis), the values used will provide a reasonable estimate on the mass and energy requirements of the synfuel production system. A review of references [3, 4, 20, 21, 74] reveals that operating parameters corresponding to a high temperature Fischer-Tropsch (HTFT) process are not appropriate because HTFT tends to produce lower hydrocarbon value products and requires a more complicated refining operation. Low temperature Fischer-Tropsch (LTFT), which is more commonly used in industry, essentially means that the operating temperature resides between 210-260 $^{\circ}$C [74]. Accounting for the promising results contained in reference [19], the patent information regarding jet fuel production contained in reference [22], and the reaction kinetics information contained in reference [75], this thesis will assume that a H_2/CO ratio of 2:1, an operating pressure of 3.0 MPa, and an operating temperature of 250 $^{\circ}$C (523 K) over a Co-based catalyst[12] will yield Fischer-Tropsch synfuel at the desired α value of 0.85.

Another important design consideration is Fischer-Tropsch reactor design. The reactor design for the proposed synfuel plant in this thesis would almost certainly have to be a custom built device, engineered not only for its α value but also for conformance to MILSPEC shipboard and shock requirements. Nevertheless, Fischer-Tropsch reactors fall into three broad categories (fixed-bed reactors, slurry bed reactors, and microchannel reactors) and an evaluation of the three options provide a sense of the size and operational characteristics of the reactors. A fixed-bed reactor has the

---

[12] The implications of a Co-based catalyst are (1) that the WGS reaction is negligible, (2) the catalyst is affordable, and (3) the catalyst has been shown to produce an α value within the desired spectrum.

advantages of smaller size compared to a fluid or slurry reactor and it is easier to extract wax buildup. Slurry bed reactors are much simpler and less costly to construct, and they require less maintenance and suffer less down time during catalyst replacement. Figure 3-25 and Figure 3-26 illustrate the difference in operation between fixed and slurry bed Fischer-Tropsch reactors [78]:
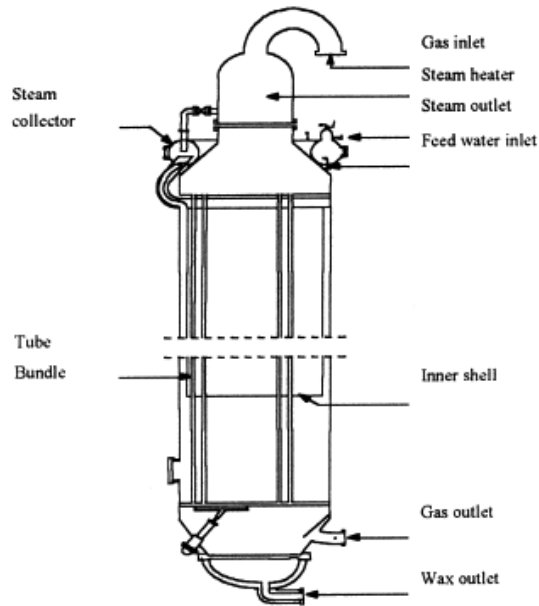
Figure 3-25 - Example of LTFT Fixed Bed Reactor
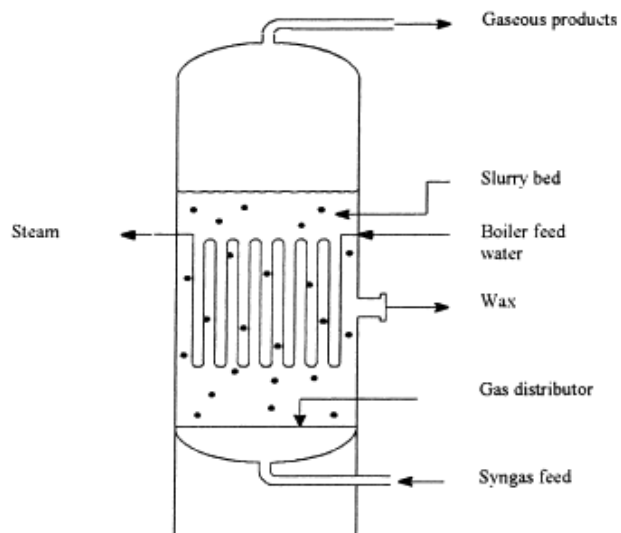
Figure 3-26 - Example of LTFT Slurry Bed Reactor

For the synfuel tanker application in this thesis, problems with both fixed and slurry bed reactors are (1) that they do not scale well, and (2) they are (generally speaking) very large vessels, as shown by Figure 3-27 and Figure 3-28 [77, 79]:

FT Technology Today – Slurry Bed

Vapor product

Liquid product

Vapor Zone

Slurry Bubble Zone

(small catalyst particles)

Catalyst/ Wax Separator

Catalyst Return

Boiler Feed Water

Syngas

Sasol's Oryx GTL

FT Reactor during shipping
Capacity = 15,000 bpd
Weight = 2,200 tons
Height = 60 m
Outer Diameter = 10m
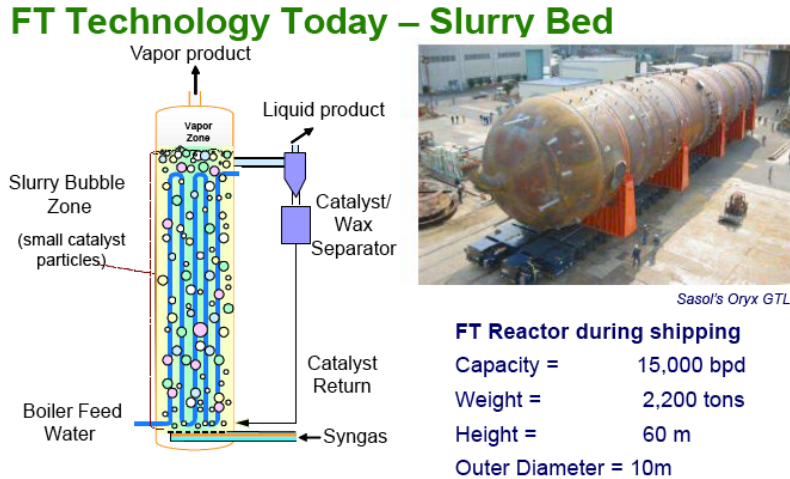
Figure 3-27 - Size Perspective of Slurry Bed Reactor

FT Technology Today – Fixed Bed

Key Reactor Stats:
– Weight: 1,200 tonnes
– Capacity: 5,800 bpd
– Diameter: 7m
– Height: 20m
– Reactor tubes: 29,000
– Tube length: 12m
– Tube diameter: 2.5cm

Fixed bed FT Reactors are also massive

Figure 3-28 - Size Perspective of Fixed Bed Reactor

The microchannel reactor (MCR) is an advanced technology concept that is undergoing pilot scale testing [77]:

Microchannel Fischer-Tropsch Reactor
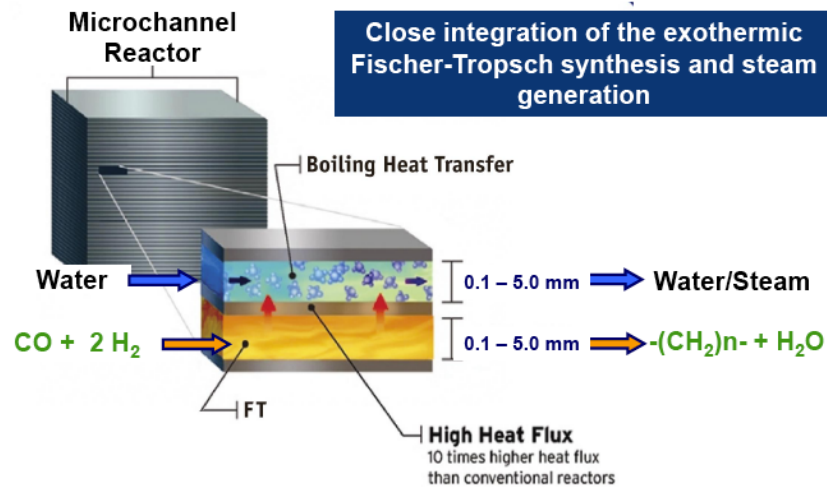
Figure 3-29 - Microchannel Fischer-Tropsch Reactor

Since conventional FT technology is an expensive, capital intensive enterprise suited for very large economies of scale, the developers of MCR technology hope to gain market share using small, modular equipment suited for small to mid scale operations [79]. Besides occupying less space, MCRs can more effectively control the reaction conditions, allow the use of more active catalysts, and accelerate processes an order of magnitude or more [77, 80]. Although this thesis does not necessarily endorse Velocys, its MCRs seem quite promising because of the ease with which they scale [79, 81]:
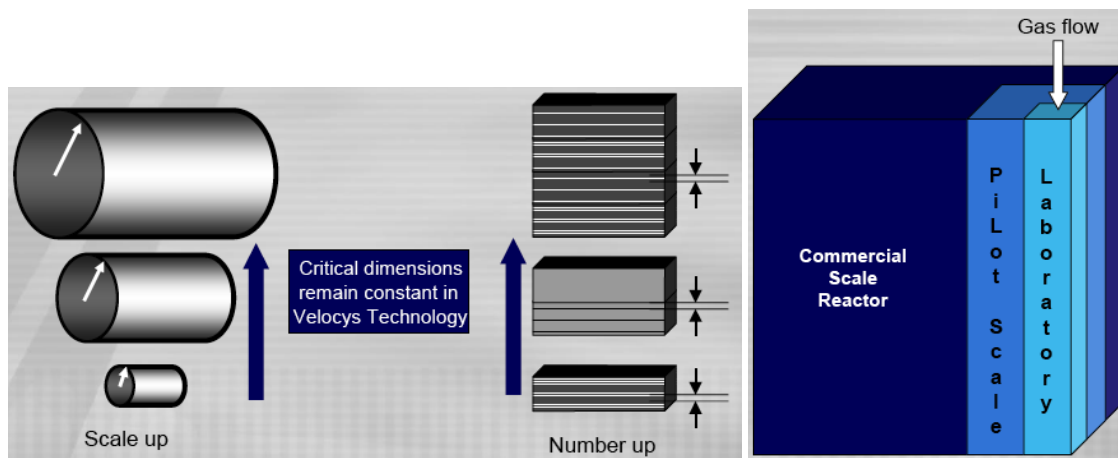
Figure 3-30 - "Numbering Up" Vice "Scaling Up"

Encouragingly, Velocys has already developed and manufactured microchannel FT reactors for field demonstrations. One of the field demonstrations set for 2011 also will incorporate the use of microchannel hydrocrackers for FT product hydroprocessing to produce JP-8 jet fuel for the US Air Force

at Wright Patterson US Air Force Base. Another demonstration already underway in Brazil utilizes the MCRs with in an ocean going GTL facility [77]:

Figure 3-31 - Microchannel FT GTL Technology on a Tanker Ship Deck

Velocys is not the only company to have had success with microchannel FT reactor technology. Eltron Research Inc. also performed bench scale testing with a variety of catalysts and achieved rather impressive results. Although Eltron Research was not able to generate a JP-5 rich hydrocarbon mixture in the MCR, it was able to demonstrate order of magnitude higher catalyst productivity than a conventional slurry or fixed bed reactor system. However, Eltron Research asserted that it would not be difficult to produce a JP-5 rich hydrocarbon mixture [19]. Because of their high throughput, modular design, and ease of scale to smaller size applications, MCRs are indeed a very attractive option for ocean tanker based synfuel generation [82].

Microchannel reactors do have some significant drawbacks that require resolution. The most significant drawback is their limited commercial and field tested operational experience; not much long-term data exists for reliability predictions and analysis. Conventional reactors are normally tested and examined after millimeters of catalyst material has been lost to allow for good system modeling; if millimeters are lost on an MCR, the entire unit would vanish! Another consideration is since MCRs are made at such a small internal scale, their resistance to mechanical shock is low [83]. This is of particular concern for a naval tanker ship because onboard components must meet stringent MILSPEC shock requirements. Thus, more evaluation is necessary before concluding that MCRs are suitable for a naval tanker ship; but they should, like SOECs, be considered as an advanced option that is likely to become feasible with additional research and development.

3.3.2.3 Fischer Tropsch Refining

After undergoing conversion in the Fischer-Tropsch reactor, the syncrude is sent to a distillation column that "discretizes" the output into multiple streams based on the boiling point corresponding to the carbon number of the hydrocarbon fraction. References [21] and [22] provide relatively detailed descriptions on how to configure a refinery to maximize the jet fuel yield from the Fischer-Tropsch process. As stated in reference [22], the refining process involves:

- **1** - Hydrocracking FT kerosene with a heavier fraction and a C_9 with a heavier fraction
- **2** - Oligomerizing FT syncrude C_2-C_8 hydrocarbons
- **3** - Hydrotreating an alkylated FT syncrude fraction with the oligomerized fraction (step 2 above)
- **4** - Aromatizing fractions of the hydrocracked, oligomerized, and hydrotreated fractions (steps 1, 2 and 3 above)
- **5** -Alkylating FT syncrude C_2-C_6 hydrocarbons with oligomerized and aromatized fractions (steps 2 and 4 above)

Reference [21] contains a convenient flow sheet of the above process description, which has been redrawn by the author for convenience:

91
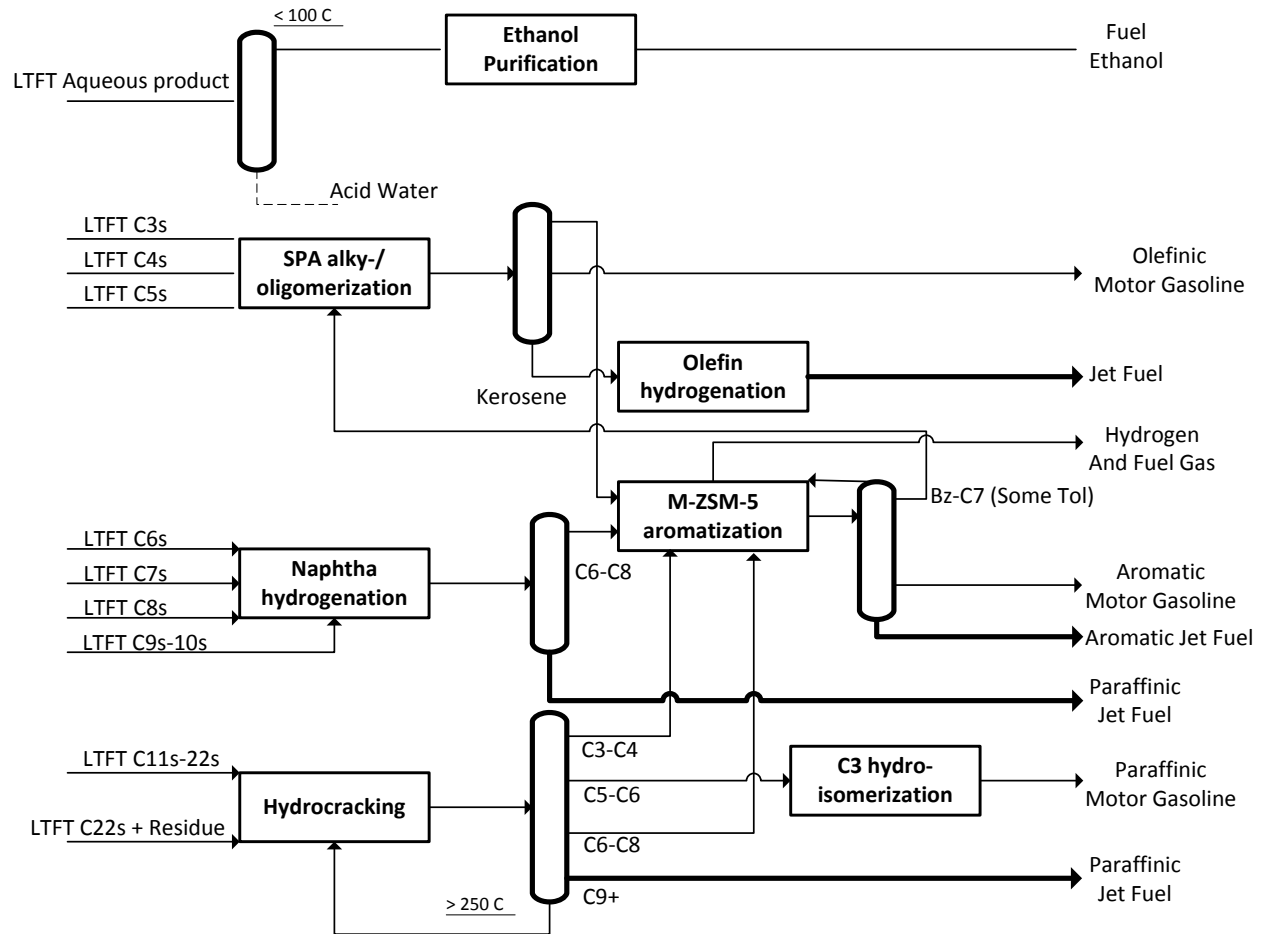
Figure 3-32 - Simplified LTFT Refining Flow Sheet

The jet fuel refining process converts molecules not suitable for jet fuel into those needed for jet fuel. Hydrocracking breaks down heavier hydrocarbons into lighter, jet fuel rich hydrocarbons; Hydrotreating increases the paraffinic composition; Oligomerization increases the hydrocarbon chain length of lighter hydrocarbons; and Aromatizing and Alkylizing adjusts the synfuel product to meet jet fuel specifications per Appendix B. All hydrocarbon products not converted to jet fuel by the refining process (i.e., motor gasoline, fuel gas, and ethanol) are recycled back into the system via ATR. Those desiring in-depth, yet excellent explanations on each of these refining steps should consult reference [84].

Fortunately, reference [22] provides enough information to allow one to assume a temperature, pressure, and catalyst for each process step. Although the actual operating parameters will vary in a real design, the values assumed in this thesis provide an adequate enough approximation to model the refinery process:

Process	Catalyst	Press (MPa)	Temp (K)
Hydrocracking	Pt-SiO2/Al2O3	5.0	423
Oligomerization	H-ZSM-5	5.0	423
Hydrotreating	Ni/SiO2	5.0	423
Aromatization	Zn/H-ZSM-5	5.0	623
Alkylation	H-ZSM-22	5.0	423

Table 3-11 - LTFT Refinery Operating Parameters

Another convenience is that reference [21] provides the weight values of the various hydrocarbon distributions for a 500,000 kg/hr refinery. By assuming a density of 0.8 kg/liter for JP-5, the required JP-5 production rate for the tanker ship is 33,958 kg/hr. The tanker ship JP-5 production rate and the assumed α value of 0.85 can thus serve as scaling factors to size the 500,000 kg/hr refinery to one suitable for the tanker ship. The first step is to scale the 500,000 kg/hr output by conveniently discretized hydrocarbon weight fraction values, which are determined by the ASF distribution (equation (3-21) above). Those values are then linearly scaled to the corresponding tanker ship values by working backwards through the refinery flow scheme. The overall result is that the mass flow rate, temperature, pressure, and estimated hydrocarbon distribution is known at each step of the refinery process. Thus, for a given JP-5 production rate and given α value, one can conveniently estimate not only the amount of LTFT raw syncrude produced, but also its hydrocarbon distribution. Furthermore, one can also determine the mass and hydrocarbon distribution of the unwanted hydrocarbons sent to the autothermal reformer. Finally, and most importantly, after determining the weight fraction of each carbon number using equation (3-21), equation (3-16) can conveniently estimate the amount of syngas feed required by the Fischer-Tropsch process and equation (3-17) can estimate the amount of syngas generated by autothermal reforming. Utilizing methodology above, ~ 4.29 kg/s (15,439 kg/hr) H_2 and ~ 30.02 kg/s (108,072 kg/hr) CO is the required syngas feed into the Fischer-Tropsch plant; similarly, the ATR produces 1.19 kg/s (4,272 kg/hr) H_2 and 11.08 kg/s (39,875 kg/hr) CO. Appendix D contains detailed spreadsheet calculations of the syngas, synfuel, and refinery plant requirements, and Appendix E contains detailed flow sheets of the various syngas, synfuel, and refinery processes.

3.3.2.4 *Estimated Power Requirements of Synfuel Production System via LTFT*

After determining the syngas feed requirements and the ATR syngas production rate using the methodology described in 3.3.2.3 above, estimating the power requirements is fairly straightforward process. Three LTFT liquid fuel production scenarios using the refinery scheme detailed in the section above were evaluated, all using CO_2 feedstock supplied by the air capture units described above in

section 3.2.1.2. The primary difference between the two scenarios is the method of hydrogen

production (alkaline electrolysis or HTCE supplemented by HTSE). The calculations utilized the following

assumptions:

- All processes are at steady state and maximum capacity
- H_2 production via alkaline electrolysis occurs precisely as claimed via Norsk Hydrotech 5040 vender data (refer to section 3.2.2.2 above) for atmospheric pressure
- H_2 production via the SOECs occurs per the simulation results of section 3.2.2.3.1 and section 3.2.2.3.2 above
- All chemical and mechanical processes are ideal and 100% efficient (perfect gas separation, perfect fractionalization in distillation column, ideal gas conversion in chemical reactors, etc.), except for compression power (90% efficient)
- The ASF model described in section 3.3.2.2 adequately describes the LTFT and refinery product distributions, and can also be used to conveniently discretize the hydrocarbon distributions
- Convenient stoichiometric relations, as stated earlier throughout this thesis in various sections, and the HTSE and HTCE models respectively described in sections 3.2.2.3.1 and 3.2.2.3.2, can be used to determine and simulate the mass flow rates and energy requirements of various process streams in the synfuel production plant
- Where necessary (RWGS, ATR, etc.) electric heaters can increase the fluid temperature as necessary at 95% efficiency
- All pump work has negligible power input
- No leakage (liquid or gas) occurs in the system
- Reference [85] can provide all required thermodynamic data (e.g., enthalpy, specific heat capacity, etc). In the event that some properties are unavailable for a given temperature range (e.g., high temperature CO), a linearly extrapolated value shall be used

By recalling Figure 3-9 from above, a clearer description of the power and infrastructure

requirements to support synfuel production via alkaline electrolysis is possible[13]:

---

[13] For those interested, a much more detailed flowsheet is available for reference in Appendix E.
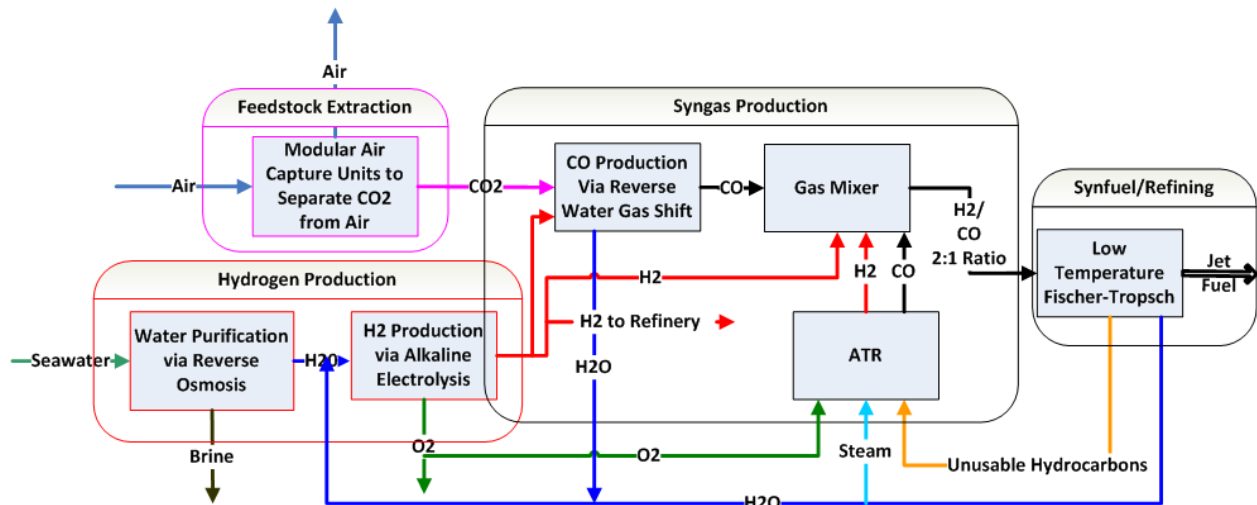
Figure 3-9 – Synfuel Production System: Baseline Option (Repeated for Convenience)

The air capture units, hydrogen electrolysis units, and the ATR must supply enough CO_2 and H_2 feed to make up for the amount of jet fuel leaving the system. Recalling 3.3.2.3, 1.88 kg/s H_2 and 13.13 kg/s CO are required by the LTFT system. However, additional H_2 is also needed to convert CO_2 to CO in the RWGS reaction and additional H_2 is also needed for the hydrotreating and hydrocracking processes. This increases the total H_2 demand to 6.93 kg/s H_2. Since the ATR produces 1.19 kg/s H_2 and 11.08 kg/s CO, the total amount of fresh H_2 and CO feed required by the electrolyzer and air capture units is 4.55 kg/s and 29.8 kg/s, respectively. Using equation (3-16) and the mass-energy relationships given in section 3.2.1.2.2, 2,573 air capture units must supply a CO_2 feed of 29.8 kg/s, which requires 20.3 MWe. Using equation (3-4) and the Norsk 5040 vendor data given in section 3.2.2.2, 378 electrolyzers, consuming a total of 789 MWe, are required to generate the requisite H_2 feed. The electrolysis operation requires four EUWP Gen 2 RO units, consuming 1.30 MWe; and 36.4 kg/s of by-product O_2 is also generated. 33.2 kg/s of the O_2 must be discharged overboard while the remainder is used as feed for ATR. To determine the required thermal power input or output for heat addition or heat rejection processes, the following relationships are used as necessary:

$$\dot{Q} = \dot{m}c_p\Delta T \tag{3-22}$$

$Where\ \dot{Q} = Thermal\ power$

$\dot{m} = Mass\ flow\ rate$

$c_p = Specific\ heat\ capacity\ (constant\ pressure)$

$\Delta T = Desired\ temperature\ difference$

$$\dot{Q} = \dot{m}\left[c_{p,0}(T_{sat} - T_1) + h_{fg} + c_{p,1}(T_2 - T_{sat})\right] \tag{3-23}$$

$where\ c_{p,0} = avg.\ specific\ heat, constant\ pressure\ (liquid\ phase)$

$T_1 = Initial\ temperature$

$T_{sat} = Saturation\ temperature\ at\ given\ pressure$

$h_{fg} = Enthalpy\ of\ vaporization$

$c_{p,1} = Avg.\ specific\ heat, constant\ pressure\ (vapor\ phase)$

$T_2 = Final\ temperature$

$$\dot{Q} = \sum \dot{m}_i * h_i \tag{3-24}$$

$$\dot{Q}_{HX,1} = \dot{Q}_{HX,2} \tag{3-25}$$

$$T_{out,2} = T_{out,1} + 15\ K \tag{3-26}$$

Equation (3-22) provides the thermal power for a process exhibiting no phase change. If a phase change is necessary, such as vaporizing water, then equation (3-23) is appropriate. Equation (3-24) is useful for situations when multiple gas streams enter a particular component, such as a gas mixer, and an unknown temperature is to be computed. By using equation (3-25), an enthalpy balance is possible, and the resultant enthalpy value will correspond to an appropriate temperature given by reference [85] (this requires an iterative approach). Equation (3-26), which is the result of one of the enumerated assumptions above, is useful when two unknown temperatures exist and a temperature difference must exist to drive the heat transfer process.

Equation (3-27) estimates the amount of compression power required by the system:

$$\dot{W}_{CP} = \frac{\dot{m}c_p T_1 \left[(r_p)^{\frac{\gamma-1}{\gamma}} - 1 \right]}{\eta}$$

$$\text{(3-27)}$$

$Where\ \dot{W}_{CP} = Power\ required\ for\ compression$

$\eta = Compressor\ efficiency$

$\dot{m} = Mass\ flow\ rate$

$C_p = Specific\ heat, constant\ pressure$

$T_1 = Initial\ temperature$

$r_p = Compression\ ratio\ \left(= \frac{P_2}{P_1} \right)$

$\gamma = \dfrac{C_p}{C_v}, (ratio\ of\ specific\ heats)$

$where\ C_v = specific\ heat, constant\ volume$

For the alkaline electrolysis case, compression power is necessary to (1) raise CO_2 and a fraction of the H_2 from ~ atmospheric to 1.0 MPa for the RWGS reaction, (2) raise H_2 and CO pressure to 3.0 MPa for LTFT, (3) compress certain gas feeds to 5.0 MPa for refining, and (4) slightly compress the required O_2 feed to 0.3 MPa for ATR. This results in 59.4 MWe for non-refining compression power and 4.85 MWe for refining compression power.

The two heat sources evaluated for this analysis are 670 ^{o}C supercritical carbon dioxide (S-CO_2) or 285 ^{o}C steam. Chapter 4 explains the basis for these temperatures; the higher temperature results from a high temperature reactor (AHTR) to heat S-CO_2 while the lower temperature is from a pressurized water reactor (PWR). Using equations (3-22)-(3-27), the total thermal power of the various processes can be determined depending on the heat source. In addition to heating the feed components, the relationship provided by equation (3-16) provides the heat input necessary to sustain the endothermic RWGS reaction. In order to ensure the syngas enters the Fischer-Tropsch reactor at 523 K, equations (3-22), (3-23) and (3-24) must be utilized in a heat balance to determine the power rejected from the ATR. Since the Fischer-Tropsch reaction is exothermic, equation (3-6) provides a relationship to determine the power rejection requirement for the Fischer-Tropsch reaction, which is -177 MWth. The refinery process requires 8.59 MWth and rejects -12.89 MWth (these heat requirements are the same regardless of the method of syngas production). Appendix E provides color-coded diagrams to conveniently trace the mass and energy transfers throughout the system. Table 3-12, also found in Appendix D, conveniently itemizes the power requirements for liquid fuels production via alkaline electrolysis:

AHTR (S-CO$_2$)-670 ^{o}C		PWR (Steam)-285 ^{o}C	
Turbine Power (MW$_e$)	875	Turbine Power (MW$_e$)	922
Power (w/ refining) (MW$_{th}$)	78.4	Power (w/ refining) (MW$_{th}$)	20.8
RWGS **(45-467 ^{o}C)**		**RWGS** **(45-285 ^{o}C)**	
RWGS RXN (Endothermic) (MW$_{th}$)	26.3	RWGS RXN (Endothermic) (MW$_{th}$)	7.70
RWGS Feed Heating (MW$_{th}$)	20.5	**RWGS Total**	**7.70**
RWGS Total (MW$_{th}$)	**46.8**		
Autothermal Reforming **(37-655 ^{o}C)**		**Autothermal Reforming** **(37-285 ^{o}C)**	
H$_2$O Heating (MW$_{th}$)	13.4	H$_2$O Heating (MW$_{th}$)	3.40
HC Heating (MW$_{th}$)	7.86	HC Heating (MW$_{th}$)	2.96
O$_2$ Heating (MW$_{th}$)	1.76	O$_2$ Heating (MW$_{th}$)	0.54
ATR Total (MW$_{th}$)	**23.0**	**ATR Total (MW$_{th}$)**	**6.90**

Table 3-12 - Power Requirements for LTFT via Alkaline Electrolysis

The steam heat source requires ~ 5.44% more electric power than the higher temperature S-CO$_2$ power cycle because electric heaters are necessary to supplement additional power for the RWGS reaction and for ATR; however, the steam cycle requires 73.4% less thermal power because the smaller temperature cannot deliver as much heat to thermal loads. During steady state operation, the system can recuperate heat from high temperature loads, such as the autothermal reformer (700 ^{o}C operating temperature). For the alkaline electrolysis case, the lower temperature steam heated cycle recuperates 2.52 MW$_{th}$, compared to only 0.25 MW$_{th}$ from the S-CO$_2$ cycle (an increase of 913%). Although the higher temperature system is slightly less efficient because of its higher heat load, it has an overall smaller heat input into the power conversion cycle because of the lower turbine power requirement.

The other case uses the advanced option of HTCE combined with HTSE (Figure 3-10 shown again for convenience):
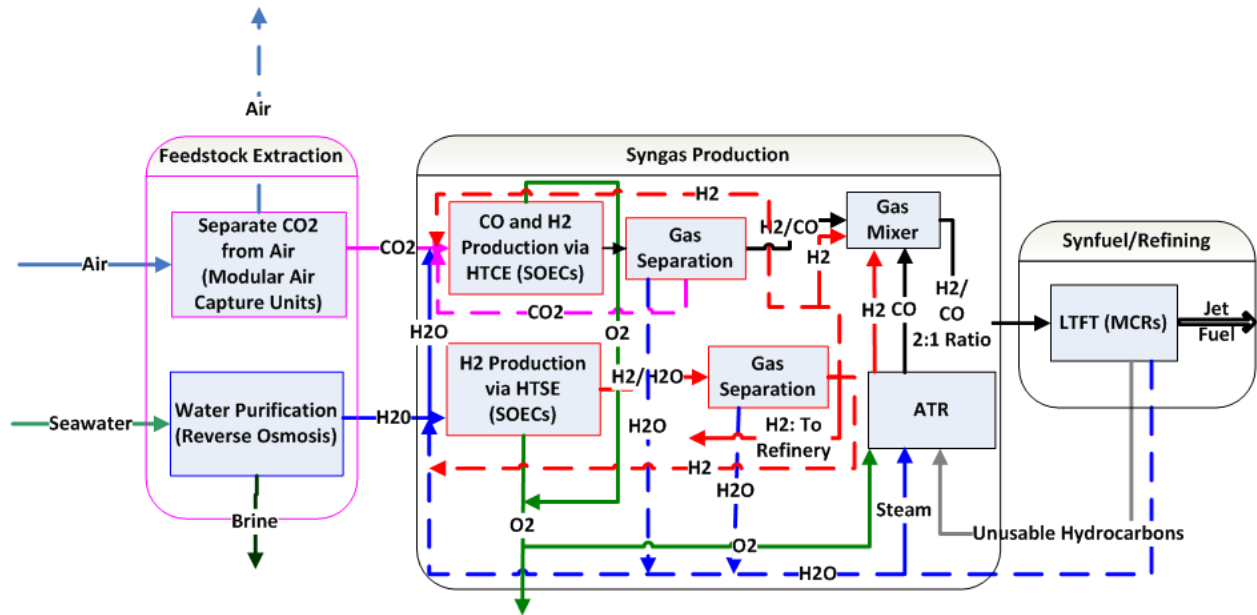
Figure 3-10 – Synfuel Production System: Advanced Option (Repeated for Convenience)

The primary purpose of the SOECs used for HTCE is to convert CO_2 to CO, but, as described by the model in section 3.2.2.3.2 and Appendix C, the process also electrolyzes water to produce H_2. However, not enough H_2 is produced to meet the demand of the synfuel system solely through HTCE. Since generating excess CO is not desired, SOECs for HTSE supplement the H_2 demand. As with the HTSE case, a portion of the product H_2 must be recycled back to the SOECs; the cells used for HTSE provide this additional H_2 for both sets of SOECs in order to minimize CO production. In total, 1,742,605 cells are necessary for HTCE (534 MWe) and 190,841 cells are necessary for HTSE (55.9 MWe). Since no RWGS reaction is necessary, the system compresses the gas streams to 3.0 MPa, vice 1.0 MPa, where appropriate. Because of the cell resistance, the gas leaves the SOECs at a higher temperature. During steady state operation, this heat can be recuperated by the incoming fluid, providing a significant energy savings. Appendix D and appendix E detail the calculations and flow diagrams, respectively, but Table 3-13 provides a summary comparison on the amount of thermal power recovered by the two cycles:

Process	(S-CO$_2$)	(Steam)
H$_2$O Heating from HTCE$_{out}$	8.27	30.6
CO$_2$ Heating from HTCE O$_2$	5.33	19.1
H$_2$O Heating from HTSE$_{out}$	1.24	4.73
H$_2$O Heating from HTSE O$_2$	0.20	22.1
H$_2$O Heating from ATR$_{out}$	0.09	2.52
Total (MW$_{th}$)	15.1	79.1
% Change from S-CO$_2$ to Steam 423%		

<div align="center">Table 3-13 - Comparison of Recuperated Heat</div>

Even though steam generated by the heat from a PWR is at a relatively low temperature compared to HTCE/HTSE, the ability to recuperate this excess heat facilitates operation of a lower temperature LWR if desired. Determining the power required by each step in the HTCE/HTSE liquid fuel production process is the same as for the alkaline electrolysis case, and the results for this more advanced option are as follows:

AHTR (S-CO$_2$)-670 ^{o}C		PWR (Steam)-285 ^{o}C	
Turbine Power (MW$_e$)	650	Turbine Power (MW$_e$)	658
Power (w/ refining) (MW$_{th}$)	171	Power (w/ refining) (MW$_{th}$)	109
HTCE (27-655 ^{o}C)		HTCE (27-285 ^{o}C)	
CO$_2$ Feed Heating (MW$_{th}$)	21.1	CO$_2$ Feed Heating (MW$_{th}$)	7.8
H$_2$O Feed Heating (MW$_{th}$)	102	H$_2$O Feed Heating (MW$_{th}$)	69.3
HTCE Total (MW$_{th}$)	123	HTCE Total (MW$_{th}$)	77.1
HTSE (27-655 ^{o}C)		HTSE (27-285 ^{o}C)	
H$_2$O Feed Heating (MW$_{th}$)	17.6	H$_2$O Feed Heating (MW$_{th}$)	12.0
HTSE Total (MW$_{th}$)	17.6	HTSE Total (MW$_{th}$)	12.0
Autothermal Reforming (37-655 ^{o}C)		Autothermal Reforming (37-285 ^{o}C)	
H$_2$O Heating (MW$_{th}$)	13.4	H$_2$O Heating (MW$_{th}$)	10.3
HC Heating (MW$_{th}$)	7.86	HC Heating (MW$_{th}$)	2.96
ATR Total (MW$_{th}$)	21.2	ATR Total (MW$_{th}$)	13.2

<div align="center">Table 3-14 – Power Requirements for LTFT via HTCE w/ HTSE</div>

Most significant is that the HTCE/HTSE case requires 25.6% less electrical power than the alkaline electrolysis case because of (1) more efficient H$_2$ hydrogen generation and (2) elimination of the RWGS process step. Because more heat can be recuperated from the synfuel production system incorporating HTCE/HTSE, less heater input is required by the steam heating option. Although some heating is still necessary to boost system temperature in some instances, the overall power requirement differs from

the high temperature S-CO$_2$ option by only ~ 1.25%. Additionally, the steam cycle has a total heat input that is ~ 36.2% smaller than the S-CO$_2$ cycle. During plant startup, however, additional heater input would be necessary to raise temperature to normal operating conditions. Chapter 4 shows that even though a PWR reactor plant could power the liquid fuel production system, significant gains in cycle efficiency are possible through the use of a S-CO$_2$ cycle; the fuel plant heat loads are small compared to the heat input to the power conversion cycle.

3.3.3   Liquid Fuels Production Summary

A comparison between the Fischer-Tropsch to the Mobil methanol conversion processes clearly shows that Fischer-Tropsch is preferred. This is primary due to the fact that a Fischer-Tropsch process can utilize ATR to recycle the non jet fuel hydrocarbon products back into the syngas production system as their original H$_2$ and CO constituents. In a MTO/MOGD production scheme, the hydrocarbon products are continuously recycled in the synfuel reactor where they iteratively undergo oligomerization until reaching the kerosene hydrocarbon range. More syngas feed, and thus more energy, is required to provide enough methanol to support the process.

Fischer-Tropsch reactors are large and complicated pieces of equipment, and are probably too large for use on a naval tanker. MCRs could serve as an attractive replacement for large, fixed and slurry-bed Fischer-Tropsch reactors if they can demonstrate durability in rugged, at-sea conditions. However, much more analysis is necessary to evaluate their suitability.

While a disadvantage of the Fischer-Tropsch process for the application in this thesis is the broad product slate, this shortcoming is minimized through the use of (1) careful adjustment of process conditions to attain an α value favorable to jet fuel production (~0.85), and (2) the use of an innovatively engineered refinery scheme designed to maximize jet fuel product. By working backwards through the refinery flow scheme, it is possible to determine the amount of syngas feed required by the LTFT system as well as the estimated H$_2$ and CO product from the ATR. An analysis of baseline and advanced H$_2$ production options (alkaline electrolysis and HTCE with HTSE) coupled to the synfuel plant, refinery, and ATR show that HTCE with HTSE is probably the best option because (1) the SOECs consume less electrical power to produce H$_2$ while operating at high temperature (compared to alkaline electrolysis) and (2) the ability to remove the RWGS system in favor of a complete SOEC system.

3.4 Chapter Summary

3.4.1 Recommended Options

After performing an assessment of the various mature, commercially available and cutting edge, prototype synfuel and syngas production technologies, the most feasible configuration utilizes CO_2 extraction via air capture, RO desalination, alkaline electrolysis, RWGS, ATR, LTFT, and a refinery specifically customized to maximize kerosene range hydrocarbon product. The optimal, cutting edge option utilizes the same features as baseline option except that HTCE and HTSE replace alkaline electrolysis and the RWGS reaction. The advanced option electrolyzes water at a much higher temperature (1,073 K) and does not need to produce excess H_2 to support the RWGS reaction; therefore ~ 25.6% electrical power less electrical power is needed for the liquid fuels production process.

3.4.2 Required Research and Design Effort

A substantial amount of additional research and design effort is necessary to improve and validate several of the subsystems utilized in the synfuel plant. Advanced technologies such as SOECs, high temperature hydrogen membranes, and microchannel Fischer-Tropsch reactors are still in development but offer marked improvement over current state of the art technology. Specifically, the following items require more investigation:

- SOEC degradation
- Corrosion inhibitor in high temperature systems
- Performance evaluation of high temperature membranes
- Performance evaluation of MCRs

Several key components of the baseline option, however, also require research investment; they are mainly the catalytic conversion devices and the air capture units. As mentioned earlier, RWGS is not a mainstream technology, nor is a LTFT reactor that is designed to maximize production of kerosene range hydrocarbons. While ATR is a well-understood process, they are seldom used in industry. The refinery system, in order to be suitable for shipboard use, will need to be designed to fit into compact, modular skids; and it will need to be designed to maximize JP-5 production. The CO_2 air capture systems are not yet suited for an at-sea environment and their present design is probably too large for shipboard use.

Recent developments in the GTL market, however, indicate that the engineering effort necessary to build such catalytic devices should not be insurmountable. This year the $18 Billion Shell Pearl natural gas-to-liquids plant is being commissioned in Qatar [86]. This single plant will consume 1.6 billion cubic feet of natural gas per day--the equivalent of 2.7% of U.S. natural gas consumption. The financial payback period is only 4 years assuming oil prices of $50/BBL [87]. Advances in technology in the next ten years will likely improve the process economics by at least 50% with better catalysts that allow production of a narrow product slate that matches market demand (essentially mitigating the inherent drawback of Fischer-Tropsch). Since more than $10 billion has been invested in such a GTL project, there is a massive economic incentive to develop better chemical reactors and catalysts to create a narrow product distribution--gasoline and diesel fuels. These are the high-value products, while natural gas is comparatively a low value product. Furthermore, the price differential between oil and natural gas in the North American market has dramatically increased. This creates additional economic incentives worldwide to improve GTL processes to convert low value natural gas into high value liquid fuels.   Thus, there will likely be massive investments (tens of millions of dollars per year) to get more selective catalysts to convert syngas to liquid fuels [88]. This implies that a lot of the technology needed for the synfuel plant is going to get pushed as if it was a crash program – major technological improvements in the next few years are highly probable.

3.5   Chapter 3 References

[1] Hall-Green, M., 2010, "Sasol Facts 2010," Sasol, -, Johannesburg, South Africa.

[2] Forsberg, C., 2005, "Nuclear Hydrogen for Production of Liquid Hydrocarbon Transport Fuels," 2005 American Institute of Chemical Engineers Fall Meeting, K. Schnelle, ed. Oak Ridge National Laboratory, Oak Ridge, TN, pp. 1-10.

[3] Dry, M., 2002, "The Fischer-Tropsch Process: 1950-2000," Catalysts Today, **71**pp. 227-241.

[4] Dry, M., 1996, "Practical and Theoretical Aspects of the Catalytic Fischer-Tropsch Process," Applied Catalysts: A General, **138**pp. 319-344.

[5] Andrews, A., 2007, "Liquid Fuels from Coal, Natural Gas, and Biomass: Background and Policy," Congressional Research Service, RL34133, Washington, DC.

[6] Muzzell, P., 2009, "Alternative Fuels," TACOM/TARDEC, 19972RC, Warren, MI.

[7] Forsberg, C., and Peterson, P., 2010, "Advanced High Temperature Reactor for Electricity and Fuels Production using High-Temperature Electrolysis and Fischer-Tropsch Synthesis," **Reply to Request for Information (RFI): Defense Advanced Research Projects Agency SN10-37**pp. 1-3.

[8] Jeckell, J.M., 2008, "Fire For Effect: Calling for a More Potent Energy System," USACGSC, Fort Leavenworth, KS.

[9] Leung, M., 2007, "S.B. Thesis: An Assessment of Carbon Sources for the Production of Synthetic Fuels from Nuclear Hydrogen," Massachusetts Institute of Technology (DSpace@mit), http://hdl.handle.net/1721.1/41598, Cambridge, MA.

[10] EPA Office of Transportation and Air Quality, 2007, "Greenhouse Gas Impacts of Expanded Renewable and Alternative Fuels Use," Environmental Protection Agency, EPA420-F-07-035, Washington, DC.

[11] Schultz, K., Bogart, L., Besenbruch, G., 2006, "Hydrogen and Synthetic Hydrocarbon Fuels-A Natural Synergy," National Annual Hydrogen Conference 2006, A. Cutair, ed. NHA, Washington, DC, pp. 1-10.

[12] Lackner, K., Dahlgren, E., Graves, C., 2010, "Closing the Carbon Cycle: Liquid Fuels from Air, Water and Sunshine," Lenfest Center for Sustainable Energy, White Paper, Columbia University.

[13] Kleiner, K., 2009, "How to Turn Seawater into Jet Fuel," NewScientist, **2010**(6/15) pp. 1.

[14] Yildiz, B., and Kazimi, M., 2006, "Efficiency of Hydrogen Production Systems using Alternative Nuclear Energy Technologies," International Journal of Hydrogen Energy, **31**pp. 77-92.

[15] O'Brien, J., Stoots, C., Herring, J., 2010, "High Temperature Electrolysis for Hydrogen Production from Nuclear Energy – Technology Summary," Idaho National Laboratory, INL/EXT-09-16140, Idaho Falls, ID.

[16] O'Brien, J., 2008, "Thermodynamic Considerations for Thermal Water Splitting Processes and High Temperature Electrolysis," Idaho National Laboratory, INL/CON-08-14376, Idaho Falls, ID.

[17] Singhal, S.C., and Kendall, K., 2003, "High Temperature Solid Oxide Fuel Cells: Fundamentals, Design and Applications," Elsevier Advanced Technology, Oxford, UK, pp. 405.

[18] Forsberg, C., 2008, "Nuclear Energy for a Low-CO2-Emission Transportation System with Liquid Fuels," Nuclear Technology, **164**(3) pp. 348-367.

[19] Fraenkel, D., White, J., Dutta, S., 2008, "Selective Fischer-Tropsch Catalyst for Producing C9-C16 Hydrocarbons," Eltron Research and Development, Inc, CLIN/SLIN 0001AC, Boulder, CO.

[20] Tatarchuk, B., and Yang, H., 2008, "Analysis & Adaptation of Advanced Fischer-Tropsch Catalyst Structures and Resulting BOP Reductions to Fulfill Future Navy Fuel Needs," Office of Naval Research, PIFR012108, Washington, DC.

[21] De Klerk, A., 2008, "PhD Thesis: Fischer-Tropsch Refining," University of Pretoria, 07282008-130342, Pretoria, South Africa.

[22] De Klerk, A., 2010, "Fischer-Tropsch Jet Fuel Process," **US 2010/018568 A1**pp. 1-14.

[23] Willauer, H., Hardy, D., Ndubizu, E., 2008, "Recovery of [CO2]T from Aqueous Bicarbonate using a Gas Permeable Membrane," Naval Research Laboratory, NRL/MR/6180--08-9129, Washington, DC.

[24] Coffey, T., Hardy, D., Besenbruch, G., 2003, "Hydrogen as Fuel for DOD," Defense Horizons, (36) pp. 1-12.

[25] Terry, K., 1995, "NEng Thesis: Synthetic Fuels for Naval Applications Produced Using Shipboard Nuclear Power," Massachusetts Institute of Technology (DSpace@mit), http://hdl.handle.net/1721.1/11590, Cambridge, MA.

[26] Werner, S., and Morgan, J., 1970, "Aquatic Chemistry: An Introduction Emphasizing Chemical Equilibrium in Natural Waters," Wiley-Interscience, New York, pp. 780.

[27] Willauer, H., Hardy, D., Ndubizu, E., 2009, "Extraction of Carbon Dioxide from Sea water by Ion Exchange Resin Part II: Using Strong Base Anion Exchange Resin," Office of Naval Research, NRL/MR/6180--09-9211, Washington, DC.

[28] Willauer, H., Hardy, D., Lewis, K., 2010, "Effects of Pressure on the Recovery of CO2 by Phase Transition from a Seawater System by Means of Multilayer Gas Permeable Membranes," Journal of Physical Chemistry, **114**pp. 4003-4008.

[29] Dooley, J., Davidson, C., and Dahowski, R., 2009, "An Assessment of the Commercial Availability of Carbon Dioxide Capture and Storage Technologies as of June 2009," Pacific Northwest National Laboratory, PNNL-18520, Richland, WA.

[30] Lackner, K. S., 2009, "Capture of Carbon Dioxide from Ambient Air," The European Physical Journal (Special Topics), **176**pp. 93-106.

[31] Ranjan, M., 2010, "M.S. Thesis: Feasibility of Air Capture," Massachusetts Institute of Technology, http://hdl.handle.net/1721.1/59782, Cambridge, MA.

[32] Lackner, K. S., 2009, "Managing Emissions from Fossil Energy Resources," pp. 1-45.

[33] Darwish, M. A., and Al-Najem, N., 2000, "Energy Consumption by Multi-Stage Flash and Reverse Osmosis Desalters," Applied Thermal Engineering, **20**pp. 399-416.

[34] Village Marine, 2009, "Military R.O. Systems," **2010**(8/10) pp. 1.

[35] Village Marine, 2009, "Expeditionary Unit Water Purification Systems, Generation 2," **2010**(8/10) pp. 1.

[36] Statoil Hydrogen Technologies, 2010, "Electrolyzer Products," **2010**(8/12) pp. 1.

[37] Stoots, C., 2010, "Production of Synthesis Gas by High-Temperature Electrolysis of H2O and CO2 (Coelectrolysis)," Sustainable Fuels from CO2, H2O, and Carbon-Free Energy, Idaho National Laboratory, Idaho Falls, ID, pp. 1-21.

[38] O'Brien, J., Herring, J., Stoots, C., 2009, "Status of the INL High-Temperature ElectrolysisResearch Program–Experimental and Modeling," Idaho National Laboratory, INL/CON-09-15618, Idaho Falls, ID.

[39] Stoots, C., O'Brien, J., McKellar, M., 2005, "Engineering Process Model For High-Temperature Electrolysis: System Performance Evaluation," Idaho National Laboratory, INL/CON-05-00725, Idaho Falls, ID.

[40] O'Brien, J., McKellar, M., Stoots, C., 2007, "Parametric Study of Large-Scale Production of Syngas via High Temperature Co-Electrolysis," AIChE Annual Meeting, R. Green, ed. Idaho National Laboratory, Idaho Falls, ID, pp. 1-20.

[41] Haratyk, G., 2010, "1-D MATLAB High Temperature Steam Electrolysis Model, MIT Department of Nuclear Science and Engineering" **R2009a**.

[42] Stoots, C., O'Brien, J., and Hartvigsen, J., 2009, "Results of Recent High Temperature Coelectrolysis Studies at the Idaho National Laboratory," International Journal of Hydrogen Energy, **34**pp. 4208-4215.

[43] Forsberg, C., 2006, "Goals, Requirements, and Design Implications for the Advanced High-Temperature Reactor," American Society of Mechanical Engineers, Paper ICONE14-89305 (CD-ROM), New York, NY.

[44] O'Brien, J., McKellar, J., Hawkes, G., 2007, "Development and Validation of a One-Dimensional Co-Electrolysis Model for Use in Large-Scale Process Modeling Analysis," Idaho National Laboratory, INL/CON-07-12236, Idaho Falls, ID.

[45] Stoots, C., 2010, "Correlation for the Reverse Gas Shift Reaction (RWGS) Equilibrium Constant as a Function of Gas Temperature, Keq(T)," **Email to author of emprically derived equilibrium constant used to solve coelectrolysis model (7/20/2010)**pp. 1-1.

[46] Haratyk, G., 2010, "1-D MATLAB Coelectrolysis Model (Rev 1), MIT Department of Nuclear Science and Engineering" **R2009a**.

[47] Stoots, C., O'Brien, J., Herring, J., 2009, "Long-Term Degradation Testing of High-Temperature Electrolytic Cells," Idaho National Laboratory, INL/EXT-09-16559, Idaho Falls, ID.

[48] Doty, F., Holte, L., and Shevgoor, S., 2009, "Securing Our Transportation Future by Using Off-Peak Wind Energy to Recycle CO2 into Fuels," ASME 3rd International Conference on Energy Sustainability, F. Doty, ed. ASME, Columbia, SC, **ES2009-90182,** pp. 1-8.

[49] Bustamante, F., Enick, R., Rothenberger, K., 2002, "Kinetic Study of the Reverse Water Gas Shift Reaction in High-Temperature, High-Pressure Homogeneous Systems," Fuel Chemistry Preprints, **47**(2) pp. 663-664.

[50] Doty, F., 2008, "Hydrocarbon and Alcohol Fuels from Variable Renewable Energy at very High Efficiency," **WO 2008/115993 A1**(N/A) pp. 1-89.

[51] Trimm, D. L., 2005, "Minimisation of Carbon Monoxide in a Hydrogen Stream for Fuel Cell Application," Applied Catalysts: A General, **296**pp. 1-11.

[52] Joo, O., Jung, K., Moon, I., 1999, "Carbon Dioxide Hydrogenation to Form Methanol Via a Reverse-Water-Gas-Shift Reaction (the CAMERE Process)," Industrial and Engineering Chemical Research, **38**pp. 1808-1812.

[53] Doty, F., Shevgoor, S., and Staab, J., 2009, "Practical Application of a Compact, High Effectiveness, Gas-to-Gas Compound Recuperator with Liquid Intermediary (CRLI)," Proceedings of the ASME 2009 Heat Transfer Conference, K. Edick, ed. ASME, San Francisco, CA, **HT2009-88372,** pp. 1-7.

[54] Kasuya, F., and Tsuji, T., 1991, "High Purity CO Gas by Pressure Swing Adsorption," Gas Separation and Purification, **5**(4) pp. 242-246.

[55] Dutta, N. N., and Patil, G. S., 1995, "Developments in CO Separation," Gas Separation and Purification, **9**(4) pp. 277-283.

[56] Damle, A., 2009, "Hydrogen Fuel: Production, Transport and Storage,"Taylor and Francis Group, LLC, London, UK, pp. 283-317, Chap. 8.

[57] Adhikari, S., and Fernando, S., 2006, "Hydrogen Membrane Separation Techniques," Industrial and Engineering Chemical Research, **45**(3) pp. 875-881.

[58] Holladay, J. D., Hu, J., King, D. L., 2009, "An Overview of Hydrogen Production Technologies," Catalysts Today, **139**pp. 244-260.

[59] Liu, K., Deluga, G., Bitsch-Larsen, A., 2010, "Hydrogen and Syngas Production and Purification Technologies,"Wiley-Interscience, New York, NY, pp. 127-151, Chap. 3.

[60] Ersoza, A., Olguna, H., Ozdoganb, S., 2003, "Autothermal Reforming as a Hydrocarbon Fuel Processing Option for PEM Fuel Cell," Journal of Power Sources, **118**pp. 384-392.

[61] Qi, A., Wang, S., Changjun, N., 2007, "Autothermal Reforming of Gasoline on Rh-Based Monolithic Catalysts," International Journal of Hydrogen Energy, **32**pp. 981-991.

[62] Lee, S., 2007, "Handbook of Alternative Fuel Technologies,"CRC Press, Boca Raton, FL, pp. 297-320, Chap. 9.

[63] Liu, X., Lu, G., Yan, Z., 2003, "Recent Advances in Catalysts for Methanol Synthesis Via Hydrogenation of CO and CO2," Industrial and Engineering Chemical Research, **42**pp. 6518-6530.

[64] Hindman, M., 2010, "Methanol to Gasoline (MTG) Technology: An Alternative for Liquid Fuel

Production," ExxonMobil,

April, http://www.exxonmobil.com/Apps/RefiningTechnologies/presentations.aspx.

[65] Tabak, S., and Yurchak, S., 1990, "Conversion of Methanol Over ZSM-5 to Fuels and Chemicals,"

Catalysts Today, **6**(3) pp. 307-327.

[66] Mavrikakis, M., Maravelias, C., Stewart, C., 2009, "Fundamentals of Synthetic Conversion of CO2 to

Simple Hydrocarbon Fuels," Sandia National Laboratory, SAND2009-7489, Albuquerque, NM.

[67] Keil, F., 1999, "Methanol-to-Hydrocarbons: Process Technology," Microporous and Mesoporous

Materials, **29**pp. 49-66.

[68] Tabak, S., Avidan, A., and Krambeck, F., 1986, "Production of Synthetic Gasoline and Diesel Fuel

from Non-petroleum Sources," Symposium on the Surface Science of Coal Liquification Catalysts: Alcohol

Synthesis, J. Bartlett, ed. American Chemical Society, New York, NY, **31,** pp. 67-73.

[69] Harandi, M., 1993, "Integrated Process for Converting Methanol to Gasoline and Distillates,"

769,508(5,117,279) pp. 1-15.

[70] Degnan, T., 2007, "Recent Progress in the Development of Zeolitic Catalysts for the Petroleum

Refining and Petrochemical Manufacturing Industries," Studies in Surface Science and Catalysts, **170**pp.

54-65.

[71] Sapre, A., Poturovic, J., Dandekar, A., 2005, "ExxonMobil Advanced Technologies: Refiner's Solution

to Present & Future Industry Challenges," 10th Annual European Refining Technology Conference,

ExxonMobil, Vienna, Austria, pp. 1-30.

[72] Kuechler, K., Brown, S., Puttemans, M., 2010, "Feedstock Preparation of Olefins for Oligomerization to Produce Fuels," **11/489,114**(US 7,741,526 B2) pp. 1-30.

[73] Kuechler, K., 2010, "Olefin Oligomerization to Produce Hydrocarbon Composition Useful as Fuels," **11/342,385**(US 7,678,954 B2) pp. 1-25.

[74] Leckel, D., 2009, "Diesel Production from Fischer-Tropsch: The Past, the Present, and New Concepts," Energy & Fuels, **23**pp. 2342-2358.

[75] Van der Laan, G., 1999, "PhD Thesis: Kinetics, Selectivity and Scale Up of the Fischer-Tropsch Synthesis," University of Groningen, http://irs.ub.rug.nl/ppn/181518880, Netherlands.

[76] Ceramatic, 2009, "Production of Military Synthetic Fuel," Office of Naval Research, N00014-09-C-0441, Arlington, VA.

[77] McDaniels, J., 2010, "Unlocking Biofuels with Microchannel Technology," Velocys, Plain City, OH.

[78] Espinoza, R., Steynberg, A., Jager, B., 1999, "Low Temperature Fischer–Tropsch Synthesis from a Sasol Perspective," Applied Catalysts: A General, **186**pp. 13-26.

[79] Tonkovich, A., Kuhlmann, D., Rogers, A., 2005, "Microchannel Technology Scale Up to Commercial Capacity," Chemical Engineering Research and Design, **83**(A6) pp. 634-639.

[80] Lerou, J., 2010, "Enabling Small Scale GTL," Velocys, Plain City, OH.

[81] Fitzgerald, S., Yang, B., Taha, R., 2008, "Reduced Complexity in Representation of Fischer-Tropsch Chemistry," Velocys, Plain City, OH.

[82] Dutta, S., 2010, "Synfuel Production on Naval Tanker," **Email communication with author regarding size of synthetic fuel system components (7/29/2010)**pp. 1.

[83] Castaldi, M., 2010, "Hydrogen and Syngas Production and Purification Technologies,"Wiley-Interscience, New York, NY, pp. 329-356, Chap. 7.

[84] Jones, D., and Pujado, P., 2006, "Handbook of Petroleum Processing," Springer, Dordrecht, Netherlands, pp. 1353.

[85] Linstrom, P., and Mallard, W., 2010, "NIST Chemistry WebBook, NIST Standard Reference Database Number 69," National Institute of Standards and Technology, Gaithersburg, MD, pp. N/A.

[86] Newswire, 2010, "Shell Kicks Off Pearl GTL Start," Upstreamonline.Com, **Exploration and Production** pp. 1.

[87] Evans, D., 2008, "Pearl GTL Set for Big Payback," Upstreamonline.Com, **Exploration and Production** pp. 1.

[88] Forsberg, C., 2010, "Pearl GTL Project in Qatar: Nuclear Tanker," **Email communication with author regarding implications of Shell GTL Project on Catalyst Design (9/15/2010)**pp. 1.

(This Page Intentionally Blank)

4   Reactor Plant and Power Cycle

4.1 Introduction

4.1.1   Power Plant Power and Temperature Requirements

Chapter 3 shows that liquid fuels production requires significant amounts of energy. Even with a nearly ideal scenario (i.e., perfect autothermal reforming (ATR), best case Fischer-Tropsch (FT) synthesis, etc.), liquid fuels production utilizing alkaline electrolysis for H_2 production and the reverse water gas shift (RWGS) reaction for CO production requires 874 MW_e and 78.4 MW_{th}. The more advanced option, which uses a combination of high temperature steam electrolysis (HTSE) and high temperature co-electrolysis (HTCE) for H_2 and CO production requires 650 MW_e and 171 MW_{th}. Both of these figures assume that an advanced power cycle provides high temperature (670 ^{o}C) heat to a system operating in a steady state condition. During plant startup, the electrical power demand is limited by the number of electrolysis cells, air capture units, compressors, etc., which limits startup electrical power to steady state electrical power. Capacity increases over time, to a maximum of 6,400 BBL/Day, as non-JP-5 hydrocarbons are recycled back into the system via ATR. However, the power plant must deliver more thermal power during startup because it cannot recuperate heat until the various liquid fuel production processes commence[14]. Although the additional plant capacity required for startup is an important consideration, the temperature of the delivered heat input is even more crucial. As chapter 3 shows, all of the processes in the liquid fuels production plant require a precise temperature and pressure in order to sustain the desired chemical reactions, which are summarized for convenience in Table 4-1:

---

[14] Precisely determining the non-steady state heat load during startup requires simulation beyond the scope of this thesis. The values given assume the most conservative case where no recycle heat is available and startup is not ramped up over a prolonged period. In reality, the required heat load decreases over time as more heat can be recuperated. Appendix D includes a calculation for the maximum required thermal power input for the alkaline electrolysis and HTCE/HTSE cases. Startup time is plant specific, but most liquid fuel production processes described in patent literature assume ~ 50 hours to attain steady state conditions.

Process	Pressure (MPa)	Temperature (^{o}C)
Fischer-Tropsch Synthesis	3.0	250
Autothermal Reforming	0.3	700
Alkylation	5.0	150
Aromatization	5.0	350
Hydrotreating	5.0	150
Hydrocracking	5.0	150
Oligomerization	5.0	150
Reverse Water Gas Shift RXN	1.0	467
High Temperature Steam Electrolysis	3.0	800
High Temperature Co-Electrolysis	3.0	800

Table 4-1 - Summary of Liquid Fuels Production Pressures and Temperatures[15]

Although the pressures required by the various processes in Table 4-1 are manageable, several of the processes require temperatures that are well above 300 ^{o}C, which is the nominal primary coolant temperature of conventional pressurized water reactors (PWRs). For liquid fuels production via alkaline electrolysis, conversion of CO_2 to CO via RWGS, refining raw Fischer-Tropsch syncrude into JP-5, and recycling unused hydrocarbon products back to H_2/CO syngas all require "high temperature" heat that exceeds PWR operating temperature. The temperature demand is even more pronounced for the HTCE/HTSE case. As chapter 3 demonstrated, however, the required temperatures for liquid fuels production could be attained by using electric heaters to increase temperatures where necessary; and intelligent heat recuperation could minimize electric heater power demand. During normal operation, each "high temperature" process should only require sets of cycling "steady state" heaters, which cycle on and off at prescribed temperatures in order to offset ambient heat losses. Such losses typically have negligible power requirements to accommodate.

The calculations performed in chapter 3 show that a PWR power source is feasible option in a liquid fuels production scheme. However, this chapter shows in the following sections that an advanced salt-cooled high temperature reactor is better suited for this purpose, especially when coupled to an advanced power cycle. Constraining the reactor plant to a PWR necessitates using a reactor core with a

---

[15] The RWGS reaction applies only to the alkaline electrolysis case. HTCE and HTSE do not apply to the alkaline electrolysis case.

higher rated power as well as PCS machinery requiring a much larger footprint. Despite the USN's familiarity with PWRs and a Rankine PCS, the advantages afforded through the use of high temperature reactors and more compact Brayton cycle machinery are too significant to ignore, especially for shipboard applications.

4.1.2   Overview of Power Plant Options

Nuclear reactors are typically classified by power output and the peak temperatures of their coolants. Light water reactors (LWRs), such as the PWRs used on nuclear-powered US Navy (USN) warships, are low-temperature, high-pressure reactors. Fast reactors cooled with liquid sodium operate at medium temperatures and low pressures. High temperature reactors can use either (1) high-pressure gases or (2) low-pressure liquids (such as salt) with boiling points above peak operating temperatures for reactor coolants [1]. Figure 4-1, adapted from reference [1], succinctly compares various reactor plant types by their temperature and power output:
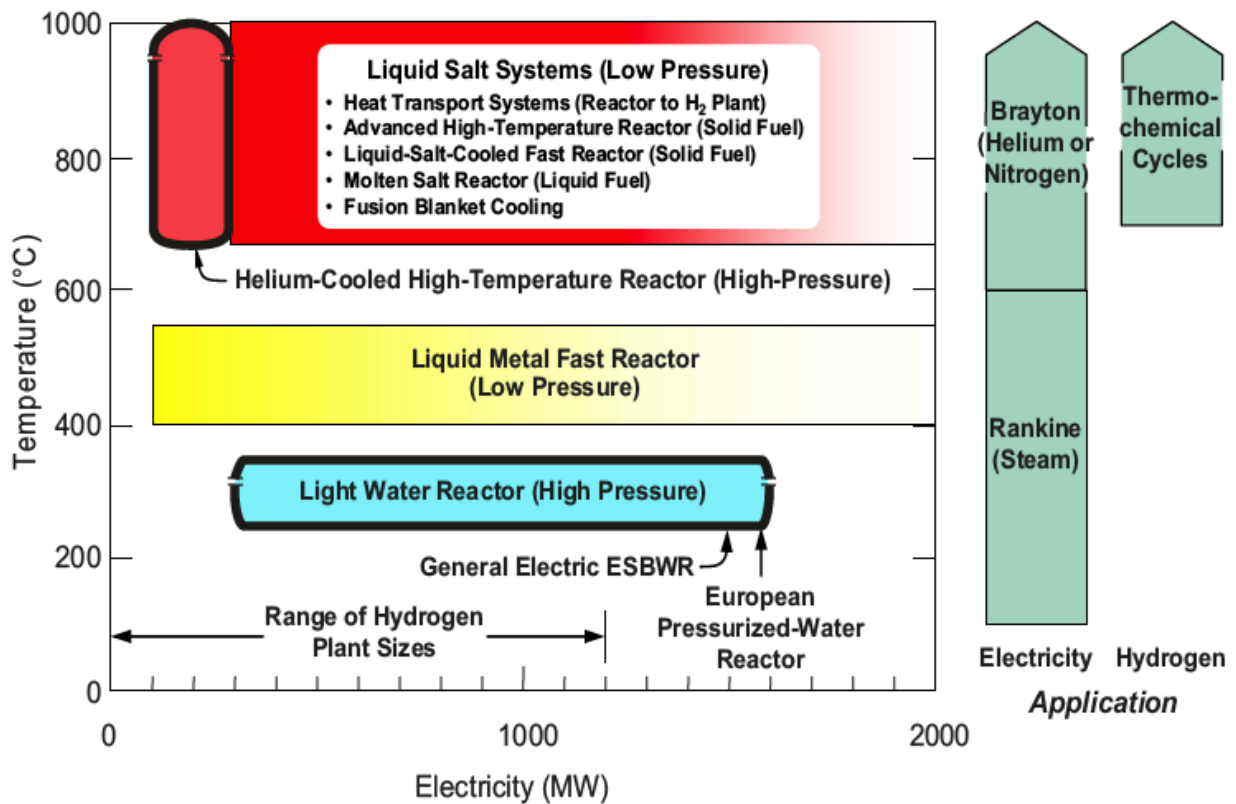
Figure 4-1 - Reactor Plant Type vs Temperature

In considering Figure 4-1, the two possible approaches for configuring a reactor plant system to supply the energy and high temperature heat for liquid fuels production are to either modify an existing reactor plant system to satisfy the power and temperature requirements of section 4.1.1 or to develop a new reactor system specifically engineered for the application.

The USN has a visceral aversion to using any reactor plant system other than a PWR [2], primarily because PWRs more than adequately satisfy the power and propulsion needs of any warship in its current or projected arsenal. Naval Reactors (NAVSEA 08) is extremely reluctant to tinker with technology that it has mastered with such an admirable safety record, especially when newer technology threatens to be much more expensive. However, the temperature requirements for the liquid fuels production plant (Table 4-1 above) provide justification for considering alternative reactor plant designs.

A limitation with using LWRs coupled to a Rankine cycle is that, for practical reasons, the peak temperature of a Rankine cycle steam turbine is ~ 550 ^{o}C [1], well below the desired temperature for ATR or high temperature H_2 production. Such a limitation would exist even if more advanced cladding materials (e.g., SiC) were available for a LWR core. As chapter 3 demonstrates, a potential solution to this problem is utilizing electric heaters (or something equivalent) to increase temperature where required to supplement recuperation and/or startup. However, a more desirable option is the use of high temperature Brayton cycles, which can utilize higher temperature heat to more efficiently produce electricity. Furthermore, Brayton cycle power conversion system (PCS) machinery tends to require a smaller footprint, an important consideration for shipboard applications.

At the present time, only gas-cooled (Helium) reactors have the capability to generate higher temperatures, but current systems are connected to steam cycles. Advanced, direct Brayton cycle gas-cooled reactor designs are under development [3]. The most promising reactor plant concept for liquid fuels production is the liquid salt cooled advanced high temperature reactor (AHTR), which is explained in more detail later in the following sections. Compared to a gas-cooled reactor, the low pressure AHTR is able to achieve superior passive safety at much higher power output for a similar size reactor due to the higher volumetric heat capacity and better natural circulation characteristics of liquid salt [4]. Another consideration is that the liquid fuels production plant contains a relatively large inventory of hazardous chemicals. With boiling points ~ 1,400 °C, a low-pressure molten salt coolant avoids the potential for chemical plant pressurization. Furthermore, the salt coolants under consideration do not react with air and only slowly react with water [5].

118

4.2 Advanced High Temperature Reactor (AHTR) Option

4.2.1 AHTR Overview

Conceptually developed in 2003 [6], the AHTR is an innovative combination of four existing reactor technologies [1]:

- Tristructural-isotropic (TRISO) particle, graphite matrix nuclear fuel (high temperature, graphite neutron moderation … derived from the high-temperature, gas-cooled reactor)
- Clean, high-temperature, low-pressure, transparent liquid salt coolant (derived from experience with the molten salt reactor)
- Passive safety systems and plant design (derived from the sodium-cooled fast reactor)
- Brayton power cycle (derived from natural gas fired plants)

Each of these technologies, discussed in more detail below, affords numerous advantages. TRISO fuel particles, which are small particles of uranium dioxide coated with layers of carbon and silicon carbide, can operate with a peak temperature of ~ 1,200 ^{o}C; significant fuel failure does not occur until ~ 1,600 ^{o}C [3]. A shortcoming of the graphite TRISO particles is that they are only compatible with helium and fluoride salts [4]. Compared to helium, liquid salt is a superior coolant. For the same power density, fuel-to-coolant temperature difference is 50 to 100 ^{o}C less in a salt-cooled reactor, with an equivalent drop in peak fuel temperature [7]. This additional thermal margin permits a higher coolant outlet temperature, a higher power density, or a smaller size core [8]. The TRISO fuel and the salt coolant provide inherent passive safety[16] to the AHTR design. In event of a reactor accident, the system design transports reactor decay heat into the ground, which (along with the high-temperature capabilities of the fuel) avoids exceeding catastrophic fuel failure temperature limits. Additionally, the low-pressure coolant (1) eliminates a driving force moving radionuclides to the environment and (2) dissolves and holds most fission products (including iodine and cesium) and actinides should these materials escape from the fuel [9]. Finally, Brayton cycle technology provides a method to efficiently utilize the AHTR's high-temperature heat for much more efficient power generation [1].

---

[16] Passive safety is defined here as a system that uses active components in a very limited way to initiate subsequent passive operation.

4.2.2 ATHR Fuel Design

4.2.2.1 Civilian Reactors vs. Naval Reactors

Generally speaking, USN reactor cores have a much different operating profile than their larger, commercial counterparts. When online, commercial reactors operate at maximum power. Naval reactors, however, are used not only for power generation but also propulsion. Therefore, USN reactor cores are designed for frequent maneuvers over a wide ranging power level. The USN claims that reactors on newer warships can last the lifetime of the ship without refueling. Because of their smaller size, different operating profile, and longer operating lifetime, USN reactors require nuclear fuel loadings that are much different from civilian reactors. One could argue that examining the merits of publically available nuclear fuel design investigations for USN reactor applications is a fruitless endeavor due to their dissimilar goals and requirements. The following assumption obviates this concern: the AHTR used for the shipboard liquid fuels production application shall be assumed to operate almost continuously at maximum power, similar to a commercial reactor's operating profile. The justifications of this assumption are:

- Warships tend to operate <15 knots more than 80% of the total time underway [10]. Fifteen knots corresponds to ~ 9.5 MW_e (brake power) for a T-AOE-187 (*Henry Kaiser* class) tanker ship [11], which is less than 1.5% of the total loading for the HTCE/HTSE option.
- Because the increased electrical demands on modern warships rival (or even exceed) propulsion system requirements, the USN desires to construct electric drive ships that are fully integrated with the ship's electrical distribution system (IPS) [12]. By utilizing energy storage devices and through load center distribution, electric drive ships provide more constant load to the prime mover.
- Conventionally powered prime movers (e.g., gas turbine or diesel engines) could also provide propulsive power to the vessel, using fuel produced via the ship's onboard liquid fuels production plant. This would decouple the reactor from the propulsion system, thereby simplifying operations by allowing operators to solely concentrate on the complicated task of liquid fuels production.

4.2.2.2   AHTR Fuel Design Options

The base fuel element is the TRISO coated fuel particle, which is about the size of a sand grain. The multiple coatings of carbon and silicon carbide act as a high-temperature equivalent of metallic cladding, and it is the only demonstrated fuel type capable of operations for extended periods of time at high-temperatures with high burnups [4]. These particles are incorporated into a graphite matrix that can be molded into any desired geometric shape, but the current designs are the prismatic block, the fuel pebble, and the stringer [3, 6]:
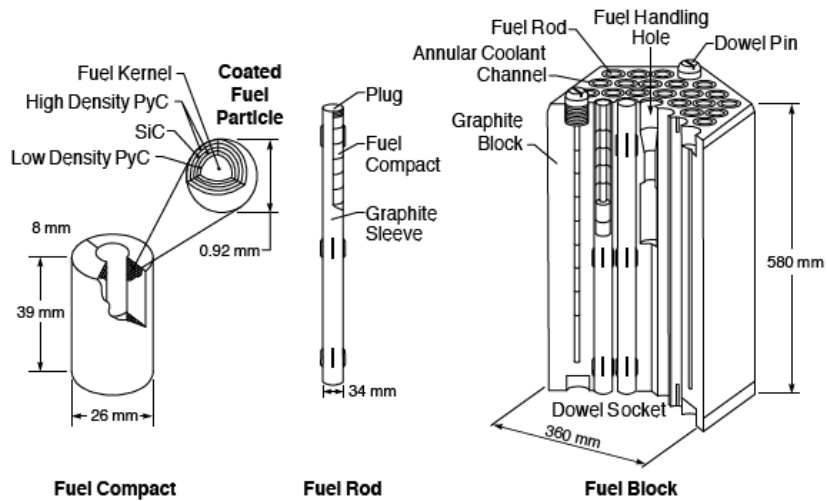
Figure 4-2 - Fuel Particles Incorporated into Prismatic Hexagonal Block Design
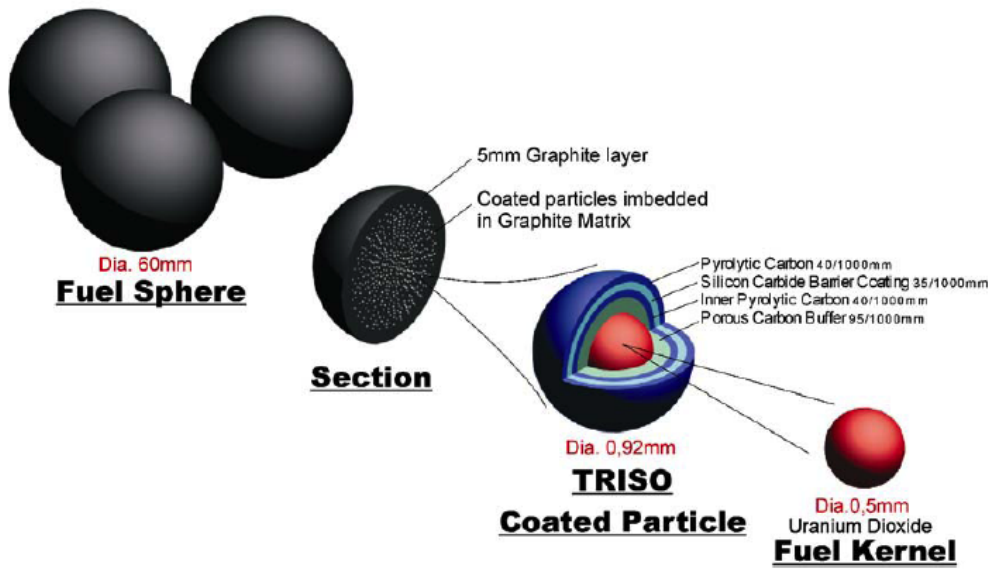
Figure 4-3 - Fuel Particles Incorporated into Pebble Fuel Design
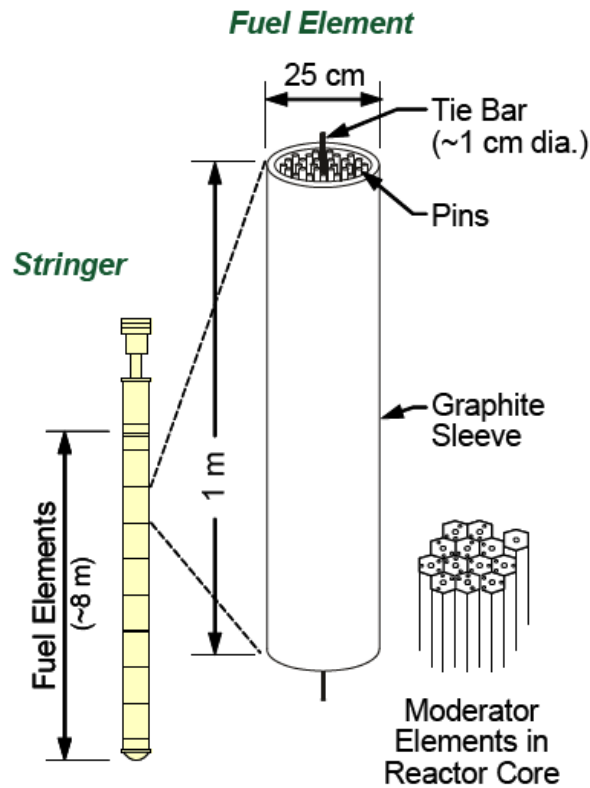
Figure 4-4 - Fuel Particles Incorporated into Stringer Design

The prismatic block fuel (Figure 4-2 above) is the baseline design that has been studied most extensively. Since the Fort St. Vrain helium cooled reactor (1973-1989) utilized this design, it is by far the most proven option [6]. Compared to the other options, it also provides maximum freedom in core design. The core designer has great flexibility in choosing (1) the ratio of the fuel to the moderator and to the coolant and (2) the three dimensional neutronic characteristics. Compared to the other options, however, the prismatic block design is more expensive and much more difficult to refuel (more-complicated three-dimensional fuel-handling operations and a fuel assembly that also contains the moderator) [4]. However, in the present application, since batch refueling is the only practical option, axial segmentation is not as significant a drawback.

The pebble bed reactor (PBR) design uses the coated-particle fuel in a graphite matrix compacted into pebbles, ~6 cm in diameter (Figure 4-3 above); the core is a bed of the fuel pebbles. Although not as proven as the prismatic block design, two helium-cooled PBRs have been built, operated, and decommissioned in Germany, and a small pebblebed test reactor has been recently built in China. PBRs are refueled online at operating temperature. A slow, continuous flow of pebbles occurs through the reactor core, with pebbles added at the top of the core and removed at the bottom. Extracted pebbles are sent through a radiation detector that determines burnup as well as the disposition of the pebble as spent nuclear fuel (SNF) for disposal or for recycle back to the core for additional burnup (a process that can repeat several times):
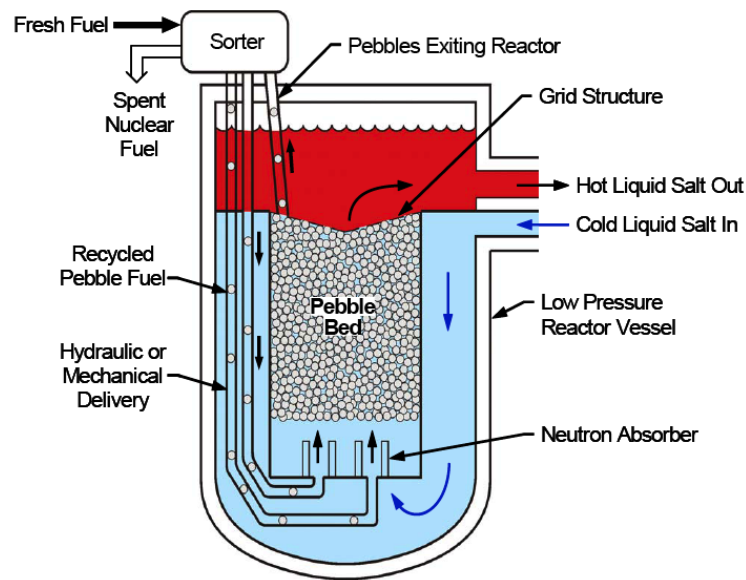
Figure 4-5 - Illustration of PBR Refueling

PBRs operate with very low excess reactivity and relatively low enrichments. Current estimates indicate that pebbles have the lowest fabrication cost of any of the three fuel geometry options [4].

Despite the reduced cost and ease of refueling, the PBR option is probably not suitable for marine applications. The core geometry is not precisely defined. Operating a reactor outside of precisely known parameters would require a change in the nuclear navy's cultural mindset. The constant pitch, roll, and yaw motions of an underway vessel (not to mention the occasional extreme maneuvers) could cause undesired perturbations in the online refueling system. Furthermore, a failure in the online refueling system while underway would be very inconvenient even in the best of circumstances. Finally, additional infrastructure and handling would be necessary to accommodate the additional refueling logistics. The increased handling of radioactive material (RAM) – especially highly radioactive SNF – would increase the risk of an incident the USN would rather avoid. Should the need ever arise, transporting additional fuel pebbles to a deployed asset could prove problematic.

The stringer fuel design (Figure 4-4 above) consists of multiple fuel assemblies, neutron moderator sections, radiation shielding, thermal insulation, pressure seals, and other components, and was designed for the advanced gas reactor (AGR);[17] it has a similar pin design to the Japanese high-temperature test reactor (HTTR). For gas-cooled reactor designs, a 1 cm nimonic® alloy PE16 tie bar goes through each fuel assembly and holds them together as a single unit on a stringer. The graphite sleeve provides a gas flow channel, serves as part of the assembly with the grid structure that holds the fuel pins in the proper geometry, and provides some radiation shielding to reduce the rate of radiation damage to the permanent graphite in the reactor core. The sleeve is part of the SNF and is separated from the SNF pins for the purposes of disposal [7]. The tubes are mounted inside individual coolant channels of the prismatic fuel block (see Figure 4-6 below) [6]. This arrangement maximizes heat transfer from fuel to coolant and is used to minimize peak fuel temperature. Separating most of the graphite from the fuel and the coolant provides extra degrees of design freedom, but the arrangement also results in significant neutron spectrum differences from inner-row to outer-row pins.

---

[17] AGR refers to the British CO_2-cooled, graphite-moderated gas reactor (~ 638 ^{o}C) coupled to a Rankine PCS.
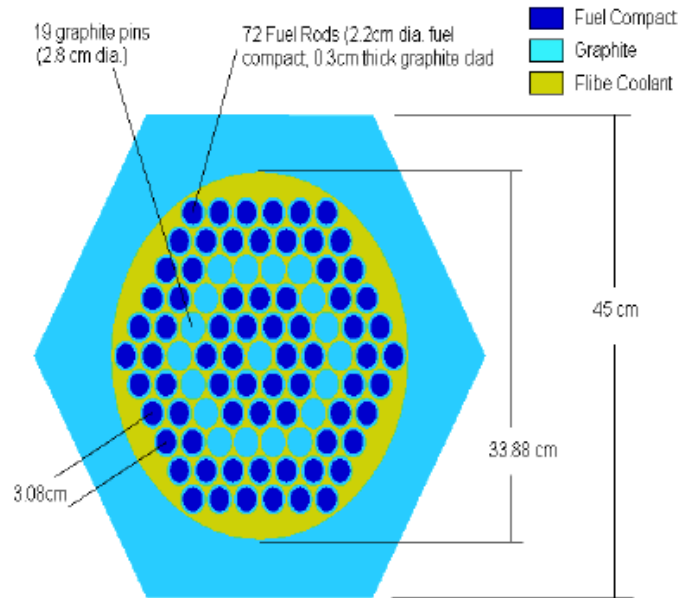
Figure 4-6 - Stringer Fuel Arrangement

The core design and stringer approach is potentially viable for the AHTR. The stainless steel grid structure that holds the AGR fuel pins in place and the tie rod could be replaced by carbon–carbon composites. A preliminary assessment of the carbon–carbon technology and the AGR design has not identified any insurmountable fabrication challenges to create an equivalent carbon–carbon composite; however, only limited analysis of such fuel designs has been performed, and significant fuel development effort would be required [7]. The main utility of the stringer fuel design is the ability to refuel the core with the reactor online. The advantages of such a feature are obvious for commercial applications; however, online refueling capability is of little use for a marine platform. The refueling would have to be completed pierside, or in drydock, which are instances where the reactor is normally shutdown and the ship is supplied by shore power. In addition to developing the additional infrastructure needed to accommodate the unique refueling operation, reactor refueling operations would become more frequent, thereby increasing the risk of a SNF related handling incident. For these reasons, the stringer fuel design is barely more suitable than the pebblebed design. Hence, prismatic block fuel is the option of choice.

4.2.2.3 *Performance Characteristics of AHTR Fuel*

Since an AHTR operates at higher temperatures compared to a PWR, it is more efficient, and therefore consumes less fuel per unit generation of electricity. Salt-cooled reactors also have superior performance to gas-cooled reactors, which is a consequence of the high coolant pumping requirements in gas-cooled reactors. In order to minimize this loss, a gas-cooled reactor must have larger temperature rises across the core than a salt-cooled reactor. Therefore, for the same peak coolant temperature, a gas-cooled reactor will have a lower average temperature of delivered heat to the power conversion system compared to a salt-cooled reactor, and therefore lower plant efficiency [13].

In reference [14], Oak Ridge National Laboratory (ORNL) demonstrates the superior fuel performance in a salt-cooled (compared to gas-cooled) reactor. The power density of the baseline AHTR (10.2 MW/m^3) is ~ 50% higher than that of the helium-cooled VHTR (6.6 MW/m^3). Parametric results of the ORNL study show that power density could be increased even higher:

Parameter	VHTR (He-Cooled)	AHTR (Salt-Cooled)		
Power (MW$_{th}$)	600	2400		
Total # Fuel Columns	102	265	211	169
Power Density (MW/m^3)	6.6	10.2	12.8	15.9
Specific Power Density (MW/t)	103	158	199	248
Single Batch — Enrichment (%)		10.4	13.0	16.3
Single Batch — Burnup (GWd/t)		78	98	122
Two Batch — Enrichment (%)	14.0	15.3	19.5	24.7
Two Batch — Burnup (GWd/t)	100	156	196	244
Three Batch — Enrichment (%)		20.6	26.2	33.1
Three Batch — Burnup (GWd/t)		234	293	366

Table 4-2 - Power Density Parametric Study Results

While the investigation of single-, two-, and three-batch refueling schemes is not particularly relevant for a USN reactor, Table 4-2 shows that increasing the reference AHTR core power density 150% requires increasing uranium enrichment to less than 20% for the single-batch fuel management scheme.

Because of the AHTR's improved efficiency and core characteristics, it actually consumes less fuel than gas-cooled reactors and LWRs as reference [6] shows in Table 4-3:

Parameter	LWR	Salt-Cooled PB-AHTR	He-Cooled PBMR
Burnup (MWt-day/kg)	55	117	80
Fuel Enrichment	5.0	10.0	8.1
Carbon/Heavy Metal	0	363	425
Thermal Efficiency (%)	33	46	42
HM Mass (g/pebble)	-	10.06	9.0
Relative U Consumption	1.00	0.70	0.90
Relative SWU Consumption	1.00	0.81	1.00
Relative Spent Fuel Volume	-	0.56	1.00

Table 4-3 - Fuel Consumption Comparison

The salt-cooled reactor, as shown in Table 4-3, consumes the least amount of fuel, has the highest burnup, and has the greatest cycle efficiency of all three reactor types. Since the AHTR uses TRISO fuel, it could also take advantage of the "deep burn"[18] concepts developed for He-cooled reactors to increase core lifetime even more (see reference [15] for details). Although an analysis of deep burn feasibility for the AHTR is beyond the scope of this thesis, subsequent deep burn investigation could make an AHTR even more attractive.

4.2.3 Reactor Size and Safety Implications of Salt-Coolant

As previously mentioned, the reduced core temperature difference for a given power density provides additional thermal margin that can be exploited to increase core outlet temperatures or increase power density and reduce core size. Table 4-2 and Table 4-3 show not only the significant increase in power density possible, but also the reduced fuel consumption. Figure 4-7 provides an illustration (not to scale) of the rather significant size difference between a gas-cooled and salt-cooled reactor [6]:

---

[18] "Deep burn" refers to the concept proposed by General Atomics (GA), where TRISO particles consume plutonium, neptunium, and americium transuranic nuclides, and are driven to more than 500 MW_e-day/kg burnup.
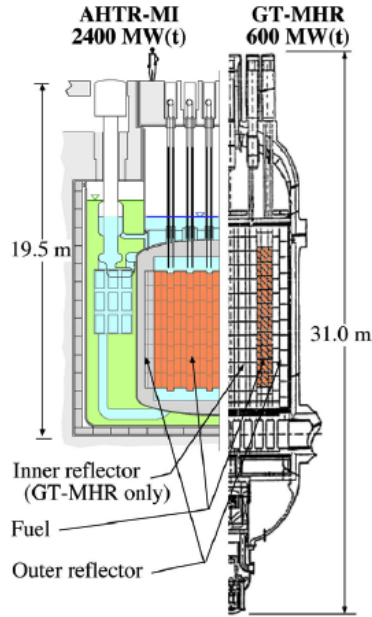
Figure 4-7 - Size Comparison of Salt-Cooled vs. Gas-Cooled Reactor (Note Rating Difference)

In addition to the 37% reduction in vessel height, Figure 4-7 and Table 4-2 also show a rather dramatic difference in rated power level, 600 MW_{th} for the He-cooled reactor and 2,400 MW_{th} for the salt-cooled reactor. This significant difference is a result of decay heat removal (DHR) requirements under accident conditions. For a gas-cooled reactor under accident conditions when the reactor is depressurized, natural circulation of gases cannot efficiently transport heat from the fuel to the reactor vessel; instead, decay heat is removed by conduction of heat from the fuel to the reactor vessel. Therefore, the rated power of the gas-cooled reactor must be limited to ~600 MW_{th} in order to ensure fuel failure does not occur. In the AHTR, natural circulation of liquid salts efficiently moves heat from anywhere in the reactor core to the reactor vessel. Reactor size is thus limited by the ability to remove heat from the vessel, not the ability to move heat from the fuel to the vessel wall, thereby facilitating a higher allowed rated power [9]. Figure 4-8 provides an explanatory illustration [8]:
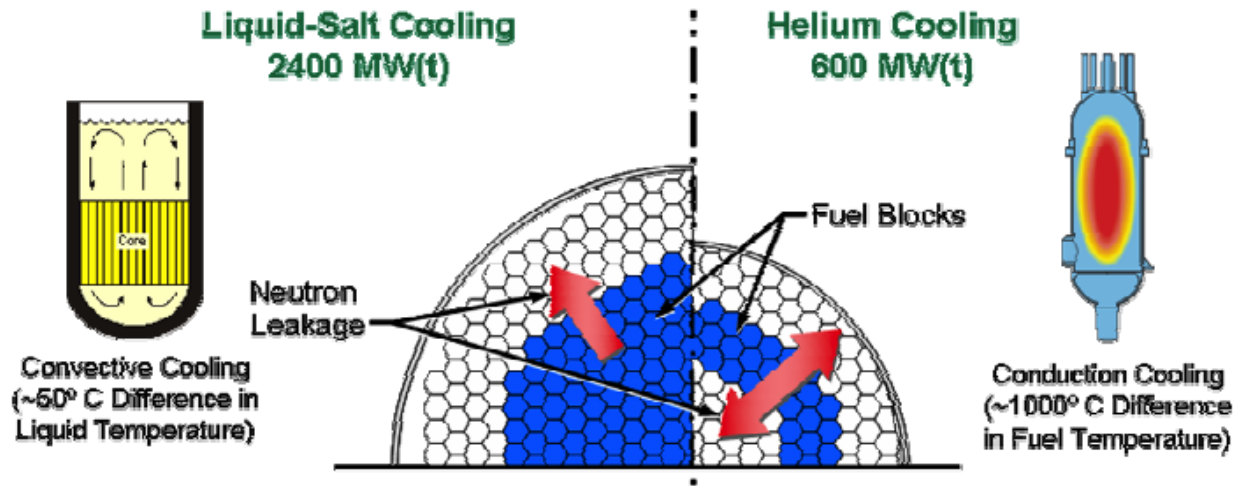
Figure 4-8 - Comparison of Liquid Salt vs. He Cooling

For commercial applications, the ability to use one larger reactor instead of several smaller reactors would obviously reduce capital costs. Furthermore, the use of a larger core for the salt-cooled reactor results in less neutron leakage, thereby achieving a higher burnup and lower SNF volume for a given enrichment [8].

4.2.4   AHTR Salt Coolant

4.2.4.1   Overview of Desired Salt Coolant Properties and Current State-of-the-Art

Previous salt-cooled reactor technological experience comes from (1) the aircraft nuclear propulsion program in the 1950s and (2) the Th-U^{233} breeder experiment in the 1960s [3]. A difference between the two earlier molten salt reactor (MSR) experiments and the current AHTR proposal is that the MSR experiment contained fertile and fissile fuel in the salt coolant, while the AHTR uses a solid fuel and "clean" salt. Even though the AHTR uses the salt solely as a coolant, the property and composition requirements remain markedly similar to the previous MSR applications [16]:

- Exhibit chemical stability >800 ^{o}C
- Stable under intense radiation
- Melt at useful temperatures (<525 ^{o}C) and are not volatile
- Compatible with high-temperature alloys and graphite
- ~~Dissolve useful quantities of fissile and fertile material~~

129

Chemical, physical, nuclear, metallurgical, and economic factors all impact the selection of a suitable salt coolant candidate that meets the above requirements. From past decades of experience, fluoride salts have an established advantage over the few other coolants that had been considered previously for service >700 °C. However, despite considerable analysis, no recommendation exists for a particular salt composition [17, 18] primarily because of the materials challenges and lack of data for a range of salt coolants in high-temperature applications. A summary listing of candidate salt coolants, as well as their associated thermodynamic properties and their comparison to other types of reactor coolants, is documented in Table 4-4 [18]:

Coolant	Formula Weight (g/mol)	Melting Point (K)	1,173 K Vapor Pressure (kPa)	Heat Transfer Properties at 973 K				
				$\rho \times 10^{-3}$ Density (kg/m^3)	$C_p \times 10^{-3}$ Heat Capacity (J/kg-K)	$\rho.C_p$ (MJ/m^3-K)	μ Viscosity (mPa-s)	K Thermal Conductivity (W/m-K)
LiF-BeF$_2$	33	733	0.16	1.94	2.41	4.68	5.6	1
LiF-NaF-BeF$_2$	38.9	588	0.226	2	2.04	4.08	5	0.97
NaF-BeF$_2$	44.1	613	0.186	2.01	2.17	4.36	7	0.87
LiF-NaF-KF	41.3	727	0.093	2.02	1.88	3.8	2.9	0.92
LiF-NaF-RbF	67.7	708	0.107	2.69	0.98	2.64	2.6	0.62
LiF-NaF-ZrF$_4$	84.2	709	~0.7	2.92	1.46	4.26	6.9	0.53
LiF-ZrF$_4$	95.2	782	10.3	3.09	1.22	3.77	>5.1	0.48
NaF-ZrF$_4$	92.7	773	0.666	3.14	1.17	3.67	5.1	0.49
KF-ZrF$_4$	103.9	663	0.16	2.8	1.05	2.94	<5.1	0.45
Rb-ZrF$_4$	132.9	683	0.173	3.22	0.83	2.67	5.1	0.39
KF-AlF$_3$	69.7	833	~1.1	1.8	1.33	2.39	1.4	0.5
NaF-NaBF$_4$	104.4	658	1270	1.75	1.5	2.63	0.9	0.4
KF-KBF$_4$	109	733	13.3	1.7	1.3	2.21	0.9	0.38
RbF-RbBF$_4$	151.3	715	<13.3	2.21	0.91	2.01	0.9	0.28
LiCl-KCl	55.5	628	0.773	1.52	1.2	1.82	1.15	0.42
LiCl-RbCl	75.4	586	-	1.88	0.89	1.67	1.3	0.36
NaCl- MgCl$_2$	73.7	718	<0.33	1.68	1.09	1.83	1.36	0.5
KCl-MgCl$_2$	81.4	699	<0.27	1.66	1.15	1.91	1.4	0.4
Na	22.9	371	13.3	0.79	1.26	1	0.2	62
Pb	207.2	600	0.001	10.54	0.16	1.69	1.37	16
Water (573 K)	18	273	8660	0.72	5.71	4.11	0.1	0.54
He (70 bars)	4	1	-	0.0035	5.21	0.02	0.4	0.0035

Table 4-4 - Summary Listing of Candidate Salt Coolants

4.2.4.2   Thermal Hydraulic Properties and Heat Transfer Comparison

From a thermal hydraulics perspective, a good salt candidate has a low melting point, high boiling temperature, low viscosity, high thermal conductivity, and high heat capacity. The thermal hydraulic characteristics of the candidate salts are known with varying degrees of certainty. Of note is that liquid salts are Newtonian fluids and exhibit normal fluid behavior [17].

Density (ρ) and dynamic viscosity (μ) are determined from the following experimentally determined relationships, which generically apply to all the salt candidates [17]:

$$\rho_{salt} = 2,270 - 0.37 \cdot T(°C); \left(\frac{kg}{m^3}\right) \tag{4-1}$$

$$\mu_{salt} = 3.4 \times 10^{-5} \cdot e^{\frac{5,165}{T(K)}}; (Pa \cdot s) \tag{4-2}$$

A cursory calculation using equations (4-1) and (4-2) reveals that for a 100 degree temperature rise across the core (700 °C to 800 °C) density only decreases by ~1.84% (effectively negligible); however, dynamic viscosity decreases 40%, a significant variation owing to the exponential nature of the relationship. Heat capacity (c_p) and thermal conductivity (k) are more difficult to determine; there is no fundamental theory to predict the heat capacity of various salt compositions, and thermal conductivity of molten salt is very challenging to measure. Reference [17] proposes using the Dulong-Petit correlation to estimate heat capacity, which is accurate to ~20% [19]:

$$c_p = 8 \cdot \frac{\sum X_i N_i}{\sum X_i M_i} \tag{4-3}$$

$Where\ X_i = mole\ fraction\ of\ component\ i$

$N_i = atoms\ per\ salt\ constituent\ i\ \left(\frac{g}{mol}\right) [= 2\ for\ NaCl, 3\ for\ BeF_2, etc.]$

$M_i = formula\ weight\ of\ component\ i\ \left(\frac{g}{mol}\right)$

While acknowledging considerable scatter exists in its experimental database, ORNL claims that its most reliable thermal conductivity measurements were obtained using a hot-wire and annular cylinder apparatus, as the results are more consistent and are amenable to modeling. According to reference [17], the most successful model for predicting the thermal conductivity of molten salts was proposed by Rao and Turnbull [20]:

$$k = 0.119 \cdot T_m^{0.5} \cdot \frac{\rho^{0.667}}{\left(\frac{M}{n}\right)^{1.167}}; \left(\frac{watt}{m-K}\right) \tag{4-4}$$

$where\ T_m = melting\ point\ (K)$

$$\rho = molar\ volume\ of\ molten\ salt\ \left(\frac{cm^3}{mol}\right)$$

$$M = avg.\ formula\ weight\ of\ salt\ \left(\sum X_i M_i\right)$$

$$n = \#\ of\ discrete\ ions\ per\ salt\ formula\ (e.g., NaCl = 2)$$

Another option suggested by reference [17] to determine thermal conductivity is the Kokholv correlation [21], which is simply a function of temperature and molecular weight:

$$k = 0.0005 \cdot T(K) + \frac{32.0}{M} - 0.34;\ \left(\frac{watt}{m-K}\right) \tag{4-5}$$

Reference [17] conveniently provides a consolidated summary of the thermal hydraulic properties of various candidate salts:

Salt Composition (mol %)	Formula Weight (g/mol)	Melting Point ($^\circ$C)	Density (g/cc) (700 $^\circ$C)	Viscosity (cP) (700 $^\circ$C)	Heat Capacity (cal/g-K) (700 $^\circ$C)	Measured Conductivity[19] (watt/m-K) (700 $^\circ$C)	Rao-Turnbull Prediction (watt/m-K) (700 $^\circ$C)	Khoklov Correlation (watt/m-K) (700 $^\circ$C)
LiF-BeF$_2$ (66.7-33.3)	33.0	460	1.94	5.6	0.577	1.0	0.79	1.1
NaF-BeF$_2$ (57-43)	44.1	340	2.01	7.0	0.520	-	0.58	0.87
LiF-NaF-BeF$_2$ (26-37-37)	38.9	315	2.0	5.0	0.489	-	0.62	0.97
LiF-NaF-KF (46.5-11.5-42)	41.3	454	2.01	6.9	0.388	0.60	0.68	0.82

Table 4-5 - Summary of Thermal Hydraulic Properties for Selected Salt Coolants

An examination of the candidate salt coolants in Table 4-5 reveals that no single salt enjoys an overwhelming thermal hydraulic advantage. Salt properties do not usually place severe limitations on the choice of coolant composition[20], and they are usually considered in combination with respect to their influence on heat transfer. However, having a salt coolant with a lower freezing point simplifies the materials, components, and system requirements; hence all candidate salts are multi-component in order to adequately reduce freezing temperature. All other factors being equal, salts with a freezing point <400 $^\circ$C should have priority [17]. In regards to freezing point, LiF-NaF-BeF$_2$ is best, followed by NaF-BeF$_2$.

---

[19] LiF-BeF$_2$ thermal conductivity measurements performed @ 600 $^\circ$C. LiF-NaF-KF thermal conductivity measurements performed @ 500 $^\circ$C.

[20] The one exception to this concerns the viscosity of BeF$_2$-containing salts. Salts rich in BeF$_2$ form extremely viscous mixtures that completely restrict their use to compositions of BeF$_2$ to ≤ 45%. Most other salts do not possess this property of forming highly viscous mixtures.

Table 4-5 also shows that density (ρ), heat capacity (c_p), and thermal conductivity (k) all trend based upon the formula weight of the salt. Within a group of salts sharing similar constituents, density increases with salts containing heavier elements, whereas heat capacity and thermal conductivity decrease with these heavier salts. The volumetric heat capacity ($\rho.c_p$) decreases with salts containing heavier elements. Therefore salts with lighter constituent elements typically display better heat transfer properties. The "figure of merit" methodology, developed by reference [22], provides a useful means to compare various coolants (superior candidate receives lowest numerical value):

$$forced\ convection\ FOM\ (turbulent) = \frac{\mu^{0.2}}{\rho^2 c_p^{2.8}} \tag{4-6}$$

$$free\ convection\ FOM\ (turbulent) = \left(\frac{\mu^{0.2}}{\beta \rho^2 c_p^{1.8}}\right)^{0.36} \tag{4-7}$$

$$free\ convection\ FOM\ (laminar) = \left(\frac{\mu}{\beta \rho^2 c_p}\right)^{0.5} \tag{4-8}$$

$$coefficient\ of\ thermal\ expansion \equiv \beta = \frac{1}{\rho} \cdot \frac{d\rho}{dT} \tag{4-9}$$

An inspection of typical FOMs for natural and forced convection confirms the superior heat transfer metrics of lighter salts. The marked advantage of molten salts over liquid metals and helium in turbulent heat transfer is due to the much larger heat capacity of the salts, as shown in Table 4-6 [18]:

Free Convection FOM @ 973 K				Forced Convection FOM @ 973 K	
Turbulent		Laminar		Turbulent Forced Convection	
Coolant	FOM	Coolant	FOM	Coolant	FOM
Water (573 K)	4.8	Water (573 K)	0.63	Water (573 K)	0.2
LiF-BeF$_2$	13.9	Na	3.51	LiF-BeF$_2$	0.7
LiF-NaF-BeF$_2$	15.6	Pb	5.36	NaF-BeF$_2$	0.91
NaF-BeF$_2$	16.5	LiCl-RbCl	6.86	LiF-NaF-BeF$_2$	1.02
Na	20.3	LiF-BeF$_2$	10.1	LiCl-RbCl	8.99
LiCl-RbCl	21.3	LiF-NaF-BeF$_2$	10.7	Na	13.1
Pb	28.5	NaF-BeF$_2$	13.5	Pb	33.6
He (70 bars)	386	He (70 bars)	504	He (70 bars)	14,500

Table 4-6 - Salt Coolant Heat Transfer Comparison (Lower is Better)

Table 4-6 shows that lighter molten salts (such as LiF-BeF$_2$) have somewhat better heat transfer performance than the heavier salts, except for natural convection in the laminar regime. Of note is that LiF-NaF-BeF$_2$ and NaF-BeF$_2$ have nearly as good FOM as LiF-BeF$_2$ but have a fairly significant lower melting temperature (see Table 4-5). However, <u>turbulent</u> natural convection is of primary importance in most passive cooling situations [17]. The most important point regarding Table 4-6 is that all of the molten salt coolant candidates would likely prove acceptable for some reactor and heat transport system designs [18].

4.2.4.3   Nuclear Properties of Salt Coolants

Since graphite has a very small probability of capturing neutrons, the major contribution to parasitic neutron capture is the salt coolant. The rate of parasitic neutron capture is directly related to the efficiency of fuel utilization; hence, more parasitic neutron capture requires additional fuel to maintain a critical system. Additionally, the relationship between capture and moderation is especially significant during a theoretical accident scenario [17]. Such a relationship is best described by the moderating ratio, a FOM relating the effectiveness of neutron moderation versus parasitic neutron capture for a given energy range:

$$\boldsymbol{Moderating\ Ratio} = \frac{\xi \Sigma_s \phi(\Delta E)}{\Sigma_c \phi(\Delta E)}$$ (4-10)

$where\ \xi \Sigma_s \phi(\Delta E) = rate\ of\ energy\ loss\ due\ to\ scattering$

$\Sigma_c \phi(\Delta E) = rate\ of\ neutron\ capture$

$(\Delta E) = 0.1\ to\ 10\ eV\ energy\ range\ used\ for\ analysis$

Table 4-7 compares the moderating ratio of various salts as well other materials of interest [17]:

Material	Total Neutron Capture (per unit volume) Relative to Graphite	Moderating Ratio (avg. 0.1-10 eV)
Heavy Water	0.2	11,449
Light Water	75	246
Graphite	1	863
Sodium	47	2
LiF-BeF$_2$	8	60
LiF-NaF-BeF$_2$	20	22
NaF-BeF$_2$	28	15
KF-ZrF$_4$	67	3

Table 4-7 - Examination of Moderating Ratio for Some Salt Coolants

Although the total neutron capture of light water (H_2O) is larger than the other materials, the excellent moderating power of light water leads to a much larger moderating ratio than that of any salt coolant. The BeF_2 salts have large moderating ratios and small parasitic capture rates (best neutronics), while the alkali fluorides have the worst. The capture rates of the salts are much larger than those of pure graphite; thus, minimizing the amount of salt coolant in the core will improve the fuel efficiency substantially from a neutronics perspective [17]. Table 4-5, Table 4-6 and Table 4-7 appear to favor LiF-NaF-BeF$_2$ for its low melting point and relatively good heat transfer and neutronics properties, but the Li component of LiF-NaF-BeF$_2$ must have a 99.99% enrichment of ^{7}Li. Although the percent natural abundance of ^{6}Li is only 7.59%, Figure 4-9 clearly shows its detrimental effect in the thermal spectrum [14]:
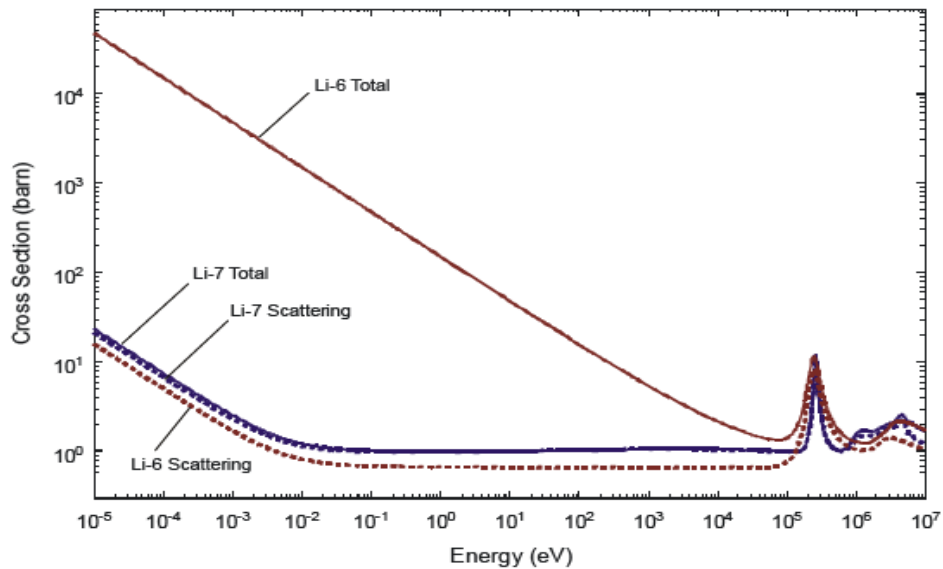
Figure 4-9 - Comparison of Li-6 and Li-7 Neutron Cross Sections

The high ^{7}Li enrichment requirement will make any Li-based salt costly. Although NaF-BeF$_2$ has slightly inferior heat transfer and neutronics characteristics, it nonetheless has relatively comparable performance and does not require any enrichment.

The other consequences of parasitic neutron capture are short and long term activation. From an activation standpoint, LiF-BeF$_2$ is clearly superior, as there are no intermediate-lived activation products in this salt. After a single day, the activation levels in LiF-BeF$_2$ are nearly zero, similar to water. Activated salts with a sodium constituent will have a significant concentration of ^{24}Na ($T_{1/2}$ = 15 h). Depending on the shielding arrangements in the reactor compartment, resulting radiation levels from ^{24}Na could preclude an emergency reactor compartment entry while underway. Salts with potassium

also have strong short-term activation levels for several days after shutdown due to ^{42}K ($T_{1/2}$=12 h). The worst salts for short-term activation, however, have either rubidium or zirconium components. Rubidium produces several significant activation products (^{86m}Rb, $T_{1/2}$=1 m; ^{88}Rb, $T_{1/2}$=18 m; and ^{86}Rb, $T_{1/2}$=18 d) with high-energy (>0.3 MeV) gamma radiation. Zirconium contains an even greater number of activation products (^{97m}Nb, $T_{1/2}$=1m; ^{97}Nb, $T_{1/2}$=1 h; ^{97}Zr, $T_{1/2}$=17 h; ^{95}Nb, $T_{1/2}$=35 d; ^{95}Zr, $T_{1/2}$=64 d), but the activity is less than that of rubidium by an order of magnitude for a time after shutdown less than 10 days. Figure 4-10 provides a useful comparison for the various candidate salt constituents [17]:
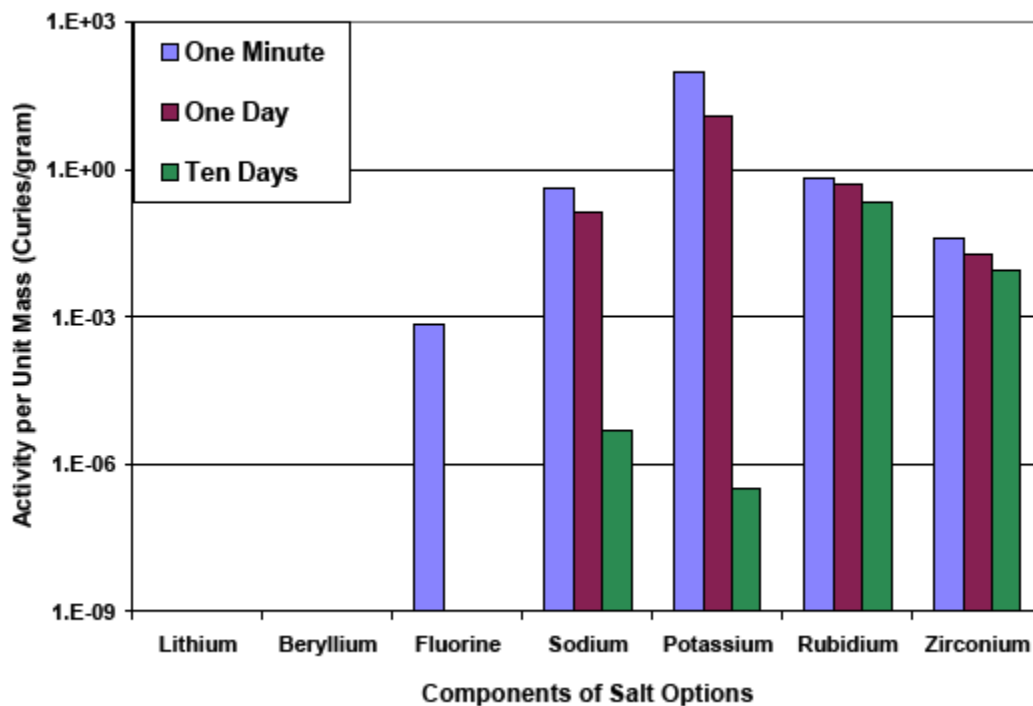
Figure 4-10 - Activity Levels for Various Candidate Salt Constituents

Figure 4-10 illustrates how salts with rubidium (Ru) components will have much higher radiation levels once time after shutdown exceeds 10 days. LiF-BeF$_2$ is obviously the most superior salt in terms of short term activation levels; however, its benefit in terms of short term activation levels should be balanced against its relatively higher melting point and higher cost (due to ^{7}Li enrichment) compared to other salts. Additionally, there are toxicity issues associated with using beryllium (Be). The other salt coolants have activation characteristics similar to that of the sodium coolant in fast reactors and should be only modestly more challenging to manage [18].

Compared with a PWR's coolant, the long term activation of the AHTR's salt coolant (whatever the salt composition) will complicate disposal. Table 4-8 contains a summary of the significant long-term activation products from potential salt coolant components [17]:

Activated Isotope	Decay Type	Radiation Gamma Energy (MeV)	Half-life	Level of Activation (µCi/g-coolant) (Parent Elements in Coolant)				
				Be	Na	K	Rb	Zr
^{10}Be	β$^-$		1.5×10^6 y	0.2				
^{22}Na	β$^+$, γ	1.3	3 y		0.002			
^{36}Cl	β$^-$		3×10^5 y			1		
^{40}K	β$^-$, γ	1.5	1×10^9 y			0.04		
^{87}Rb	β$^-$		50×10^9 y				0.02	
^{93}Zr	β$^-$, γ	0.03	1.5×10^6 y					0.4
^{93m}Nb	β$^-$, γ	0.03	1.5×10^6 y					0.3
Cumulative Activity from Coolant Constituent				0.2	0.002	1.04	0.02	0.7
Total Activity Level (µCi/g-coolant)								2

Table 4-8- Activity Level of Salt Coolant Constituents (10 yr Decay)

Of the isotopes above, the gamma emitters are of concern. ^{10}Be is long-lived and has uncertain environmental mobility properties. ^{93}Zr, the parent of ^{93m}Nb, has a very long, 1.5 million year half-life and it cannot be easily removed from salt. Although the ^{93m}Nb poses the most significant disposal challenge, ORNL believes that its predicted activity levels after long-term operation in an AHTR will almost certainly be sufficiently low to qualify as low level waste (LLW); however, this assessment has not been corroborated by any other investigation and deserves more analysis. In summary, ORNL's assessment is that the disposal of all of the salt candidates as LLW after 10 years of cooling should be possible, provided that certain salt coolants receive appropriate chemical pretreatment [18]. One should note, however, that the salt coolant is indefinitely reusable; no need exists to dispose of the salt coolant until the core is decommissioned, and even then it could be transferred to another reactor.

Neutron capture and moderation also play a role in determining core reactivity coefficients, which are especially important parameters for any transient. Investigation by reference [17] reveals that all salts except LiF-BeF$_2$ contribute a positive coolant density coefficient[21] (CDC) as well as a positive coolant void ratio[22] (CVR).[23] The AHTR, however, is a pool-type reactor (essentially operating at

---

[21] The coolant density coefficient is the reactivity change due to coolant expansion upon heating.
[22] The coolant void ratio is the change in reactivity due to a 100% coolant voiding scenario.
[23] Calculations performed by investigators at ORNL using TRITON with SCALE 5.1 solvers for resonance processing (CENTRM), 2-D deterministic transport (NEWT), isotropic transmutation/depletion/decay (ORIGEN-S), and 238-

atmospheric pressure with a very large margin to boiling); hence, there can be no depressurization leading to a sudden, rapid loss of coolant. Since any "loss" of coolant from the core will be caused or accompanied by a temperature change, the total temperature coefficient must also be considered. Any reactivity insertion causing a rise in coolant temperature will lag behind the corresponding rise in fuel temperature; therefore, the relative magnitude and sign of the total coolant temperature coefficient must be evaluated in relation to the noncoolant (fuel and graphite) temperature coefficient. By assuming that complete voiding without a temperature change is not possible, then the significance of any coolant density change can only be considered when accounting for all other temperature coefficients. Although the (negative) fuel coefficient dominates the core's response to reactivity insertions (despite the coolant temperature coefficient), the net reactivity effect can only be precisely understood through a coupled neutronics/thermal-hydraulic analysis.[24] ORNL has defined a convenient parameter, the coolant safety ratio[25], in order to compare various salt coolants. Table 4-9 provides a concise summary of the reactivity coefficients and safety ratio for various salt coolants[26] [18]:

---

group ENDF/B-IV cross section library. Refer to reference [17] for model details. Calculations used the standard hexagonal prismatic fuel block with TRISO fuel particles (25% packing fraction, 15% enriched), 1.27 cm diameter fuel channels (216 total), and 0.935 cm diameter coolant channels (108 total, 7% block volume).

[24] PARCS or NESTLE coupled with RELAP.

[25] The safety ratio is defined as the ratio of the magnitude of a positive (total) coolant temperature coefficient to the total noncoolant temperature coefficient. For instance, a coolant safety ratio of 1.0% means that the fuel and graphite must only increase temperature 1 K to offset the reactivity increase caused by a 100 K rise in coolant temperature. Thus, a smaller (or even negative) safety ratio is best.

[26] Calculations assume a uniform temperature rise across the core, which is a conservative approximation in that it exaggerates the salt coolant's positive reactivity contributions.

Salt (mol% composition)	^{235}U Enrichment (Wt %)	Coolant Void Ratio ($)	Total Coolant Coefficient ($/100 K)	Salt Coolant Safety Ratio (%)	Total Thermal Coefficient ($/100 K)
Coefficients Without Er$_2$O$_3$ Poison, 7% Coolant Fraction					
LiF-BeF$_2$ (67-33)	14.1	$0.28	$0.00	-0.10%	-$0.58
NaF-BeF$_2$ (57-43)	15.4	$2.71	$0.07	17.0%	-$0.32
LiF-NaF-ZrF$_4$ (26-37-37)	15.5	$2.83	$0.09	21.5%	-$0.32
NaF-ZrF$_4$ (59.5-40.5)	15.8	$3.35	$0.11	30.5%	-$0.24
NaF-RbF-ZrF$_4$ (33-23.5-43.5)	16.5	$4.39	$0.13	53.8%	-$0.11
Coefficients with Er$_2$O$_3$ Poison, 7% Coolant Fraction					
LiF-BeF$_2$ (67-33)	14.3	-$0.11	-$0.09	-3.70%	-$2.54
NaF-BeF$_2$ (57-43)	15.6	$2.45	-$0.01	-0.60%	-$2.26
LiF-NaF-ZrF$_4$ (26-37-37)	15.8	$2.89	$0.04	1.90%	-$2.23
NaF-ZrF$_4$ (59.5-40.5)	16.1	$3.44	$0.06	2.90%	-$2.14
NaF-RbF-ZrF$_4$ (33-23.5-43.5)	16.9	$4.91	$0.11	5.10%	-$2.00
Coefficients with Er$_2$O$_3$ Poison, 7% Coolant Fraction, 99.9% ^{7}Li					
LiF-BeF$_2$ (67-33)	19.2	$9.56	$0.17	9.40%	-$1.62
LiF-NaF-ZrF$_4$ (26-37-37)	16.9	$4.99	$0.12	5.10%	-$2.16
Coefficients with Er$_2$O$_3$ Poison, 15% Coolant Fraction					
LiF-BeF$_2$ (67-33)	15.5	-$0.64	-$0.19	-8.80%	-$2.40
NaF-BeF$_2$ (57-43)	18.0	$4.63	-$0.04	-2.20%	-$1.81
LiF-NaF-ZrF$_4$ (26-37-37)	18.7	$5.83	$0.08	4.20%	-$1.78
NaF-ZrF$_4$ (59.5-40.5)	19.3	$6.98	$0.12	7.20%	-$1.57
NaF-RbF-ZrF$_4$ (33-23.5-43.5)	21.2	$10.41	$0.21	15.0%	-$1.21

Table 4-9 - Effect of Core Parameters on AHTR Reactivity Coefficients

Analysis of Table 4-9 reveals that, with the exception of CVR, the reactivity coefficients have a much stronger dependence on coolant fraction and burnable poison content than on salt coolant type. All salt coolant options have a negative total thermal reactivity coefficient. Therefore, any type of salt coolant can provide protection against a temperature transient when coupled to a properly designed fuel block [18]. LiF-BeF$_2$ once again demonstrates the best neutronic performance, but not to the extent that it is clearly favored over other salt coolant candidates when cost and thermal hydraulic performance are considered as well. Encouragingly, an independent analysis of AHTR reactivity coefficients for both uranium and plutonium fuels[27] also concludes that the temperature coefficients are negative; additionally, the void coefficient can be made negative as long as the core is undermoderated and the

---

[27] The study used a prismatic hexagonal block and Pu or U TRISO fuel particles. Although different dimensions were used for the fuel and coolant channels, they do not differ significantly from reference [17]. Refer to reference [23] for core design details. Additionally, the study utilized MCNP (4c3) and the JEFF-3.0 nuclear data library for computational analysis.

salt coolant has a large moderating ratio [23]. These results were consistent for 5 different candidate salts (NaF, BeF_2, LiF, ZrF_4, and Li_2BeF_2).

4.2.4.4   Chemical Compatibility and Material Suitability of Salt Coolants

Compared to He or other gas coolants, molten salts provide much more effective heat transfer; however, unlike He, salt coolants present numerous challenging (and unresolved) materials issues. Above 750 ^{o}C, materials performance for data in liquid fluorides is sparse [24]. ORNL completed a detailed review of corrosion testing of alloys for fluoride-salt service; however, no compelling evidence favors one particular salt [18]. Simply stated, no consensus exists to select a particular salt based on its corrosion behavior with high-temperature alloys [17]. The need to investigate and resolve this issue, however, is absolutely critical. Since fluorides remove the passive oxide layers from metals, traditional corrosion approaches do not apply and alternate, innovative strategies are necessary for several key reactor plant components. The AHTR requires extremely durable components to (1) withstand thermal cycling between large temperatures, (2) withstand a large pressure difference between the salt coolant loop and the PCS, and (3) resist wear at elevated temperatures [24].

The principle challenge is that not enough research examining salt-coolant compatibility with candidate materials at operating temperatures has been performed. References [14] and [17] assume a reactor outlet temperature of 1,000 ^{o}C in their analyses; however, ASME approved nuclear materials capable of withstanding temperatures at that magnitude are highly unlikely to be developed any time soon. The most promising material candidate, Hastelloy-N, is rated to 704 ^{o}C by the ASME code, but not for class 1 components (boilers and pressure vessels) [24].

Despite the desire to operate at 1,000 ^{o}C, sparse data exists to suggest the viability of any salt coolant candidate for temperatures at or above 700 ^{o}C. Appendix A of reference [17] contains a summary of the corrosion results for various salt coolant candidates. Several of the salt candidates only had a 500-hour test duration, and many salts also had a thorium-fluoride constituent; however the results unambiguously confirm that Hastelloy-N demonstrates superior performance to stainless steel or Inconel. Table 4-10 contains a partial summary of some salts among the candidate materials [17]:

Alloy	Salt	Duration (hours)	Temperature (^{o}C)	Corrosion Depth (mills)
316 SS	FLiNaK	500	815	4
Inconel	FLiFaK	1,000	815	13
Inconel	36LiF-49NaF-15BeF$_2$	1,000	815	3
Hastelloy-N	FLiNaK	8,760	677	1
Hastelloy-N	67LiF-33BeF$_2$	26,000	649	0

Table 4-10 - Material Performance of Some Salt Coolant Candidates

The 67LiF-33BeF$_2$ salt was evaluated in the molten salt reactor experiment test loop, and its results appear quite promising. However, no research to date conclusively confirms its viability in nuclear applications of temperatures at or above 700 ^{o}C.

4.2.4.5   Summary of Salt Coolant Attribute Analysis

Endorsing a specific salt coolant is problematic, primarily because numerous suitable candidates have adequate thermal-hydraulic and neutronics properties. Researchers must determine how particular salt candidates perform with various materials suitable for key reactor plant functions at desired operating temperatures before enough information is available to make an informed decision. Two promising salt candidates are LiF-NaF-BeF$_2$ and NaF-BeF$_2$. Both salts have a low melting point as well as good thermal hydraulic and neutronics characteristics. The key consideration when selecting between LiF-NaF-BeF$_2$ and NaF-BeF$_2$ is the additional cost of enriching the [7]Li constituent to 99.99%. LiF-NaF-BeF$_2$ provides only a relatively modest performance boost over NaF-BeF$_2$, but the additional margin could be desirable and worth the cost in specialized, high performance (i.e., military) applications.

Although LiF-BeF$_2$ has somewhat better nuclear and thermal hydraulic performance, its higher melting point is undesirable. However, LiF-BeF$_2$ has much lower short-term activation levels (similar to water) that facilitate reduced shielding, which is very desirable for marine platforms. Furthermore, LiF-BeF$_2$ may be the only salt candidate that has activation levels low enough to facilitate an emergency reactor compartment entry at sea, but further investigation is necessary to make any definite statement regarding this scenario. An additional consideration is that of all the salt candidates considered, LiF-BeF$_2$ is the only one that has negative coolant, void, and fuel reactivity temperature coefficients across the board. Even though all of the other salt coolant candidates have a clearly acceptable total (net) thermal reactivity coefficient, positive coolant and void reactivity coefficients are anathema to the nuclear navy's reactor design philosophy. However, detailed design within the analysis of alternatives (AOA) design process could show that the lower melting point of other salts dramatically simplifies the overall reactor

plant design, as well as provides a more comfortable margin to a postulated casualty that cools the salt temperature towards its freezing point.

The key issue requiring resolution is demonstrating salt coolant compatibility with a material rated to 700 $^{\circ}$C or higher by the ASME code. Hastelloy-N appears promising, but more investigation in necessary to prove its suitability as an ASME class 1 component at 700 $^{\circ}$C. In addition to monitoring its performance in a radiation field, its suitability must also be demonstrated in heat exchangers subjected to thermal cycling and a large pressure difference as well pumps and valves that are subjected to mechanical wear.

4.2.5   AHTR Passive Safety Systems

4.2.5.1   Safety Overview

As previous sections have already alluded, the fact that the AHTR essentially operates near atmospheric pressure nearly makes it immune to the dreaded large break loss of coolant accident (LOCA) that gas-cooled reactor and LWR designers must contemplate. Barring catastrophic rupture of the reactor pressure vessel (RPV) from either battle damage or willful negligence in adhering to RPC brittle fracture prevention limit (BFPL) criteria, a LOCA is of limited concern. As previous sections have already shown, even if complete voiding of the core were to occur, the associated rise in fuel temperatures will insert enough negative reactivity to shut down the reactor.

More likely casualties are freezing of the salt coolant or a loss of forced circulation (LOFC). Of these two scenarios, LOFC has been investigated in much more detail by ORNL (refer to references [14] and [25]); the important points of its investigations are detailed below. Three options exist for passive decay heat removal (explained in more detail below); each of them has corresponding advantages and tradeoffs.

4.2.5.2   Salt Freezing

No detailed analysis exists of response to events causing a rapid drop in salt temperature (e.g., catastrophic rupture of Brayton PCS or secondary salt system). In contrast to LWRs, the salt coolant does not simultaneously serve as the moderator, which consequently eliminates the "moderator induced reactivity insertion casualties" (e.g., steam system rupture or other cold water insertion). Any

sudden drop in coolant temperature actually inserts negative reactivity (since a slightly more dense coolant will absorb more neutrons, leaving less for the fuel); however, coolant temperature reactivity effects are very modest (see Table 4-9 above). Although the results of a coupled neutronics/thermal-hydraulics analysis of such an event could be insightful, such an investigation is beyond the scope of this thesis.

To mitigate the effect of any salt freezing, most AHTR designs utilize the guard vessel concept utilized in sodium-cooled reactors (essentially a "tank within a tank"). The interior tank is the RPV, which contains the core and primary (radioactive) salt coolant. The exterior vessel contains the RPV (interior tank), as well as the secondary (non-irradiated) salt coolant, IHX, and piping. This arrangement minimizes the heat transfer surface area for accidental freezing [6]. Figure 4-11 shows a conceptual, two-tank system design for a commercial-sized (2,400 MW$_{th}$) AHTR:
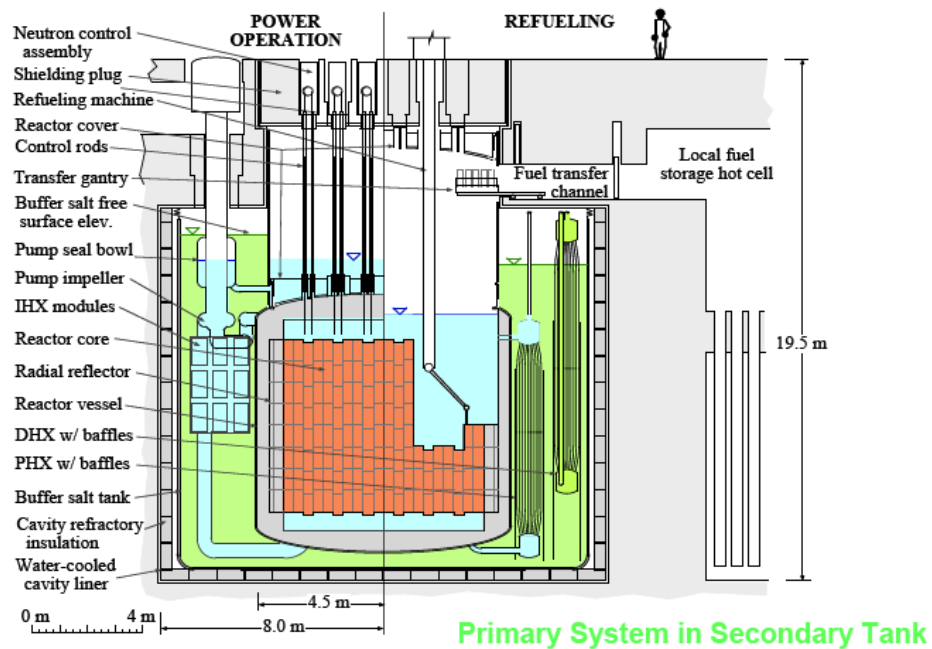
Figure 4-11 - Conceptual Design of Two-Tank System

4.2.5.3   Loss of Forced Circulation (LOFC) Analysis

ORNL has performed two independent analyses for the LOFC. The earlier (2004) analysis, utilized the Graphite Reactor Severe Analysis Code (GRSAC), adapted to accommodate AHTR thermal

hydraulics characteristics (see reference [25] for details). Figure 4-12 shows the results of a LOFC with a scram occurring at t=0:
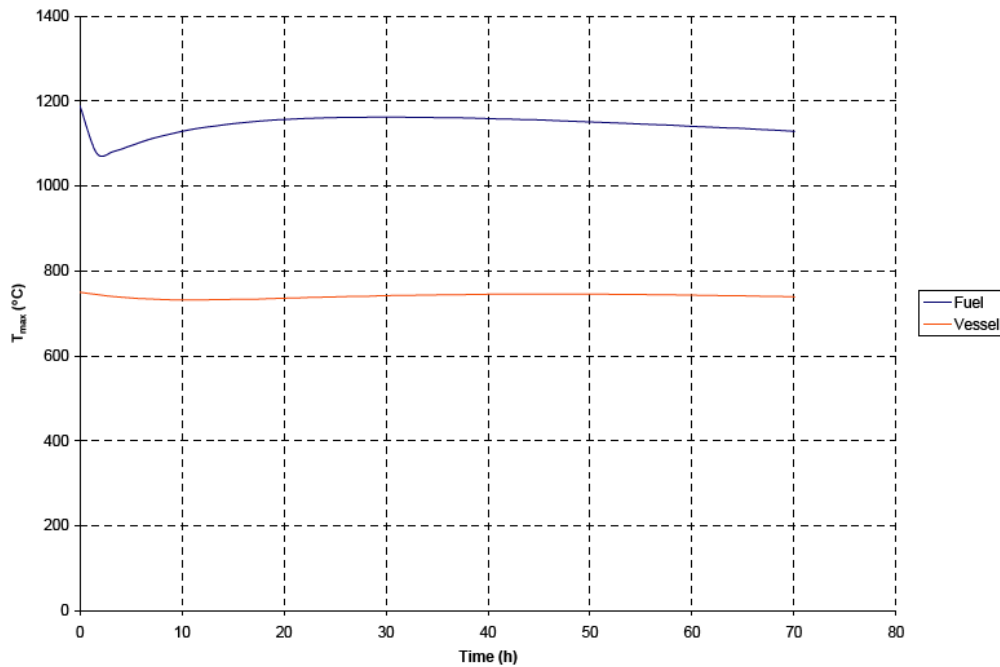
Figure 4-12 - GRSAC Simulation of LOFC

During the LOFC event, the molten salt naturally circulates up the fuel channels in the core and down by the edge, which results in a nearly isothermal core. The fuel reaches a peak temperature of ~1,160 $^{\circ}$C in ~30 hours. The average core temperature rises to approximately the same temperature as the hottest fuel during normal operations. Such relatively mild accident conditions are indicative of an AHTR's passive safety [25].

The later (2005) analysis utilized the RELAP-5 3D thermal/hydraulics code that was specifically configured for the AHTR design (see reference [14] for model details) and assumed decay heat removal using the reactor vessel auxiliary cooling system (RVACS, explained in more detail in the following section). Figure 4-13 shows the effect of a LOFC on fuel temperature, including a simulation <u>with a failure to scram</u>:
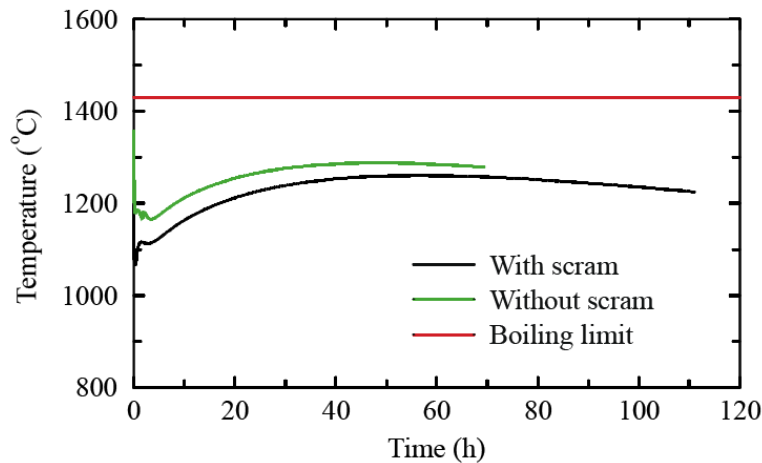
Figure 4-13 - RELAP-5 Model Fuel Temperature Due to LOFC

The LOFC event (coupled with failure to scram) causes the average fuel temperature to increase until reaching a peak in ~90 seconds; fuel temperature then decreases in response to the reduction in power caused by (1) negative thermal reactivity feedback and (2) the establishment of natural circulation flow. Fuel temperature rises over the long-term (peaking at ~ 50 hours) because the core decay power exceeds that removed by the RVACS; however, the long-term peak temperature value is ~ 70 ^{o}C less than the peak temperature occurring early in the transient [14]. The RELAP-5 results are consistent with the GRSAC model, and they suggest that the AHTR can withstand a LOFC (and a simultaneous failure to scram) and fuel temperature remains below the boiling limit.

Although these results appear promising, they require more analysis. The model uses ANS 5.1 for the infinite irradiation of ^{235}U (UO$_2$) to evaluate decay heat power. The ANS 5.1 Standard was developed specifically to evaluate decay heat power for LWRs with low enriched uranium fuel. However, this model was chosen because ANS 5.1 predicts 30% higher decay heat than the model specifically developed for the gas-cooled VHTR (thereby implying a degree of conservatism) [14]. However, reference [26] notes that the ANS 5.1 Standard only considers 4 fissionable nuclides (^{235}U, ^{238}U, ^{239}Pu, and ^{241}Pu), all of which are fissioned by thermal neutrons (except ^{238}U); reactor designs other than the baseline LWR considered by ANS 5.1 may generate actinides whose decay and fission products generate a non-negligible contribution to decay heat power. Reactor physics codes such as MCNP are excellent in modeling the probabilistic treatment of neutron transport, but poor in modeling depletion; conversely, codes such as Origen are effective in modeling depletion, but poor in modeling neutron transport. Therefore, Ben-Gurion University developed a code BGCore, which performs detailed calculations of in-core fuel composition and post-irradiation fuel characteristics, including decay heat,

145

for any existing reactor types and those under development. In contrast to the common approach used by most of the reactor analysis codes of tracking only the most neutronically important nuclide densities, BGCore computes the entire set of over 1,700 nuclides during all stages of fuel depletion and subsequent decay. Figure 4-14 demonstrates the validity of BGCore decay heat prediction by comparing it with the ANS model for a 4.0% UO_2 enriched LWR irradiated for 1,350 EFPD at a constant specific power of 37.7 W/g-HM (1 yr=3.16×10^7 sec):
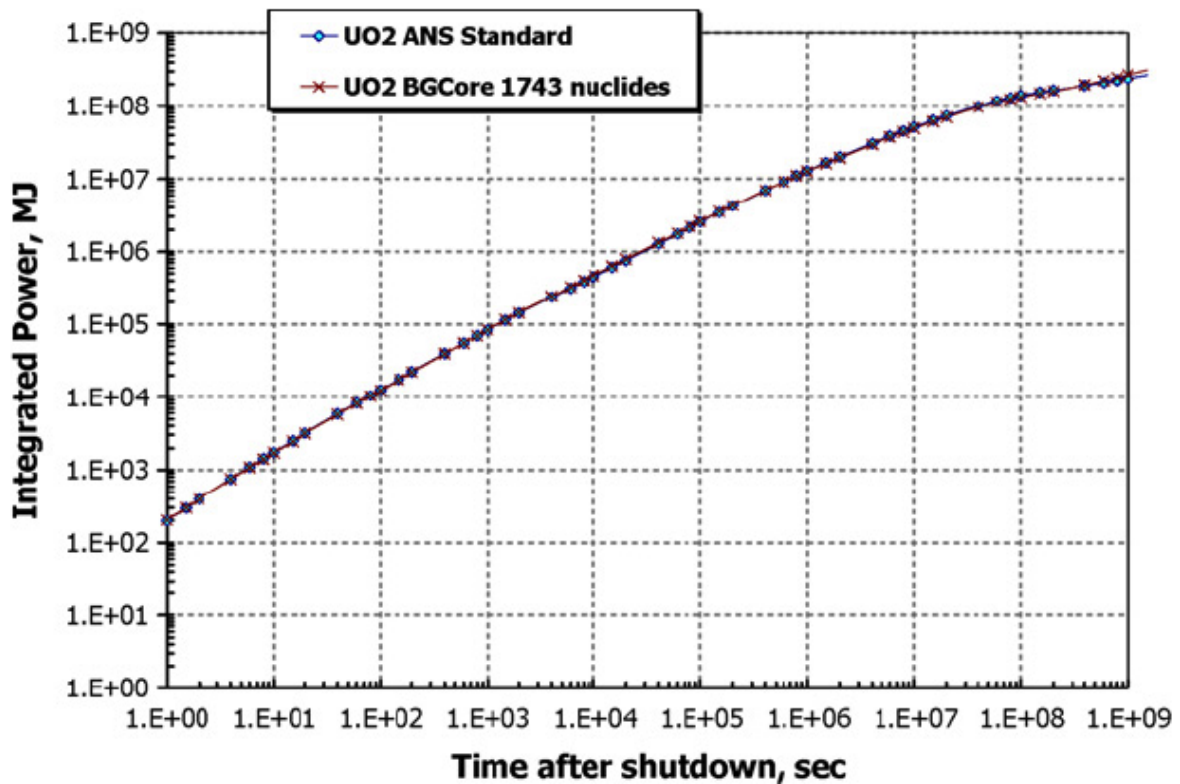
Figure 4-14 - Benchmarking BGCore with ANS 5.1

Reference [26] compares the results of the ANS decay heat model to BGCore for a lead-bismuth cooled reactor suffering a LOFC accident similar to the case analyzed by ORNL for the AHTR. As with the AHTR case, the transient was modeled with the RELAP5-3D thermal hydraulics code, with decay heat removal via the RVACS. Calculations were performed using the ANS 79 decay heat model available in RELAP 5, which considers only the same 4 fissionable nuclides, and with BGCore. The results show that for the advanced reactor design, the ANS decay heat model under-predicts the decay heat power:
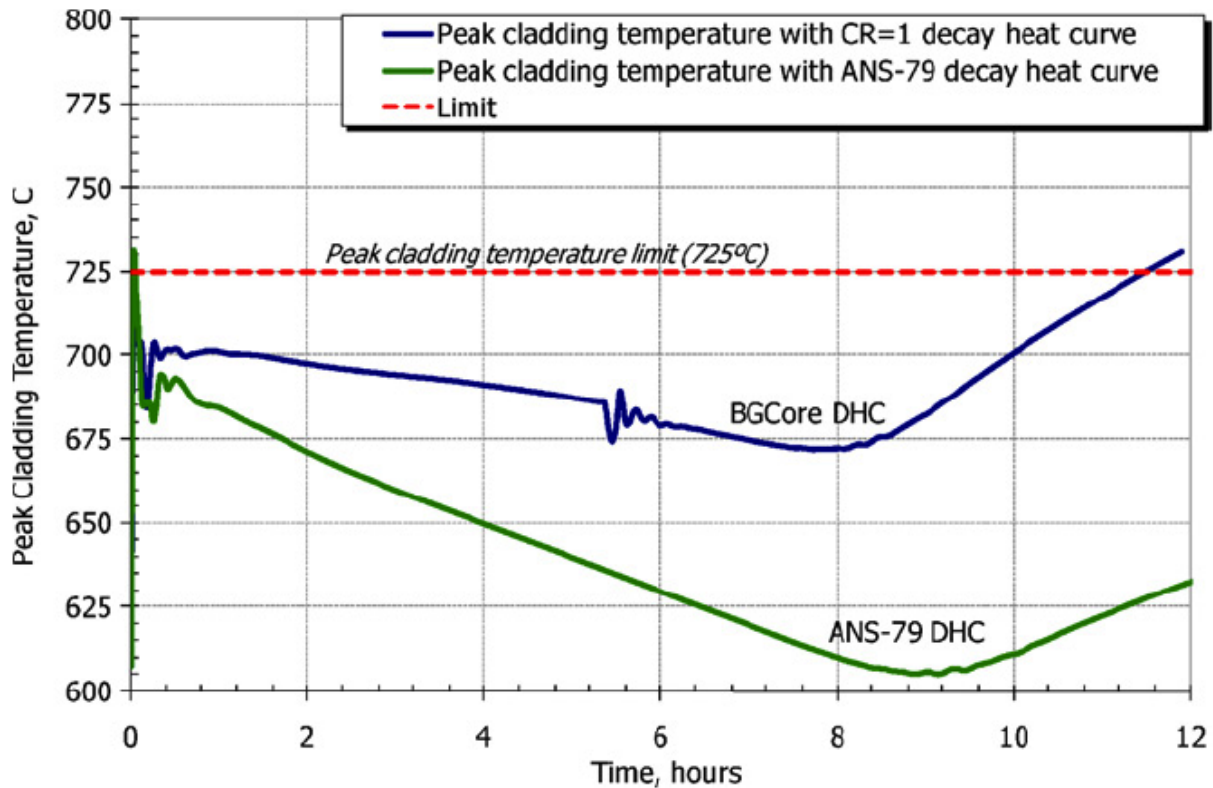
Figure 4-15 - Comparison of ANS Decay Heat Model with BGCore

Although the reactor used in this analysis has a 1.0 conversion ratio, the results indicate that the ANS standard might not be suitable for the AHTR.

4.2.5.4   Passive Decay Heat System Options

ORNL has identified three potential passive decay heat removal (DHR) system options, all of them based on technologies originally developed for sodium-cooled fast reactors (SFR). All three options are common in that they (1) have significant heat capacity to absorb reactor decay heat for many hours following shutdown, (2) each system is passive and is able to match the decay heat generation rate 30-60 hours following shutdown, and (3) all systems are situated in a silo to ensure that no credible accident results in uncovering the reactor core. The differences between the DHR systems designed for the SFR and the AHTR are (1) the AHTR's peak temperatures are 200-450 $^{\circ}$C higher than the SFR, (2) the melting points of molten salt are higher than sodium (98 $^{\circ}$C), and (3) the volumetric heat capacity ($\rho * c_p$) of salt is about four times that of sodium. The higher operating temperatures and freezing points necessitate alternate materials and design constraints, as well as leading to the increased

importance of thermal radiation transport. The salt coolant's better volumetric heat capacity, however,
is favorable in that it reduces the size of DHR system components and presents fewer size constraints.
Table 4-11 presents a synopsis of the three options [27]:

DHR Concept	Principle of Operation	Advantages	Disadvantages
Reactor Vessel Auxiliary Cooling System (RVACS)	• Core decay heat to reactor vessel via natural circulation (NC) of salt coolant. • Heat conduction through graphite reflector and vessel wall • Radiation heat transfer across argon gap to guard vessel (primary mechanism affecting heat transfer rate) • Heat conduction through guard vessel • Heat removal of guard vessel via NC of ambient air	• Relatively simple system • Previously developed for SFR • Well understood	• DHR capacity limited by RPV size • Integral effects testing (IET, required for licensing) difficult to perform for RVACS design • Multifunction reactor vessel must satisfy two conflicting requirements: ➢ contain reactor system ➢ transfer decay heat under accident events
Direct Reactor Auxiliary Cooling System (DRACS)	• Heat removed via NC from a HX in the primary reactor vessel to a HX with the ultimate heat sink (e.g., the atmosphere)	• Located inside RPV, helping to minimize system temps • Higher heat rejection temps reduce system size • Reactor power output not limited by ability of RPV to reject heat • Modular design; ease of IET validation	• Not fully developed • Material compatibility of salt coolants not fully evaluated

Pool Reactor Auxiliary Cooling System (PRACS)	• Reactor and auxiliary components contained within larger tank • Larger tank has a secondary salt • Heat rejected from reactor salt system to secondary salt tank • Heat rejection from secondary salt to environment (via DRACS)	• Two salt system can be also be used for reactivity control • Buffer salt can absorb large amounts of decay heat relative to other designs • Buffer salt pool limits primary metal temps independent of any insulation system • DRACS HXs can be positioned to maximize heat transfer • Lower costing, lower enriched ^{7}Li buffer salt can provide secondary Rx shutdown mechanism • Modular design	• Newest system design concept with most design uncertainties • Dual salt system adds a significant amount of system complexity • DRACS for AHTR not fully developed

Table 4-11 - Summary of DHR System Design Options

The simplistic design of the RVACS is attractive, provided more detailed analysis demonstrates that the system adequately meets the needs of the reactor necessary for the ship's mission. The RELAP-5 LOFC analysis from the previous section demonstrates RVACS effectiveness for an AHTR rated at 2,400 MW$_{th}$; however, additional core and vessel design criteria dictated by subsequent, more detailed analyses could determine that RVACS does not provide enough assurance. Since salt coolant compatibility material issues must be resolved anyway for the AHTR concept to materialize, the most prudent course of action would be to perform a comparative analysis on the three designs when certain that they are all feasible. Since PRACS and DRACS share similar design features, and since development of both systems is also contingent upon resolving salt compatibility, no particular urgency exists to endorse the use of any particular DHR system. The main point is that passive DHR system options do exist, and each option is probably capable of providing passive DHR assurance.

4.2.5.5   Safety Systems Summary

The preliminary safety evaluation of the AHTR is promising. Since the AHTR operates near atmospheric pressure, practically no scenario exists to cause a LOCA. Negative net thermal reactivity

coefficients provide a feedback mechanism to mitigate the impact of any event inserting positive reactivity into the core. If core voiding were to somehow occur, the net thermal reactivity coefficient is sufficient to confer protection. Additional investigation could prove useful in demonstrating reactor response to various salt coolant temperature transients, but changing salt coolant temperature (especially in comparison to LWRs) should only have a very modest impact.

A RELAP-5 thermal-hydraulics analysis suggests that a baseline AHTR core, with a RVACS DHR system, can show sufficient protection against a complete LOFC event with no scram. Throughout the entire transient, fuel temperatures remain well below salt coolant boiling temperatures, thereby assuring fuel integrity. An independent evaluation using GRSAC yields similar conclusions. However, the models utilized in these analyses may not adequately predict the AHTR's decay heat power. More analysis is needed with a more robust decay heat model to confirm the adequacy of the AHTR's design in a LOFC scenario.

The RVACS DHR system is simple and can provide protection against the LOFC events postulated in the RELAP-5 simulation, but alternate AHTR designs might preclude its use. The DRACS and PRACS designs present attractive alternatives to RVACS; however, material compatibility issues with the salt coolants present challenges in actually implementing their design. Once the DRACS and PRACS designs are confirmed to be feasible, a more comprehensive investigation should identify the most appropriate DHR system for a specific AHTR design.

4.2.6   AHTR Power Cycle Analysis

4.2.6.1   *PCS Requirements and Options for Consideration*

Compared to a Rankine cycle, a Brayton power cycle affords the opportunity for a more efficient, as well as a more compact, PCS. Reference [28] shows that a S-CO$_2$ cycle has a small footprint (shown in more detail later), as well as high thermodynamic efficiency ~47-48%; reference [29] reports a thermodynamic efficiency of ~43% with a gas-cooled fast reactor (GFR) using a S-CO$_2$ coolant. Additionally, He Brayton cycles can be designed to have thermodynamic efficiencies exceeding 50% (at sufficiently high temperatures), as shown in reference [30]. Gas-cooled reactor studies in references [31] and [32] show similar results. The motivation for a higher thermodynamic efficiency for the shipboard liquid fuels production application, as compared to a Rankine cycle with a PWR, is that a higher efficiency will reduce the rated power (and footprint) required by the reactor.

Thoroughly evaluating options to integrate the reactor plant and PCS with the shipboard propulsion system is an entire study itself, but a reasonable estimation of the additional power required is not difficult. Since the liquid fuels production loads are much more significant than even the top speed propulsion load, an integrated power system (IPS) (Figure 4-16) with electric drive propulsion makes the most sense:
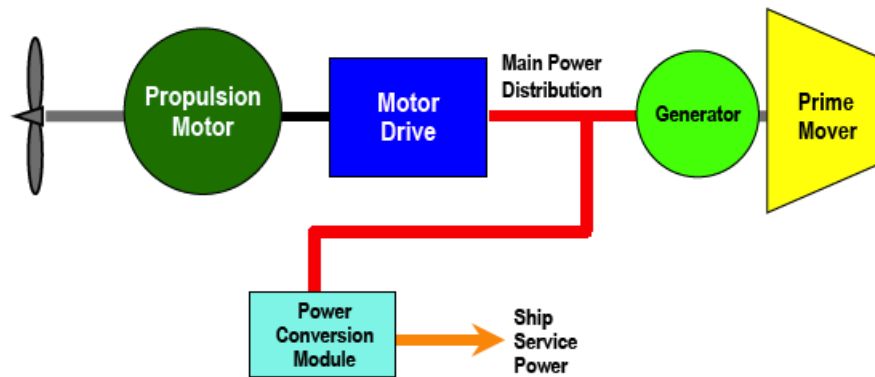
Figure 4-16 - Integrated Power System Architecture

An IPS architecture has several key advantages:

- Fewer prime movers (none needed for propulsion), thereby providing naval architectural flexibility
- Power tailored to system requirements; operators can determine how best to use power
- Producibility advantages
- Facilitates fault and transient isolation, thereby preventing warfighting disruptions

Electric drive propulsion is fundamental to an IPS. The capability exists and IPS designs are being implemented on naval platforms [33]. The primary disadvantages of electric drive are (1) that it requires more components to form a propulsion system, and (2) the process of converting mechanical energy to electrical energy and then back to mechanical energy is a more inefficient process, as Figure 4-17 illustrates [34]:
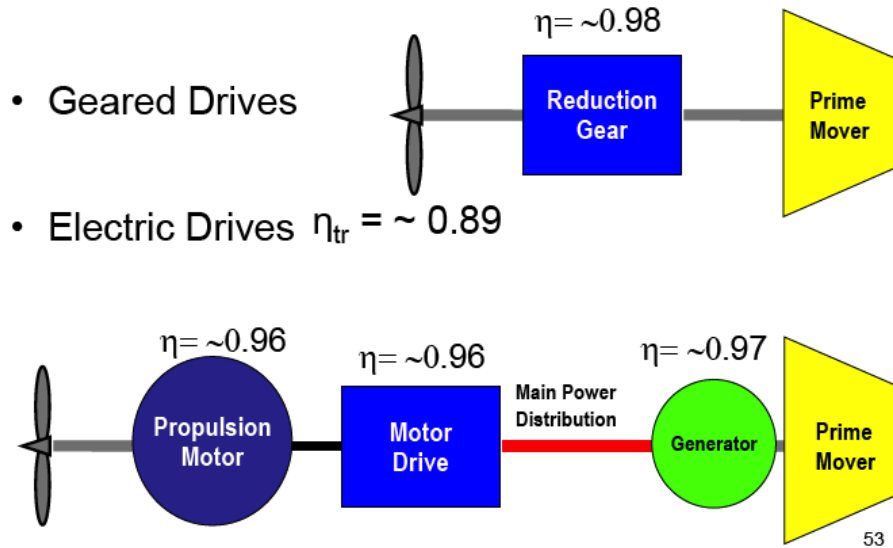
Figure 4-17 - Comparison of Traditional and Electric Drive Propulsion Efficiencies

From ASSET, the maximum electrical loading for the T-AO-187 *Henry Kaiser* class tanker ship is 4.82 MW_e and its top (flank) speed propulsion load (20.14 knots) is 23.7 MW_e (brake power) at full displacement (41,319 MT) [11]. However, most navy ships frequently operate at 15 knots or less, which is only 9.44 MW_e. Considering that the amount of power required by the liquid fuel production system is more an order of magnitude higher, the propulsion system need not be considered in the power cycle calculation.

Multiple options exist for the PCS working fluid. Several references demonstrate that S-CO_2 power cycles are very compact and efficient. The primary utility with S-CO_2 is that it affords comparable efficiency to a He power cycle at a much lower temperature (~600 ^{o}C vice ~800°C). Operating at lower temperatures obviates many materials challenges, and it also facilitates compatibility with a SFR or GFR [35]. Although reference [36] shows that S-CO_2 efficiency increases with higher temperatures (as expected), little investigation discusses the suitability of S-CO_2 at temperatures desirable for heat input to HTCE/HTSE processes (>700 ^{o}C) [37]. Another alternative is He, which is desirable for being inert. Unfortunately, He is becoming scarcer [38], and is the most expensive fluid option. Because of He's small atomic size, designing a completely leak-proof system is nearly impossible [30]. Replenishment of He inventory on station could prove problematic, whereas CO_2 is available from the ship's air capture units. A 80%/20% N_2/He mixture or a pure N_2 fluid could serve as an alternative to He; but N_2's low heat capacity will result in large mass flow rates for the same power output.

152

Compared to helium, a supercritical CO_2 cycle has several advantages. At room temperature (300 K), CO_2 can be stored in the liquid phase at a relatively low pressure of 6.71 MPa [39]. Since He must be stored in a gaseous or supercritical phase, it will require significantly more space than CO_2 storage. Another advantage is that, for a given power, S-CO_2 turbomachinery components will be smaller. As reference [35] shows, the number of turbine stages is as follows:

$$N = c_p \frac{\Delta T}{\Delta h_{stage}}$$
(4-11)

$Where\ N = \#\ Stages$

$c_p = specific\ heat\ capacity\ (constant\ pressure), \dfrac{kJ}{(kg - K)}$

$\Delta T = Temperature\ drop\ across\ Tubine, K$

$\Delta h_{stage} = Enthalpy\ drop\ per\ stage, \dfrac{kJ}{kg}$

As equation (4-11) shows, the number of stages, and therefore turbine length, is proportional to the c_p value at the same ΔT and Δh_{stage} conditions. At 700 °C and 20 MPa, the c_p of He is ~ 5.2 kJ/kg-K while the c_p of CO_2 is ~ 1.2 kJ/kg-K; therefore, the He turbine will require over four times the number of stages of the equivalent S-CO_2 turbine.

Figure 4-18 shows a power conversion unit (PCU)[28] size comparison between a S-CO_2 system and a gas turbine-modular helium reactor (GT-MHR) [40]:
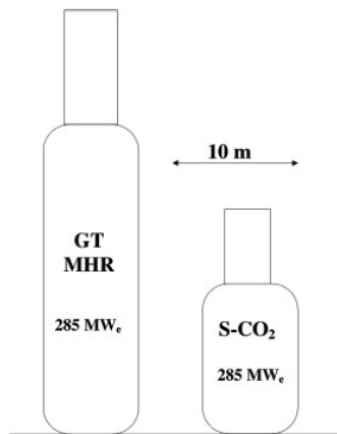
Figure 4-18 - Size Comparison of GT-MHR PCU and S-CO₂ PCU

---

[28] The power conversion units (PCUs) in Figure 4-18 depict the "first generation" PCS layout [28]. These PCUs house all components necessary for a direct, recompression cycle: generator, turbine, main compressor, recompressing compressor, high-temperature recuperator, and low temperature recuperator. Other designs are possible and are described in detail in reference [28].

The 285 MW$_e$ PCU is 7.6 meters in diameter for both fluids, but 18 meters tall for the S-CO$_2$ unit and 34 meters tall for the GT-MHR unit. Thus, the S-CO$_2$ cycle PCU has ~ 89% higher power density. Another benefit of the S-CO$_2$ machines is that CO$_2$ does not leak out as easily as helium, which allows shaft sealing between the generator and turbine using proven technology [40]. The following section also shows that S-CO$_2$ cycles have a better cycle efficiency than helium for a simple Brayton cycle. Since the S-CO$_2$ PCS is more efficient, it can utilize a smaller reactor plant for the same power output.

The tradeoff with using S-CO$_2$ is that its corrosion performance in higher temperature systems (700-900 $^\circ$C) requires more investigation. At higher temperatures, CO$_2$ dissociates as follows [41]:

$$CO_2 \leftrightarrow CO + \frac{1}{2}O_2, \Delta H \ (700 \ ^\circ C) \cong +565 \frac{kJ}{mol} \ (endothermic) \tag{4-12}$$
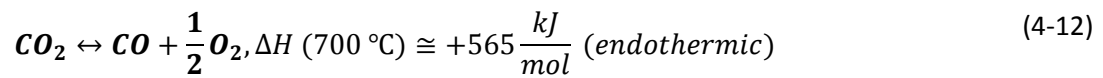
Although equation (4-12) is not favored thermodynamically, small concentrations of O$_2$ will nevertheless result [37]:
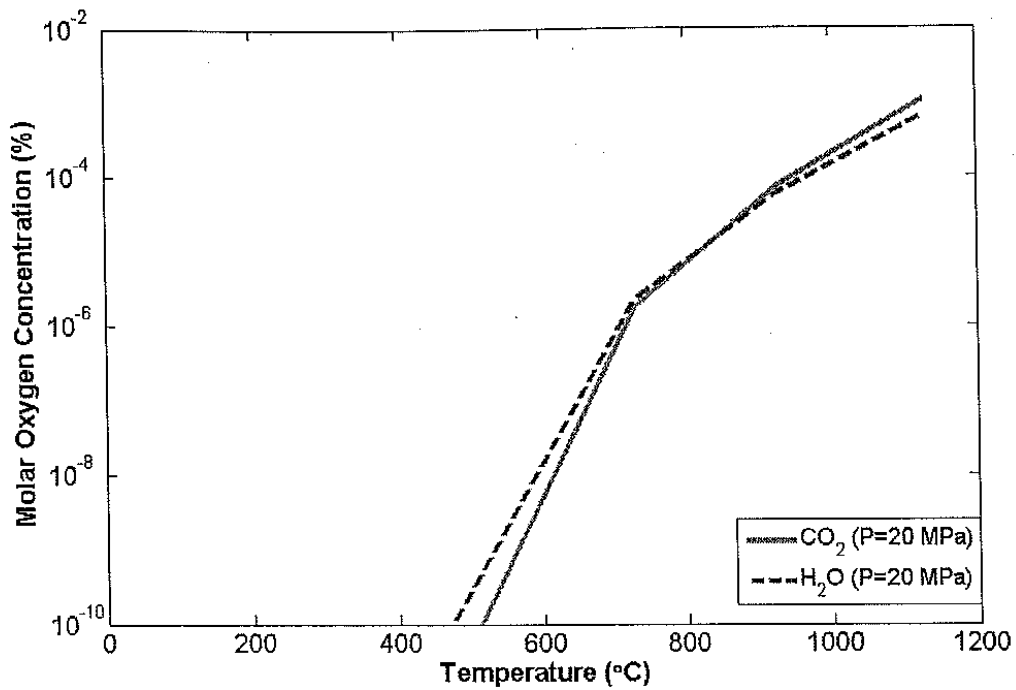
Figure 4-19 - Equilibrium O$_2$ Concentration vs. Temperature at 20 MPa

Until ~ 800 $^\circ$C, S-CO$_2$ has better performance than water (a smaller O$_2$ concentration in principle results in a reduced corrosion rate). Reference [42] reports very small corrosion rates for Type 316 stainless steel (316SS) specimens at 10 MPa, 600 $^\circ$C S-CO$_2$ flow: after 10,000 hours of operation, only 1x10^{-4} g/cm^2 weight gain was reached, forming an ~5 μm continuous oxide layer. More recently, the corrosion

resistance of ten engineering alloys (F91, HCM12A, 316SS, 310SS, AL-6XN, 800H, Haynes 230, Alloy 625, PE-16, and PM 2000) were tested in S-CO_2 for 3000 hours at 610 °C and 20 MPa. Alloys F91 and HCM12A developed porous oxide layers and experienced substantial weight gain (~ 5x10^{-3} mg/cm^2, nearly two orders of magnitude higher than the remaining eight alloys); however the remaining eight alloys formed stable, dense, and corrosion resistant oxide layers with a weight gain of ~4x10^{-5} mg/cm^2. The high chromium and nickel content alloys performed best, followed by the stainless steel alloys with intermediate chromium content [43]. Another study evaluated 6 nickel based and 1 austenitic stainless steel (AUSS) alloys at temperatures ranging from 650 °C to 750 °C, pressures from 12.5 to 20 MPa, and for durations of up to 1000 hours. At 750°C and a pressure of 12.5 MPa, the nickel based alloys revealed weight gain rates of 0.0063 mg/cm^2-day, which were almost an order of magnitude lower than the stainless steel (0.096 mg/cm^2-day) over the 1,000 hour test period. The reduced corrosion rate results from the combination of nickel and chromium that forms a higher integrity and more stable passive film than iron and chromium. The migration of cations into the scale is lower because nickel has a lower oxygen affinity than iron. The study also concludes that the lower chromium content in AUSS 316L most likely contributed to the high oxidation rates [44].

A potentially problematic trend with the studies conducted in references [43] and [44] is that they unambiguously demonstrate S-CO_2's superior performance for a chromium rich alloy. However, numerous references report that any chromium rich alloy performs poorly with any of the AHTR salt coolant candidates. Although Hastelloy-N appears to show resistance to fluoride salts, it has not been evaluated with S-CO_2. In order to ensure a S-CO_2 power cycle is compatible with the AHTR, a material must be evaluated that is resistant to both fluids and has the structural capacity to withstand the demanding temperature and differential pressure environment; or a complex heat exchanger must be designed that contains separate channels for each coolant yet still enables efficient heat transfer within a relatively compact unit.

4.2.6.2   Simple Brayton Cycle

This thesis compared S-CO_2, He, N_2 and an 0.8/0.2 N_2/He mixture in a simple Brayton cycle scheme in order to objectively evaluate the power cycle performance of each fluid. Figure 4-20 provides an illustration of the simple Brayton power cycle scheme:
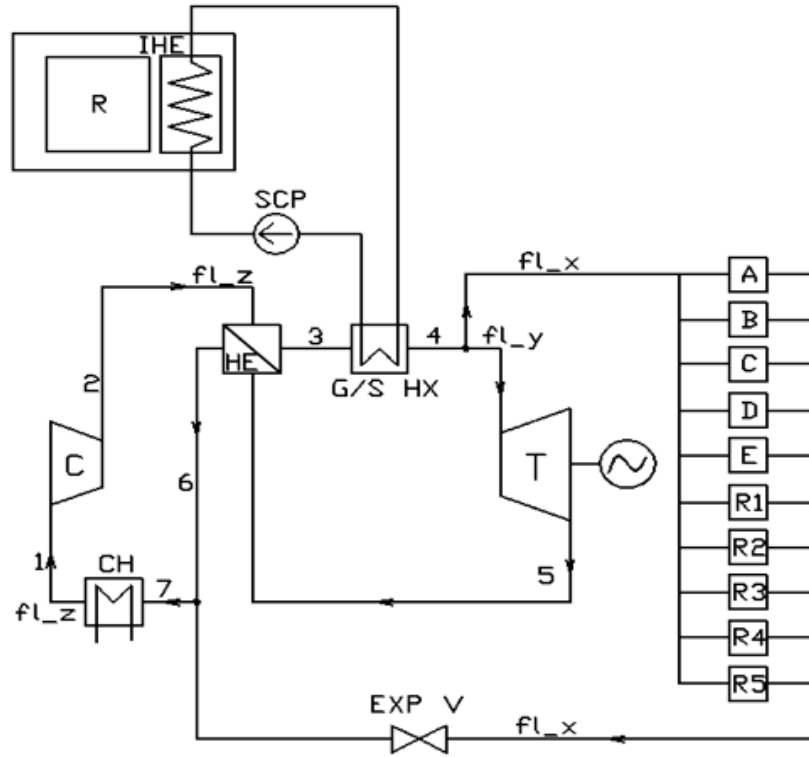
Figure 4-20 - Schematic of Proposed Brayton PCS

Alkaline Electrolysis and HTCE/HTSE Liquid Fuels Production Options			
R		Reactor (AHTR)	
IHE		Intermediate Heat Exchanger (IHE)	
SCP		Salt Coolant Pump	
G/S HX		Salt-to Gas HX	
T		Turbine	
C		Compressor	
HE		Recuperative Heat Exchanger	
CH		Chiller	
fl_x , fl_y, fl_z		Flow Rate	
EXP V		Expansion Valve	
Alkaline Electrolysis Option Only		**HTCE/HTSE Option Only**	
A	RWGS Reaction	A	HTCE (CO_2)
B	ATR (H_2O)	B	HTCE (H_2O)
C	ATR (O_2)	C	HTSE (H_2O)
D	ATR (Hydrocarbons)	D	ATR (H_2O)
E	N/A	E	ATR (Hydrocarbons)
R1	Alkylation	R1	Alkylation
R2	Hydrocracking	R2	Hydrocracking
R3	Aromatization	R3	Aromatization
R4	Oligomerization	R4	Oligomerization
R5	Hydrotreating	R5	Hydrotreating

Table 4-12 - Brayton PCS Legend

Appendix F contains a detailed description of the thermodynamic principles and algorithm methodology used in the power cycle calculations.

The cycle pressure ratio was varied over a range between 1.1 and 5.0. For the alkaline electrolysis case, the assumed working fluid temperature is 700 ^{o}C; the HTCE/HTSE case uses an 800 ^{o}C fluid temperature. The results with highest cycle thermal efficiency (max Eff) and highest turbine work (max Wrk) - lowest flow rate – are shown in a series of figures in the following paragraphs. Because integrating the liquid fuels production plant and refinery heat loads into the cycle consumes a portion of heat transferred to the cycle without producing any power, the resulting cycle thermal efficiency is somewhat lower than a simple Brayton cycle.

The optimization computations reveal somewhat mixed results for best cycle efficiency. None of the options with N_2 (N_2 or He/N_2 mixture) are ever optimal. For the alkaline electrolysis case, which requires lower temperatures, the He cycle is slightly better when the goal is maximizing cycle efficiency; however, S-CO_2 has somewhat superior cycle efficiency when the goal is maximizing work (lowest mass flow rate):
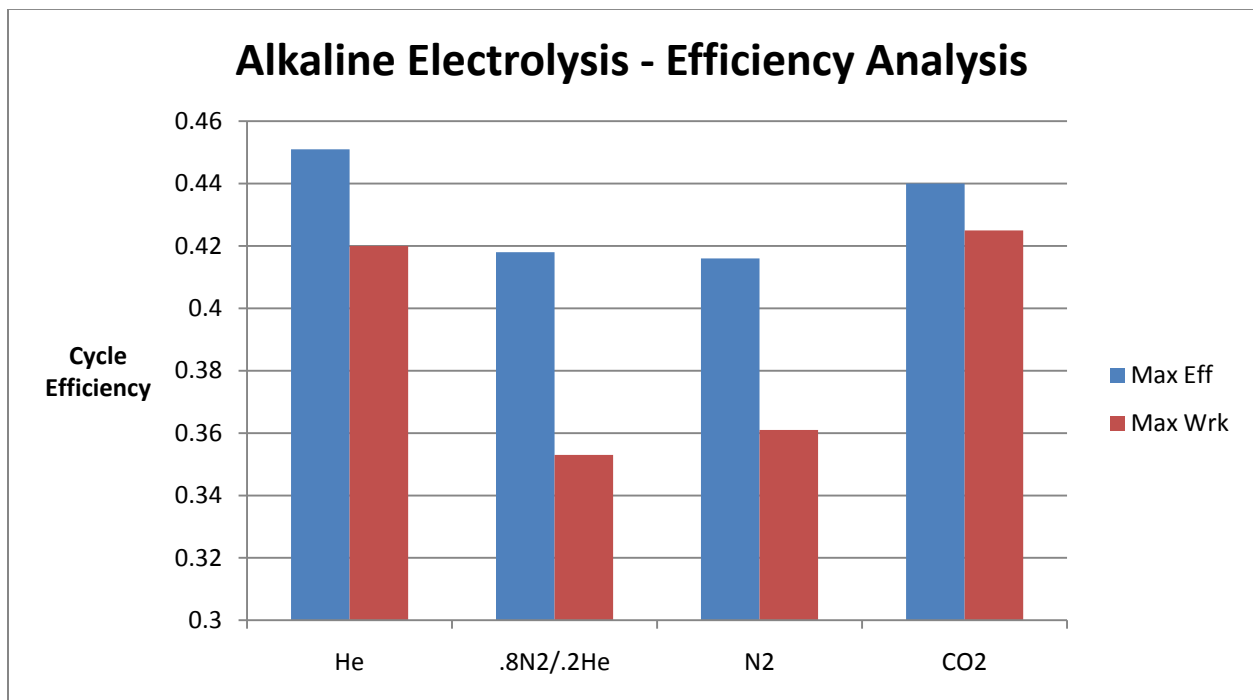
Figure 4-21 - Comparison of Cycle Efficiencies, Simple Brayton (Alkaline Electrolysis Case)

However, for the HTCE/HTSE case (which has a peak operating temperature of 800 ^{o}C instead of 700 ^{o}C), S-CO_2 has a better cycle efficiency:

HTCE/HTSE - Efficiency Analysis
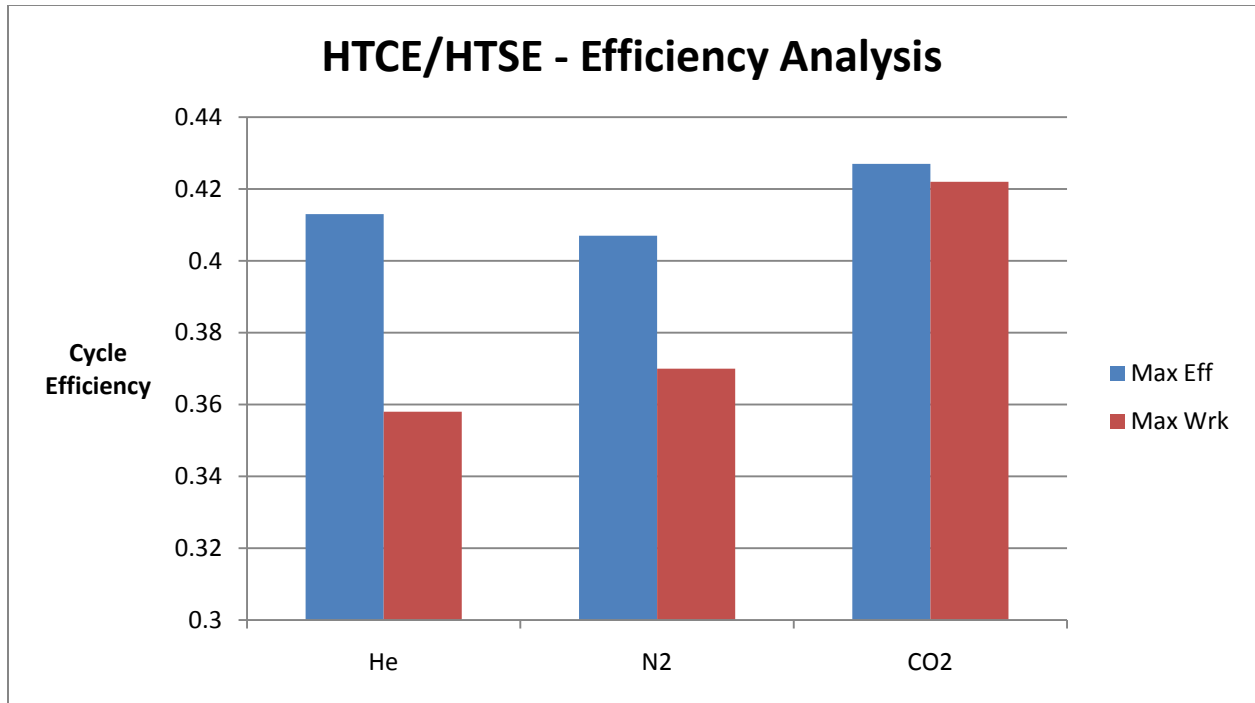
Figure 4-22 - Comparison of Cycle Efficiencies (HTCE/HTSE Case)

The He PCS efficiency is only better for the alkaline electrolysis case with the cycle optimized to maximize thermal efficiency. The S-CO_2 PCS has slightly superior efficiency when the cycle is optimized to maximize efficiency for the HTCE/HTSE case, and has a much better efficiency than He when the cycle is optimized to maximize work. The S-CO_2 cycle has a much higher mass flow rate, but considering the gram atomic weight of CO_2 is 11 times higher than He, the higher mass flow rate is not surprising. (At 800°C and 20 MPa, CO_2 fluid density is 10.72 times greater than helium [39].) As explained by equation (4-11) S-CO_2 will have a smaller turbine than helium. Furthermore, the following parametric relationship used to compare heat exchanger sizes (derived in detail in reference [45]) shows that S-CO_2 will also have somewhat smaller heat exchangers:

$$\frac{W}{Q} \propto \left(\rho^2 c_p^3\right)^{-1} \tag{4-13}$$

$$where \; W = circulator \; work$$
$$Q = channel \; thermal \; power$$

Substituting density and heat capacity values for 700 °C and 800 °C (20 MPa) yields a CO_2/He ratio of 0.59 and 0.57, respectively.[29]

---

[29] The flow rates are high enough for helium and S-CO_2 to ensure a turbulent flow regime for both fluids for all pipes with equivalent hydraulic diameters larger than 1×10^{-6} meters. Since the heat exchanger channel diameters

Simply stated, the S-CO$_2$ PCS will be considerably smaller than a He PCS despite the higher mass flow rate. N$_2$ or a N$_2$/He mixture is probably not suitable for a shipboard application because pure He or S-CO$_2$ cycles tend have better efficiency. N$_2$ would be relatively easy to obtain, but obtaining CO$_2$ would not be difficult either considering that the ship is equipped with CO$_2$ air capture units. Additionally, CO$_2$ can be liquefied at a relatively low pressure, which facilitates more convenient storage. Helium is more expensive, and it presents challenges due to its tendency to leak out of the system. Compared to He, S-CO$_2$ tends to have a higher cycle efficiency. A S-CO$_2$ PCS also has a considerably smaller footprint. While helium is an inert gas, S-CO$_2$ is reactive; however, previous investigation shows that several alloys are promising.

4.2.6.3 S-CO$_2$ Recompression Cycle Analysis

While the previous section shows that S-CO$_2$ has somewhat better cycle efficiency in a simple Brayton cycle, figure shows S-CO$_2$ is an obvious choice for a recompression cycle, even at 800 ^{o}C:
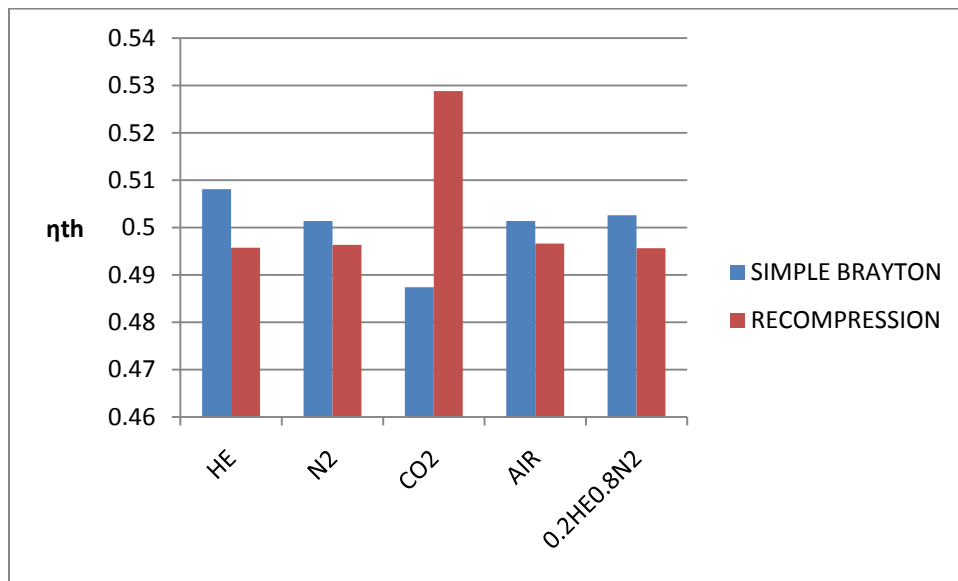
Figure 4-23 - Recompression Cycle Comparison

The difference between a recompression cycle and a simple Brayton cycle is the use of at least two additional components: a recompression compressor and a low temperature recuperator (LTR). For a S-CO$_2$ system, incorporating these two additional components into the PCU provides a remarkable efficiency increase for a relatively modest increase in PCU footprint [28]:

---

for a 150 MW heat exchanger in reference [28] is 0.002 meters, one can easily conclude from a Reynolds number calculation that helium and CO$_2$ would have turbulent flow.
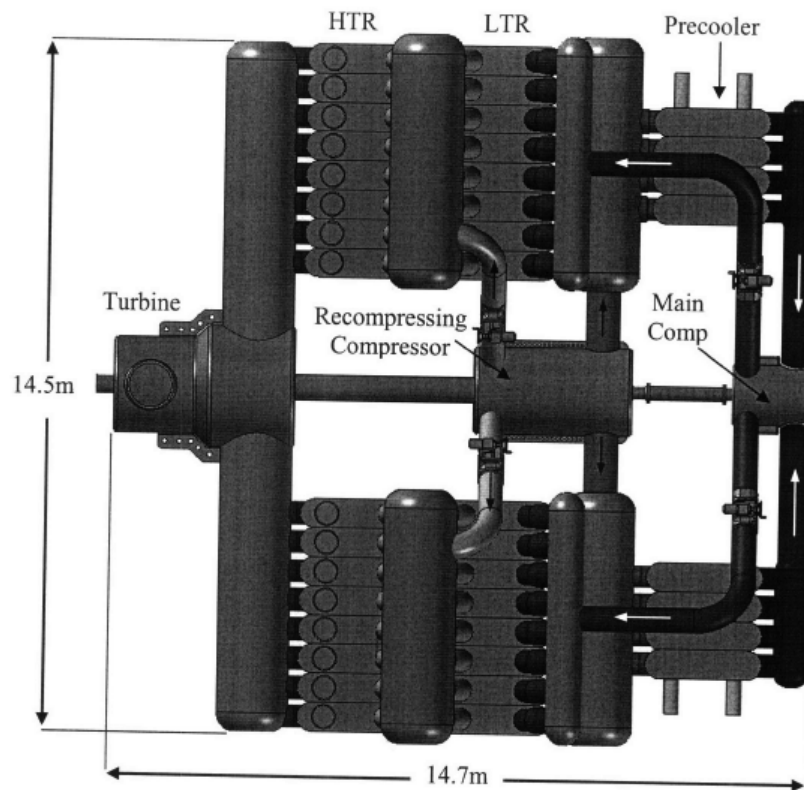
Figure 4-24 - S-CO₂ Recompression PCU (300 MWₑ)

As following sections will show, the S-CO₂ recompression PCU is much more compact than a comparable Rankine PCS design.

As noted in section 4.2.4.4, high operating temperatures in excess of 800 ^{o}C may be desirable, but ASME certification for a 700 ^{o}C reactor outlet temperature is much more realistic in the near term. Because the AHTR uses an intermediate heat exchanger (IHX) to separate the low pressure reactor from the high pressure PCS, 670 ^{o}C is a realistic maximum operating temperature for the S-CO₂ fluid.

Like the simple Brayton cycle, the S-CO₂ cycle efficiency was computed for liquid fuels production using alkaline electrolysis as well as HTCE/HTSE using the liquid fuel plant performance parameters that were calculated in chapter 3 for a 670 ^{o}C working fluid. Figure 4-25 shows the recompression scheme used to compute cycle performance, which is similar to a simple Brayton cycle, while Appendix F contains the algorithm used to compute the cycle efficiency:

160
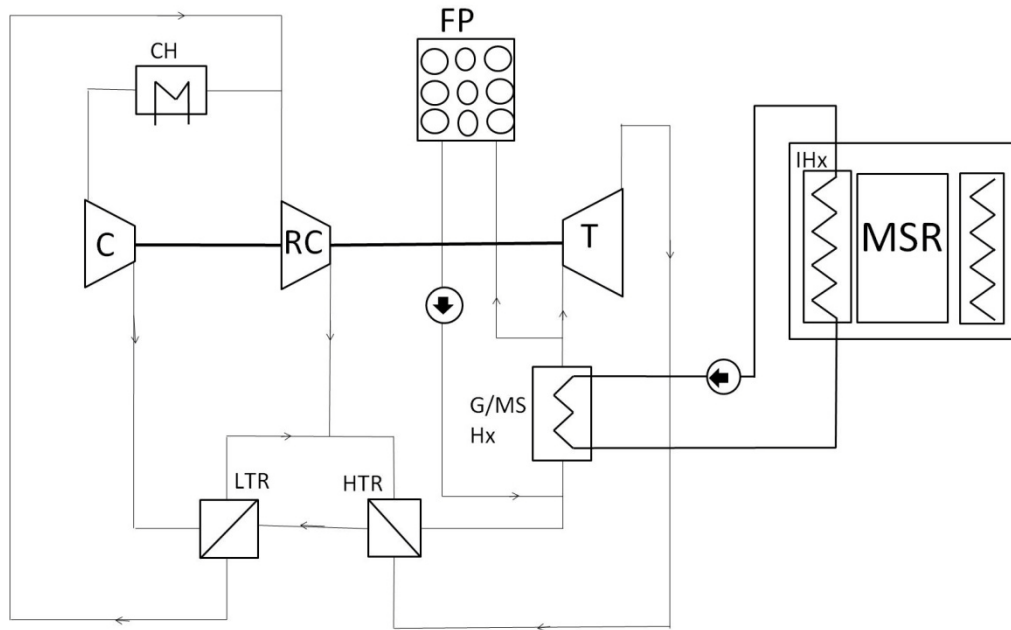
Figure 4-25 - S-CO2 Recompression Cycle Scheme

Table 4-13 summarizes the cycle results:

Max Press (MPa)	25.0	Power Required for Alkaline Electrolysis (MW$_e$)			874
Pressure Ratio	3.20	Power Required for HTCE/HTSE (MW$_e$)			650
T_cond (^{o}C)	32.0				
Alkaline Electrolysis					
Flow Rates (kg/s S-CO$_2$)		**Heat Input (MW$_{th}$)**		**Power (MW$_e$)**	
PCS	6,960	Refining	8.59	Turbine	1,253
Heat Loads	316	RWGS/ATR	69.8	Compressor	105
Total Flow Rate	**7,275**	PCS	1,729	Recompressor	274
		Total Heat Input	**1,807**	**Net Power**	**874**
				Efficiency	**48.3%**
HTCE/HTSE					
Flow Rates (kg/s S-CO$_2$)		**Heat Input (MW$_{th}$)**		**Power (MW$_e$)**	
PCS	5,176	Refining	8.59	Turbine	932
Heat Loads	686	HTCE-HTSE Heating/ATR	162	Compressor	78.1
Total Flow Rate	**5,862**	PCS	1,286	Recompressor	204
		Total Heat Input	**1,456**	**Net Power**	**650**
				Efficiency	**44.6%**

Table 4-13 - S-CO$_2$ Recompression Cycle Results (S-CO$_2$, 670 ^{o}C)

As expected, the alkaline electrolysis case has higher cycle efficiency because less heat input is required to support HTCE/HTSE. However, much more overall heat input and net power is necessary to support alkaline electrolysis.

4.3   Pressurized Water Reactor Option

4.3.1   Basis for PWR Consideration

USN reactors have always been PWRs.[30] All US commercial power reactors are either PWRs or, its LWR cousin, boiling water reactors (BWRs).[31] Despite their relatively low operating temperature compared to newer conceptual reactor plant designs, the USN has extensive operating experience as well as a rigorously demonstrated safety record with PWRs. The Naval Nuclear Propulsion Program (NAVSEA 08) eschews reactor plant designs other than PWRs because it is difficult to show that a different reactor plant design would afford the same levels of reliability and survivability given the typical power demands of a naval vessel [2]. Although the higher temperatures necessary for the RWGS reaction or HTCE/HTSE, ATR, and refining suggest that another reactor plant design might be more prudent, a PWR could hypothetically serve as the power source for either the alkaline electrolysis case or the HTCE/HTSE case.

4.3.2   PWR Feasibility

The required temperatures for liquid fuels production could be attained by using electric heaters to increase temperatures where necessary; and intelligent heat recuperation could minimize electric heater power demand. During normal operation, each "high temperature" process has relatively negligible power requirements to accommodate compared to the power needed for electrolysis. For the alkaline electrolysis case using 285 ^{o}C as the working fluid, 40.6 MW$_e$ is necessary to maintain the RWGS reaction (467 ^{o}C); 4.61 MW$_e$ of heater power is needed to raise steam, O$_2$, and hydrocarbon temperature to 700 ^{o}C for ATR; and an additional 2.49 MW$_e$ is required to boost temperature to 350 ^{o}C for aromatization. These figures are small considering that alkaline electrolysis requires 789 MW$_e$. Since

---

[30] The only exception is the USS Seawolf, SSN 575, which had a liquid sodium cooled reactor from 1957-1958 (one year of its 30 year service life). The sodium-cooled reactor plant was converted to a PWR in 1958. See http://en.wikipedia.org/wiki/USS_Seawolf_%28SSN-575%29 for more details regarding USS Seawolf.

[31] Because of radiation shielding and containment concerns, direct cycle nuclear power plants are not suitable for shipboard use; hence BWRs shall not be discussed further.

only 2.52 MW$_{th}$ is recuperated during the alkaline electrolysis case, plant startup only requires a modest amount of additional heater power. HTCE/HTSE is feasible using 285 ^{o}C steam as well. In the HTCE/HTSE case, the heater power for refining remains the same, but 0.77 MW$_e$ is necessary to boost steam temperature to 800 ^{o}C for HTSE and 5.38 MW$_e$ is necessary for ATR. Since 79.1 MW$_{th}$ are recuperated in the HTCE/HTSE cycle, the startup operation will not be as trivial as for the alkaline electrolysis case. However, given that 590 MW$_e$ are necessary for HTCE and HTSE, the additional power requirements for startup should be manageable.

Since a PWR is a feasible option, it deserves consideration. The previous section identifies numerous AHTR design issues requiring additional investigation and resolution, particularly when coupled to a S-CO$_2$ PCS. The AHTR will require a large amount of research and design effort to validate its suitability, whereas the PWR uses a mature, well-understood design. By utilizing an already approved naval reactor plant design, the USN would undoubtedly save on research and design costs as well as assume less technological risk.

In order to make an objective evaluation regarding the AHTR's potential benefit to the PWR, the cycle efficiency was computed for a Rankine cycle for the alkaline electrolysis and HTCE/HTSE fuel production schemes with the following assumptions using the well-known Rankine cycle problem solving process that reference [46] explains in detail:

- 285 ^{o}C steam temperature (15 ^{o}C less than nominal PWR operating temperature)
- Saturated vapor upon exiting steam generator (S/G)
- 30 ^{o}C condenser temperature with 10 ^{o}C condensate subcooling
- 90% turbine and pump efficiencies
- Steam flow rate such that flow rate steam supplied to heat loads (ATR, HTSE, etc.) enters heat exchanger as saturated vapor and leaves as saturated liquid

The alkaline electrolysis case has a total S/G flow rate of 1,021 kg/s, a 2,722 MW$_{th}$ heat input, and a 33.6% cycle efficiency. Recalling Table 4-13, the AHTR coupled to a S-CO$_2$ PCS is able to power the alkaline liquid fuels production process with a 33.6% lower heat input (1,087 MW$_{th}$) and a 44.1% higher cycle efficiency (48.3%). For the HTCE/HTSE case, the S/G flow rate is 807 kg/s, 2,082 MW$_{th}$ heat input is necessary, and cycle efficiency is 31.3%. For this more advanced fuel production option, the AHTR requires 30.1% less heat input (1,456 MW$_{th}$) and has a 42.4% higher cycle efficiency (44.6%).

Another significant advantage of the S-CO$_2$ system is that the PCS is much more compact. Figure 4-26 and Figure 4-27, adapted from reference [28], succinctly demonstrate the reduced footprint of an indirect, 300 MW$_e$, supercritical-CO$_2$ (S-CO$_2$) cycle over a Rankine cycle:
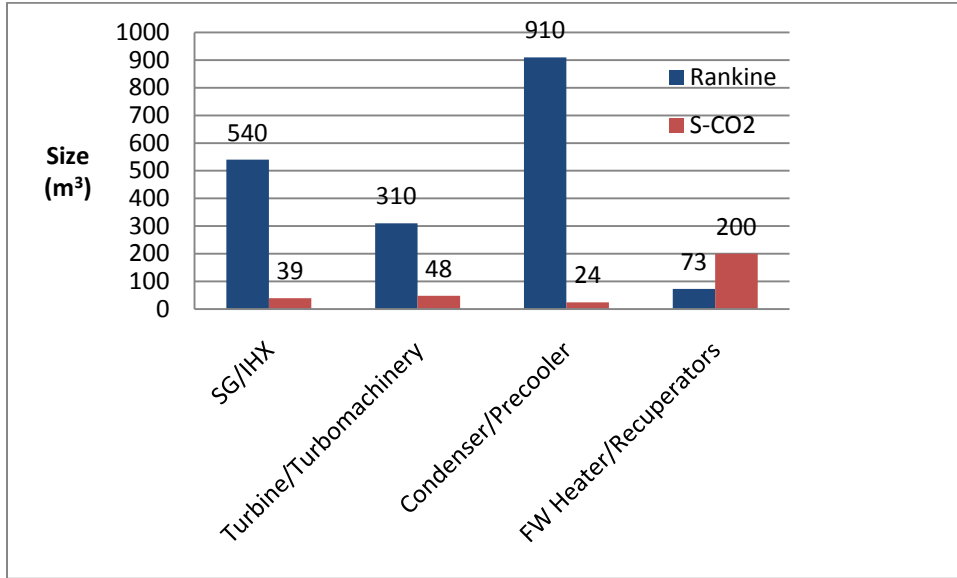
Figure 4-26 - Overall Comparison of S-CO2 vs Rankine Cycle Machinery Footprint

230MWth Steam Generator (6 units required to generate 388MWe)

Figure 2.43 IHX vs. steam generator size comparison. (top view)

Total steam generator volume = 540m³ (includes total volume for 6 units)

Total IHX volume = 39m³ (includes total volume for 16 modules)

300MWth IHX (2 units required to generate 300MWe)

Figure 2.42 IHX vs. steam generator size comparison. (front view)
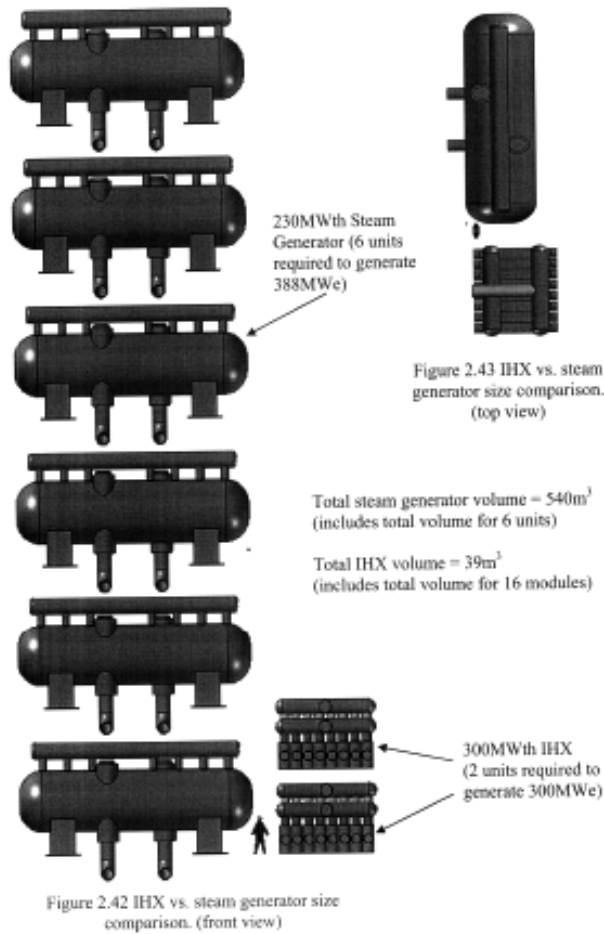
Figure 4-27 - Comparison of S-CO2 vs Rankine Cycle Heat Exchangers

For those interested, reference [28] contains several more figures that further illustrate the reduced footprint of S-CO_2 components. However, the important point is that for a 300 MW_e PCS, Rankine cycle machinery requires 1,833 m^3; but S-CO_2 machinery requires only 311 m^3, a reduction of 83%.

A PWR could hypothetically be coupled to a S-CO_2 PCS; however, S-CO_2 turbine inlet temperature sensitivity studies in reference [28] demonstrated that for a turbine inlet temperature of 300 ^{o}C, the best possible cycle efficiency is ~ 20%, and that cycle efficiency worsens as temperature decreases. Nevertheless, calculations were performed for the S-CO_2 recompression cycle proposed in section 4.2.6.3 for the alkaline electrolysis and HTCE/HTCE case, assuming a temperature of 285 ^{o}C. Although PCS turbo machinery volume could hypothetically be reduced by using a S-CO_2 cycle instead of a traditional Rankine cycle, Table 4-14 shows that the efficiency penalty of adopting a S-CO_2 for a PWR is probably not worth the tradeoff:

S-CO$_2$, 285 ^{o}C (PWR)			
Max Press (MPa)	25.0	Power Required for Alkaline Electrolysis (MW$_e$)	921
Pressure Ratio	2.40	Power Required for HTCE/HTSE (MW$_e$)	658
T_cond (^{o}C)	32.0		
Alkaline Electrolysis			
Flow Rates (kg/s S-CO$_2$)		Heat Input (MW$_{th}$)		Power (MW$_e$)	
PCS	22,263	Refining	6.24	Turbine	2,073
Heat Loads	141	RWGS/ATR	14.6	Compressor	326
Total Flow Rate	**22,404**	PCS	3,290	Recompressor	826
		Total Heat Input	**3,311**	**Net Power**	**921**
				Efficiency	**27.8%**
HTCE/HTSE					
Flow Rates (kg/s S-CO$_2$)		Heat Input (MW$_{th}$)		Power (MW$_e$)	
PCS	15,906	Refining	6.24	Turbine	1,481
Heat Loads	734	HTCE-HTSE Heating/ATR	102	Compressor	233
Total Flow Rate	**16,640**	PCS	2,351	Recompressor	590
		Total Heat Input	**2,459**	**Net Power**	**658**
				Efficiency	**26.7%**

Table 4-14 - S-CO$_2$ PCS Performance with PWR

Recalling Table 4-13 and the Rankine cycle results above, a S-CO$_2$ PCS is not well suited for a PWR. Compared to the higher temperature case, S-CO$_2$ flow rates are over 200% higher. The cycle efficiency is 17.2% lower for the alkaline electrolysis case (27.8% vs. 33.6%) and 14.7% lower for the HTCE/HTSE case (26.7% vs 31.3%). In summary, constraining the reactor plant to a PWR necessitates using a reactor core with a higher rated power as well as PCS machinery requiring a much larger footprint. Despite the USN's familiarity with PWRs and a Rankine PCS, the advantages afforded through the use of high temperature reactors and more compact Brayton or recompression cycle machinery are too significant to ignore, especially for shipboard applications.

4.4 Power Plant Summary

Of the three options available to design the AHTR's core with TRISO fuel particles, the prismatic block is probably most suited for the USN, which has little need for on-line or frequent refueling. Compared to the other options, it provides the most freedom in core design because the core designer has great flexibility in choosing (1) the ratio of the fuel to the moderator and to the coolant and (2) the three dimensional neutronic characteristics. Follow-on investigation could reveal the possibility of incorporating deep burn concepts with the AHTR.

Several salt coolant candidates appear feasible, but researchers must determine how particular salt candidates perform with various materials suitable for key reactor plant functions at desired operating temperatures before enough information is available to make an informed decision. Of the materials evaluated so far, Hastelloy-N appears most promising. Investigation is necessary to determine its ASME suitability. Although LiF-BeF_2 is has somewhat better nuclear and thermal hydraulic performance, its higher melting point is undesirable. However, LiF-BeF_2 has much lower short-term activation levels (similar to water) that facilitate reduced shielding, which is very desirable for marine platforms. Furthermore, LiF-BeF_2 may be the only salt candidate that has activation levels low enough to facilitate an emergency reactor compartment entry at sea; but, further investigation is necessary to make any definite statement regarding this scenario. The other two promising options are LiF-NaF-BeF_2 and NaF-BeF_2. The key consideration between selecting between LiF-NaF-BeF_2 and NaF-BeF_2 is the additional cost of enriching the ^7Li constituent to 99.99%. LiF-NaF-BeF_2 provides only a relatively modest performance boost over NaF-BeF_2, but the additional margin could be desirable and worth the cost.

The preliminary safety evaluation of the AHTR is promising. Since the AHTR operates near atmospheric pressure, practically no scenario exists to cause a LOCA. Negative net thermal reactivity coefficients provide a feedback mechanism to mitigate the impact of any event inserting positive reactivity into the core. Additional investigation could prove useful in demonstrating reactor response to various salt coolant temperature transients, but changing salt coolant temperature (especially in comparison to LWRs) should only have a very modest impact. A RELAP-5 thermal-hydraulics analysis shows that a baseline AHTR core, with a RVACS DHR system, can show sufficient protection against a complete LOFC event with no scram. Throughout the entire transient, fuel temperatures remain well below salt coolant boiling temperatures, thereby assuring fuel integrity. An independent evaluation using GRSAC yields similar conclusions. However, additional analysis using a decay heat model other than the ANS standard may be necessary.

Although the RVACS DHR system is simple and can provide protection against the LOFC events postulated in the RELAP-5 simulation, alternate AHTR designs might preclude its use. The DRACS and PRACS designs present attractive alternatives to RVACS; however, material compatibility issues with the salt coolants presents challenges in actually implementing their design. Once the DRACS and PRACS designs are confirmed feasible, a more comprehensive investigation should identify the most appropriate DHR system for a specific AHTR design.

Analysis of simple Brayton PCS alternatives shows that N_2, a N_2/He mixture, and pure helium are not as competitive as S-CO_2. S-CO_2 tends to operate at higher cycle efficiency for a simple Brayton cycle, and a much higher efficiency in a recompression cycle. Additionally CO_2 is easier to obtain than He, and is much more convenient to store than any of the other fluids. Compared to the other variants, S-CO_2 has the smallest PCS footprint. Although previous investigation into S-CO_2 compatibility with various alloys has demonstrated promising trends, additional investigation of material compatibility with salt coolants and S-CO_2 is necessary.

Despite the USN's familiarity with PWRs and a Rankine PCS, the advantages afforded through the use of high temperature reactors and more compact Brayton cycle machinery are too significant to ignore, especially for shipboard applications of the type proposed in this thesis. For the same 6,400 BBL/Day JP-5 production rate, the AHTR coupled to a S-CO_2 PCS is able to power the alkaline liquid fuels production process with a 33.6% lower heat input and a 44.1% higher cycle efficiency. For the HTCE/HTSE case, the AHTR requires 30.1% less heat input and has a 42.4% higher cycle efficiency. Using a S-CO_2 recompression cycle also affords a compact PCS with desirable efficiency. A PWR cannot utilize a S-CO_2 recompression cycle without suffering a significant efficiency penalty.

Since the required reactor heat input for liquid fuels production is known, the efficiency of the entire liquid fuel production process can be determined. A 6,400 BBL/day production rate of JP-5 is ~ 0.074 BBL/sec. Per Appendix B, the enthalpy of combustion for JP-5 is ~ 48,500 kJ/kg. Assuming a density of 0.8 kg/liter, and by assuming 3.79 liter/gal and 42 gal/BBL, the combustion of 0.074 BBL/sec of JP-5 is ~ 453,000 kW$_{th}$ (453 MW$_{th}$). Dividing this value by the reactor heat input provides the overall process efficiency (Rankine cycle assumed for PWR):

Option	Efficiency
AHTR – Alkaline Electrolysis	25.1%
AHTR – HTCE/HTSE	31.1%
PWR – Alkaline Electrolysis	16.6%
PWR – HTCE/HTSE	21.8%

Table 4-15 - Overall Liquid Fuel Production Efficiencies (Combustion Heat Output to Reactor Heat Input)

Assuming the technological issues facing the AHTR, S-CO_2, and SOECs are resolved sometime in the future, the AHTR reactor generating liquid fuels via HTCE/HTSE offers an attractive efficiency compared to the other options evaluated in this thesis.

The baseline reactor plant design recommended for additional analysis should include the salt-cooled AHTR with a prismatic block fuel design and LiF-BeF$_2$ coolant; this will be the assumed configuration in the next chapter. The prismatic block design provides the core designer maximum flexibility, which is highly desirable for USN reactor cores. The ease of refueling benefits conferred through the use of pebble bed or stringer fuel designs are more suited for a civilian facility than a military warship. Although LiF-BeF$_2$ does not have the lowest freezing point, it has the lowest short-term activation, best neutronic performance, and best free and forced convection FOMs. Its better performance is probably worth its relatively higher cost due to ^{7}Li enrichment, especially considering that the salt should be indefinitely reusable.

The baseline PCS will use a S-CO$_2$ recompression power cycle. Although the HTCE/HTSE liquid fuels production system is a more advanced option, the HTCE/HTSE case promises the most benefit. The next chapter will determine the feasibility of the nuclear powered liquid fuels production plant by inserting a parallel midbody section into the T-AO-187 tanker ship (USS Henry Kaiser) and estimate the cost of constructing an entirely new platform. A more ambitious engineering effort should also be undertaken in the future to design a new hull form using the baseline liquid fuels production plant, reactor plant, and PCS designs developed in this thesis.

4.5 Chapter 4 References

[1] Forsberg, C., 2005, "Brayton Power Cycles and High-Temperature Salt-Cooled Reactors," Transactions of the American Nuclear Society, **92**(1) pp. 231-233.

[2] Donald, K. A., 2010, "Naval Sea Systems Command, Director of Nuclear Propulsion (NAVSEA 08) Statement regarding US Navy use of Non-PWR Reactor Technology," **Statement from head of NAVSEA 08 to author and other MIT afflliated Engineering Duty Officers during an MIT luncheon on 29 Sep 2010 that, at the present time, the US Navy is not interested in implementing non-PWR reactor technology on its warships.**pp. 1.

[3] Forsberg, C., 2003, "Hydrogen, Nuclear Energy, and the Advanced High-Temperature Reactor," International Journal of Hydrogen Energy, **28**pp. 1073-1081.

[4] Forsberg, C., Ingersoll, D., Peterson, P., 2006, "Refueling Options and Considerations for Liquid-Salt-Cooled Very High-Temperature Reactors," Oak Ridge National Laboratory, ORNL/TM-2006/92, Oak Ridge, TN.

[5] Forsberg, C., 2002, "Nuclear Hydrogen Production: Isolating the Nuclear Reactor and Chemical Facilities," Transactions of the American Nuclear Society, **87**(1) pp. 78-79.

[6] Forsberg, C., 2010, "High-Temperature Salt-Cooled Reactors," Massachusetts Institute of Technology, Presentation to 22.39 (Integration of Reactor Design, Operations, and Safety), MIT, 10/05/2010, Cambridge, MA.

[7] Forsberg, C., Peterson, P., and Pickard, P., 2003, "Molten-Salt-Cooled Advanced High-Temperature Reactor for Production of Hydrogen and Electricity," Nuclear Technology, **144**(3) pp. 289-302.

[8] Forsberg, C., 2006, "Fuel Characteristics and Requirements for the Advanced High-Temperature Reactor," Transactions of the American Nuclear Society, **94**pp. 645-647.

[9] Forsberg, C., 2006, "Goals, Requirements, and Design Implications for the Advanced High-Temperature Reactor," American Society of Mechanical Engineers, Paper ICONE14-89305 (CD-ROM), New York, NY.

[10] Schrady, D., Smyth, G., and Vassian, R., 1996, "Predicting Ship Fuel Consumption: Update," Naval Postgraduate School, NPS-OR-96-007, Monterey, CA.

[11] Carderock Division, Naval Surface Warfare Center (NSWC), 2003, "ASSET - Advanced Surface Ship and Submarine Evaluation Tool," **5.3**.

[12] Hoffman, D., Borraccini, J., Swindler, S., 2010, "Next Generation Power and Energy: Maybe Not So Next Generation," Engineering the Total Ship (ETS) 2010 Proceedings, J. Pazik and S. Wallace, eds. American Society of Naval Engineers, Falls Church, VA, pp. 1-23.

[13] Forsberg, C., 2006, "Advanced High Temperature Reactor Spent Fuel Characteristics and Repository Impacts," Oak Ridge National Laboratory, HLW06/147924, Oak Ridge, TN.

[14] Ingersoll, D., Clarno, K., Forsberg, C., 2005, "Status of Physics and Safety Analyses for the Liquid-Salt-Cooled Very High-Temperature Reactor (LS-VHTR)," Oak Ridge National Laboratory, ORNL/TM-2005/218, Oak Ridge, TN.

[15] Kim, T., Taiwo, T., and Williamson, M., 2005, "A Feasibility Study of Reactor-Based Deep-Burn Concepts," Argonne National Laboratory, ANL-AFCI-155, Argonne, IL.

[16] Grimes, W., 1967, "Chemical Research and Development for the Molten-Salt Breeder Reactor," Oak Ridge National Laboratory, ORNL/TM-1853, Oak Ridge, TN.

[17] Williams, D., Toth, L., and Clarno, K., 2006, "Assessment of Candidate Molten Salt Coolants for the Advanced High-Temperature Reactor (AHTR)," Oak Ridge National Laboratory, ORNL/TM-2006/12, Oak Ridge, TN.

[18] Williams, D., and Clarno, K., 2008, "Evaluation of Salt Coolants for Reactor Applications," Nuclear Technology, **163**(3) pp. 330-343.

[19] Grimes, W., 1966, "Reactor Chemistry Division Annual Progress Report for Period Ending December 31, 1965," Oak Ridge National Laboratory, ORNL-3913, Oak Ridge, TN.

[20] Cornwell, K., 1971, "The Thermal Conductivity of Molten Salts," Journal of Physics D: Applied Physics, **4**pp. 441-445.

[21] Khokhlov, V., 1998, "Light Metals,"TSM, San Antonio, TX, pp. 501-506, Chap. 10.

[22] Bonilla, C., 1958, "Nuclear Engineering Handbook, Edited by H. Etherington,"McGraw-Hill, New York, NY, pp. 9, Chap. Ch 6.5, Sec 9-3.

[23] Zakova, J., and Talamo, A., 2008, "Analysis of the Reactivity Coefficients of the Advanced High-Temperature Reactor for Plutonium and Uranium Fuels," Annals of Nuclear Energy, **35**pp. 904-916.

[24] Corwin, D., and Wilson, D., 2010, "Fluoride Salt Cooled High Temperature Reactor (FHR) Materials Challenges," Oak Ridge National Laboratory, FHR Workshop Presentation (9/20/2010), Oak Ridge, TN.

[25] Ball, S., and Forsberg, C., 2004, "Advanced High-Temperature Reactor (AHTR) Loss-of-Forced-Circulation Accidents," 2nd International Topical Meeting on HTR Technology, Reproduced by IAEA, Vienna, Austria, ed. Oak Ridge National Laboratory, Oak Ridge, TN, pp. 1-10.

[26] Shwageraus, E., and Hejzlar, P., 2009, "Decay Heat in Fast Reactors with Transuranic Fuels," Nuclear Engineering and Design, **239**pp. 2646-2653.

[27] Forsberg, C., 2006, "Alternative Passive Decay-Heat Systems for the Advanced High-Temperature Reactor," International Congress on Advanced Nuclear Power Plants, Paper 6055 (CD-ROM), Reno, NV.

[28] Gibbs, J., 2008, "M.S. Thesis: Power Conversion System Design for Supercritical Carbon Dioxide Cooled Indirect Cycle Nuclear Reactors," Massachusetts Institute of Technology, http://hdl.handle.net/1721.1/44765, Cambridge, MA.

[29] Memmott, M., 2007, "M.S. Thesis: Hydrogen Production Using a Supercritical CO_2-Cooled Fast Reactor and Steam Electrolysis," Massachusetts Institute of Technology, http://hdl.handle.net/1721.1/41307, Cambridge, MA.

[30] Dostal, V., Hejzlar, P., and Driscoll, M., 2006, "The Supercritical Carbon Dioxide Power Cycle: Comparison to Other Advanced Power Cycles," Nuclear Technology, **154**pp. 283-301.

[31] Oh, C., Moore, R., Davis, C., 2005, "Power Conversion Study for High Temperature Gas-Cooled Reactors," Idaho National Engineering and Environmental Laboratory, INEEL/CON-05-02618, Idaho Falls, ID.

[32] Wang, J., and Yihua, G., 2005, "Parametric Studies on Different Gas Turbine Cycles for a High Temperature Gas-Cooled Reactor," Nuclear Engineering and Design, **235**pp. 1761-1772.

[33] Convert Team, 2010, "Advanced Propulsion Motor," Convert Team, APM Fact Sheet, Warwickshire, UK.

[34] Woud, H., and Douwe, S., 2002, "Design of Propulsion and Electric Power Generation Systems," Institute of Marine Engineering, Science and Technology, London, UK, pp. 494.

[35] Kato, Y., Nitawaki, T., and Muto, Y., 2004, "Medium Temperature Carbon Dioxide Gas Turbine Reactor," Nuclear Engineering and Design, **230**pp. 195-207.

[36] Dostal, V., 2004, "Sc.D. Thesis: A Supercritical Carbon Dioxide Cycle for Next Generation Nuclear Reactors," Massachusetts Institute of Technology, http://hdl.handle.net/1721.1/17746, Cambridge, MA.

[37] Forrest, E., and Stefano, P., 2010, "Alternative Power Cycles for Nuclear Power Plants," Massachusetts Institute of Technology, Spring 2010 Report for "Fundamentals of Advanced Energy Conversion", Cambridge, MA.

[38] Tamura, L., 2010, "Nation's Helium Reserve Running on Empty?" Washingtonpost.Com, **Politics**pp. http://www.washingtonpost.com/wp-dyn/content/article/2010/10/11/AR2010101104496.html.

[39] Linstrom, P., and Mallard, W., 2010, "NIST Chemistry WebBook, NIST Standard Reference Database Number 69," National Institute of Standards and Technology, Gaithersburg, MD, pp. N/A.

[40] Dostal, V., Hejzlar, P., and Driscoll, M., 2006, "High-Performance Supercritical Carbon Dioxide Cycle for Next-Generation Nuclear Reactors," Nuclear Technology, **154**pp. 265-282.

[41] Outotec Research Oy, 2007, "HSC Chemistry," **6.12**.

[42] Kato, Y., 2005, "Overview of Supercritical CO2 Cycle Studies at Tokyo Tech," Massachusetts Institute of Technology, Proc. MIT-Tokyo Tech Symp. Innovative Nuclear Energy Systems (CD-ROM), Cambridge, MA.

[43] Gibbs, J., 2010, "M.S. Thesis: Corrosion of Various Engineering Alloys in Supercritical Carbon Dioxide," Massachusetts Institute of Technology, http://hdl.handle.net/1721.1/59247, Cambridge, MA.

[44] Dunlevy, M., 2009, "M.S. Thesis: An Exploration of the Effect of Temperature on Different Alloys in a Supercritical Carbon Dioxide Environment," Massachusetts Institute of Technology, http://hdl.handle.net/1721.1/57777, Cambridge, MA.

[45] Lyall, H., 1972, "A Comparison of CO2 and Helium as Reactor Coolants," Journal of Nuclear Energy, **26**(2) pp. 49-60.

[46] Todreas, N., and Kazimi, M., 1989, "Nuclear Systems 1: Thermal Hydraulic Fundamentals,"Taylor and Francis Group, New York, NY, pp. 192-208, Chap. 6.

(This Page Intentionally Blank)

5   Naval Platform Integration

5.1   Parallel Midbody Feasibility Determination

5.1.1   Concept Description

One method of demonstrating feasibility of the liquid fuels production process explained in the previous chapters is by incorporating the synfuel plant and power plant into a modular, parallel midbody plug that is inserted into an existing ship.[32] The TAO-187 *Henry Kaiser* class oiler will be the test case for this thesis; it will be split at a logical and convenient watertight bulkhead and the midbody module containing the power plant and fuel plant will be inserted at the break. The first step in the process is estimating the weight and volume of the equipment needed in the midbody section (including the ship systems and structure), and then checking that the equipment desired in the midbody section can (1) fit within the volume and (2) be supported by the buoyant force.

The goal of this investigation is to design a midbody section that accommodates the synfuel plant variant that utilizes <u>high temperature electrolysis</u> for syngas production and a <u>salt-cooled advanced high-temperature reactor</u> (AHTR) coupled to a <u>supercritical CO_2 ($S\text{-}CO_2$) PCS</u> for power production. The PCS shall not supply any propulsion power. Despite the lack of available detailed design work for some of these advanced systems, enough information exists to make reasonable approximations for the major components; these estimates could always be refined through more detailed investigation at a later time. Pressurized water reactors (PWRs), Rankine power conversion systems (PCSs), and alkaline electrolysis units are all commercially established, but, as chapters 3 and 4 show, they are very large, heavy machines; the PWR alone requires the rating of ~ 6 Nimitz-sized A4W reactors operating almost continuously at or above 85% rated power. A $S\text{-}CO_2$ recompression cycle is less than $1/5^{th}$ the size of an equivalent Rankine cycle. Simply stated, a high-temperature reactor coupled to an advanced recompression power cycle is better suited for liquid fuels production. However, future investigation could and should contemplate the use of commercially mature technology in a completely custom built marine platform.

---

[32] A parallel midbody is simply a modular plug containing the desired equipment.

5.1.2 Determining Space and Weight for Power Plant Components

5.1.2.1 Reactor Size and Weight

Conveniently, Figure 1.2, Table 1.1, Table 3.5, and Table 6.1 of reference [1] contain all the
Conceptually designs exist only for a 2,400 MW$_{th}$ AHTR, and the designs under consideration are for a civilian variant that is housed in concrete and equipped with a refueling apparatus. However, Oak Ridge National Laboratory (ORNL) has developed some useful parametrics to scale the reactor to ~1,456 MW$_{th}$. The components of significant weight are the reactor pressure vessel (RPV), fuel, graphite, and coolant. Since the reactor considered by this thesis has the same power density as the AHTR designed by ORNL, its geometric parameters should scale linearly with power. Other reactor plant devices requiring consideration are the decay heat removal system, the primary shield, and the secondary shield.

Conveniently, Figure 1.2, Table 1.1, Table 3.5, and Table 6.1 of reference [1] contain all the desired parameters necessary to estimate the size and weight of the RPV, the fuel/graphite core, and the reactor vessel auxiliary cooling system (RVACS) by linearly scaling the geometric parameters as a function of power. Admittedly, changing a reactor's geometry changes the neutron leakage probabilities and thermal/hydraulic performance, but the goal is to estimate the reactor's size and weight; a reactor designer could certainly adjust the baseline core design to accommodate the desired geometry, especially with the design freedom conferred by the prismatic block core. Thus, the new RPV has a diameter of ~ 4.87 m and a height of ~ 12.7 m. By assuming a 0.1 m thickness, the RPV's weight can be determined from the density of steel (7,750 kg/m^3), which is 30.8 MT. A similar procedure for the RVACS dimensions provided in Table 6.1 shows that the RVACS weighs only 0.052 MT, not including ancillary components; more accurate design details regarding the AHTR's ancillary systems would undoubtedly yield more accurate estimates. Table 1.1 of reference [1] indicates that the core power density is 10 MW/m^3. Since the core volume is known, and the core graphite density of 1.74 g/cm^3 is given, the weight of the graphite in the core is ~253 MT. Table 3.5 shows that the heavy metal mass is 158 MW$_{th}$/MT, from which the heavy metal mass is 9.22 MT.

Determining the coolant mass is not as convenient. Although the LiF-BeF$_2$ density at operating temperature (700 ^{o}C) is known from reference [2], the total amount of salt-coolant is not known.

Therefore, expert opinion was solicited from ORNL and the volume assumed for the baseline variant is 2,561 m^3 [3]. By linearly scaling the vessel's geometry, the coolant has an estimated mass of 253 MT.

5.1.2.2 Reactor Shielding

The reactor has two radiation shields. The primary shield tank (PST), which is essentially a cylinder that surrounds the RPV, attenuates gammas and neutrons escaping the reactor. The PST also houses the nuclear instruments, which provide an indication of reactor power level based on the amount of neutrons and gammas leaking from the core. The secondary shield protects against fast neutron flux escaping the PST as well as capture gammas resulting from neutron activation of primary plant components (especially water within the PST). This thesis will not attempt to propose an optimum radiation shield design because such a problem is an entire investigation itself. Rather, this thesis shall approximate the reactor's shielding requirements using convenient approximations.

Since the neutron and gamma radiation fields have not yet been computed [3]), this thesis shall assume that the AHTR has the same gamma and neutron radiation fields as a PWR since they have a similar neutron spectrum. Reference [4] provides a convenient chart to estimate the radiation field in the immediate vicinity of the reactor vessel:
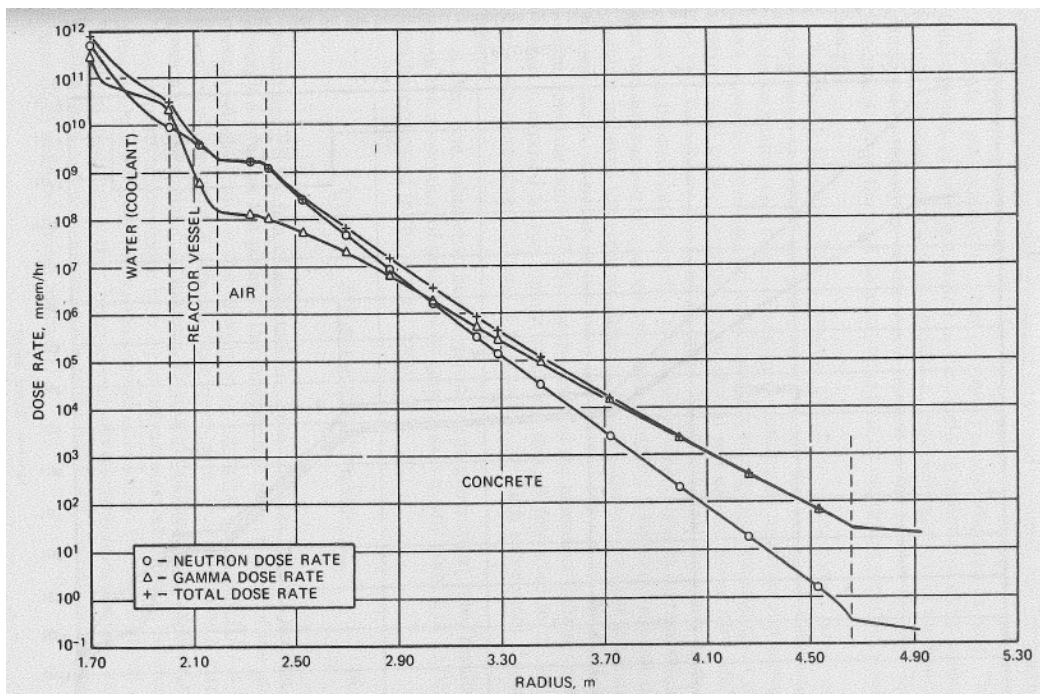
Figure 5-1 - Estimated Radiation Field IVO Reactor Vessel

As Figure 5-1 shows, the gamma dose rate immediately outside the reactor vessel is ~ 2×10^8 mrem/hr while the neutron dose rate is ~ 3×10^9 mrem/hr for a 2,900 MW$_{th}$ PWR. By assuming that the PWR and the AHTR have a comparable neutron spectrum, the radiation level can scaled linearly, resulting in dose rates of ~ 1×10^5 Rem/hr gamma and ~ 1.51×10^6 Rem/hr neutron.

Since the radiation field and the height of the reactor vessel is known, the following relationships can be used to roughly approximate radiation dose rate as functions of distance and shielding [5]:

$$DR_2 = \frac{DR_1 r_1}{r_2} \tag{5-1}$$

$$DR_2 = \frac{DR_1 r_1{}^2}{r_2{}^2} \tag{5-2}$$

Where DR = dose rate

r = radius

$$DR_s = DR_u(0.1)^N \tag{5-3}$$

$$N = {}^x/x_{1/10}$$

Where DR_u = unshielded dose rate

DR_s = shielded dose rate

X = shielding thickness (inches)

$X_{1/10}$ = shielding tenth thickness

For gamma radiation:

$X_{1/10}$ =2" for lead,

$X_{1/10}$ =4" for steel,

$X_{1/10}$ =24" for polyethylene and water

For neutron radiation:

$X_{1/10}$ =10" for polyethylene and water

Equation (5-1) is the "line/cylinder source" approximation, and it is used to estimate the radiation dose at point 2 when the dose at point 1 is known and the distance from r$_1$ to r$_2$ is less than ½ the height of the source (i.e., less than ½ the height of the reactor vessel). After this distance has been exceeded, the "point source" approximation is used (equation (5-2)). In addition to distance, shielding also attenuates the radiation fields and equation (5-3) must be used to estimate the shielded radiation dose.

Since the radiation dose immediately outside the reactor vessel is known, equations (5-1), (5-2) and (5-3) shall be used to estimate the composition of the primary (PST) and secondary radiation shields. Although PST designs can vary, this thesis shall assume that the primary shield tank has 0.0254 m (1.0 inches) of steel on the top, bottom and inner and outer walls. In order to reduce the neutron dose to 100 mrem/hr at the PST outer radius, 1.758 m of water is required. This amount of shielding attenuates the gamma radiation field to ~ 22.8 Rem/hr. The resulting PST weight is 127.55 MT.

The dimensions chosen for a six-sided reactor compartment secondary shield box are 20.0 m x 22.4 m x 16.9 m, thereby yielding a volume of ~7,576 m^3. A 20 m length is conveniently 4 times the diameter of the reactor vessel, the 22.4 m width spans the beam of the ship, and the 16.9 m height spans the height of the inner platforms within the vessel. Assuming the reactor vessel is located in the center of the compartment, the estimated neutron does rate at the inner surface of the secondary shield wall is merely 0.28 mrem/hr. The gamma dose, however, is ~ 6.4 Rem/hr. By using the guidance contained in reference [6], the amount of shielding should reduce the dose rate to less than 2.5 mrem/hr. A person exposed to this dose rate for 40 hours/week for 50 weeks will just meet the maximum allowable dose of 5.0 rem. Assuming 0.0254 m of steel on each side of the wall, ~ 0.15 m (5.82 inches) of lead are required to attenuate the gamma field to an acceptable level. Assuming a uniform, six-sided shielding configuration results in a secondary shield weight of 3,110 MT. Although assuming a uniform shielding configuration probably overestimates the shielding weight, this is justifiable because the size and weight of the AHTR's ancillary systems are not provided.

5.1.2.3 Power Conversion System

Conveniently, reference [7] has performed a relatively detailed analysis of the size and weight required by a S-CO$_2$ recompression cycle. Tables 2.5(a-d) are particularly helpful. A 300 MW$_e$ indirect cycle PCS weights 1,005 MT and consumes ~1,102 m^3. Since 650 MW$_e$ are necessary, three 300 MW$_e$ PCS modules are appropriate. The PCS exists to provide 650 MW$_e$ to electrical generators, and the following relationships are useful estimating electrical generator size and weight [8]:

$$W \approx 1.02 \cdot (P)^{0.252} \tag{5-4}$$

$$Where\ W = weight\ density\ \left(\frac{kw}{kg}\right)$$

$$P = Power\ (MWe)$$

$$V \approx 0.37 \cdot (P)^{0.31} \tag{5-5}$$

$$Where\ V = volume\ density\ (\frac{kw}{m^3})$$

Because the PCS is divided into 3 sections, three 217 MW$_e$ generators are necessary, and equations (5-4) and (5-5) show that each electrical generator weighs ~54.8 MT and consumes 111 m^3 of volume.

5.1.2.4   Overall Power Plant Summary

Table 5-1 summarizes the weight and volume estimations for the power plant components:

Power Plant Systems	Weight (MT)	Volume (m^3)
Reactor Plant		
Fuel	9.22	-
Graphite	253	145.6
Coolant	9.04	-
RPV	12.7	235.7
RVACS	0.052	256.2
Reactor Total	**284**	**256**
Shielding		
PST	128	7,576
Secondary Shield	3,110	2,873
Shielding Total	**3,238**	**7,576**
PCS		
S-CO$_2$ HXs/Machines	2,088	3,306
Electrical Generator	164	332
PCS Total	**2,252**	**3,638**
Grand Total	**5,774**	**11,213**

Table 5-1 - Power Plant Size Estimation Summary

As Table 5-1 shows, refinement of the secondary shielding could yield significant savings in weight and volume.

5.1.3   Space and Weight Estimation of Chemical Plant Components

Table 5-2 identifies the major components of the liquid fuels production plant, which includes the devices necessary for syngas generation:

Component (unit capacity)
Fischer-Tropsch (FT) Reactors (BBL/day)
Product Upgrading/Refining (BBL/Day)
Autothermal Reforming (ATR) (BBL/day)
HTCE SOECs (kg/s H_2)
HTSE SOECs (kg/s H_2)
Air Capture Units (MT CO_2/Day)
H_2 Separation (kg/s)
CO_2 Separation (kg/s)
RO Units (kg/s)
Reserve H_2O Feed Tanks (m^3)
Major Compressors (m^3/hr)
Steam Generators (MW_{th})
Other Significant Heat Exchangers (MW_{th})

Table 5-2 - Major Liquid Fuel Production Plant Components

5.1.3.1 Synfuel Production Components

Recalling chapter 2, the desired capacity of the synfuel plant is 6,400 BBL/Day, which is less than 1% of the throughput of a world-class refinery. Although liquid fuel production facilities exist, most of the technology used by industry is far too large for offshore use. However, as offshore gas-to-liquids (GTL) is becoming more lucrative, companies are starting to invest in offshore liquid fuels production technology. Velocys is a company that specializes in small scale, modularly constructed liquid fuel production and product upgrading equipment. Some of their technology under development seeks to produce jet fuel and distillate using gas-to-liquids (GTL) process onboard offshore platforms. Reference [9] contains the estimated size and weight of the FT microchannel reactor (MCR) modules, which reference [10] confirmed, except with a unit capacity of 300 BBL/Day vice 360 BBL/Day. Since an ATR is similar to a steam methane reformer (SMR), the ATR's size and footprint was estimated from reference [10] and reference [11] as well. Although Velocys has not published any information regarding the size of its product upgrading modules, reference [10] suggested using the space and weight of the FT MCR apparatus, except with double capacity (600 BBL/Day vice 300 BBL/Day). Table 5-3 provides a footprint summary of the major synfuel production components:

Component	Capacity (BBL/Day)	Number Req'd	L (m)	W (m)	H (m)	Vol (m³)	Total Vol (m³)	Weight (MT)	Total Weight (MT)
Fischer-Tropsch MCRs	300	22	7.62	1.52	1.52	13.9	306	20	440
Product Upgrading Modules	600	11	7.72	1.52	1.52	13.9	153	20	220
Autothermal Reformer	3,000	2	5.79	3.96	3.96	91	182	50	100

Table 5-3 - Synfuel Production Footprint Summary

5.1.3.2 HTCE/HTSE SOECs

Technical reports [12] and [13] have performed space and weight estimations for solid oxide cells, which are in close agreement. Table 8 in reference [13] is particularly useful because the estimate includes the support structure, which increases the area by a factor of four. After linearly scaling the dimensions for the cell area assumed in chapter 3 (225 cm^2 vice 400 cm^2) and applying the support structure factor, each stack has an area of 0.3654 m^2. Each 1,000 cell stack is 4.06 m tall; therefore each stack consumes ~1.484 m^3 of volume. 1,743,000 co-electrolysis cells (HTCE) and 191,000 HTSE cells are assumed since 1,742,605 HTCE cells and 190,841 HTSE cells are the minimum required, thereby resulting in 1,743 HTCE stacks and 191 HTSE stacks. Therefore, a footprint of ~ 640 m^2 is needed for the HTCE cells and 70.0 m^2 is needed for the HTSE cells (effectively 26.0 m x 26.0 m for the HTCE cells and 9.0 m x 9.0 m for the HTSE cells). Since the stack volume is known, the weight can be computed by linearly scaling the weight value provided in reference [13], which results in 5.97 MT per 1,000 cell stack. The total weight of the HTCE stacks is 10,406 MT and the HTSE stacks weigh 1,140 MT (11,546 MT total).

5.1.3.3 Gas Separation, Desalination and Feed Equipment, and Compressors

Most gas separation equipment manufacturers state on their websites that their equipment is custom built; however, references [14] and [15]provide a general weight and volume estimate for modular gas separation units that shall be used since no other information is readily available: 9.14 m x 3.66 m x 3.05 m and 25 MT. Village Marine, however, precisely defines the space and weight needed by the each of three required EUWP Gen-2 RO units: 12.2 m x 7.62 m x 2.80 m and 25.4 MT [15]. This thesis shall assume three reserve tanks, with a combined capacity equal to 24 hours of demand, are necessary. Since the demand is 28.5 kg H_2O/sec, ~ 2,462,400 kg H_2O/day is necessary. Thus, three 1,000

MT reserve feed tanks (RFTs), each with a volume of 1,000 m^3 (assumed water density 10^3 kg/m^3) are needed. The RFTs' footprint can be adjusted as necessary to accommodate other equipment.

The compressors have a high enough throughput that their weight and footprint is not negligible. Table 5-4 shows the most significant compressors in the synfuel production plant:

Compressor Type	Required Capacity (m^3/hr)
CO_2 Compressor	54,804
H_2 Refining Compressor	3,813
Syngas Compressor	30,903

Table 5-4 - Significant Synfuel Plant Compressors

Based on the compressor flow rate, reference [16] provided a reasonable size and weight for each unit. They require a total volume of 73.0 m^3 and weigh ~102 MT.

5.1.3.4   Steam Generators and Heat Exchangers

As with the gas separation units, the steam generators and heat exchangers are custom built devices, especially so for shipboard liquid fuels production applications. Fortunately, reference [7] contains the ratings, dimensions, and weights of steam generators and S-CO_2 heat exchangers. However, the components provided in reference [7] could have a different configuration and specific power density than the actual heat exchangers selected. Therefore, the following assumptions shall be used for scaling plant components with dissimilar power densities:

- Capacity is proportional to volume, V

- Weight and cost are proportional to surface area, S

- For any geometric solid of fixed aspect ratio:

$$S \propto V^{\frac{2}{3}}$$
(5-6)

Equation (5-6) is a frequently used relationship in the chemical and electric power industries for "economy-of-scale" cost considerations, which suggest that plant size increases at less than a 1:1 ratio with plant rating (i.e., output per unit time). Indeed, references [17] and [18] suggest that the capital cost of facilities scale with capacity at a power ~0.6-0.7. Since cost and weight are generally proportional to each other, equation (5-7) should provide a close enough first order estimate.   Since

only a rough estimate of a component's size and weight is necessary for this analysis, the following

relationships will be used as necessary to scale the appropriate weight or volume:

$$W_2 = W_1 \left(\frac{C_2}{C_1}\right)^{\frac{2}{3}}$$

$Where\ W = Weight\ (MT)$

$C = Capcity\ (MW_{th}, MW_e, \frac{kg}{s}, etc.)$

$$V_2 = V_1 \left(\frac{C_2}{C_1}\right)$$

$Where\ V = Volume\ (m^3)$

(5-7)

(5-8)

In this analysis, equations (5-7) and (5-8) are used to scale a larger component down to size; thus, the

estimated weight (and cost) is reduced in a less than linear manner, thereby making the approximation

more conservative than scaling versus capacity to the first power.   Table 5-5 and Table 5-6 summarize

the space and weight consumed by all steam generators and significant steam generators in the liquid

fuels production plant:

S/G Type	Capacity (MW_{th})	Scaling Factor	Volume (m^3)	Weight (MT)
Baseline S/G (Russian VVER 440/213)	230	1	95.5	165
HTCE S/G	102	0.582	42.4	96.0
HTSE S/G	17.6	0.180	7.31	29.7
ATR S/G	13.4	0.150	5.55	24.8
Total Boiler Weight/Volume			55.2	151

Table 5-5 - Summary of Significant Steam Generators

IHX Type	Capacity (MW_{th})	Scaling Factor	Volume (m^3)	Weight (MT)
Baseline IHX (S-CO_2)	300	1	20.412	81
HTCE CO_2 HE	21.1	0.170	1.44	13.8
ATR HC HE	7.86	0.088	0.535	7.10
Alkylation HE	0.42	0.013	0.029	1.00
Hydrocracking HE	5.24	0.067	0.357	5.50
Aromatization HE	1.92	0.034	0.131	2.80
Oligomerization HE	0.51	0.014	0.035	1.20
Hydrotreating HE	0.5	0.014	0.034	1.10
Total HX Wt/Vol			2.56	32.5

Table 5-6 - Summary of Significant Heat Exchangers

5.1.3.5 Air Capture Units

Reference [19] claims that the entire air capture unit apparatus can fit into a 12 m x 2.5 m x 3m container box, and each unit requires 2,500 kg of resin. An additional 1,000 kg will be used to account for the drying chamber and other ancillary equipment. Per reference [20], the actual dimensions of the cargo container box referred to in [19] are 12.192 m x 2.438 m x 2.896 m, and each cargo box has an empty weight of 3.7 MT. Chapter 3 determined that ~2,584 air capture units are necessary. Assuming 2,600 units, the entire air capture system requires a significant volume of 234,000 m^3 and weighs 18,723 MT. Since the air capture units must be exposed to the environment, they will be stacked on the main deck of the midbody.

5.1.3.6 Overall Liquid Fuels Production Plant Summary

The synfuel production plant consumes a significant volume of the ship, and it displaces nearly five times as much weight as the entire power plant (34,155 MT vs 5,774 MT). 85% of the total liquid fuel plant weight results from the SOECs (30%) and the air capture units (55%).

5.1.4 Determining Weight of Essential Ship Systems

Although the function of the midbody section housing the synfuel production system and its associated power plant, other ancillary ship systems are required for operation at sea. Such systems include firefighting and dewatering systems, ventilation, and the hull structure. All of these items must be included in the midbody's weight. ASSET provides the weight for all of these systems in the TAO-187's weight report module, which is known as the ship weight breakdown structure (SWBS) [21].

Since the ship's SWBS is available, parametric "ratiocination" relationships provided in reference [22] can estimate the weight of ship systems in the midbody. The relationships, which are typically a function of geometry, scale as follows:

$$W_n = W_p \cdot \left[ratio\ of\ ^{New}/_{Parent}\right]$$ (5-9)

$$Where\ W_n = Weight\ new\ ship\ system$$
$$W_p = Weight\ of\ parent\ ship\ system$$

An example use of equation (5-9) to estimate the midbody's shell plating using reference [22] is as follows:

$$W_n = W_p \cdot [L(B + 2D)] \tag{5-10}$$

$$Where\ L = Length$$

$$B = Beam$$

$$D = Depth$$

The "[L(B+2D)]" quantity in equation (5-10) is the geometric parameter that is scaled in the new/parent ratio in equation (5-9) above. Each item in the SWBS report has a unique parametric relationship in the form of equations (5-9) and (5-10). Some items, such as sonar domes, will not exist in the midbody, so their contribution is excluded from the calculation. Table 5-7 is a summary of the SWBS group 1, 3, 4, 5, and 6 weights for the midbody section with the original ship weight provided for comparison[33]:

Ship System	TAO-187 (MT)	110 m Midbody (MT)
Grp1-Structural Components	7,161	4,787
Grp3-Electrical Components (non power plant)	337	26,750
Grp4-I&C Components	80.2	42.9
Grp-5 Auxiliary Components	790	591
Grp6-Outfittings	927	519
Total	9,295	32,690

Table 5-7 - Summary of Ship System Weights in Midbody Section

All weight groups except for group 3 nearly scale as a function of length (198 m ship length vs. 110 m midbody length). By varying the midbody's length, the linear relationship between overall midbody weight vs. length becomes obvious:

---

[33] Groups 2 (propulsion) and 7 (armament) are not shown since none of their systems apply to the midbody section.

Midbody Weight vs Length for TAO-187
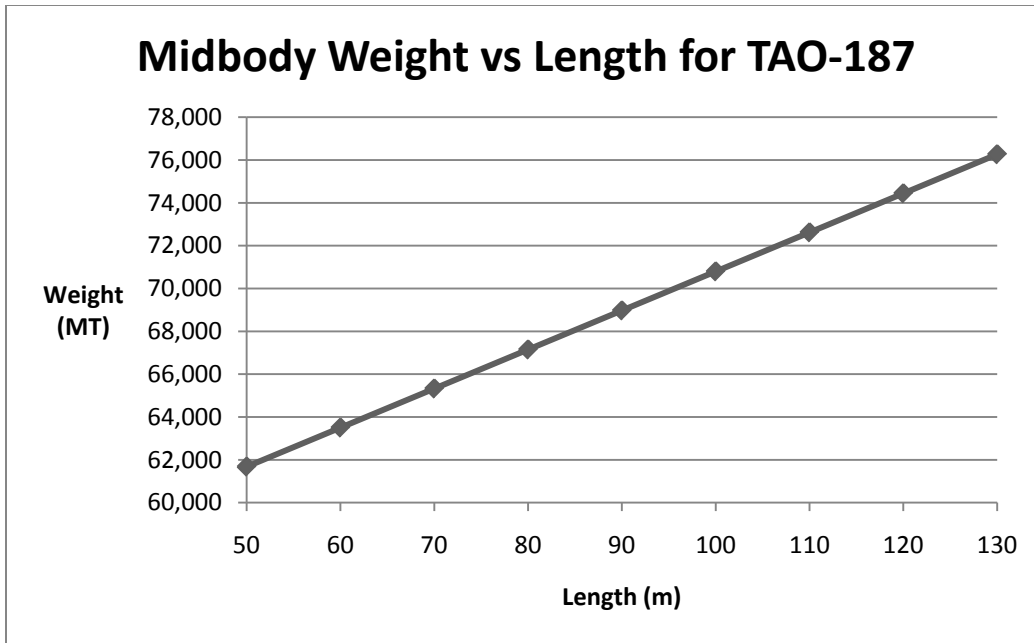
Figure 5-2 - Parallel Midbody Weight as a Function of Length

Recalling Table 5-7, SWBS group three does not scale linearly because the power requirements of the midbody section are more than two orders of magnitude higher than for the original ship (4.82 MW_e for the ship vs. 650 MW_e for the midbody). According to the parametrics 14,085 MT of shipboard cabling and 8,546 MT of switch gear and distribution panels are necessary to accommodate the power demand. Considering the significant electric power demands of the liquid fuel production system in comparison to typical ship systems, there is little reason to doubt the validity of the parametric values.

5.1.5 Determining Size and Location of Parallel Midbody Section

A rule of thumb for determining a ship's allowable length before bending moments could exceed a hull's structural design limits is the length-to-draft (L/T) or length-to-depth (L/D) ratio. For a bulk carrier, this value is ~ 30 per Table 3-1 of reference [23]. Additionally, the length-to-beam ratio (L/B) should remain ~10 or less for these types of vessels. These rules of thumbs merely provide a starting point to estimate the midbody's geometry. The length between perpendiculars (LPP or "L") for the TAO-187 is 198.12 m, its beam is 29.718 m, and its DWL is 10.52 m [21], thereby resulting with a L/T of ~18.83. For the TAO-187 to achieve a L/T of ~ 30 would require the insertion of a midbody of ~117.5 m, which would increase its L/B ratio from 6.66 to 10.62. Using ASSET to insert a 120 m midbody into the TAO-187 results in a warning message effectively stating that the maximum recommended midbody length for the TAO-187 is 110 m, a difference of only 6.38% from the rule of thumb provided in

189

reference [23].   Table 5-8 summarizes the TAO-187's geometry provided by ASSET's design summary module:

Platform	TAO-187
Lightship Weight (MT)	14,852
LPP (m)	198
Beam @ DWL (m)	29.7
Draft (m)	10.5
Maximum Midbody Length (L/T=30; L/B~10)	110

Table 5-8 - Ship's Geometry Summary

The ASSET graphical displays from the hull subdivision module that show the locations of the watertight bulkheads are helpful for determining where to place the midbody because they provide a general sense of where the machinery rooms and bulk cargo locations are. Additionally, cross referencing the bulkhead location with the section number in the hull geometry module provides the corresponding sectional area. Since the sectional area is given for the DWL, one can easily compute the midbody's displacement by multiplying by the midbody's length and the seawater density (assumed 1,025 kg/m^3). Placing the midbody closer to the center provides more volume and displacement per unit length while also minimizing the amount of trim. However, arranging the midbody section closer to the machinery space helps maintain a more logical arrangement and it also minimizes the interference with the fuel and cargo handling systems. Figure 5-3 shows the bulkhead locations for T AO-187 while Figure 5-4 (courtesy of reference [24]) provides a better illustration of where the major cargo handling systems are located for the two platforms:
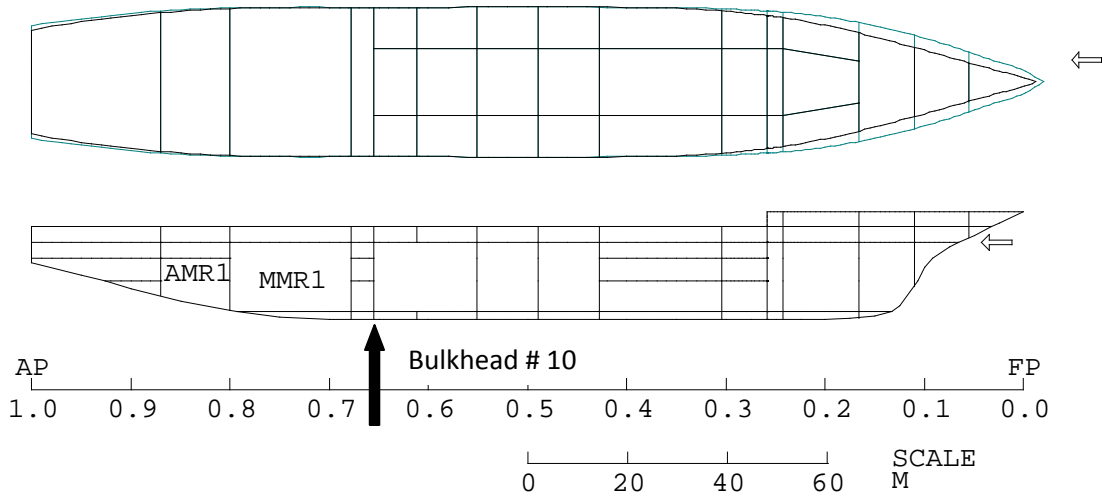
Figure 5-3 - Layout of AO-187 Bulkheads (Main Deck)
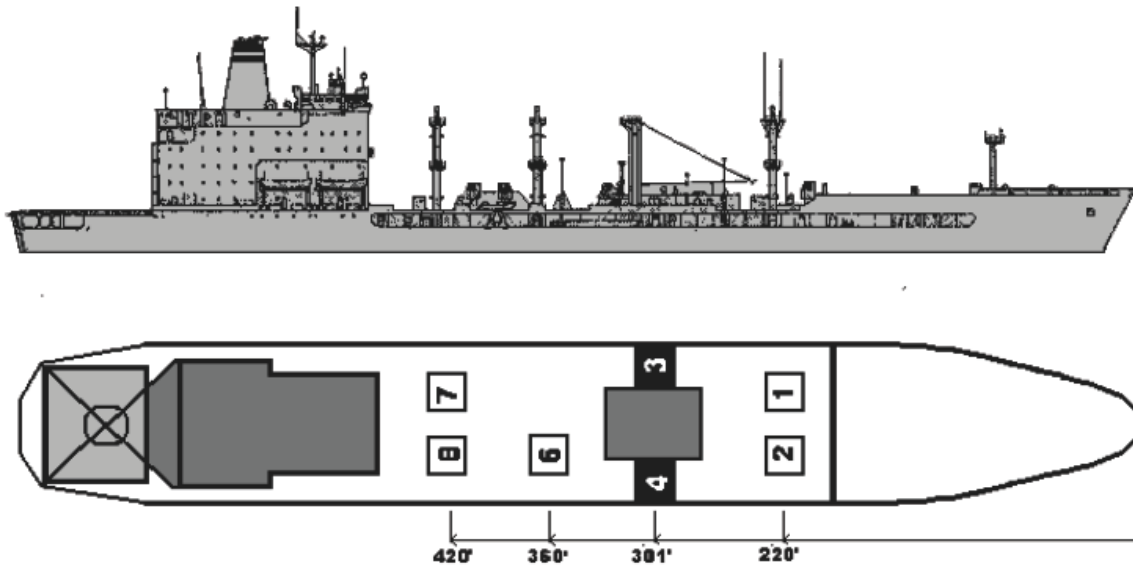
Figure 5-4 - Illustration of AO-187 Handling Systems

For both vessels, inserting the parallel midbody section just forward of the space separating MMR1 from the "large object void space" is probably the best location (i.e., just forward of transverse bulkhead #10). Co-locating the midbody section in the vicinity of the machinery spaces (1) conveniently arranges all of the major machinery spaces in one area of the ship, (2) places the midbody section out of the way of the

cargo handling equipment, and (3) inserts the midbody in a relatively central location on the vessel. For the TAO-187, the location of the midbody section (~station 22) provides a sectional area of ~ 303 m^2.

5.1.6 Midbody Feasibility Issues

Inserting the maximum 110 m midbody for the TAO-187, with sectional area of 303 m^2, results in a displaced water volume of 33,316 m^3 and a displaced weight of 34,149 metric tons (MT). ASSET also provides the half-breadth offsets, which are convenient for determining the available volume of the midbody using trapezoidal rule integration. The total volume available for equipment below the main deck is 59,437 m^3. Table 5-9 provides a summary of the midbody section's geometry and weight:

Midbody Parameters, TAO 187	
Length (m)	110
Beam (m)	29.718
Draft (m)	10.52
Sectional area (m^2)	302.87
Volume (m^3)	59,437
Displacement Volume (m^3)	33,316
Displacement (MT)	34,149

Table 5-9 - Midbody Geometry Design Summary

Table 5-10 summarizes estimated equipment weight within a 110 m long midbody[34]:

System	Weight (MT)	Volume (m^3)
Chemical Plant	34,155	12,874
Power Plant	5,774	11,213
Grp1-Structural Components	4,797	-
Grp3-Electrical Components (non PCS)	26,750	-
Grp4-I&C Components	42.9	-
Grp-5 Auxiliary Components	680	-
Grp6-Outfittings	519	-
Total	72,718	24,087
Assumed Midbody Capacity	34,149	59,437
Difference (Displacement - Weight)	-38,570	35,349
Difference (%)	-113%	59.5%

Table 5-10 - Overall Parallel Midbody Size Summary

---

[34] The volumes from the ship systems are not listed because they are homogenously mixed throughout the midbody section. While they will occupy some volume, it should not be difficult to accommodate them since ~80% of the midbody volume remains free for use; hence their volume contribution is neglected.

Since the weight exceeds the displacement by a significant margin, the midbody will not be able to accommodate a full scale synfuel production system. As Table 5-10 shows, the significant weight drivers are the fuel production system (air capture units, SOECs) and the electrical components (cabling, switchgear).

Improved weight estimates that would serendipitously cause the weight to more closely match displacement will not remedy the problem either because it is simply not possible to accommodate enough air capture units on the ship's deck. Recall that each air capture unit is ~ 2.90 m tall. Since the pilot house is ~ 18.0 m above the main deck, the highest the air capture units could conceivably be stacked is 6 units tall. Each unit has a width of ~ 2.5 m; therefore only 10 units can fit across the beam of the ship. Accommodating all 2,600 units 10 wide and 6 high requires that they extend 43 units long, which is over 525 m. For comparison, a Nimitz-class supercarrier is only 333 m long, and the largest supertankers (such as the Ultra Large Crude Carrier *Jarhe Viking*) are ~ 458 m long.

Improvements to the prototype air capture unit design that result in a more compact design might make them feasible for a tanker ship specifically designed to accommodate them; however, even the most optimistic assumptions will not facilitate a parallel midbody in an existing tanker ship. Recalling chapter 3, the relationship describing the air capture units' capture rate is as follows:

$$\Delta CO_2 = C_{CO_2} \cdot f \cdot A \cdot v \qquad\qquad (5\text{-}11)$$

$Where\ \Delta CO_2 = Capture\ Rate$

$C_{CO_2} = CO_2\ concentration$

$f = fraction\ of\ CO_2\ captured$

$A = absorber\ area$

$v = linear\ velocity$

Theoretically, the area/volume of the air capture units can be reduced as follows:

- Reduce the fraction of CO_2 captured (not advisable, will require more units)

- Increase the fraction of CO_2 captured (not possible, requires alternate system)

- Increase the CO2 concentration in air (not possible, function of surrounding environment)

- Increase the linear velocity in the column

The assumption generally used is the flow rate is 2-3 meters per second (~5 knots) [19,25]. Assuming that the increased air speed resulting from the ship's movement (typically ~ 15 knots) reduces the absorber contact area by a factor of 4 would require the number required to 650 units. Because of the

power plant's size, inserting a well deck into the midbody would not be feasible. Assuming the units can fit in a section 10 m long and 10 m wide, the units will stack either 6 or 7 units tall (the design will not be completely symmetric); of course, this midbody design assumes that a 130 m midbody length is feasible. Since some of the units will extend as high as 21 m, they will partially obstruct the view of the pilot house. The ship has a righting moment (GM) of only 3.08 m, so arranging the units so high on the ship will probably pose an intact stability concern. Extending the midbody length to 130 meter results in ~ 40,375 MT of buoyancy; however, the remaining equipment (with only 650 air capture units) weighs 49,272 MT.   If the midbody is reduced to the more appropriate 110 m length, the displacement deficit increases to ~ 11,477 MT and the air capture units would have to be stacked even higher (all of them would be at least 7 units high and some would be 8). If jet fuel production capacity is reduced to that only required to sustain peacetime operations (5,200 BBL/day), the amount of power required only decreases to ~ 529,000 kWe (only a18.7% reduction).   2,090 air capture units are required to supply this load. Optimistically assuming once again that the number required can actually be reduced by a factor of 4, a total of 522 units must fit on the 110 m deck, which results in many of the units still stacking 6 units high. The 110 m midbody can support 38,481 MT; however, the weight is still 4,332 MT over the limit.

The electrical equipment weight is a significant factor in being over the weight limit. Producing power on this scale has never been done on a navy platform. There is also no reason to assume that the weight estimate is not accurate because a significant amount of electrical gear is necessary. Other issues exist that also frustrate the midbody feasibility concept. In the liquid fuel production analysis, 100% autothermal reforming efficiency was assumed; however, if the efficiency of the autothermal reformer is only ~ 70 %, then the number of air capture units increases more than 17% to 614 (assuming a factor of 4 size reduction and the peacetime demand requirement). Another issue is that even if the flow rate is substantially increased through the air capture units, the CO2 capture rate will probably not increase a proportional amount because of the reduced amount of time that the air contacts the resin. Additional investigation is necessary to establish the reaction kinetics of the resin with the CO_2 to determine what the best case size reduction could be.   Finally, the air capture units (as designed) are not suited for topical or humid environments [19], thereby implying that even more units would be necessary in order to accommodate their reduced at-sea performance. Determining the actual performance characteristics of the air capture units on a sea-based platform is something experimental research is best suited to investigate.

5.2 Cost Estimation of a New Synfuel Tanker

5.2.1 Overview

A rigorous cost estimation is well beyond the scope of this thesis. Because many of the proposed systems are still in their design phase, accurately determining their operating, maintenance, personnel and disposal costs is not possible. The primary benefit the nuclear powered synfuel tanker provides the fleet is the elimination of fuel logistics; however, quantifying this benefit in terms of dollars would require substantial investigation. In addition to the commodity price of fuel, the future mix of naval combatants and their primary area of operation could likely change by the time the tanker ship is even deployed. Any change in force structure results in the changes to the logistics structure as well. Since the life-cycle cost/benefit analysis is an enormously complicated problem requiring focused attention, this thesis will only compare the acquisition cost of the ship against the commodity price of fuel.

This thesis will assume that the new tanker will resemble the TAO-187. Since the weight and geometry of the TAO-187 are known from reference [21], reference [22] can be used to estimate the weight of a similar ship. By knowing the weight of the ship, reference [26] can be used to estimate the ship's cost. Reference [26], similar to reference [22], uses parametrics to estimate the cost of common ship systems. However, the cost model is not adequate for determining the cost of special systems such as reactor and fuel production plants. Since many of the systems conceived for the liquid fuel production plant and reactor plant in this thesis have not yet been built, soliciting expert opinion is necessary to estimate their cost.

5.2.2 Ship Cost

5.2.2.1 Ship Geometry

As the previous section explains, implementing an air capture CO_2 production system with enough capacity to supply a 6,400 BBL/Day synfuel plant is not possible on any sea-based platform without a significant size reduction. In order to calculate a cost estimate, this thesis will assume that the number of air capture units can be reduced by a factor of 4, thereby requiring only 650 units for the entire air capture system. The basis of this assumption is that the prototype air capture units identified in this thesis are designed for land base where there is no size penalty. Furthermore, there is a

significant of research on removal of carbon dioxide from air as part of climate change mitigation projects; because this is a new area of research, major improvements in technology are expected. If the units are stacked 10 across and 5 high, the total length necessary to accommodate the units is 169 m. Since the original length of the ship is 198 m, the length of the new ship will be 367 m. However, it is necessary to adjust the beam and depth in order to maintain a similar hull shape. Since the original L/B and L/D ratios for the ship are 6.65 m and 10.70 m, respectively, the new hull will have a beam of 55.2 m and a depth of 34.3 m. As the original depth-to-draft (D/T) ratio is 1.76 m, the ship's new draft is 19.5 m (~ 64 feet). Although these dimensions are feasible, the ship would not be able to transit via the Suez or Panama canals.

5.2.2.2   Integrated Power System (IPS)

Since the new ship will have a very capable nuclear reactor, no need exists to maintain the conventional propulsion system. As chapter 4 explains, an electric drive propulsion system coupled with an integrated power system is the most appropriate solution. The size and weight of the propulsion system depends on the propulsion power requirement. Because the new ship has similar geometry, convenient scaling factors can estimate the power requirement. The geometric scaling factor, λ, is the ratio of ship lengths:

$$\lambda = \frac{L_1}{L_2} \tag{5-12}$$

For the current design, λ is 1.90. Thus, the new displacement (Δ) can be estimated as follows:

$$\Delta_2 = \Delta_1 \cdot \lambda^3 \tag{5-13}$$

Since the full load displacement of the TAO-187 is 41,319.3 MT, the new ship's full load displacement is 283,409 MT. The following relationship, known as the "Admiralty Coefficient" provides a means to estimate the required propulsion power assuming a similar top speed of 20.14 knots:

$$C = \frac{V^3 \Delta^{2/3}}{BHP} \tag{5-14}$$

$Where\ C = Constant$

$V = Speed$

$BHP = Brake\ Power$

Because the BHP at 20.14 knots for the TAO-187 is ~ 23.7 MW_e, the BHP needed by the new ship is ~ 85.6 MW_e, which is helpful for estimating the weight of propulsion machinery. Since the transmission

efficiency for electric drive propulsion is ~ 0.89, but only ~ 0.98 for the TAO-187's mechanical drive, the turbines must actually produce ~ 94.3 MW_e to compensate for the additional losses [27]. Assuming the ship's 4.8 MW_e "hotel loads" increase by a factor of λ, and additional 4.34 MW_e of shipboard power is also required (9.16 MW_e total). The reactor plant, must now supply the additional 94.3 MW_e of propulsion power and 9.16 MW_e of hotel loads (103 MW_e total). Since the reactor plant thermodynamic cycle efficiency is 0.446, the reactor's rating must increase 231 MW_{th} to 1,687 MW_{th} (~ 15.8% increase). However, the S-CO_2 PCS need not change because the midbody design assumed three 300 MW_e units, and the new design remains within the original PCS's capability. Because most navy ships have two propulsion trains for reliability, the 85.6 MW_3 load can be divided between two motors and equation (5-4) can be used to estimate the weight.

5.2.2.3   Cost Model Input/Output and Vessel Size Refinement

Since the new ship's geometry is known, and the power requirement of the IPS has been determined, reference [22] can be used to scale values from the ASSET weight report. The group 1-7 SWBS weights (light ship) in the cost model are as follows:

Category	Group Weight (Long Tons)
SWBS 100 (Structure)	29,937
SWBS 200 (Propulsion)	823
SWBS 300 (Electrical)	68,695
SWBS 400 (Inst. & Comms)	378
SWBS 500 (Auxiliary)	5,490
SWBS 600 (Outfittings)	3,619
SWBS 700 (Armament)	0

Table 5-11 - MIT Ship Cost Model Inputs (Light Ship): Initial Estimate

 Excluding the cost of S-CO_2 power conversion system, the reactor plant, and the liquid fuel production plant, the acquisition cost of the lead ship is ~ $20.9 billion (2010 dollars), which is ~ double the cost of a nuclear-powered aircraft carrier.

Maintaining geometric similitude for all three dimensions (L, B, and T) partially contributes to the high cost, but (as will be shown below) the primary cost driver is the large amount of electrical infrastructure required to support the synfuel plant. However, the ship's current beam and draft dimensions preclude it from transiting the Suez Canal; therefore, a better approach is to utilize the geometric constraints presented in section 5.1.5 in order to minimize the ship's beam and draft (ship's

length is the primary constraint). Hence, the beam and depth will be adjusted such that L/B=10 and L/T=30. In addition to reducing the vessel's cost, the ship would have the capability to transit the Suez Canal.

Thus, for a 367 m long hull, the minimum beam and draft are 36.7 m and 12.2 m, respectively. λ in equation (5-12) must be recomputed for each dimension; therefore, λ (L$_2$/L$_1$)=1.90 as before, while ζ (B$_2$/B$_1$) = 1.24 and ξ (T$_2$/T$_1$)=1.17. Modifying equation (5-13) such that $\lambda^3=\lambda\xi\zeta$ results in a new full load displacement of 110,260 MT, a substantial 61.1% decrease. Substituting this new displacement value into equation (5-14) results in a required brake power of 45.6 MW$_e$, which means that the turbines must supply 50.2 MW$_e$ after accounting for the difference in transmission efficiencies. Since the 9.16 MW$_e$ of "hotel" loads remains the same (length didn't change), the amount of power supplied by the reactor is now ~709 MW$_e$ (1,589 MW$_{th}$). The new cost model inputs are as follows:

Category	Group Weight (Long Tons)
SWBS 100 (Structure)	15,789
SWBS 200 (Propulsion)	413
SWBS 300 (Electrical)	66,105
SWBS 400 (Inst. & Comms)	152
SWBS 500 (Auxiliary)	2,680
SWBS 600 (Outfittings)	1,612
SWBS 700 (Armament)	0

Table 5-12 - MIT Cost Model Inputs (Light Ship): Final Estimate

Per the cost model, the lead ship procurement cost will be ~ 18.6 billion ($2010). Although the structural dimensions (L, B, and T) and the displacement changed somewhat significantly (SWBS 100 is about half), the SWBS 300 weight (electrical) only decreased 2,590 long tons (~ 3%). Thus, the modest 11% decrease in price is expected as electrical systems are more costly than structural materials and outfittings. In addition to the rather modest price decrease, the nuclear power tanker ship with the light ship displacement proposed for the revised estimate will only have a cargo capacity of 22,117 MTs, while the original TAO-187 has a 26,467 MT capacity (the fuel production plant remains the same size; only the cargo capacity changes). Assuming a 0.8 kg/liter density, the new capacity is enough to supply over 33 days of peacetime operations and 27 days of combat operations of a carrier strike group. A more rigorous ship design effort in the future should be able produce a ship that has a larger cargo capacity while still meeting the ship's design constraints. However, $18.6 billion is a significant sum, and future ship design must also determine if it is possible to design a ship with equivalent capability for about half the current cost estimate.

5.2.3   Power Plant Cost

Because a S-CO$_2$ recompression cycle offers attractive thermodynamic efficiency, several assessments (notably references [28] and [29]) have attempted to quantify the cost benefit value of an S-CO$_2$ power cycle. However, previous analysis has examined the cost of the components in a piecemeal fashion, coupled the overall S-CO$_2$ PCS cost with a cost of gas-cooled reactor, or has demonstrated the cost savings a S-CO$_2$ system can provide a utility over a He or Rankine PCS. While insightful, these analyses are not quite appropriate for providing the approximate capital cost of an S-CO$_2$ PCS on a US Navy tanker ship. As for the AHTR, some believe that the capital cost will be 75% lower than for a LWR because its near atmospheric pressure system facilitates less costly piping and containment infrastructure [30]; however, this logic is not applicable to a shipboard reactor plant system. Another consideration reducing the AHTR's cost is the higher efficiency, which significantly impacts the power cycle because the system handles less thermal power per unit of electricity [31]. Although the AHTR power plant will be more efficient, it must also be constructed out of more exotic materials (e.g., Hastelloy-N) that are rated for high temperature operation. Given the lack of precedent in constructing a high-temperature, salt-cooled, S-CO$_2$ power plant, the following assumptions will be used to estimate the power plant's cost:

- The cost of the power plant includes the S-CO$_2$ PCS and the AHTR
- Baseline US Navy nuclear power plant cost is for two Nimitz-class A4W reactors
- Two A4W reactors have a combined rating of 1,000 MW$_{th}$ and 30% thermal efficiency
- Cost estimate does not include research and design or other lifecycle costs
- Cost will based on the following relationship suggested by reference [31]:

$$C_{AHTR} = C_{A4W} \cdot \left(\frac{MWe_{AHTR}}{MWe_{A4W}}\right)$$
(5-15)

$$Where\ C = cost\ (2010\ dollars)$$

Recalling section 5.2.2.2, the AHTR's anticipated rating is 709 MW$_e$, and from the assumptions above, the A4W reactor plant has a rating of 300 MW$_e$. Reference [32] reports that the fiscal year 2007 cost of two A4W reactors is $600 million, which is $642 million in 2010 dollars. Therefore, the estimated acquisition cost of the tanker ship's power plant is estimated at $1.52 billon.

While $1.52 billion is a significant cost increase from $600 million, the much more expensive cost will be in the research and design work for this new reactor plant system. A $10+ billion cost just

for research and design would not be surprising, which would probably include a prototype model prior to fielding on a naval platform. Part of the US Navy's reluctance to investigate wholly new reactor concepts is that the research and design costs are large and, some would say, not justifiable considering the USN has already mastered PWR technology [33]. If the navy does decide to research a high temperature reactor, perhaps as part of a joint DOE program for electricity and high temperature heat, then the new reactor would likely become the replacement for an aircraft carrier's reactor [31].

5.2.4   Synfuel Plant Cost

The synfuel plant cost will be estimated by summing the cost estimates of the major components within the system:

- Air capture units
- SOECs
- Fuel production/reformer modules

Although the modular, microchannel fuel production modules are still in the prototype stage of design, reference [34] suggested $15,000 per BBL/day. Per section 5.1.3.1, twenty-two 300 BBL/Day Fischer-Tropsch MCRs and eleven 600 BBL/Day product upgrading modules are required. Additionally, a 3,000 BBL/Day ATR is necessary to recycle unused hydrocarbons back as syngas. Using the estimate provided, the total acquisition cost of this system is $243 million.

The cost of the SOECs appears more significant. Reference [35] estimates the cost at $200/kW, with 1/3 of the stacks replaced annually. The electrolysis cells in the synfuel plant require 589.9 MW_e. The initial cost of the SOECs is $118 million; however, assuming the rate of replacement quoted in reference [35] is correct, the SOEC cost over the life of the ship exceeds $1.57 billion. The annual SOEC replacement cost is nearly $35.4 million dollars, a rather significant figure. Clearly, more research and design effort is necessary to reduce their replacement rate to make SOECs viable. At the fiscal year 2010 commodity price of $2.84 per gallon JP-5, the SOEC degradation cost equates to 296,781 BBL of fuel. Assuming the peacetime fuel delivery rate of 5,200 BBL/Day, over 57 days of fuel delivery are necessary to compensate. However, this analysis is only considering the initial acquisition cost, so the assumed SOEC cost will be $118 million.

Reference [19] quotes a price of $200,000 per air capture unit, which includes all ancillary components. However, the current prototype design is not adequate; the design needs to be four times

more compact. This thesis will assume that a device that consumes four times less space will have four times the cost, per equation (5-8). Since 650 units are required at $800,000 per unit, the capital cost of the air capture system is $520 million. Therefore, considering the fuel modules, SOECs, and air capture units, the total acquisition cost of the synfuel plant is ~ $881 million.

5.2.5   Synfuel Platform Cost Summary

Table 5-13 summarizes the acquisition cost as follows:

Component	Cost ($ billion)
Ship	18.6
Power Plant	1.52
Synfuel Plant	0.88
Total	21.0

Table 5-13 - Cost Estimation Summary

 Per reference [36], the fiscal year 2010 commodity price of JP-5 is $2.84 per gallon ($119.28 per BBL). Assuming peacetime fuel consumption (5,200 BBL./Day), the daily commodity fuel cost is $620,256 per day. Assuming the tanker ship is available to deliver fuel 180 days per year results in an annual fuel savings of $112 million. Therefore, at current fuel prices (and excluding all associated lifecycle costs associated with maintaining the ship and its personnel) the tanker would pay for itself after 188 years of service. Admittedly, this time frame is unrealistic; however, fuel prices will undoubtedly rise in the coming years. Assuming delivery of 5,200 BBL/Day of fuel for 50% of the time of its 40-year service life, Figure 5-5 shows that the fuel pays for the acquisition cost of the first tanker ship when the price reaches $13.35 per gallon:

Time to Payback Ship Acquisition Cost as Function of Fuel Price
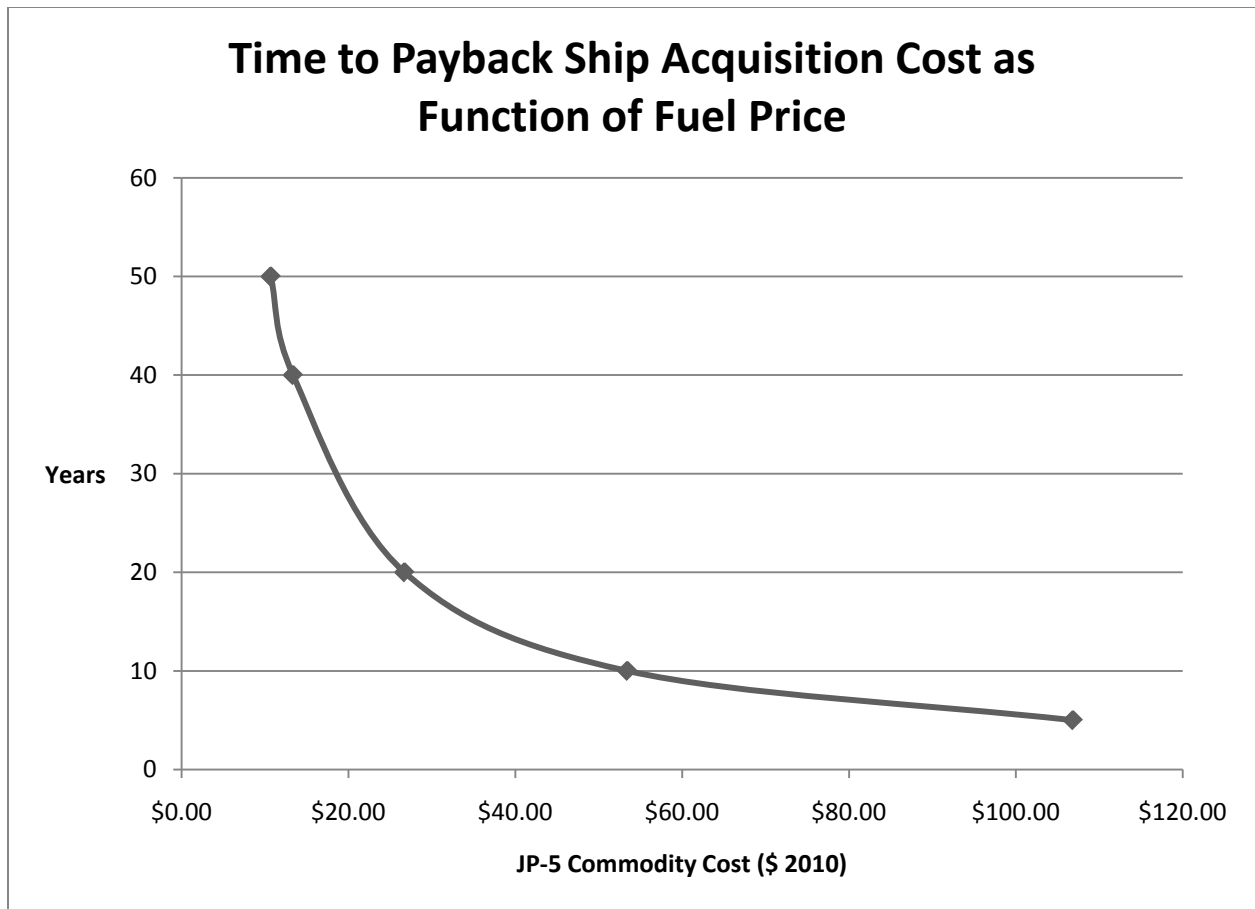
Figure 5-5 - Tanker Payback as Function of Fuel Price

Of course, the fuel commodity price will need to be higher to also cover operating, maintenance, personnel, and other lifecycle costs. However, if the fully burdened costs of delivering fuel are considered (refer to chapter 1), the tanker appears to be a relatively attractive option. A fully burdened (i.e., delivered on station) fuel cost of $53.42 per gallon results in tanker payback in just 10 years.

5.3   Ship Design Summary

The electrical power requirements for liquid fuel production are high, thereby resulting in significant amounts of electrical infrastructure to transfer power to the synfuel plant. The electrical power infrastructure and the air capture units account for over 62% of the 72,718 MT weight in a 110 m long parallel midbody for the TAO-187 tanker ship. Although large components such as reactor plant shielding and steam generators cannot be neglected during design, their contributions are not significant enough to preclude the midbody concept. Because of the 110 m midbody length limit, even reducing the size of the air capture units by a factor of four is not sufficient enough to make the

midbody concept viable. Assuming the air capture units can be reduced to ¼ of their current volume while maintaining their current capacity, the liquid fuel plant could probably fit within a 169 m long module.

A synfuel tanker should have all the capabilities of the present TAO-187 platform. Therefore, the new ship would probably need an overall length of ~ 376 m (TAO-187 length + synfuel module length) to accommodate all desired ship requirements. In order to maintain geometric similitude, the ship's beam, depth, and draft would increase to 55.2 m, 22.1 m, and 12.56 m, respectively. These dimensions should facilitate acceptable stability and structural performance; however, displacement would increase from 41,319.3 MT to 283,409 MT, and the tanker would be precluded from transiting via the Suez Canal. In order to provide some cost reduction and to maintain the capability to transit the Suez Canal, the tanker's length was kept at 376 m but its beam and draft were reduced to 36.7 m and 12.2 m. These dimensions are the customary L/B and L/T geometric proportion limits for a bulk carrier, and result in a full load displacement of 110,260 MT. However, designing the tanker ship to these limits might not be desirable because of the tanker ship's reduced cargo capacity compared to the original TAO-187 (22,117 MT vs. 26,467 MT). A more rigorous, detailed design in the future should determine a more optimal hull geometry.

Because the electrical power demands are so significant, an IPS architecture with electric drive is the most logical propulsion solution. Assuming the same 20.14 knot top speed, the tanker's BHP must increase from 23,720 kW, to ~ 45,600 kW_e, Since the transmission efficiency for electric drive propulsion is lower the current tanker's mechanical drive (0.89 vs. 0.98), the turbines must actually supply ~ 50,200 kW_e in order to provide the required delivered power to the propellers.

By using the MIT cost model for ship construction costs, and by soliciting expert opinion for power plant and fuel production plant acquisition costs, the lead ship acquisition cost was determined to be $21.0 billion ($2010). This figure excludes research and design or any other lifecycle costs. The primary cost driver for the ship is the large amount of electrical infrastructure (SWBS 300) required for the synfuel production plant. A future ship design study should determine the feasibility of reducing the current cost estimate by a factor of two or more.

At the current JP-5 commodity cost of $2.84 per gallon, and assuming delivery of the peacetime demand requirement (5,200 BBL/Day) 50% of the year, the fuel cost would pay for the acquisition cost in just over 188 years. However, Figure 5-5 shows that payback time is extremely sensitive to fuel price.

Increasing the fuel price to $13.35 reduces the payback time to 40 years. Since the fully-burdened cost of fuel is often much more than the commodity cost, the cost benefit of the nuclear power tanker is potentially favorable. More detailed analysis that considers the tanker's total lifecycle costs and the fully burdened fuel cost should be performed to precisely quantify the potential cost benefit.

5.4 Chapter 5 References

[1] Ingersoll, D., Clarno, K., Forsberg, C., 2005, "Status of Physics and Safety Analyses for the Liquid-Salt-Cooled Very High-Temperature Reactor (LS-VHTR)," Oak Ridge National Laboratory, ORNL/TM-2005/218, Oak Ridge, TN.

[2] Williams, D., Toth, L., and Clarno, K., 2006, "Assessment of Candidate Molten Salt Coolants for the Advanced High-Temperature Reactor (AHTR)," Oak Ridge National Laboratory, ORNL/TM-2006/12, Oak Ridge, TN.

[3] Holcomb, D., 2011, "Re: Salt Cooled Reactor Questions--Nuclear Tanker," **Email communication to author discussing salt coolant volume in reactor plant**pp. 1-1.

[4] Glasstone, S., and Sesonske, A., 1994, "Nuclear Reactor Engineering: Reactor Design Basics,"Chapman and Hall, Inc., New York, NY, pp. 322-405, Chap. 6.

[5] Eshleman, R., 2003, "Applied Engineering Principles Manual," Naval Sea Systems Command, Rev 1, ACN-1 http://www.usna.edu/EE/ee301/internal/Applied_EngineeringPrinciples.pdf, Washington, DC.

[6] Bureau of Medicine and Surgery, 2001, "Radiation Health Protection Manual," Department of the Navy, NAVMED P-5055, Washington, DC.

[7] Gibbs, J., 2008, "M.S. Thesis: Power Conversion System Design for Supercritical Carbon Dioxide Cooled Indirect Cycle Nuclear Reactors," Massachusetts Institute of Technology, http://hdl.handle.net/1721.1/44765, Cambridge, MA.

[8] Welsh, M., 2010, "Marine Electrical Systems," Massachusetts Institute of Technology, Presentation of Marine Electrical Systems to 2.611 (Marine Power and Propulsion), Cambridge, MA.

[9] Simmons, W., 2008, "Offshore GTL Enabled by Microchannel Process Technology," Velocys, 7th

GTLTec, February 18-19,

2008: http://www.google.com/url?sa=t&source=web&cd=1&ved=0CBcQFjAA&url=http%3A%2F%2Fvelo

cys-

files.gripmanager.com%2Fconferences%2F19%2FGTLTec_Presentation_final.pdf&rct=j&q=simmons%20

Offshore%20GTL%20Enabled%20by%20Microchannel%, Plain City, OH.

[10] Dritz, T., and McDaniel, J., 2011, "Email Communication on 01/30/2011 with Velocys, Inc." **Email

discussion regarding the estimated size and weight of reforming, fischer-tropsch, and product

upgrading modules.**pp. 1-1.

[11] Brophy, J., 2004, "Modular Gas-to-Liquids Technology," Velocys, 10th PIN Meeting, Heriot-Watt

University, Edinburgh: http://www.pinetwork.org/whatsnew/brophy_10.pdf, Plain City, OH.

[12] Stoots, C., O'Brien, J., McKellar, M., 2005, "Engineering Process Model For High-Temperature

Electrolysis: System Performance Evaluation," Idaho National Laboratory, INL/CON-05-00725, Idaho

Falls, ID.

[13] Tornabene, R., Wang, X., Steffen, J., C., 2005, "Development of Parametric Mass and Volume

Models for an Aerospace SOFC/Gas Turbine Hybrid System," Glenn Research Center, NASA/TM—2005-

213819, Cleveland, OH.

[14] Gottschlich, D., 2007, "Membrane Technology Research (MTR) Frequently Asked Questions (FAQ) -

"what is the Footprint of a VaporSep Membrane System? how Much does it Weight?"," **2011**(2/2) pp. 1.

[15] Village Marine, 2009, "Expeditionary Unit Water Purification Systems, Generation 2," **2010**(8/10)

pp. 1.

[16] Ebra Corporation, E.G., 2010, "Multistage Centrifugal Compressors," Elliot Group, http://www.elliott-turbo.com/Files/Admin/Literature/compressors.pdf, Jeanette, PA.

[17] Canada, J., Sullivan, W., Kulonda, D., 2005, "Capital Investment Analysis for Engineering and Management," Pearson - Prentice Hall, Upper Saddle River, NJ, pp. 585.

[18] Popper, H., 1970, "Modern Cost Engineering Techniques," McGraw-Hill, New York, NY, pp. 538.

[19] Lackner, K. S., 2009, "Capture of Carbon Dioxide from Ambient Air," The European Physical Journal (Special Topics), **176**pp. 93-106.

[20] Transworld Logistics Group, 2010, "Ocean Container Dimensions," **2011**(2/3) pp. 1.

[21] Carderock Division, Naval Surface Warfare Center (NSWC), 2003, "ASSET - Advanced Surface Ship and Submarine Evaluation Tool," **5.3**.

[22] Cimino, D., and Tellet, D., 2007, "Marine Vehicle Weight Engineering,"Society of Allied Weight Engineers, Los Angeles, CA, pp. 91-130, Chap. 8.

[23] Gillmer, T., and Johnson, B., 1982, "Introduction to Naval Architecture," Naval Institute Press, Annapolis, MD, pp. 324.

[24] Barzashka, I., 2/29/2000, "Nuclear Propulsion," **2011**(2/2) pp. 1.

[25] Ranjan, M., 2010, "M.S. Thesis: Feasibility of Air Capture," Massachusetts Institute of Technology, http://hdl.handle.net/1721.1/59782, Cambridge, MA.

[26] Smith, M., 2008, "M.S. Thesis: Updating MIT's Cost Estimation Model for Shipbuilding," Massachusetts Institute of Technology, http://hdl.handle.net/1721.1/44876, Cambridge, MA.

[27] Woud, H., and Douwe, S., 2002, "Design of Propulsion and Electric Power Generation Systems," Institute of Marine Engineering, Science and Technology, London, UK, pp. 494.

[28] Dostal, V., 2004, "Sc.D. Thesis: A Supercritical Carbon Dioxide Cycle for Next Generation Nuclear Reactors," Massachusetts Institute of Technology, http://hdl.handle.net/1721.1/17746, Cambridge, MA.

[29] Driscoll, M., 2004, "Supercritical CO2 Plant Cost Assessment," Massachusetts Institute of Technology, MIT-GFR-019, Cambridge, MA.

[30] Ingersoll, D., 2004, "Status of Preconceptual Design of the Advanced High-Temperature Reactor (AHTR)," Oak Ridge National Laboratory, ORNL/TM-2004/104, Oak Ridge, TN.

[31] Forsberg, C., 2011, "RE: AHTR Cost, MIT Department of Nuclear Science and Engineering" **Email communication to author discussing cost scaling for AHTR power plant**pp. 1-1.

[32] O'Rourke, R., 2010, "Navy Nuclear-Powered Surface Ships: Background, Issues, and Options for Congress," Congressional Research Service, RL33946, Washington, DC.

[33] Donald, K. A., 2010, "Naval Sea Systems Command, Director of Nuclear Propulsion (NAVSEA 08) Statement regarding US Navy use of Non-PWR Reactor Technology," **Statement from head of NAVSEA 08 to author and other MIT afflliated Engineering Duty Officers during an MIT luncheon on 29 Sep 2010 that, at the present time, the US Navy is not interested in implementing non-PWR reactor technology on its warships.**pp. 1.

[34] Dutta, S., 2010, "Re: Synfuel Production on a Naval Tanker," **Microchannel reactor performance characteristics**pp. 1-2.

[35] O'Brien, J., McKellar, M., Harvego, E., 2009, "High-Temperature Electrolysis for Large- Scale

Hydrogen and Syngas Production from Nuclear Energy – System Simulation and Economics," Idaho

National Laboratory, INL/CON-09-15563, Idaho Falls, ID.

[36] DESC, 2010, "FY 2010 Prices," DESC, http://www.desc.dla.mil/DCM/DCMPage.asp?pageid=722, Fort

Belvoir, VA.

(This Page Intentionally Blank)

6 Summary, Conclusions, and Recommendations for Future Work

6.1 Summary and Conclusions

Emerging technologies in CO_2 air capture, high temperature electrolysis, microchannel catalytic conversion, and Generation IV reactor plant systems have the potential to create a shipboard liquid fuel production system that will ease the burdened cost of supplying fuel to deployed naval ships and aircraft. By integrating these technologies together in a naval nuclear tanker ship platform, the wartime demand of a Carrier Strike Group (GSG) (6,400 BBL/Day of JP-5) could be satisfied using only air and water feedstocks. A commitment to this technology, while bold and challenging, promises to enhance US national security by providing a marked first step toward US energy independence. Because of rapid industrialization of population-dense Asian nations such as China and India, the steep climb in the fuel prices witnessed over the previous decade will likely become even more pronounced [1]:
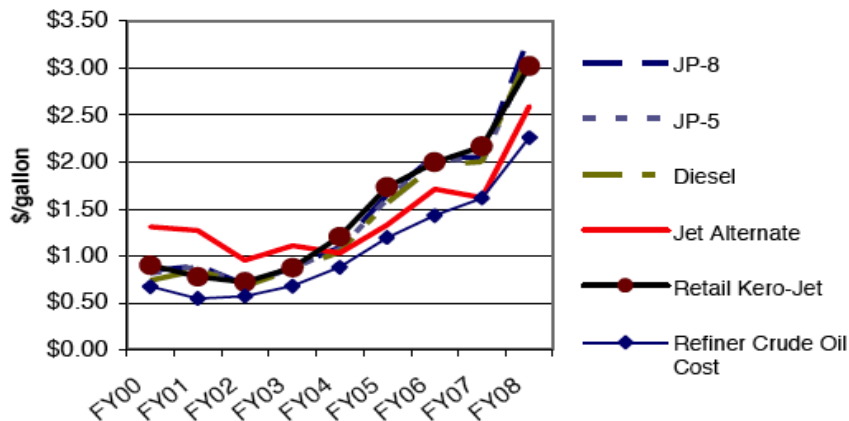
Figure 6-1 - Average Defense Department Fuel Costs

Previous investigation suggested implementing shipboard a liquid fuel production system using commercially mature processes such as alkaline electrolysis, light water reactors (LWRs), and methanol synthesis; however, more detailed analysis shows that such an approach is not practical. The methanol synthesis option utilizing alkaline electrolysis would require over 711 Norsk 5040 electrolyzers, each with a 13.5 m x 4 m footprint [2]:

Figure 6-2 - Size Perspective of Conventional Alkaline Electrolysis Technology

In addition to the obvious challenge of accommodating so many large units on board a tanker ship, the power plant would have to generate 1,482 MW_e in order to produce 6,400 BBL/Day JP-5 via methanol synthesis. Assuming a 33% thermodynamic efficiency, a LWR system on the order of 4,491 MW_{th} would be necessary; and these power requirements do not include shipboard propulsion or other hotel loads. These power requirements are large even for shore-based facilities; therefore, such an approach is not recommended.

Although Fischer-Tropsch synthetic fuel production technology has traditionally been designed to accommodate large economies of scale, recent advances in modular, microchannel technology have the potential to facilitate a shipboard solution. More research and design is necessary to evaluate their suitability, but initial results appear promising. Recent advances in high temperature co-electrolysis (HTCE) and high temperature steam electrolysis (HTSE) have been even more critical. All of the solid-oxide electrolytic cells (SOECs) necessary for H_2 and CO production of a 6,400 BBL/Day system would occupy only 35 m x 35 m footprint; only 16 Norsk 5040 electrolyzers could fit in the same area. Furthermore, higher temperature allows SOECs to electrolyze water and CO_2 more efficiently, requiring only ~ 75% of the electrical power needed for an equivalent alkaline electrolysis process (590 MW_e vs. 789 MW_e). However, the SOEC degradation rate must be resolved before they can be considered a viable alternative. Recent 25 cell SOEC stack tests at Idaho National Laboratory (INL) demonstrated an area specific resistance (ASR) increase of 40% in only 400 hours [3]. The current assumption is that 1/3 of the SOECs in a facility will be replaced annually [4]. At the estimated price of $200/$kW_e$, the current failure rate translates to an annual cost of nearly $35.4 million. At the fiscal year 2010 commodity price of $2.84 per gallon JP-5 [5], the SOEC degradation cost equates to 296,781 BBL of fuel. Assuming the peacetime fuel delivery rate of 5,200 BBL/Day, over 57 days of fuel delivery are necessary to

compensate. Additionally, more investigation is necessary to validate the design of the high temperature infrastructure and to resolve corrosion concerns.

After performing an assessment of various CO_2 feedstock sources, atmospheric CO_2 extraction using an air capture system appears the most promising option. Traditional synfuel feedstocks (i.e., coal and natural gas) have potential for shore based facilities, but are of limited utility for a naval platform. In addition to not being carbon neutral, their use would complicate military logistics even more and while not addressing the problem of supplying fuel to deployed forces. Similar problems exist with using municipal solid waste (MSW) and biomass, thus leaving CO_2 extraction from the air or sea as the only viable alternatives. Seawater is an attractive feedstock source since it contains 140 times the CO_2 concentration as the equivalent air volume. Unfortunately, the majority of seawater CO_2 is in a bicarbonate form, which makes using vacuum degassing/evaporation impractical. Using a strong anion based resin is impractical because of (1) the extremely large amounts of resin required to accommodate their low CO_2 capacity and (2) the need to use large amounts of a strong base elution chemical such as sodium hydroxide aboard ship [6]. Laboratory scale results of CO_2 extraction using gas permeable membranes are trending in the right direction; however, much more progress is required before they can be considered as an option [7]. This leaves atmospheric air capture as the most promising approach. Modular and transportable 1 MT/day CO_2 air capture prototypes exist [8]; although encouraging, the current design requires improvement. In order to be feasible for shipboard use, they must be able to capture CO_2 in a system only ¼ of the present size. Additionally, they require enhancement to facilitate their use at sea; the present design is optimized for dry, desert climates. However, there is a significant amount of climate change mitigation research and design underway, which implies substantial potential for technological improvement.

In order to improve the efficiency of the liquid fuel production process, improvements in modular, high temperature gas separation technology and autothermal reforming (ATR) are highly desirable. A significant limitation of all of current gas separation technologies is that they require cooling the inlet gas stream to near ambient temperature prior to separation, thus imposing an additional and significant energy penalty if using high temperature processes. Also, reforming the unwanted (non JP-5) hydrocarbons back into syngas via ATR significantly reduces CO_2 and H_2 feed demand by the synfuel production system. Rather than being completely discarded overboard, the plant can use a significant fraction of the generated O_2 to recycle hydrocarbons back into syngas feed. Compared to steam methane reforming or partial oxidation, ATR is not as common in the chemical

industry because of the process's need for oxygen; hence the more limited technological experience with this capability. However, the process is well-understood and could probably be implemented onboard a tanker ship with a modest research and design investment.

After synthesizing these cutting edge technologies into a coherent system, the proposed shipboard liquid fuel production system using water, air, and nuclear power is shown in Figure 6-3:
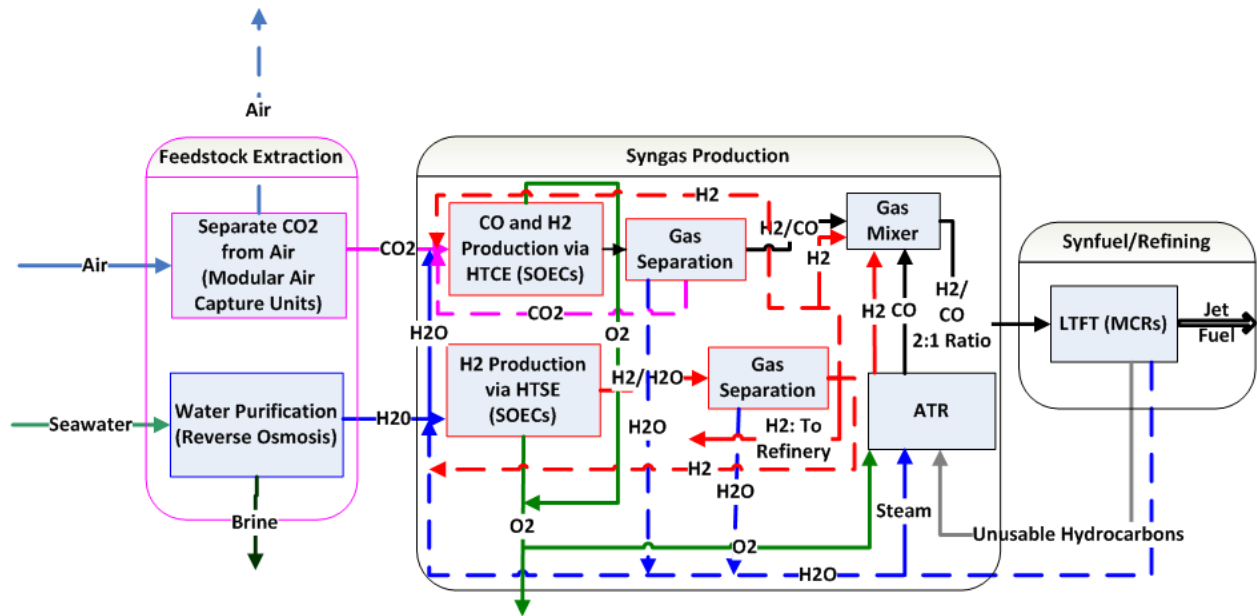
Figure 6-3 - Proposed Liquid Fuel Production System

Table 6-1 summarizes the liquid fuel production system's power requirements for both a Pressurized Water Reactor (PWR) Rankine cycle plant, and an advanced high temperature reactor (AHTR) coupled to a supercritical carbon dioxide (S-CO₂) power cycle:

AHTR (S-CO2)-670 ^{o}C			PWR (Steam)-285 ^{o}C		
Reactor Power			**Reactor Power**		
Total Thermal Power (MW$_{th}$)	1,456		Total Thermal Power (MW$_{th}$)		2,082
Thermal Power to Power Cycle (MW$_{th}$)	1,285		Thermal Power to Power Cycle (MW$_{th}$)		1,973
Electrical Power from Power Cycle (MW$_e$)	650		Electrical Power from Power Cycle (MW$_e$)		658
Thermal Power for Process Heat (MW$_{th}$)	171		Thermal Power for Process Heat (MW$_{th}$)		109
HTCE **(27-655 ^{o}C)**			**HTCE** **(27-285 ^{o}C)**		
CO_2 Feed Heating (MW$_{th}$)	21.1		CO_2 Feed Heating (MW$_{th}$)		7.80
H_2O Feed Heating (MW$_{th}$)	102		H_2O Feed Heating (MW$_{th}$)		69.3
HTCE Total (MW$_{th}$)	**123**		**HTCE Total (MW$_{th}$)**		**77.1**
HTSE **(27-655 ^{o}C)**			**HTSE** **(27-285 ^{o}C)**		
H_2O Feed Heating (MW$_{th}$)	17.6		H_2O Feed Heating (MW$_{th}$)		12.0
HTSE Total (MW$_{th}$)	**17.6**		**HTSE Total (MW$_{th}$)**		**12.0**
Autothermal Reforming **(37-655 ^{o}C)**			**Autothermal Reforming** **(37-285 ^{o}C)**		
H_2O Heating (MW$_{th}$)	13.4		H_2O Heating (MW$_{th}$)		10.3
HC Heating (MW$_{th}$)	7.86		HC Heating (MW$_{th}$)		2.96
ATR Total (MW$_{th}$)	**21.2**		**ATR Total (MW$_{th}$)**		**13.2**
Product Upgrading (7-350 ^{o}C) (MW$_{th}$)	**8.59**		**Product Upgrading (7-285 ^{o}C) (MW$_{th}$)**		**6.24**
Overall Cycle Performance			**Overall Cycle Performance**		
Cycle Efficiency (η_{th})	44.6%		Cycle Efficiency (η_{th})		33.1%
Heat JP-5 Combustion/Reactor Heat Input	31.1%		Heat JP-5 Combustion/Reactor Heat Input		21.8%

Table 6-1 – Liquid Fuel Production System Temperature and Power Requirements Summary for 6,400 BBL/Day JP-5

Although a PWR power plant is not the recommended option, its use is feasible. The required temperatures for liquid fuels production could be attained by using electric heaters to increase temperatures where necessary; and intelligent heat recuperation could minimize electric heater power demand. During normal operation, each "high temperature" process has relatively negligible power requirements to accommodate compared to the power needed for electrolysis. Operating with a Rankine cycle, a PWR could power the recommended liquid fuel production plant with a 2,082 MW$_{th}$ reactor and 33.1% cycle efficiency.

The Naval Nuclear Propulsion Program (NAVSEA 08) eschews reactor plant designs other than PWRs because it is difficult to show that a different reactor plant design would afford the same levels of reliability and survivability given the typical power demands of a naval vessel [9]. Although the research and development costs associated with an AHTR design would be significant [10], the potential benefits

afforded by more advanced reactor and power cycle designs are too significant to ignore. For the recommended liquid fuel production option, the salt-cooled AHTR requires 30.1% less heat input (1,456 MW_{th} vs. 2,082 MW_{th}) and has a 42.4% higher cycle efficiency (44.6% vs. 33.1%) when coupled to a S-CO_2 recompression cycle operating at 25.0 MPa and 670 ^{o}C. Analysis of simple Brayton power conversion system (PCS) alternatives shows that N_2, a N_2/He mixture, and pure helium are not as competitive as S-CO_2. S-CO_2 tends to operate at higher cycle efficiency for a simple Brayton cycle, and a much higher efficiency in a recompression cycle. Additionally CO_2 is easier to obtain than helium (especially in the present application, which removes it from air), and is much more convenient to store than any of the other fluids. Compared to the other variants, S-CO_2 has the smallest PCS footprint. Compared to a Rankine cycle, the compactness of the S-CO_2 system is readily apparent, as Figure 6-4 shows [11]:
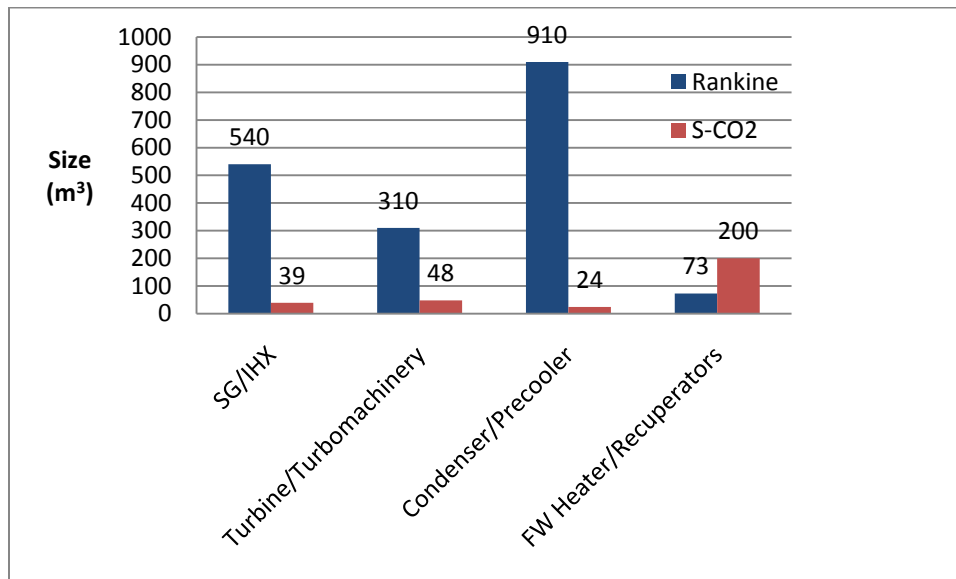
Figure 6-4 - Comparison of Rankine to S-CO2 Machinery from a 300 MW_e Plant

A PWR cannot take advantage of a S-CO_2 cycle without suffering a severe efficiency penalty. A S-CO_2 coupled to a PWR results in a 18.1% higher heat input (2,459 MW_{th} vs. 2,082 MW_{th}) and a 14.7% lower thermal efficiency (26.7% vs. 33.1%) than an equivalent Rankine cycle. Given the magnitude of the liquid fuel production plant's power requirements, these penalties significantly increase the size and cost of the reactor plant. Finally, Table 6-2 shows that in terms of reactor power heat input to JP-5 combustion heat output, the AHTR option operating with a S-CO_2 is clearly the most desirable choice:

Option	Efficiency
AHTR – Alkaline Electrolysis	25.1%
AHTR – HTCE/HTSE	31.1%
PWR – Alkaline Electrolysis	16.6%
PWR – HTCE/HTSE	21.8%

Table 6-2 – Ratio of JP-5 Combustion Heat Output to Reactor Heat Input

The key issue requiring resolution with the AHTR's design is demonstrating satisfactory salt coolant compatibility with ASME certified components at operating temperatures. Hastelloy-N appears to be a promising material for the reactor vessel and salt coolant piping for temperatures 700 ^{o}C and lower [12], but additional performance evaluation with a variety of salt coolant candidates is necessary before its viability can be confirmed. Another issue is that chromium rich materials appear to offer the best corrosion resistance to S-CO_2 [13, 14]; however, chromium rich materials exhibit the worst material performance with the fluoride based molten salts considered for use in the AHTR [12]. Subsequent investigation should evaluate the corrosion resistance of Hastelloy-N with S-CO_2 fluids and molten salt candidates in a common heat exchanger in order to validate concept feasibility.

The feasibility of incorporating the liquid fuel production and power plant systems into a module inserted as a parallel midbody into the TAO-187 *Henry Kaiser* class oiler was evaluated. The maximum 110 m midbody length does not provide enough buoyancy to accommodate the equipment's weight, and not enough deck surface area exists to accommodate the air capture units. The electrical power requirements for liquid fuel production are high, thereby resulting in significant amounts of electrical infrastructure to transfer power to the synfuel plant. The electrical power infrastructure and the air capture units account for over 62% of the 72,718 MT weight in a 110 m long parallel midbody for the TAO-187 tanker ship. Although large components such as reactor plant shielding and steam generators cannot be neglected during design, their contributions are not by themselves significant enough to preclude the midbody concept. Because of the 110 m midbody length limit, even reducing the size of the air capture units by a factor of four is not sufficient to make the midbody concept viable. Assuming the air capture units can be reduced to ¼ of their current volume while maintaining their current capacity, the liquid fuel plant could probably fit within a 169 m long module.

Since the synfuel tanker would likely need to retain all of the capabilities of the present TAO-187 platform, the new ship would need an overall length of ~ 376 m (TAO-187 length + synfuel module length) to accommodate all desired requirements. In order to minimize cost as much as possible, and to

maintain the capability of transiting the Suez Canal, the beam was increased to 36.7 m and the draft was increased to 12.2 m, while keeping the original 376 m length. These dimensions are the customary L/B and L/T geometric proportion limits for a bulk carrier, and result in a full load displacement of 110,260 MT. However, designing the tanker ship to these limits might not be desirable because of the tanker ship's reduced cargo capacity compared to the original TAO-187 (22,117 MT vs. 26,467 MT). Assuming a 0.8 kg/liter density, the tanker's capacity is sufficient to supply over 33 days of peacetime operations and 27 days of combat operations for a CSG. A more rigorous, detailed design in the future should determine a more optimal hull geometry. Because the electrical power demands are so significant, an IPS architecture with electric drive is the most logical propulsion solution [15]. Assuming the same 20.14 knot top speed, the tanker's BHP must increase from 23.7 MW_e to ~ 45.6 MW_e. Since the transmission efficiency for electric drive propulsion is lower than the current tanker's mechanical drive (0.89 vs. 0.98), the turbines must actually supply ~ 50.2 MW_e in order to provide the required delivered power to the propellers [16]. After accounting for additional 9.16 MW_e in shipboard hotel loads, the total power required for liquid fuels production, propulsion, and electrical power for shipboard systems is ~ 709 MW_e, which corresponds to an overall reactor rating of 1,589 MW_{th}.

By using the MIT cost model for ship construction costs [17], and by soliciting expert opinion for power plant and fuel production plant acquisition costs [10, 18, 19], the lead ship acquisition cost was determined to be $21.0 billion ($2010). This figure excludes research and design or any other lifecycle costs. At the current JP-5 commodity cost of $2.84 per gallon, and assuming delivery of the peacetime demand requirement (5,200 BBL/Day) 50% of the year, the fuel cost would pay for the acquisition cost in just over 188 years. However, Figure 6-5 shows that payback time is extremely sensitive to fuel price:
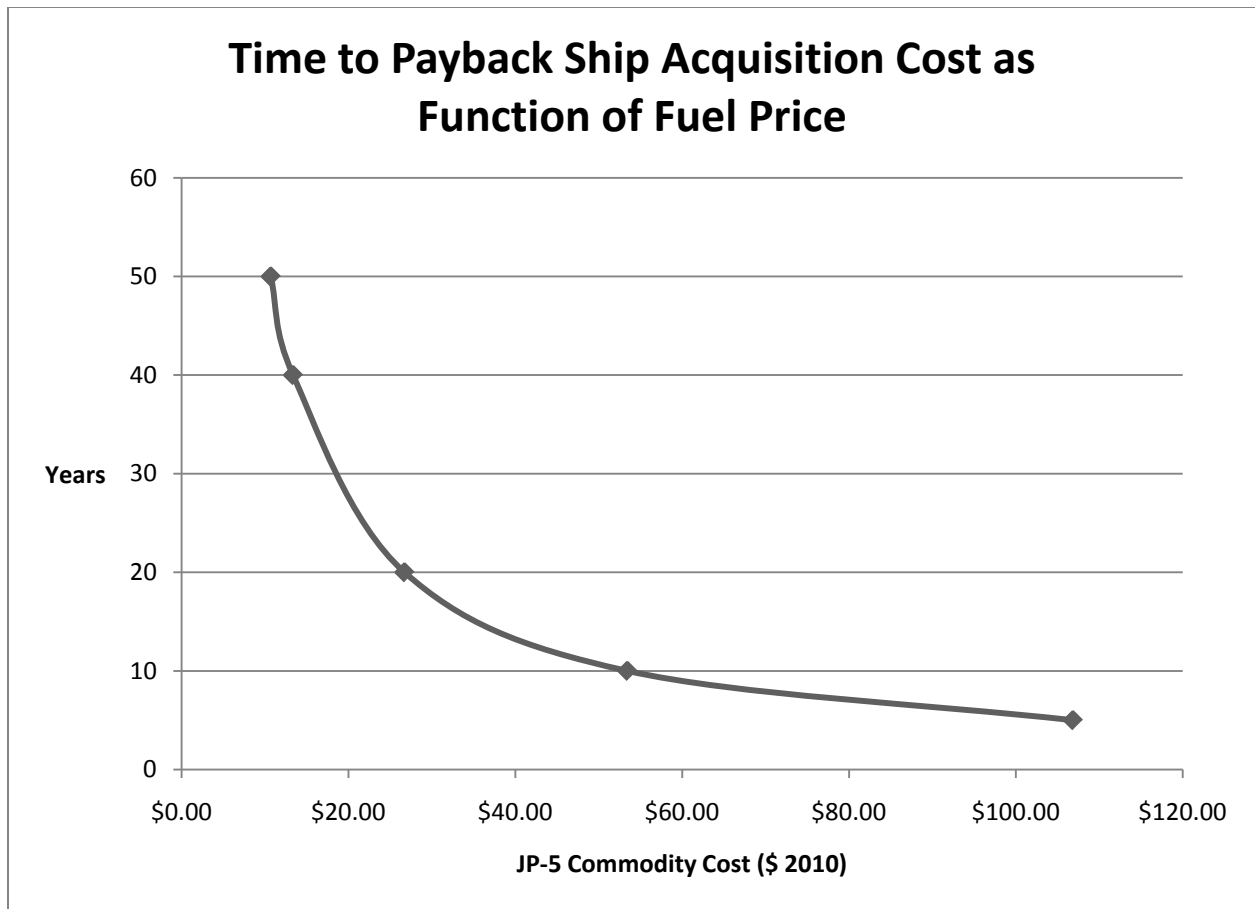
Figure 6-5 - Tanker Payback as Function of Fuel Price

Increasing the fuel price to $13.35 reduces the payback time to 40 years. Since the fully-burdened (i.e., delivered on station) cost of fuel is often much more than the commodity cost [20], the cost benefit of the nuclear power tanker is potentially favorable. More detailed analysis that considers the tanker's total lifecycle costs and the fully burdened fuel cost should be performed to precisely quantify the potential cost benefit.

6.2   Recommendations for Future Work

A significant amount of investigation is necessary to confirm the proposed concept's technological feasibility, precisely quantify the cost benefit, and complete the detailed design work. Numerous issues, spanning a broad range of academic disciplines, require resolution. Although additional topics could also receive attention, more investigation is clearly necessary for the following topics:

6.2.1 CO$_2$ Feedstock Extraction
- Reduce the current air capture unit system size by a factor of four or more.
- Improve current air capture system design to facilitate operation at sea.
- Determine if the gas permeable separation membrane design can be improved in order to facilitate adequate CO$_2$ extraction from seawater.

6.2.2 High Temperature Electrolysis
- Resolve the mechanisms responsible for accelerated degradation in SOECs. Engineer a solution that extends cell lifetime to 50,000 hours or more.
- Validate material resistance to corrosion at operating temperatures of 800 ^{o}C and higher.

6.2.3 Gas Cleanup
- Identify the most promising high temperature gas cleanup technologies (H$_2$ and CO separation), and perform a detailed analysis on their impact on the liquid fuel production system. Quantify their associated energy penalties and their impact on system efficiency.

6.2.4 Liquid Fuels Production/Product Refinement
- Engineer a catalyst within a microchannel Fischer-Tropsch reactor that maximizes the JP-5/kerosene hydrocarbon fraction and minimizes the product upgrading requirements. Quantify the catalyst's syngas to synfuel conversion ratio and evaluate its overall impact on system efficiency.
- Design an autothermal reformer that can be accommodated in the proposed liquid fuel production scheme. Establish its efficiency in reforming non JP-5 hydrocarbons back to syngas feed, and calculate its impact on the cycle.

6.2.5 Power Plant Design
- Design a compact, highly enriched (>90% ^{235}U), salt-cooled AHTR (700 ^{o}C) optimized for shipboard use. Evaluate its performance under credible accident scenarios.
- Evaluate the corrosion resistance of Hastelloy-N with S-CO$_2$ fluids and molten salt candidates in a common heat exchanger at temperatures of 700 ^{o}C.
- Demonstrate Hastelloy-N's suitability for ASME certification as a reactor pressure vessel material.
- Demonstrate material compatibility of prospective salt coolants at operating temperature in order to conclusively determine the best salt coolant candidates.

6.2.6 Tanker Ship Design
- Design a nuclear tanker ship that can accommodate the proposed liquid fuel production design, and evaluate if smaller ships with reduced capacity is more desirable and cost effective. The design should consider the tanker's total lifecycle cost as well as the ancillary costs associated with fully burdened fuel cost in order to precisely quantify the concept's cost benefit.

6.2.7   Future Work Summary

Although an extensive amount of research and development work remains just to demonstrate the concept's feasibility, there is extensive synergism with work underway on several new technologies:

- Evaluation of the salt-cooled AHTR
- CO_2 capture/sequestration
- H_2 production
- Conversion of syngas to liquid fuels

In each area, rapid technological progress is being made because there are large incentives to develop each technology independent of possible naval applications. No single entity has the resources to investigate all of these concepts; however, the US Navy, as well as other entities with a vested interest in energy security, could concentrate on one or two aspects of the design effort as well as the technological integration. For example, it could focus on an advanced, high temperature reactor design with an advanced power cycle because the developments from that research would be useful for next generation reactor plants. It should also focus on how to make the air capture units more compact because shoreside facilities have little need reduce their present size; or, perhaps, it could sponsor new, innovative approaches of effectively removing CO_2 from seawater. Finally, it must integrate the results from the research and design efforts of individual technologies into a viable platform that suits its specific requirements.   Presently, producing jet fuel from water and air seems like a bold, expensive, radical concept; however, launching ballistic missiles from nuclear powered submarines would have seemed just as bold to someone in the 1930's. Given enough investment and determination, a fully viable concept could be available in within a 10-20 year time frame.

6.3 Chapter 6 References

[1] Andrews, A., 2009, "Department of Defense Fuel Spending, Supply, Acquisition, and Policy," Congressional Research Service, R40459, Washington, DC.

[2] Statoil Hydrogen Technologies, 2010, "Electrolyzer Products," **2010**(8/12) pp. 1.

[3] Stoots, C., O'Brien, J., Herring, J., 2009, "Long-Term Degradation Testing of High-Temperature Electrolytic Cells," Idaho National Laboratory, INL/EXT-09-16559, Idaho Falls, ID.

[4] O'Brien, J., McKellar, M., Harvego, E., 2009, "High-Temperature Electrolysis for Large- Scale Hydrogen and Syngas Production from Nuclear Energy – System Simulation and Economics," Idaho National Laboratory, INL/CON-09-15563, Idaho Falls, ID.

[5] DESC, 2010, "FY 2010 Prices," DESC, http://www.desc.dla.mil/DCM/DCMPage.asp?pageid=722, Fort Belvoir, VA.

[6] Willauer, H., Hardy, D., Ndubizu, E., 2009, "Extraction of Carbon Dioxide from Sea water by Ion Exchange Resin Part II: Using Strong Base Anion Exchange Resin," Office of Naval Research, NRL/MR/6180--09-9211, Washington, DC.

[7] Willauer, H., Hardy, D., Lewis, K., 2010, "Effects of Pressure on the Recovery of CO2 by Phase Transition from a Seawater System by Means of Multilayer Gas Permeable Membranes," Journal of Physical Chemistry, **114**pp. 4003-4008.

[8] Lackner, K. S., 2009, "Capture of Carbon Dioxide from Ambient Air," The European Physical Journal (Special Topics), **176**pp. 93-106.

[9] Donald, K. A., 2010, "Naval Sea Systems Command, Director of Nuclear Propulsion (NAVSEA 08) Statement regarding US Navy use of Non-PWR Reactor Technology," **Statement from head of NAVSEA 08 to author and other MIT afflliated Engineering Duty Officers during an MIT luncheon on 29 Sep 2010 that, at the present time, the US Navy is not interested in implementing non-PWR reactor technology on its warships.**pp. 1.

[10] Forsberg, C., 2011, "RE: AHTR Cost, MIT Department of Nuclear Science and Engineering" **Email communication to author discussing cost scaling for AHTR power plant**pp. 1-1.

[11] Gibbs, J., 2008, "M.S. Thesis: Power Conversion System Design for Supercritical Carbon Dioxide Cooled Indirect Cycle Nuclear Reactors," Massachusetts Institute of Technology, http://hdl.handle.net/1721.1/44765, Cambridge, MA.

[12] Williams, D., Toth, L., and Clarno, K., 2006, "Assessment of Candidate Molten Salt Coolants for the Advanced High-Temperature Reactor (AHTR)," Oak Ridge National Laboratory, ORNL/TM-2006/12, Oak Ridge, TN.

[13] Gibbs, J., 2010, "M.S. Thesis: Corrosion of Various Engineering Alloys in Supercritical Carbon Dioxide," Massachusetts Institute of Technology, http://hdl.handle.net/1721.1/59247, Cambridge, MA.

[14] Dunlevy, M., 2009, "M.S. Thesis: An Exploration of the Effect of Temperature on Different Alloys in a Supercritical Carbon Dioxide Environment," Massachusetts Institute of Technology, http://hdl.handle.net/1721.1/57777, Cambridge, MA.

[15] Welsh, M., 2010, "Marine Electrical Systems," Massachusetts Institute of Technology, Presentation of Marine Electrical Systems to 2.611 (Marine Power and Propulsion), Cambridge, MA.

[16] Woud, H., and Douwe, S., 2002, "Design of Propulsion and Electric Power Generation Systems," Institute of Marine Engineering, Science and Technology, London, UK, pp. 494.

[17] Smith, M., 2008, "M.S. Thesis: Updating MIT's Cost Estimation Model for Shipbuilding," Massachusetts Institute of Technology, http://hdl.handle.net/1721.1/44876, Cambridge, MA.

[18] Dutta, S., 2010, "Re: Synfuel Production on a Naval Tanker," **Email communication with author describing microchannel reactor performance characteristics** pp. 1-2.

[19] O'Rourke, R., 2010, "Navy Nuclear-Powered Surface Ships: Background, Issues, and Options for Congress," Congressional Research Service, RL33946, Washington, DC.

[20] Corley, R., 2009, "M.S. Thesis: Evaluating the Impact of the Fully Burdened Cost of Fuel," Naval Postgraduate School, http://handle.dtic.mil/100.2/ADA508983, Monterey, CA.

Appendix A – US Navy Fuel Consumption

The figures in this appendix provide the reader perspective on (1) the amount of fuel consumed in relation to other US Government entities, (2) the amount of fuel consumed by various combatant platforms within the navy, and (3) the amount of fuel consumed by the deployed forces that the nuclear synfuel tanker would supply.

Overall US Navy Fuel Consumption
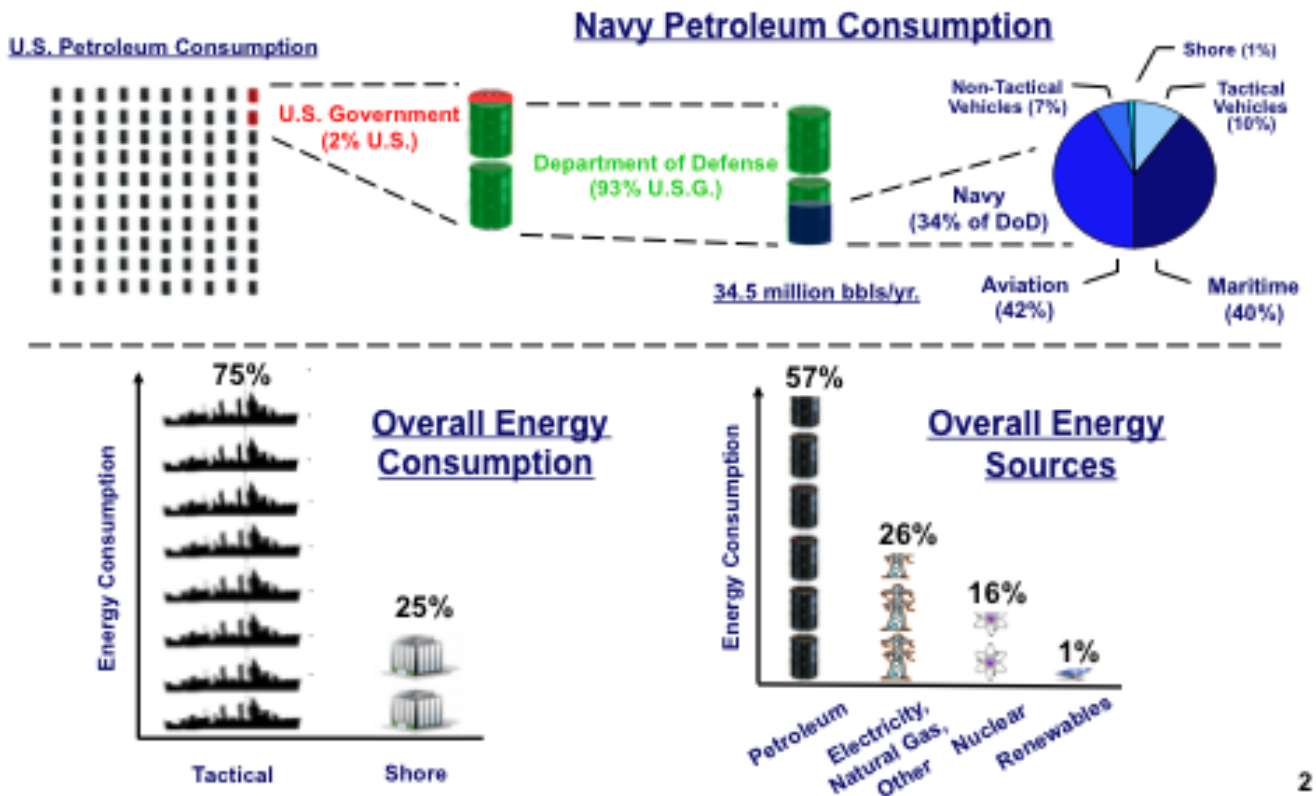
Figure A-1 – Overall US Navy Petroleum Consumption [1]
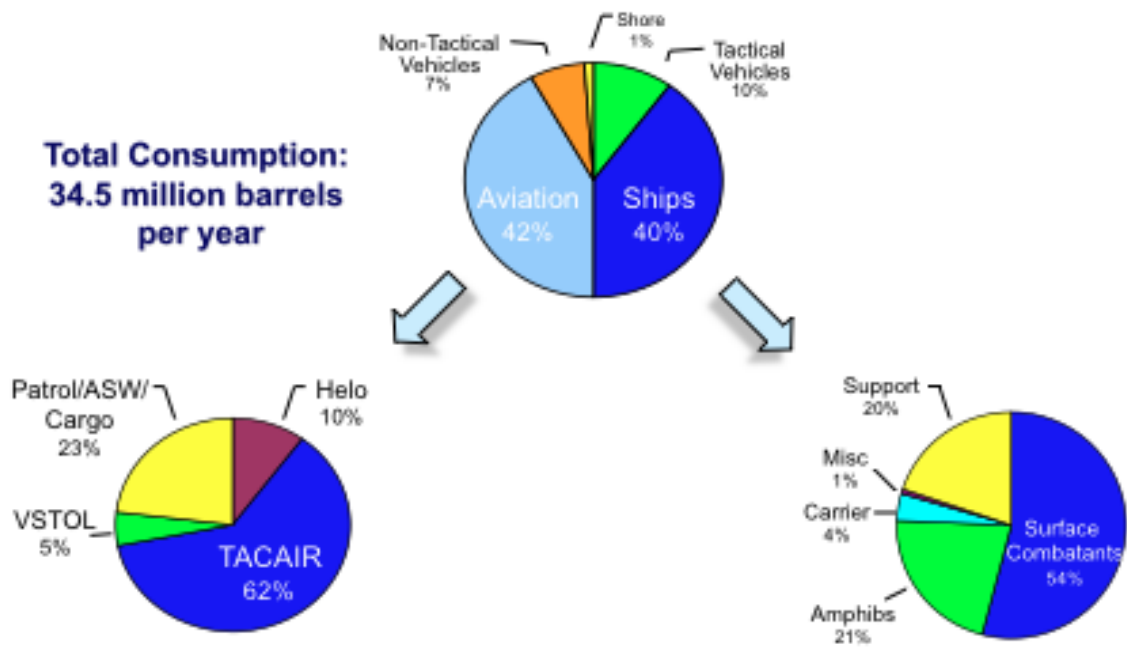
Figure A-2 – US Navy Consumption by Capability [1]
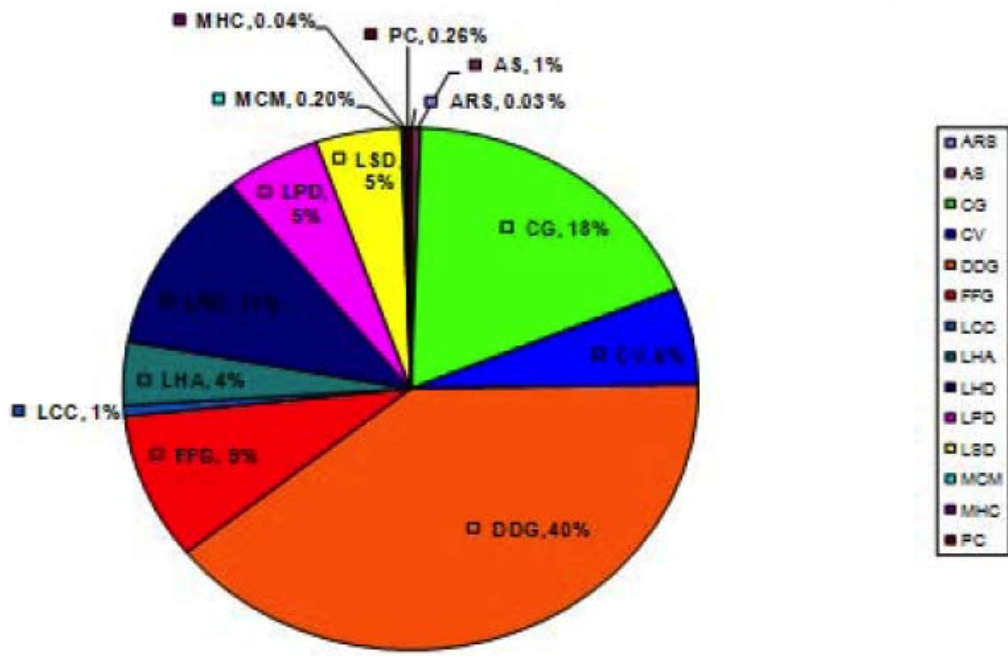
Figure A-3 – US Navy FY07 Surface Ship Fuel Consumption [2]

Carrier Strike Group and Amphibious Ready Group Fuel Consumption

Platform	Status	FY 03 (BBL/Day)	FY 09 (BBL/Day)
CSG	Deployed	3,214	2,005
	Non-deployed	2,112	1,317
ESG/ARG	Deployed	1,424	827
	Non-deployed	714	415

Table A-1- US Navy JP-5 Consumption Figures [3]

BSO	Weapon System Detail	EMP Code	Deployed (BBLs/Day)		Non-deployed (BBLs/Day)	
			Underway	Not Underway	Underway	Not Underway
60	CVN-0065	CSG	3.00	3.00	3.00	3.00
60	CVN-0068	CSG	3.00	3.00	3.00	0.00
60	CG-0047	CSG	691.00	210.00	569.00	20.00
60	DDG-0051	CSG	529.00	183.00	498.00	17.00
60	SSN-0688	CSG	0.00	0.00	0.00	0.00
60	SSN-0774	CSG	0.00	0.00	0.00	0.00
70	CVN-0068	CSG	3.00	3.00	3.00	3.00
70	CG-0047	CSG	714.00	155.00	575.00	16.00
70	DDG-0051	CSG	583.00	153.00	502.00	13.00
70	SSN-0688	CSG	0.00	0.00	0.00	0.00
70	SSN-0774	CSG	0.00	0.00	0.00	0.00
60	LHA-0001	ESG	1,094.00	519.00	895.00	72.00
60	LHA-0006	ESG	0.00	0.00	0.00	0.00
60	LHD-0001	ESG	1,105.00	457.00	937.00	80.00
60	LHD-0008	ESG	0.00	0.00	0.00	0.00
60	LPD-0004	ESG	472.00	258.00	377.00	30.00
60	LPD-0017	ESG	401.00	106.00	250.00	13.00
60	LSD-0041	ESG	305.00	78.00	237.00	7.00
60	LSD-0049	ESG	297.00	135.00	237.00	11.00
70	LHA-0001	ESG	1,375.00	635.00	969.00	65.00
70	LHA-0006	ESG	1,375.00	635.00	969.00	65.00
70	LHD-0001	ESG	1,243.00	534.00	958.00	65.00
70	LHD-0008	ESG	1,243.00	543.00	958.00	65.00
70	LPD-0004	ESG	548.00	271.00	419.00	31.00
70	LPD-0017	ESG	466.00	203.00	255.00	17.00
70	LSD-0041	ESG	326.00	102.00	246.00	14.00
70	LSD-0049	ESG	326.00	102.00	246.00	14.00

Table A-2 – US Navy F-76 Consumption By Platform (FY07/08/09 3-yr Avg) [4]

Appendix A References

[1] Kaptur, M., 2009, "Navy Energy Perspectives (Power Point Presentation)," Reserve Officer's Association, www.roa.org/site/DocServer/Kaptur_Navy_Energy_Brief_v6.ppt?, Washington, DC.

[2] Fonte, S., 2009, "M.S. Thesis: A Cost Estimation Analysis of US Navy Ship Fuel-Saving Techniques and Technologies," Naval Postgraduate School, http://handle.dtic.mil/100.2/ADA510113, Monterey, CA.

[3] Greg, R., 2010, "RE: Fuel Consumption Data," **Email to Author of JP5 Fuel Consumption Data (.xls format), FY03 and FY09**pp. 1.

[4] Dimirack, S., 2010, "RE: Fuel Consumption Data," **Email to Author of Historical Three Year Average of F76 Consumption in BBLs/day (.xls format)**pp. 1.

Appendix B – Fuel Specifications

JP-5 and F-76 Fuel Specifications

Table B-1 summarizes the important JP-5 specifications. F-76, JP-8, and Jet A-1 specifications are provided for comparison. However, the list below is not a complete listing, and the US military frequently revises fuel specifications. Detailed specifications, along with approved testing methods, are found in references [1-4].

Requirement	JP-5	F-76	JP-8	Jet A-1
Max Aromatics (% vol)	25.0	--	25.0	25.0
Max Sulfur (% mass)	0.30	0.50	0.30	0.30
Distillation Temp (^{o}C)				
10% Recovered, temp	205	--	205	205
End Point, temp	300	385	300	300
Min Flash Point (^{o}C)	60	60	38	38
Density @ 15°C (kg/liter)				
Min	0.788	--	0.775	775
Max	0.845	0.876	0.840	0.840
Max Freezing Point (^{o}C)	-46	--	-47	-47
Min Heat of Combustion (MJ/kg)	42.6	--	42.8	42.8
Min Hydrogen Content (% mass)	13.4	12.5	13.4	13.4
Min Smoke Point (mm)	19.0	--	19.0	19.0
Fuel System Icing Inhibitor (% vol)				
Min	0.10	--	0.10	--
Max	0.15		0.15	

Table B-1 – Fuel Specifications

JP-5 Chemical Properties

Appendix C of reference [5] contains an excellent summary of JP-5 composition and properties. Of particular note is Table B-2 below, which contains the typical hydrocarbon families that compose JP-5, as well as Table B-3, which contains the composition and heat of combustion of JP-5. While Table B-2 is mainly useful as a frame of reference, Table B-3 shows that the differences for the three suggested chemical formulas of JP-5 are negligible. Hence, using the simpler version, $(CH_2)_n$ for n=10, is convenient and sufficiently accurate for this thesis' scoping analysis.

Paraffins	26%
Naphthenes	**50%**
Aromatics	**22%**
Olefins	**2%**

Table B-2 – Typical Avcat JP-5 Hydrocarbon Distribution [6]

Type	Formula	% H_2	% C	ΔH $_{combustion}$ (kJ/kg)	ΔH $_{formation}$ (kJ/kg)
Avcat	$CH_{1.83}$	13.3	86.7	47,254	-2,814
Theoretical JP-5	$CH_{1.94}$	14	86	48,005	-2,941
Practical JP-5	CH_2	14.4	85.6	48,410	-2,998

Table B-3 – Composition and Heat of Combustion of JP-5 [7]

Appendix B References

[1] Department of Defense, 2006, "Detail Specification: Fuel, Naval Distillate," Department of Defense, MIL-DTL-16884L, Arlington, VA.

[2] Department of Defense, 2004, "Detail Specification Turbine Fuel, Aviation Grades JP-4 and JP-5," Department of Defense, MIL-DTL-5624U, Alexandria, VA.

[3] Department of Defense, 1999, "Detail Specification Turbine Fuels, Aviation, Kerosene Types, NATO F-34 (JP-8), NATO F-35, AND JP-8+100," Defense Quality and Standardization Office, MIL-DTL-83133E, Falls Church, VA.

[4] ExxonMobil, 2005, "World Jet Fuel Specifications (with Avgas Supplement)," ExxonMobil, 2005 Edition, Leatherhead, UK.

[5] Terry, K., 1995, "NEng Thesis: Synthetic Fuels for Naval Applications Produced Using Shipboard Nuclear Power," Massachusetts Institute of Technology (DSpace@mit), http://hdl.handle.net/1721.1/11590, Cambridge, MA.

[6] Coordinating Research Council, 2004, "Handbook of Aviation Fuel Properties, 3rd Ed," CRC Press, 635, Alpharetta, GA.

[7] Smith, M., 1970, "Aviation Fuels," G.T. Foulis & Co. LTD, Oxfordshire, UK, .

(This Page Intentionally Blank)

Appendix C - High Temperature Electrolysis Model

Introduction

Idaho National Laboratory (INL) has performed and published much of the research and development regarding high temperature steam electrolysis (HTSE) and co-electrolysis (HTCE) in free, publically available reports. Although INL utilizes sophisticated software modeling programs, the researchers involved have lucidly explained the thermodynamic principles that describe HTSE and HTCE in many of their reports. They also show in their reports how closely their theoretical modeling predictions correlate to their empirical observations. The intent of this appendix is to show the thermodynamic concepts that were used to develop HTSE and HTCE electrolyzer models in MATLAB.

Nomenclature

ASR	Area specific resistance, ohm-cm^2
F	Faraday number, 96,487 C/mol
ΔG_R	Gibbs free energy of reaction, J/mol
ΔH^o_f	Enthalpy of formation, J/mol
ΔH_i	Component sensible enthalpy, J/mol
ΔH_R	Enthalpy of reaction, J/mol
i	Current density, Amps/cm^2
I	Current, Amps
$\dot{N}$	Molar flow rate, mol/s
$\Delta\dot{N}$	Molar production rate, mol/s
P	Pressure, kPa
$\dot{Q}$	Rate of heat transfer, watts
R_u	Universal gas constant, J/mol-K
T	Temperature, K
T_o	Standard temperature, K
T_R	Reactant temperature, K
T_p	Product temperature, K
V	Voltage, volts
V_n	Nernst potential, volts
V_{op}	Operating voltage, volts
V_{tn}	Thermal neutral voltage, volts
$\dot{W}$	Work rate (power), watts
Y	Mole fraction

Thermodynamics of HTSE

The following discussion regarding HTSE thermodynamics is paraphrased from references [1, 2]. Figure C-1 below shows the control volume (CV) of an isothermal process with heat and work crossing the CV boundary:
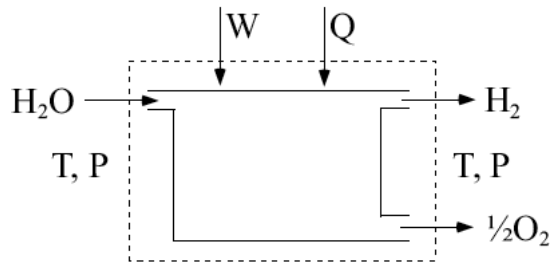
Figure C-1 - Schematic of HTSE CV

In HTSE, the steam reduction reaction is endothermic, and depending on the operating voltage of the stack, the net heat generation may be positive, negative, or zero as shown by figure below:
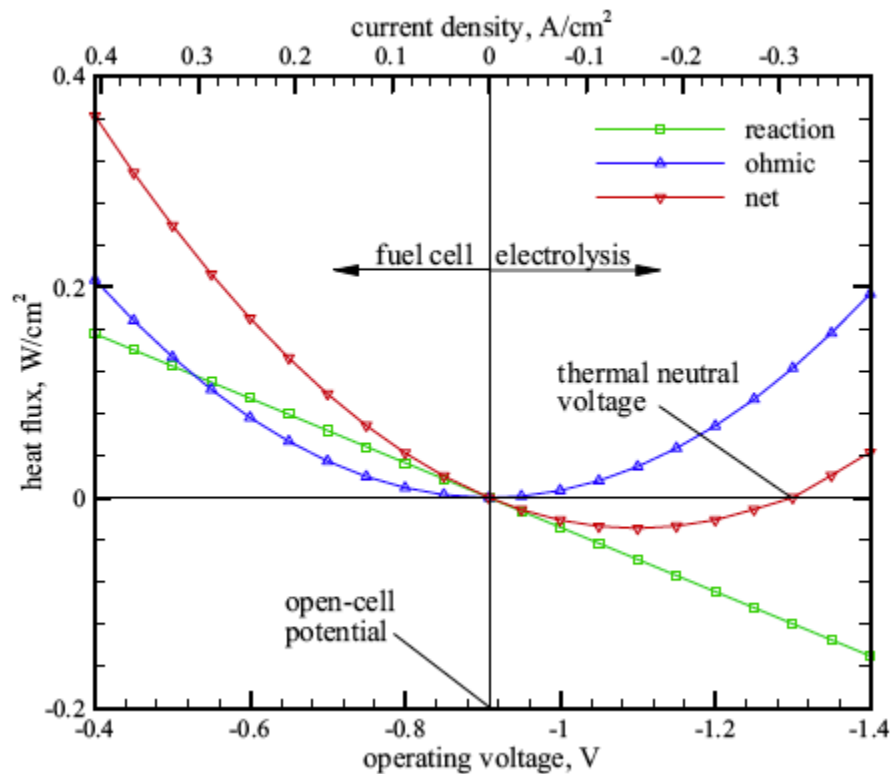
Figure C-2 - Thermal Contributions in Electrolyzer and Fuel Cell Modes

In electrolysis mode, the net heat flux is zero for "thermal neutral voltage (TNV)", which can be predicted from the following equation:

$$\dot{Q} - \dot{W} = \Delta \dot{N}_{H_2} \Delta H_R \qquad \text{(C-1)}$$

Where, from Faraday's Law:

$$\Delta \dot{N}_{H_2} = I / 2F \qquad \text{(C-2)}$$

To solve equation (C-1) for TNV, assume no heat transfer and work equal to electrical power. Hence,

$$\dot{Q} = 0 \qquad \text{(C-3)}$$

$$\dot{W} = IV_{tn} \qquad \text{(C-4)}$$

$$V_{tn} = \Delta H_R / 2F \qquad \text{(C-5)}$$

Using the ideal gas law approximation, ΔH_R, the enthalpy of reaction, is a function of temperature, TNV is also a function of temperature and independent of cell area specific resistance (ASR) and gas compositions. Operation at or near TNV simplifies thermal management of the cell stack since no significant excess gas flow is required and component thermal stresses are minimized.

The magnitude of heat transfer required to maintain isothermal operation is,

$$\dot{Q}_T(T) = \Delta \dot{N}_{H2} \Delta H_R(T) - IV_{op} \qquad \text{(C-6)}$$

Using equations (C-2) and (C-5) above,

$$\dot{Q}_T(T) = I(V_{tn} - V_{op}) \qquad \text{(C-7)}$$

Where,

$$V_{op} = \overline{V}_N + i \times ASR \qquad \text{(C-8)}$$

$$\overline{V}_N = \frac{1}{2F(T_P - T_R)(y_{o,O2,A} - y_{i,O2,A})(y_{o,H2,C} - y_{i,H2,C})} \times \qquad \text{(C-9)}$$

$$\int_{T_R}^{T_P} \int_{y_{i,O2,A}}^{y_{o,O2,A}} \int_{y_{i,H2,C}}^{y_{o,H2,C}} \Delta G_R(T) + R_u T \ln\left(\frac{1 - y_{H2} - y_{N2}}{y_{H2} y_{O2}^{1/2}}\right) dy_{H2} dy_{O2} dT$$

For non-isothermal cases, the following conservation equations are used to describe the energy balance across the electrolyzer:

$$\dot{Q} - \dot{W} = \sum_{P} \dot{N}_i [\Delta H^o_{f_i} + H_i(T_P) - H^o_i] -$$

(C-10)

$$\sum_{R} \dot{N}_i [\Delta H^o_{f_i} + H_i(T_R) - H^o_i]$$

$$\dot{W} = -V_{op}I$$

(C-11)

Thus, the difference between thermal and electrolyzer power is equal to the difference between the product and reactant mass flow rates and enthalpies for all process streams (including the sweep gas). Since enthalpy is a function of temperature, determining the outlet temperature (T_p) is an iterative process requiring a numerical algorithm.

To solve the system of equations, the cathode side inlet flow rates and molar fractions of steam and hydrogen are specified, along with the anode side sweep gases. The current density and active cell area are also specified, yielding total operating current. The corresponding hydrogen production rate is obtained from Faraday's law. Once the per-cell hydrogen production rate is known, the outlet flow rates of hydrogen and steam on the cathode side and oxygen on the anode side can be determined. Once the flow rates are known, a value of product temperature, T_p, is assumed, thereby allowing a summation of all the terms in equation (C-10).

Thermodynamics of HTCE

The following discussing regarding HTCE model development is paraphrased from references [3, 4]. HTCE is a more complicated process because it also includes a chemical equilibrium model to account for RWGS reaction kinetics. As with HTSE, analyzing the HTCE system begins with analyzing the processes within the CV:
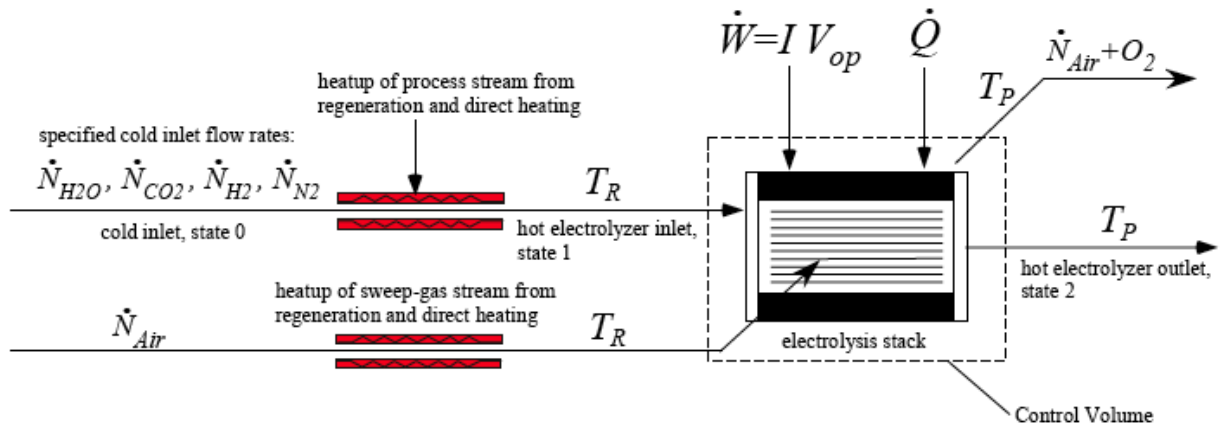
Figure C-3 - HTCE CV

While H_2 generation occurs from HTSE, CO production occurs from the RWGS reaction as shown:

$$CO_2 + H_2 <=> H_2O + CO \tag{C-12}$$

The overall shift reaction that occurs during heatup from the cold unmixed inlet condition to the hot mixed pre-electrolyzer state is represented as:

$$y_{0,CO}\,CO + y_{0,CO2}\,CO_2 + y_{0,H2}\,H_2 + y_{0,H2O}\,H_2O \rightarrow y_{1,CO}\,CO + y_{1,CO2}\,CO_2 + y_{1,H2}\,H_2 + y_{1,H2O}\,H_2O \tag{C-13}$$
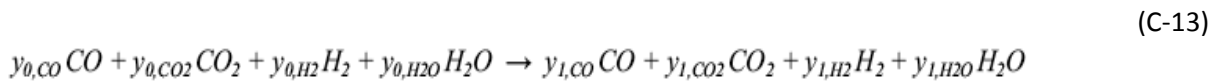
The $y_{0,j}$ values represent the cold inlet mole fraction values of CO, CO_2, H_2, and H_2O, which are specified in the inlet composition molar flow rates. The equilibrium mole fractions of the four species at electrolyzer temperature, prior to electrolysis, are represented by $y_{1,j}$ values. The three governing chemical balance equations for carbon, hydrogen, and oxygen corresponding to equation (C-13) are:

$$y_{0,CO} + y_{0,CO2} = y_{1,CO} + y_{1,CO2} \tag{C-14}$$

$$2y_{0,H2} + 2y_{0,H2O} = 2y_{1,H2} + 2y_{1,H2O} \tag{C-15}$$

$$y_{0,CO} + 2y_{0,CO2} + y_{0,H2O} = y_{1,CO} + 2y_{1,CO2} + y_{1,H2O} \tag{C-16}$$

The final equation invokes the equilibrium constant for the shift reaction, which completes a system of equations, thereby providing hot inlet gas composition[35] [5]:

$$K_{eq}(T) = \frac{y_{1,CO2} y_{1,H2}}{y_{1,CO} y_{1,H2O}}$$

(C-17)

To determine the outlet gas composition, equation (C-16) must be modified to account for oxygen removal from the CO_2/steam mixture:

$$y_{1,CO} + 2y_{1,CO2} + y_{1,H2O} = y_{2,CO} + 2y_{2,CO2} + y_{2,H2O} + \Delta n_O$$

(C-18)

Where Δn_0 is the rate of monatomic oxygen removal by the CO_2/steam mixture given by:

$$\Delta n_O = \frac{I_e}{2F\dot{N}_{Tot}}$$

(C-19)

$$I_e = i \cdot A_{cell} \cdot N_{cells}$$

(C-20)

Using equations (C-18), (C-19), and (C-20), another complete set of equations is available to solve the post electrolyzer equilibrium concentration. However, after the electrolysis, the reaction continues until an empirically derived temperature of about 700 °C (973K). The post electrolyzer molar fractions are then input into equations (C-14), (C-15), (C-16), and (C-17) and the final molar concentrations are determined for a value to T=979 K.

As with HTSE, the energy conservation for HTCE is

$$\dot{Q} - \dot{W} = \sum_P \dot{N}_i [\Delta H_{f_i}^o + H_i(T_P) - H_i^o] - \sum_R \dot{N}_i [\Delta H_{f_i}^o + H_i(T_R) - H_i^o]$$

(C-21)

The rate of heat transfer is specified (zero for adiabatic), and the temperature-dependent enthalpy values of all species are obtained from curve fits or a database such as NIST. The cathode-side hot electrolyzer inlet molar composition and flow rates of steam, hydrogen, CO_2, CO and any other inert gases are determined from specification of the cold inlet flow rates of all components and solution of

---

[35] K_{eq} is an empirically derived value and was provided by INL per request. Its value is:
$K_{eq}(T) = \exp(A/T + B*\ln(T) + CT + DT^2 + E)$, where $A = 4.92194 \times 10^3$, $B = -7.78386 \times 10^{-1}$, $C = 2.5559 \times 10^{-3}$, $D = -5.0983 \times 10^{-7}$, $E = -1.24911$, and T is in Kelvin.

equations (C-14), (C-15), (C-16), and (C-17) above. The inlet side flow rate of the anode side sweep gas must also be specified. Thus, the second summation on the right hand side of equation (C-21) can be evaluated. The current density, cell area, and number of cells are specified, yielding total ionic current. However, care must be taken to ensure that specified inlet gas flow rates and total ionic current are compatible. Thus, the minimum inlet steam and CO_2 molar flow rates must satisfy the following constraint to avoid oxygen starvation[36]:

$$\dot{N}_{H_2O} + \dot{N}_{CO_2} \geq \frac{I_e}{2F}$$

(C-22)

The solution for the system of equations for power output now follows the same iterative process used for the HTSE model above (equations (C-8), (C-9), (C-11)).

---

[36] Oxygen starvation will create deposits of carbon soot on the cells, damaging them.

HTSE Model MATLAB Code

Developed by reference [6].

```
% Main function for High Temperature Steam Electrolysis
calculations
%
% Tin        : Electrolyzer inlet temperature (K)
% Tout_guess : guess for outlet temperature (K)
% ASR        : Area Specific Resistance (A.cm2)
% i          : current density (A/cm2) per cell
% P          : Pressure (MPa)
% The cell has an area of 225cm2
%
% Ntot_St    : total molar flow rate (including any inert gas
flows) per
%              cell on the CO2/steam side (mol/s)
% Ntot_airIn : total molar flow rate (including any inert gas
flows) per
%              cell on the air sweep (mol/s)
%
% Molar fractions:
% yH refers to H2
% yHO refers to H2O
% yN refers to N2
% yO refers to the molar fraction of O2 on the air sweep side
% 1 refers to pre-eletrolysis, equilibrium values (calculated
before)
% 2 refers to post-eletrolysis, equilibrium values at T2

function
HTSE_OneCell(Tin,Tout_guess,ASR,i,P,Ntot_St,Ntot_airIn,yH1,yHO1,y
O1,yN1)

AreaOfCell = 225; % cm2
F=96485.3399; % Faraday constant (C/mol)

if (Ntot_St*(yHO1))<(2*i*AreaOfCell/(4*F))
    disp(' ');
    disp('Oxygen starvation. Please increase oxygen atoms in
input streams or reduce current density');
    return
end

if (yH1+yHO1+yN1)~=1
    disp(' ');
    resp = input('Sum of the molar fractions non equal to 1. Lets
normalize? (yes type 1) ');
    if resp== 1
        ntot=yH1+yHO1;
        yH1=yH1/ntot;
        yHO1=yHO1/ntot;
```

```matlab
        yN1=yN1/ntot;
        disp(' ');
    else return
    end
end


Res1=PostElecMolFrac(i,Ntot_St,yH1,yHO1);
yH2=Res1(1);
yHO2=Res1(2);



Res2=convi(Tin,Tout_guess,ASR,i,P,Ntot_St,Ntot_airIn,yH1,yHO1,yO1
,yN1);

Vop=Res2(1);
Tout=Res2(2);

DeltaNO = i*AreaOfCell/(4*F);
Ntot_airOut = Ntot_airIn + DeltaNO;
yO2 = (yO1 + DeltaNO/Ntot_airIn)/(1+DeltaNO/Ntot_airIn);

disp(' ');
disp('--RESULTS--');
disp(' ');
disp(' ');
disp(['Electrolyzer inlet temperature: ', num2str(Tin), ' K']);
disp(['Electrolyzer outlet temperature: ', num2str(Tout), ' K']);
disp(' ');
disp(['Cell operating voltage : ', num2str(Vop) , ' V']);
disp(['Cell current density : ', num2str(i) , ' A/cm2']);
disp(['Area of cell : ', num2str(AreaOfCell) , ' cm2']);
disp(['Cell power requirement : ', num2str(Vop*225*i) , ' W']);
disp(' ');
disp( 'H2/Steam stream');
disp( '  Electrolyzer inlet');
disp(['    Molar flow rate at the inlet: ', num2str(Ntot_St), '
mol/s']);
disp( '    Molar fraction at the inlet for ');
disp(['      H2: ', num2str(yH1)]);
disp(['      H2O: ', num2str(yHO1)]);
disp(['      N2: ', num2str(yN1)]);
disp( '  Electrolyzer outlet');
disp(['    Molar flow rate at the outlet: ', num2str(Ntot_St), '
mol/s']);
disp( '    Molar fraction at the outlet for ');
disp(['      H2: ', num2str(yH2)]);
disp(['      H2O: ', num2str(yHO2)]);
disp(['      N2: ', num2str(yN1)]);
disp(' ');
disp( 'Air stream');
disp( '  Electrolyzer inlet');
disp(['    Molar flow rate at the inlet: ', num2str(Ntot_airIn),
' mol/s']);
disp( '    Molar fraction at the outlet for ');
```

```matlab
disp(['      O2: ', num2str(yO1)]);
disp(['      N2: ', num2str(1-yO1)]);
disp( '  Electrolyzer outlet');
disp(['    Molar flow rate at the outlet: ',
num2str(Ntot_airOut), ' mol/s']);
disp( '    Molar fraction at the outlet for ');
disp(['      O2: ', num2str(yO2)]);
disp(['      N2: ', num2str(1-yO2)]);


% V_nernst integrated over the cell
% for T (Kelvin) and P (MPa)
% y mole fraction of H2, O2, H2O
% Result in volts

function V=V_nernst_Int(Tin,Tout,P, yH1, yH2 , yO1, yO2, yHO1,
yHO2)

% be careful of the units!

F=96485.3399; % Faraday constant (C/mol)
R= 8.314472; % Gas Constant (J/(K.mol))
L=0.15;

deltaX=0.001;

% yO depends on the inlet mass flow rate

X=0:deltaX:L;
yH=yH1+(yH2-yH1)*X/L;
yO=yO1+(yO2-yO1)*X/L;
yHO=yHO1-(yHO2-yHO1)*X/L;
T=Tin+(Tout-Tin)*X/L;

V=0;

for k=1:length(X)
   V= V+deltaX*(V_nernst(T(k),P,yH(k),yO(k),yHO(k)));
end

V=V/L;


% V_op
% for T (Kelvin) and i (A/cm2)
% Tin and Tout inlet and outlet temperature of the electrolyzer
% Result in volts
% ASR is the Area Specific Value of the cell (A.cm2)
% P pressure in MPa
% Ntot_St is the total molar flow rate (including any inert gas
flows) per
% cell on the CO2/steam side (mol/s)
%
% yH refers to H2
```

```matlab
% yHO refers to H2O
% yO refers to the molar fraction of O2 on the air sweep side
% 1 refers to pre-eletrolysis values at Tin
% 2 refers to post-eletrolysis values at Tout
%
% Ntot_airIn is the total molar flow rate (including any inert
gas flows) per
% cell on the air sweep side (mol/sec)

function V=V_op_Eq(Tin,Tout,ASR, i,P, Ntot_St, Ntot_airIn, yH1,
yHO1 , yO1)

AreaOfCell = 225; % cm2
F=96485.3399; % Faraday constant (C/mol)

DeltaNO = i*AreaOfCell/(4*F);
yO2 = (yO1 + DeltaNO/Ntot_airIn)/(1+DeltaNO/Ntot_airIn);

Res= PostElecMolFrac(i,Ntot_St,yH1, yHO1);

yH2=Res(1);
yHO2=Res(2);


V = V_op(Tin,Tout,ASR, i,P,  yH1, yH2 , yO1, yO2, yHO1, yHO2);


% V_op
% for T (Kelvin) and i (A/cm2)
% Tin and Tout inlet and outlet temperature of the electrolyzer
% Result in volts
% ASR is the Area Specific Value of the cell (A.cm2)
% P pressure in MPa

function V=V_op(Tin,Tout,ASR, i,P, yH1, yH2 , yO1, yO2, yHO1,
yHO2)

L=0.15; % cm

Vasr=0;
deltaX=0.001;

X=0:deltaX:0.15;
T=Tin+(Tout-Tin)*X/L;

for k=1:length(X)
   Vasr= Vasr+deltaX*(ASR - 0.463 + 3.973*(10^(-
5))*exp(10300/T(k)));
end
Vasr=Vasr/L;

V= V_nernst_Int(Tin,Tout,P, yH1, yH2 , yO1, yO2, yHO1, yHO2) +
i*Vasr;
```

```matlab
% Standard entropy of formation H2O(g)
% at T (Kelvins) and 1 bar
% in J/(mol.K)
% from NIST WebBook

function S=Sf_H2O(T)

if (T>=500)&&(T<=1700)

    a=30.09200;
    b=6.832514;
    c=6.793435;
    d=-2.534480;
    e=0.082139;
    f=-250.8810;
    g=223.3967;
    h=-241.8264;

end

if (T>1700)&&(T<=6000)

    a=41.96426;
    b=8.622053;
    c=-1.499780;
    d=0.098119;
    e=-11.15764;
    f=-272.1797;
    g=219.7809;
    h=-241.8264;

end


t=T/1000;
S= a*log(t) + b*t +c*(t^2)/2 + d*(t^3)/3 - e/(2*t^2) + g;


% Standard entropy of formation H2(g)
% at T (Kelvins) and 1 bar
% in J/(mol.K)
% from NIST WebBook

function S=Sf_H(T)

if (T>=298)&&(T<=1100)

    a=33.066178;
    b=-11.363417;
    c=11.432816;
    d=-2.772874;
    e=-0.158558;
    f=-9.980797;
    g=172.707974;
```

```matlab
    h=0;

end

if (T>1100)&&(T<=2500)

    a=18.563083;
    b=12.257357;
    c=-2.859786;
    d=0.268238;
    e=1.977990;
    f=-1.147438;
    g=156.288133;
    h=0;

end

t=T/1000;


% Standard enthalpy of formation N2(g)
% at T (Kelvins) and 1 bar
% in kJ/mol
% from NIST WebBook

function H=Hf_N(T)

if (T>=100)&&(T<=500)

    a=28.98641;
    b=1.853978;
    c=-9.647459;
    d=16.63537;
    e=0.000117;
    f=-8.671914;
    g=226.4168;
    h=0;

end

if (T>500)&&(T<=2000)

    a=19.50583;
    b=19.88705;
    c=-8.598535;
    d=1.369784;
    e=0.527601;
    f=-4.935202;
    g=212.3900;
    h=0;

end

t=T/1000;
```

```matlab
H= a*t + 0.5*b*t^2 +c*(t^3)/3 + d*(t^4)/4 - e/t + f -h;


% Standard enthalpy of formation H2(g)
% at T (Kelvins) and 1 bar
% in kJ/mol
% from NIST WebBook

function H=Hf_H(T)

if ((T>=298)&&(T<=1100))

    a=33.066178;
    b=-11.363417;
    c=11.432816;
    d=-2.772874;
    e=-0.158558;
    f=-9.980797;
    g=172.707974;
    h=0;

end

if (T>1100)&&(T<2500)

    a=18.563083;
    b=12.257357;
    c=-2.859786;
    d=0.268238;
    e=1.977990;
    f=-1.147438;
    g=156.288133;
    h=0;

end

t=T/1000;
H= a*t + 0.5*b*t^2 +c*(t^3)/3 + d*(t^4)/4 - e/t + f -h;


function [hg]=h_O(T)
  %oxygen gas enthalpy [kJ/kg] at T [kelvin] and 7 MPa


Tk=[200,250,300,350,400,450,500,550,600,650,700,750,800,850,900,9
50,1000];
  %saturation temperature in kelvin


h=[141,203,256,307,357,407,457,507,558,609,661,714,767,820,874,92
8,983];
 %vapor saturation enthalpy in kJ/kg

 % figure;
```

```
 % plot(Tk,h);

if T<=1000
hg=interp1(Tk,h,T);
 else
    hg=928+(983-928)*(T-950)/(1000-950);
 end


function [hg]=h_HO(T)
  %water steam enthalpy [kJ/kg] at T [kelvin] and 7 MPa


Tk=[273,323,373,423,473,500,550,558.98,559,573,623,673,723,773,82
3,873,923,973,1023,1073,1123,1173,1223,1240,1260];
  %saturation temperature in kelvin


h=[7,215,424,636,855,976,1220,1268,2773,2840,3017,3159,3288,3411,
3532,3651,3769,3888,4007,4129,4250,4373,4497,4539,4589];
 %vapor saturation enthalpy in kJ/kg

 %figure;
  %plot(Tk,h);

 if T<1200
hg=interp1(Tk,h,T);
 else
    hg=4539+(4589-4539)*(T-1240)/(1260-1240);
 end


% Standard Gibbs free energy of formation H2O(g)=>H2(g)+0.5*O2(g)
% at T (Kelvins) and 1 bar
% in kJ/mol
% from NIST WebBook

function G=DeltaR0_G(T)

G = 1*(Hf_H(T) - T*Sf_H(T)/1000)...
    + 0.5*(Hf_O(T) - T*Sf_O(T)/1000)...
    - 1*(Hf_H2O(T) - T*Sf_H2O(T)/1000);


% gives the operating voltage and the outlet temperature for one
cell
%
% Tin inlet temperature (K)
% guess: guess for outlet temperature (K)
% i current density (A/cm2) ; requires 4 significant digits!!
%
% Ntot_St is the total molar flow rate (including any inert gas
flows) per
% cell on the CO2/steam side in mol/s
```

```matlab
% Ntot_airIn is the total molar flow rate (including any inert
gas flows) per
% cell on the air sweep side in mol/s
%
% yH refers to H2
% yHO refers to H2O
% yN refers to N2
% yO refers to the molar fraction of O2 on the air sweep side
% 1 refers to pre-eletrolysis, equilibrium values (calculated
before)
% 2 refers to post-eletrolysis, equilibrium values at T2

function
Res=convi(Tin,guess,ASR,i,P,Ntot_St,Ntot_airIn,yH1,yHO1,yO1,yN1)

AreaOfCell = 225; % cm2
F=96485.3399; % Faraday constant (C/mol)

I=i*AreaOfCell;
W=V_op_Eq(Tin,guess,ASR, i,P, Ntot_St, Ntot_airIn, yH1, yHO1 ,
yO1)*I;
% elecrical power supplied in watt per cell

H=H_prodI(Tin,guess, i, Ntot_St, Ntot_airIn, yH1, yHO1 , yO1,
yN1);
% in J/sec

h=0.5; % temperature step in K

delta=(H-W)/H;

% convergence criteria 1%
while delta^2>0.005^2
    delta1=V_op_Eq(Tin,guess+h,ASR, i,P, Ntot_St, Ntot_airIn,
yH1, yHO1 , yO1)*I-...
        H_prodI(Tin,guess+h, i, Ntot_St, Ntot_airIn, yH1, yHO1 ,
yO1, yN1);
    delta2=V_op_Eq(Tin,guess-h ,ASR, i,P, Ntot_St, Ntot_airIn,
yH1, yHO1 , yO1)*I-...
        H_prodI(Tin,guess-h, i, Ntot_St, Ntot_airIn, yH1, yHO1 ,
yO1, yN1);
    if delta1^2<delta2^2
        delta=delta1/H_prodI(Tin,guess+h, i, Ntot_St, Ntot_airIn,
yH1, yHO1 , yO1, yN1);
        guess=guess+h;
    else
        delta=delta2/H_prodI(Tin,guess-h, i, Ntot_St, Ntot_airIn,
yH1, yHO1 , yO1, yN1);
        guess=guess-h;
    end

end

end
```

```matlab
V=V_op_Eq(Tin,guess,ASR, i,P, Ntot_St, Ntot_airIn, yH1, yHO1 ,
yO1);

Tout=guess;

Res=[V,Tout]; % T oulet (K) and Operating Voltage
```

HTCE MATLAB Model

Developed by reference [7].

```matlab
% Main function for coelectrolysis calculations
%
% Tin        : Electrolyzer inlet temperature (K)
% Tout_guess : guess for outlet temperature (K)
% Tfroz      : temperature at which the reverse-gas-shift
reaction
%              equilibirum is frozen while cooling down the
outlet stream
% ASR        : Area Specific Resistance (A.cm2)
% i          : current density (A/cm2) per cell
% P          : Pressure (MPa)
% The cell has an area of 225cm2
%
% Ntot_St    : total molar flow rate (including any inert gas
flows) per
%              cell on the CO2/steam side (mol/s)
% Ntot_airIn : total molar flow rate (including any inert gas
flows) per
%              cell on the air sweep (mol/s)
%
% Initial molar fractions at cold temperature:
% a0        : CO carbon monoxide
% b0        : CO2 carbone dioxide
% c0        : H2 hydrogen
% d0        : H2O water steam
% e0        : N2 nitrogen

function Coelectrolysis_OneCell(Tin,Tout_guess, Tfroz
,ASR,i,P,Ntot_St,Ntot_airIn,a0,b0,c0,d0,e0)

%user_entry = input('Isothermal conditions? (y/n)')

AreaOfCell = 225; % cm2
F=96485.3399; % Faraday constant (C/mol)

if (Ntot_St*(d0+2*b0))<(2*i*AreaOfCell/(4*F))
    disp(' ');
    disp('Oxygen starvation. Please increase oxygen atoms in
input streams or reduce current density');
    return
end

if (a0+b0+c0+d0+e0)~=1
    disp(' ');
    resp = input('Sum of the molar fractions non equal to 1. Lets
normalize? (yes type 1) ');
    if resp== 1
        ntot=a0+b0+c0+d0+e0;
```

```matlab
        a0 = a0/ntot;
        b0 = b0/ntot;
        c0 = c0/ntot;
        d0 = d0/ntot;
        e0 = e0/ntot;
        disp(' ');
    else return
    end
end

yO1 = 0.21;

Res1=PreElecMolFrac(Tin, a0, b0, c0, d0);
a1=Res1(1);
b1=Res1(2);
c1=Res1(3);
d1=Res1(4);

Res2=convi(Tin,Tout_guess,ASR,i,P,Ntot_St,Ntot_airIn,a1,b1,c1,d1,
yO1,e0);

Vop=Res2(1);
Tout=Res2(2);

Res3=PostElecMolFrac(i,Ntot_St, Tout, a1, b1, c1, d1);
a2=Res3(1);
b2=Res3(2);
c2=Res3(3);
d2=Res3(4);

DeltaNO = i*AreaOfCell/(4*F);
Ntot_airOut = Ntot_airIn + DeltaNO;
yO2 = (yO1 + DeltaNO/Ntot_airIn)/(1+DeltaNO/Ntot_airIn);

Res4=PostFrozElecMolFrac(Tfroz, a2, b2, c2, d2);
a3=Res4(1);
b3=Res4(2);
c3=Res4(3);
d3=Res4(4);

disp(' ');
disp('--RESULTS--');
disp(' ');
disp(' ');
disp(['Electrolyzer inlet temperature: ', num2str(Tin), ' K']);
disp(['Electrolyzer outlet temperature: ', num2str(Tout), ' K']);
disp(' ');
disp(['Cell operating voltage : ', num2str(Vop) , ' V']);
disp(['Cell power requirement : ', num2str(Vop*225*i) , ' W']);
disp(' ');
disp( 'CO2/Steam stream');
disp( '  Electrolyzer inlet');
disp(['    Molar flow rate at the inlet: ', num2str(Ntot_St), '
mol/s']);
```

```matlab
disp( '     Molar fraction at the inlet for ');
disp(['       CO: ', num2str(a1)]);
disp(['      CO2: ', num2str(b1)]);
disp(['       H2: ', num2str(c1)]);
disp(['      H2O: ', num2str(d1)]);
disp(['       N2: ', num2str(e0)]);
disp( '  Electrolyzer outlet');
disp(['    Molar flow rate at the outlet: ', num2str(Ntot_St), '
mol/s']);
disp( '     Molar fraction at the outlet for ');
disp(['       CO: ', num2str(a2)]);
disp(['      CO2: ', num2str(b2)]);
disp(['       H2: ', num2str(c2)]);
disp(['      H2O: ', num2str(d2)]);
disp(['       N2: ', num2str(e0)]);
disp( '  After cooling down');
disp(['    Freeze temperature chosen: ', num2str(Tfroz), ' K']);
disp(['    Molar flow rate: ', num2str(Ntot_St), ' mol/s']);
disp( '    Molar fraction for ');
disp(['       CO: ', num2str(a3)]);
disp(['      CO2: ', num2str(b3)]);
disp(['       H2: ', num2str(c3)]);
disp(['      H2O: ', num2str(d3)]);
disp(['       N2: ', num2str(e0)]);
disp(' ');
disp( 'Air stream');
disp( '  Electrolyzer inlet');
disp(['    Molar flow rate at the inlet: ', num2str(Ntot_airIn),
' mol/s']);
disp( '     Molar fraction at the outlet for ');
disp(['       O2: ', num2str(yO1)]);
disp(['       N2: ', num2str(1-yO1)]);
disp( '  Electrolyzer outlet');
disp(['    Molar flow rate at the outlet: ',
num2str(Ntot_airOut), ' mol/s']);
disp( '     Molar fraction at the outlet for ');
disp(['       O2: ', num2str(yO2)]);
disp(['       N2: ', num2str(1-yO2)]);


% gives the operating voltage and the outlet temperature for one
cell
%
% Tin inlet temperature (K)
% guess: guess for outlet temperature (K)
% i current density (A/cm2) ; requires 4 significant digits!!
%
% Ntot_St is the total molar flow rate (including any inert gas
flows) per
% cell on the CO2/steam side in mol/s
% Ntot_airIn is the total molar flow rate (including any inert
gas flows) per
% cell on the air sweep side in mol/s
%
```

```matlab
% a refers to CO
% b refers to CO2
% c refers to H2
% d refers to H2O
% e refers to N2
% yO refers to the molar fraction of O2 on the air sweep side
% 1 refers to pre-eletrolysis, equilibrium values (calculated
before)
% 2 refers to post-eletrolysis, equilibrium values at T2

function
Res=convi(Tin,guess,ASR,i,P,Ntot_St,Ntot_airIn,a1,b1,c1,d1,yO1,e0
)

AreaOfCell = 225; % cm2
F=96485.3399; % Faraday constant (C/mol)

I=i*AreaOfCell;
W=V_op_Eq(Tin,guess,ASR,i,P,Ntot_St,Ntot_airIn,a1,b1,c1,d1,yO1)*I
;
% elecrical power supplied in watt per cell

H=H_prodI(Tin,guess, i, Ntot_St, Ntot_airIn,  a1, b1 , c1 , d1 ,
yO1,e0);
% in J/sec

h=0.5; % temperature step in K

delta=(H-W)/H;

% convergence criteria 1%
while delta^2>0.01^2

delta1=V_op_Eq(Tin,guess+h,ASR,i,P,Ntot_St,Ntot_airIn,a1,b1,c1,d1
,yO1)*I-...
        H_prodI(Tin,guess+h, i, Ntot_St, Ntot_airIn,  a1, b1 , c1
, d1 , yO1,e0);
    delta2=V_op_Eq(Tin,guess-
h,ASR,i,P,Ntot_St,Ntot_airIn,a1,b1,c1,d1,yO1)*I-...
        H_prodI(Tin,guess-h, i, Ntot_St, Ntot_airIn,  a1, b1 , c1
, d1 , yO1,e0);
    if delta1^2<delta2^2
        delta=delta1/H_prodI(Tin,guess+h, i, Ntot_St, Ntot_airIn,
a1, b1 , c1 , d1 , yO1,e0);
        guess=guess+h;
    else
        delta=delta2/H_prodI(Tin,guess-h, i, Ntot_St, Ntot_airIn,
a1, b1 , c1 , d1 , yO1,e0);
        guess=guess-h;
    end

end

V=V_op_Eq(Tin,guess,ASR,i,P,Ntot_St,Ntot_airIn,a1,b1,c1,d1,yO1);
```

```matlab
%W=V_op(Tin,guess,i)*I;
%H=H_prod_react(Tin, guess);
Tout=guess;

Res=[V,Tout]; % T oulet (K) and Operating Voltage



% Standard Gibbs free energy of formation H2O(g)=>H2(g)+0.5*O2(g)
% at T (Kelvins) and 1 bar
% in kJ/mol
% from NIST WebBook

function G=DeltaR0_G(T)

G = 1*(Hf_H(T) - T*Sf_H(T)/1000)...
    + 0.5*(Hf_O(T) - T*Sf_O(T)/1000)...
    - 1*(Hf_H2O(T) - T*Sf_H2O(T)/1000);



% Gives the change in enthalpy carried by the species along the
cell
%
% in J/sec
% T in kelvin
% Beware the units!!
%
% Ntot_St is the total molar flow rate (including any inert gas
flows) per
% cell on the CO2/steam side in mol/s
% Ntot_airIn is the total molar flow rate (including any inert
gas flows) per
% cell on the air sweep side in mol/s
%
% a refers to CO
% b refers to CO2
% c refers to H2
% d refers to H2O
% yO refers to the molar fraction of O2 on the air sweep side
% 1 refers to pre-eletrolysis, equilibrium values (calculated
before)
% 2 refers to post-eletrolysis, equilibrium values at T2

function En=H_prodI(Tin,Tout, i, Ntot_St, Ntot_airIn,  a1, b1 ,
c1 , d1 , yO1,e0)

AreaOfCell = 225; % cm2
F=96485.3399; % Faraday constant (C/mol)

DeltaNO = i*AreaOfCell/(4*F);
yO2 = (yO1 + DeltaNO/Ntot_airIn)/(1+DeltaNO/Ntot_airIn);

Res= PostElecMolFrac(i,Ntot_St, Tout, a1, b1, c1, d1);
a2=Res(1);
b2=Res(2);
```

```matlab
c2=Res(3);
d2=Res(4);

% The total molar flow rate is not modified in the CO2/steam side
% For the air sweep side:
Ntot_airOut = Ntot_airIn + DeltaNO;


% Hf free enthalpy of formation at T(K) , in kJ/mol
En= Ntot_St*( c2*Hf_H(Tout) + d2*Hf_H2O(Tout) + ...
      a2*Hf_CO(Tout) + b2*Hf_CO2(Tout) +e0*Hf_N(Tout))+...
    -Ntot_St*( c1*Hf_H(Tin) + d1*Hf_H2O(Tin) + ...
      a1*Hf_CO(Tin) + b1*Hf_CO2(Tin) +e0*Hf_N(Tin))+...
    -Ntot_airIn*( yO1*(Hf_O(Tin)) + (1-yO1)*Hf_N(Tin) )+...
    Ntot_airOut*( yO2*(Hf_O(Tout)) + (1-yO2)*(Hf_N(Tout)));

En=En*1000; % to get the result in J/sec


% Standard enthalpy of formation CO(g)
% at T (Kelvins) and 1 bar
% in kJ/mol
% from NIST WebBook

function H=Hf_CO(T)

if (T>=298)&&(T<=1300)

    a=25.56759;
    b=6.096130;
    c=4.054656;
    d=-2.671301;
    e=0.131021;
    f=-118.0089;
    g=227.3665;
    h=-110.5271;

end

if (T>1300)&&(T<=6000)

    a=35.15070;
    b=1.300095;
    c=-.205921;
    d=0.013550;
    e=-3.282780;
    f=-127.8375;
    G=231.7120;
    H=-110.5271;

end

t=T/1000;
H= a*t + 0.5*b*t^2 +c*(t^3)/3 + d*(t^4)/4 - e/t + f -h;
```

```matlab
H = H +h; % not equal to 0 at 298K !!


% Standard enthalpy of formation CO2 (g)
% at T (Kelvins) and 1 bar
% in kJ/mol
% from NIST WebBook

function H=Hf_CO2(T)

if (T>=298)&&(T<=1200)

    a=24.99735;
    b=55.18696;
    c=-33.69137;
    d=7.948387;
    e=-0.136638;
    f=-403.6075;
    g=228.2431;
    h=-393.5224;

end

if (T>1200)&&(T<=6000)

    a=58.16639;
    b=2.720074;
    c=-.492289;
    d=0.038844;
    e=-6.447293;
    f=-425.9186;
    G=263.6125;
    H=-393.5224;

end

t=T/1000;
H= a*t + 0.5*b*t^2 +c*(t^3)/3 + d*(t^4)/4 - e/t + f -h;

H = H +h; % not equal to 0 at 298K !!


% Standard enthalpy of formation H2(g)
% at T (Kelvins) and 1 bar
% in kJ/mol
% from NIST WebBook

function H=Hf_H(T)

if ((T>=298)&&(T<=1100))

    a=33.066178;
    b=-11.363417;
```

```matlab
    c=11.432816;
    d=-2.772874;
    e=-0.158558;
    f=-9.980797;
    g=172.707974;
    h=0;

end

if (T>1100)&&(T<2500)

    a=18.563083;
    b=12.257357;
    c=-2.859786;
    d=0.268238;
    e=1.977990;
    f=-1.147438;
    g=156.288133;
    h=0;

end

t=T/1000;
H= a*t + 0.5*b*t^2 +c*(t^3)/3 + d*(t^4)/4 - e/t + f -h;


% Standard enthalpy of formation H2O(g)
% at T (Kelvins) and 1 bar
% in kJ/mol
% from NIST WebBook

function H=Hf_H2O(T)

if (T>=500)&&(T<=1700)

    a=30.09200;
    b=6.832514;
    c=6.793435;
    d=-2.534480;
    e=0.082139;
    f=-250.8810;
    g=223.3967;
    h=-241.8264;

end

if (T>1700)&&(T<=6000)

    a=41.96426;
    b=8.622053;
    c=-1.499780;
    d=0.098119;
    e=-11.15764;
    f=-272.1797;
```

```matlab
    G=219.7809;
    H=-241.8264;

end

t=T/1000;
H= a*t + 0.5*b*t^2 +c*(t^3)/3 + d*(t^4)/4 - e/t + f;


% Standard enthalpy of formation N2(g)
% at T (Kelvins) and 1 bar
% in kJ/mol
% from NIST WebBook

function H=Hf_N(T)

if (T>=100)&&(T<=500)

    a=28.98641;
    b=1.853978;
    c=-9.647459;
    d=16.63537;
    e=0.000117;
    f=-8.671914;
    g=226.4168;
    h=0;

end

if (T>500)&&(T<=2000)

    a=19.50583;
    b=19.88705;
    c=-8.598535;
    d=1.369784;
    e=0.527601;
    f=-4.935202;
    g=212.3900;
    h=0;

end

t=T/1000;
H= a*t + 0.5*b*t^2 +c*(t^3)/3 + d*(t^4)/4 - e/t + f -h;


% Standard enthalpy of formation O2(g)
% at T (Kelvins) and 1 bar
% in kJ/mol
% from NIST WebBook

function H=Hf_O(T)

if (T>=100)&&(T<=700)
```

```matlab
    a=31.32234;
    b=-20.23531;
    c=57.86644;
    d=-36.50624;
    e=-0.007374;
    f=-8.903471;
    g=246.7945;
    h=0;

end

if (T>700)&&(T<=2000)

    a=30.03235;
    b=8.772972;
    c=-3.9881133;
    d=0.788313;
    e=-0.741599;
    f=-11.32468;
    g=236.1663;
    h=0;

end

t=T/1000;
H= a*t + 0.5*b*t^2 +c*(t^3)/3 + d*(t^4)/4 - e/t + f -h;


% equilibrium constant for the gas shift reaction
% CO + H2O -> H2 + CO2
%
% T in Kelvin
function k=k(T)

a=4.92194*1000;
b=-7.78386*0.1;
c=2.5559*0.001;
d=-5.0983*0.0000001;
e=-1.24911;

k=exp(a/T + b*log(T) + c*T + d*T^2 + e);


% Equilibrium mole fractions of the four species prior to
electrolysis
%
% a refers to CO
% b refers to CO2
% c refers to H2
% d refers to H2O
% 0 refers to initial values (cold)
% 1 refers to pre-eletrolysis, equilibrium values at T
% T is the electrolyzer inlet temperature in Kelvin
```

```matlab
function Res = PreElecMolFrac(T, a0, b0, c0, d0)

SecondHalf = [ a0 + b0  ;
    2*c0 + 2*d0 ;
    a0 + 2*b0 + d0 ;
    k(T) ];

Res = fsolve(@(x)set1(x) - SecondHalf, [a0; b0; c0; d0],
optimset('Display','off'));

% a1=Res(1);
% b1=Res(2);
% c1=Res(3);
% d1=Res(4);


% Equilibrium mole fractions of the four species after the
electrolysis
%
% i is the current density (A/cm2)
% a refers to CO
% b refers to CO2
% c refers to H2
% d refers to H2O
% 1 refers to pre-eletrolysis, equilibrium values (calculated
before)
% 2 refers to post-eletrolysis, equilibrium values at T2
% T is the electrolyzer inlet temperature in Kelvin
% Ntot is the total molar flow rate (including any inert gas
flows) per
% cell on the CO2/steam side in mol/s


function Res = PostElecMolFrac(i,Ntot, T2, a1, b1, c1, d1)

AreaOfCell = 225; % cm2
F=96485.3399; % Faraday constant (C/mol)

DeltaNO = i*AreaOfCell/(4*F*Ntot); % moles of O2 produced by
electrolysis

SecondHalf = [ a1 + b1  ;
    2*c1 + 2*d1 ;
    a1 + 2*b1 + d1 - 2*DeltaNO;
    k(T2) ];

Res = fsolve(@(x)set1(x) - SecondHalf, [a1; b1; c1;
d1],optimset('Display','off'));

% a2=Res(1);
% b2=Res(2);
% c2=Res(3);
% d2=Res(4);
```

```matlab
% Equilibrium mole fractions of the four species after the
electrolysis
% and after beeing cooled down to the frozen temperature
%
% a refers to CO
% b refers to CO2
% c refers to H2
% d refers to H2O
% 2 refers to post-eletrolysis, equilibrium values at Tout
% 3 refers to post-electrolysis, equilibrium values at Tfroz
% Tfroz is the temperature below which the equilibrium don't
change anymore
%  - is frozen (Kelvin)

function Res = PostFrozElecMolFrac(Tfroz, a2, b2, c2, d2)

SecondHalf = [ a2 + b2  ;
    2*c2 + 2*d2 ;
    a2 + 2*b2 + d2 ;
    k(Tfroz) ];

Res = fsolve(@(x)set1(x) - SecondHalf, [a2; b2; c2; d2],
optimset('Display','off'));

% a3=Res(1);
% b3=Res(2);
% c3=Res(3);
% d3=Res(4);


% Set of equations to be solved in "PreElecMolFrac"

function s = set1(x)

s = [ x(1) + x(2)   ;
    2*x(3) + 2*x(4) ;
    x(1) + 2*x(2) + x(4) ;
    x(2)*x(3)/(x(1)*x(4)) ];


% Standard entropy of formation CO(g)
% at T (Kelvins) and 1 bar
% in J/(mol.K)
% from NIST WebBook

function S=Sf_CO(T)

if (T>=298)&&(T<=1300)

    a=25.56759;
    b=6.096130;
    c=4.054656;
```

```
    d=-2.671301;
    e=0.131021;
    f=-118.0089;
    g=227.3665;
    h=-110.5271;

end

if (T>1300)&&(T<=6000)

    a=35.15070;
    b=1.300095;
    c=-.205921;
    d=0.013550;
    e=-3.282780;
    f=-127.8375;
    G=231.7120;
    H=-110.5271;

end

t=T/1000;
S= a*log(t) + b*t +c*(t^2)/2 + d*(t^3)/3 - e/(2*t^2) + g;


% Standard entropy of formation CO2 (g)
% at T (Kelvins) and 1 bar
% in J/(mol.K)
% from NIST WebBook

function S=Sf_CO2(T)

if (T>=298)&&(T<=1200)

    a=24.99735;
    b=55.18696;
    c=-33.69137;
    d=7.948387;
    e=-0.136638;
    f=-403.6075;
    g=228.2431;
    h=-393.5224;

end

if (T>1200)&&(T<=6000)

    a=58.16639;
    b=2.720074;
    c=-.492289;
    d=0.038844;
    e=-6.447293;
    f=-425.9186;
    G=263.6125;
```

```matlab
    H=-393.5224;

end

t=T/1000;
S= a*log(t) + b*t +c*(t^2)/2 + d*(t^3)/3 - e/(2*t^2) + g;


% Standard entropy of formation H2(g)
% at T (Kelvins) and 1 bar
% in J/(mol.K)
% from NIST WebBook

function S=Sf_H(T)

if (T>=298)&&(T<=1100)

    a=33.066178;
    b=-11.363417;
    c=11.432816;
    d=-2.772874;
    e=-0.158558;
    f=-9.980797;
    g=172.707974;
    h=0;

end

if (T>1100)&&(T<=2500)

    a=18.563083;
    b=12.257357;
    c=-2.859786;
    d=0.268238;
    e=1.977990;
    f=-1.147438;
    g=156.288133;
    h=0;

end

t=T/1000;
S= a*log(t) + b*t +c*(t^2)/2 + d*(t^3)/3 - e/(2*t^2) + g;


% Standard entropy of formation H2O(g)
% at T (Kelvins) and 1 bar
% in J/(mol.K)
% from NIST WebBook

function S=Sf_H2O(T)

if (T>=500)&&(T<=1700)
```

```matlab
    a=30.09200;
    b=6.832514;
    c=6.793435;
    d=-2.534480;
    e=0.082139;
    f=-250.8810;
    g=223.3967;
    h=-241.8264;

end

if (T>1700)&&(T<=6000)

    a=41.96426;
    b=8.622053;
    c=-1.499780;
    d=0.098119;
    e=-11.15764;
    f=-272.1797;
    g=219.7809;
    h=-241.8264;

end


t=T/1000;
S= a*log(t) + b*t +c*(t^2)/2 + d*(t^3)/3 - e/(2*t^2) + g;


% Standard entropy of formation O2(g)
% at T (Kelvins) and 1 bar
% in J/(mol.K)
% from NIST WebBook

function S=Sf_O(T)

if (T>=100)&&(T<=700)

    a=31.32234;
    b=-20.23531;
    c=57.86644;
    d=-36.50624;
    e=-0.007374;
    f=-8.903471;
    g=246.7945;
    h=0;

end

if (T>700)&&(T<=2000)

    a=30.03235;
    b=8.772972;
    c=-3.9881133;
```

```matlab
    d=0.788313;
    e=-0.741599;
    f=-11.32468;
    g=236.1663;
    h=0;

end

t=T/1000;
S= a*log(t) + b*t +c*(t^2)/2 + d*(t^3)/3 - e/(2*t^2) + g;


% V_nernst integrated over the cell
% for T (Kelvin) and P (MPa)
% y mole fraction of H2, O2, H2O
% Result in volts

function V=V_nernst_Int(Tin,Tout,P, yH1, yH2 , yO1, yO2, yHO1,
yHO2)

% be careful of the units!

F=96485.3399; % Faraday constant (C/mol)
R= 8.314472; % Gas Constant (J/(K.mol))
L=0.15;

deltaX=0.001;

% yO depends on the inlet mass flow rate

X=0:deltaX:L;
yH=yH1+(yH2-yH1)*X/L;
yO=yO1+(yO2-yO1)*X/L;
yHO=yHO1-(yHO2-yHO1)*X/L;
T=Tin+(Tout-Tin)*X/L;

V=0;

for k=1:length(X)
   V= V+deltaX*(V_nernst(T(k),P,yH(k),yO(k),yHO(k)));
end

V=V/L;


% Nernst Potential
% for T (Kelvin) and P (MPa)
% y mole fraction of H2, O2, H2O
% Result in volts
%
% For Syngas production, although theoritically we have two
electrolysis
% reactions (steam-hydrogen and CO2-CO), we can use either one
Nernst
```

```matlab
% equation or the other. Provided the equilibirum composition of
the
% components is used in evaluating the equation.

function V=V_nernst(T,P,yH,yO,yHO)

F=96485.3399; % Faraday constant (C/mol)
R= 8.314472; % Gas Constant (J/(K.mol))

V= (1000*DeltaR0_G(T)-R*T*log(
(yHO/(yH*sqrt(yO)*sqrt(P/0.1))))))/(2*F);


% V_op
% for T (Kelvin) and i (A/cm2)
% Tin and Tout inlet and outlet temperature of the electrolyzer
% Result in volts
% ASR is the Area Specific Value of the cell (A.cm2)
% P pressure in MPa
% Ntot_St is the total molar flow rate (including any inert gas
flows) per
% cell on the CO2/steam side
%
% a refers to CO
% b refers to CO2
% c refers to H2
% d refers to H2O
% yO refers to the molar fraction of O2 on the air sweep side
% 1 refers to pre-eletrolysis, equilibrium values (calculated
before)
% 2 refers to post-eletrolysis, equilibrium values at T2
%
% Ntot_airIn is the total molar flow rate (including any inert
gas flows) per
% cell on the air sweep side

function V=V_op_Eq(Tin,Tout,ASR, i,P, Ntot_St, Ntot_airIn,  a1,
b1 , c1 , d1 , yO1)

AreaOfCell = 225; % cm2
F=96485.3399; % Faraday constant (C/mol)

DeltaNO = i*AreaOfCell/(4*F);

yO2 = (yO1 + DeltaNO/Ntot_airIn)/(1+DeltaNO/Ntot_airIn);

Res= PostElecMolFrac(i,Ntot_St, Tout, a1, b1, c1, d1);

c2=Res(3);
d2=Res(4);


V = V_op(Tin,Tout,ASR, i,P, c1, c2 , yO1, yO2, d1, d2);
```

```matlab
% V_op
% for T (Kelvin) and i (A/cm2)
% Tin and Tout inlet and outlet temperature of the electrolyzer
% Result in volts
% ASR is the Area Specific Value of the cell (A.cm2)
% P pressure in MPa

function V=V_op(Tin,Tout,ASR, i,P, yH1, yH2 , yO1, yO2, yHO1,
yHO2)

L=0.15; % cm

Vasr=0;
deltaX=0.001;

X=0:deltaX:0.15;
T=Tin+(Tout-Tin)*X/L;

for k=1:length(X)
    Vasr= Vasr+deltaX*(ASR - 0.463 + 3.973*(10^(-
5))*exp(10300/T(k)));
end
Vasr=Vasr/L;

V= V_nernst_Int(Tin,Tout,P, yH1, yH2 , yO1, yO2, yHO1, yHO2) +
i*Vasr;
```

Appendix C References

[1] O'Brien, J., 2008, "Thermodynamic Considerations for Thermal Water Splitting Processes and High Temperature Electrolysis," Idaho National Laboratory, INL/CON-08-14376, Idaho Falls, ID.

[2] Stoots, C., O'Brien, J., McKellar, M., 2005, "Engineering Process Model For High-Temperature Electrolysis: System Performance Evaluation," Idaho National Laboratory, INL/CON-05-00725, Idaho Falls, ID.

[3] M. G. McKellar, M., O'Brien, J., Stoots, C., 2007, "Process Model for the Production of Syngas Via High Temperature Co-Electrolysis," Idaho National Laboratory, INL/CON-07-12818, Idaho Falls, ID.

[4] O'Brien, J., McKellar, M., Stoots, C., 2007, "Parametric Study of Large-Scale Production of Syngas via High Temperature Co-Electrolysis," AIChE Annual Meeting, R. Green, ed. Idaho National Laboratory, Idaho Falls, ID, pp. 1-20.

[5] Stoots, C., 2010, "Correlation for the Reverse Gas Shift Reaction (RWGS) Equilibrium Constant as a Function of Gas Temperature, Keq(T)," **Email to author of empirically derived equilibrium constant used to solve coelectrolysis model (7/20/2010)**pp. 1-1.

[6] Haratyk, G., 2010, "1-D MATLAB High Temperature Steam Electrolysis Model," **Original**.

[7] Haratyk, G., 2010, "Computer Program of 1-D MATLAB Coelectrolysis Model (Unpublished)," **Rev 1**.

Appendix D - Supporting Calculations for Liquid Fuels Production

This appendix contains the calculations performed for the chapter 3. The first section pertains to the fuel demand and refinery requirements, and following sections analyze liquid fuels production via alkaline electrolysis, high temperature electrolysis, and methanol synthesis.

D - Fuel, Feed, and Refining Requirements*

Fuel Consumption

Deployed CSG JP-5 Consumption (BBL/Day)

Avg Wartime (FY 03)	Avg Peacetime (FY 09)
3,214	2,005

*Not all of the calculations may perfectly sum to 100% due to rounding.

Deployed, Underway CSG F-76 Consumption (BBL/Day)

Platform	# in CSG	Consumption	Total
CG	2	714	1,428
DDG	3	583	1,749

Assumed JP-5 Density (kg/L)	0.8

	BBL/Day	GPD	LPD	kg/day	kg/hr	kg/s
Total Peacetime	5,200	218,400	827,736	662,189	27,591	7.66
Total Wartime	6,400	268,800	1,018,752	815,002	33,958	9.43

D - Fuel, Feed, and Refining Requirements*

Synfuel Production Via LTFT

Assumed A-S-F α value	0.85
LTFT Inlet Temperature (K)	523
LTFT Pressure (MPa)	3.0

LTFT Inlet

	kg/day	kg/hr	kg/s	mol/s	liter/s (STP)
Syngas Feed Rate	2,964,264	123,511	34.31	1,072	24,016
H2 Feed Rate	**370,533**	**15,439**	**4.29**	**2,144.29**	**48,032**
CO Feed Rate	**2,593,731**	**108,072**	**30.02**	**1,072**	**24,016**

LTFT Outlet

	kg/day	kg/hr	kg/s	mol/s	Dist. Temp
C2 and C1 HCs	126,311	5,263	1.46	71.5	422
C3 HCs	63,246	2,635	0.73	17.43	380
C4-C8 HCs	377,390	15,725	4.37	54.9	280
C9+ HCs	729,918	30,413	8.45	42.8	240
H2O (waste by-product)	1,667,399	69,475	19.30	1072	
			34.31		

LTFT Thermal Output

Exothermic Output (kJ/mol)	-165
Number of moles reacting	1,072
Ouput Power (MWth)	**-177**

Fractionalization Process

Assumed Pressure (MPa):	0.1				
Hydrocarbon Fraction	Initial Destination	flow rate (kg/s)	Enthalpy_o (kJ/kg)	Final Temp (K)	Enthalpy_f (kJ/kg)
C2 and C1 HCs	Autothermal Reformer	1.46	1287.42	240	649.825
C3 HCs	Alkylation	0.73	1117	280	600
C4-C8 HCs	Oligomerization	4.37	745	380	410.3
C9+ HCs	Hydrocracking	8.45	464.3	423	-69.654
H2O (waste by-product)	ATR, waste	19.3	2974.2	310	154.45

Total Power Rejected (MWth)	**-61.7**

D - Fuel, Feed, and Refining Requirements*

LTFT Refining

Process Stream Description	Feed	From	To	kg/hr	kg/s
a1 - Hydrocracker H2 Feed	H2	H2	a	454	0.13
a2 - Hydrocracker waste H2O	waste H2O	a	waste	54	0.02
b1 - Oligomerization waste H2O	waste H2O	b	waste	245	0.07
c1 - Hydrotreater H2 feed	H2	H2	c	89	0.02
d1 - Aromatization fuel gas	Fuel Gas	d	ATR	1,275	0.35
e1 - Alkylation waste	Waste HC	e	ATR	122	0.03
1 - C9+ Hydrocracker feed	LTFT C9+ product	LTFT	a	30,413	8.45
2a - C3-C8 from Hydrocracker	C3-C8	a	d	13,432	3.73
2b - Hydrocracker kero product	Kerosene	a	tank	18,340	5.09
3a - C3 feed to Alkylation unit	LTFT C3 product	LTFT	e	2,635	0.73
3b -C4-C8 feed to Oligomerizaiton	LTFT C4-C8 product	LTFT	b	15,725	4.37
4ai - Oligomerization LPG product	LPG	b	ATR	1,154	0.32
4aii - Oligom. naphtha product	Naphtha	b	ATR	5,471	1.52
4b - Oligom. ASA Kero product	ASA kerosene	b	c	5,958	1.66
4c - Oligom. ASA C16+ product	ASA C16+	b	c	2,896	0.80
5b - Hydrotreater kero product	Kerosene	c	tank	6,021	1.67
5c - Hydrotreater C16+ product	C16+	c	a	2,922	0.81
6a - Aromatizer H2 by product	H2	d	H2	203	0.06
6bi - Aromatizer Bz product	Bz rich	d	e	4,242	1.18
6bii - Aromatizer Tol/Xyl product	Tol/Xyl rich	d	ATR	4,170	1.16
6biii - Aromatizer kero product	Kerosene	d	tank	3,541	0.98
7ai - Alkylation LPG product	LPG	e	ATR	597	0.17
7aii - Alkylation naphtha product	Naphtha	e	ATR	1,885	0.52
7b - Alkylation kerosene product	Kerosene	e	tank	6,056	1.68

			Process	Catalyst	Press (MPa)	Temp (K)
Total JP-5 (kerosene) (kg/s):	9.43		Hydrocrack	Pt-SiO2/Al2O3	5	423
Req'd H2 for Refining (kg/s):	0.095		Oligom.	H-ZSM-5	5	423
HCs sent to ATR (kg/s):	4.08		Hydrotreat	Ni/SiO2	5	423
			Aromatization	Zn/H-ZSM-5	5	623
			Alkylation	H-ZSM-22	5	423

D - Fuel, Feed, and Refining Requirements*

CO2 Production via Air Capture

Energy Requirement of Air Capture System (kJ/mol CO2)	30
Projected Production Capacity of Air Capture System (MT CO2/day)	1
Estimated Unit Volume of Modular Air Capture System (m^3)	90
CO2 Discharge Temperature (K)	318
CO2 Discharge Pressure (MPa)	0.116325
Estimated CO2 to CO Conversion Ratio	1
Required CO Production Rate, w/ ATR recycle (mol/s)	677

	(mol/s)	(kg/s)	(MT/day)
Required CO2 Production Rate	677	29.8	2572

	w/ Recycle via ATR
Required Number of Air Capture Units	**2,573**
Power Consumption (MWe)	**20.3**
Required Volume Onboard Ship (m^3)	**231,570**

D - Fuel, Feed, and Refining Requirements*

Seawater Desalination

	GPD	LPD	kg/s	mol/s
Projected Deionized Water Production Capacity of EUWP Gen2 RO Unit	250,000	947,500	11.0	609.2
Anticipated H2O Feed Demand			4.29	2,275
H2/H2O Molar Ratio	1			
Unit Power Consumption (kWe)	325			
Unit Volume Consumption (m^3)	85.5			
Minumum Number of EUWP Gen2 RO Units	4			
Maximum Power Consumption (MWe)	1.30			
Space Consumption (m^3)	342			
	GPD	LPD	kg/s	mol/s
Maximum DI Water Production Capacity	1,000,000	3,790,000	43.9	2,437

Autothermal Reforming (ATR) Approximation

ATR EQN:

$$C_m H_n + \tfrac{1}{2}m H_2O + \tfrac{1}{4}m O_2 = mCO + (\tfrac{1}{2}m + \tfrac{1}{2}n)H_2$$
$$\Delta H = \text{hydrocarbon dependent, thermally neutral}$$
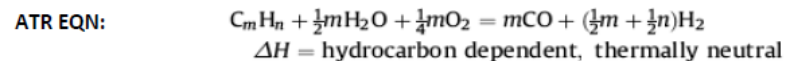
ATR Temperature (K)	973
ATR Pressure (MPa)	0.3

	ATR Inlet						
	kg/day	kg/hr	kg/s	mol/s	liters/s (STP)	Assumed C #	Assumed H#
LTFT C1 HCs	46,782	1,949	0.54	38.7		1	2
LTFT C2 HCs	79,529	3,314	0.92	32.9		2	4
Aromatization fuel gas	30,608	1,275	0.35	8.43		3	6
Alkylation HC waste	2,937	122	0.03	2.43		1	2
Oligomerization LPG	27,704	1,154	0.32	7.63		3	6
Oligomerization naphtha	131,298	5,471	1.52	21.7		5	10
Aromatizer Tol/Xyl	100,079	4,170	1.16	82.7		1	2
Alkylation LPG	14,332	597	0.17	3.95		3	6
Alkylation naphtha	45,234	1,885	0.52	7.48		5	10
Required H2O Feed	307,608	12,817	3.56	197.8			
Required O2 Feed	273,429	11,393	3.16	98.9	2,215		

	ATR Outlet				
	kg/day	kg/hr	kg/s	mol/s	liter/s (STP)
Estimated CO Product	957,003	39,875	11.08	396	8,861
Estimated H2 Product	102,536	4,272	1.19	593	13,292

273

Synfuel Refining Process

Compressor Efficiency: 0.9

Process step	Alkylation		Oligomerization	Hydrotreating	Hydrocracking	Heat Rejection				
Feed	LTFT C3 HCs	Bz Rich	LTFT C4-C8	H2	H2	Kero	kero	kero	Naphtha	Tol/Xyl
Flow Rate (kg/s)	0.73	1.18	4.37	0.02	0.13	5.09	0.98	3.35	2.04	1.16
Initial Temp (K)	280	623	380	423	623	623	623	423	423	748
Enthalpy_o (kJ/kg)	219.67	1183.76	99.942	neg	neg	742	1171.53	-76.6	502.26	1098
Final Temp (K)	423	423	423	neg	neg	300	300	300	300	300
Enthalpy_f (kJ/kg)	788.73	142.76	217.12	neg	neg	-367	-367	-367	-98.5	-155
P_1 (Mpa)	0.1	0.1	0.1	0.101325	0.101325					
P_2 (Mpa)	5	5	5	5	5					
r_p	50			49.3	49.3					
$c_{p\ (kJ/kg\text{-}K)}$	2.05			14.52	14.571					
$c_{v\ (kJ/kg\text{-}K)}$	1.51			10.38	10.446					
γ	1.36			1.40	1.39					
K	0.27			0.29	0.28					
Power (MWe)	**0.85**	**neg (liquid)**	**neg (liquid)**	**0.34**	**2.57**	**neg**	**neg**	**neg**	**neg**	**neg**
Power (MWth)	**0.42**	**-1.23**	**0.51**	**neg**	**neg**	**-5.04**	**-0.97**	**-2.65**	**-1.07**	**-1.05**

Process step	Hydrocracking		Aromatization	ATR					
Feed	LTFT C9+	Hyd Trt C16+	C3-C8	Arom. LPG	Alk HC Waste	Olg. LPG	Alk LPG	LTFT C1	LTFT C2
Flow Rate (kg/s)	8.45	0.80	3.73	0.35	0.03	0.32	0.17	0.54	0.92
Initial Temp (K)	423	423	423	623	423	423	423	240	240
Enthalpy_o (kJ/kg)	-63.552	-75	964	1897.39	1210	788.73	788.73	neg	neg
Final Temp (K)	623	623	623	280	240	280	280	240	240
Enthalpy_f (kJ/kg)	556.41	550	1479	219.67	783	219.67	219.67	neg	neg
P_1 (Mpa)				0.1	0.1	0.1	0.1	0.1	0.1
P_2 (Mpa)				0.3	0.3	0.3	0.3	0.3	0.3
r_p				3	3	3	3	3	3
$c_{p\ (kJ/kg\text{-}K)}$				1.64	2.14	1.64	1.64	2.14	1.58
$c_{v\ (kJ/kg\text{-}K)}$				1.42	1.61	1.42	1.42	1.61	1.27
γ				1.15	1.33	1.15	1.15	1.33	1.24
K				0.13	0.25	0.13	0.13	0.25	0.20
Power (MWe)	**neg**	**neg**	**neg**	**0.03**	**0.01**	**0.03**	**0.01**	**0.10**	**0.09**
Power (MWth)	**5.24**	**0.50**	**1.92**	**-0.59**	**-0.01**	**-0.18**	**-0.09**	**0**	**0**

Overall Refinery Power Requirements	
Compression Power (MWe)	**4.85**
Heat input (MWth)	**8.59**
Heat rejected (MWth)	**-12.89**

Additional Heater Power for PWR Option (MWe)

Hydrocracking	Hydrotreating	Aromoatizing	Total
1.70	0.16	0.62	**2.49**
3.62	0.35	1.33	(MWth)

PWR Heat Input (MWth)	6.22

274

D - Synfuel via Alkaline Electrolysis, RWGS, and LTFT with Recycle via Autothermal Reforming

Alkaline Electrolysis

Overall Electrolysis Reaction: $H_2O \rightarrow \frac{1}{2} O_2 + H_2$

	kg/hr	kg/s	mol/s	liter/s (STP)
H2 Production Required for LTFT	15,439	4.29	2,144	48,032
H2 Production Required for RWGS	4,871	1.35	677	15,155
H2 Production Required For Refining	340	0.09	47	
H2 Produced From ATR	4,272	1.19	593	
Total Required Steady State H2 Production via Electrolysis	**16,378**	**4.55**	**2,275**	**50,954**
Total Required DI H2O Feed	147,404	40.9	2,275	
Total Amount of O2 Produced	131,026	36.4	1,137	25,477
O2 for Disposal (Less ATR Recycle)	119,633	33.2	1,038	23,262

Performance Characteristics of Hydrotech 5040 Alkaline Water Electrolyzer

Number of Cells	230
Assumed Operating Pressure (MPa)	0.101325
Assumed Operating Temperature (K)	373
Max H2 Production/cell (Nm^3 H2/hr-cell)	2.11
Cell Power Consumption (kWhr/Nm^3 H2-cell)	4.3
Max H2 Production (Nm^3 H2/hr)	485.3
Max Power/Electrolyzer (MWe)	2.09
Nm^3 H2/mol H2	0.0224

Required Power for H2 Production (MWe)	**789**
Number of Electrolyzers Required	**378**

D - Synfuel via Alkaline Electrolysis, RWGS, and LTFT with Recycle via Autothermal Reforming

RWGS (S-CO2)

# Stages for 100% Conversion	5		CO2:CO Conversion Ratio		1.0
Catalyst	Cu/Alumina		H2O Product Pressure		0.118325
RWGS Temperature (K)	740		H20 Temp (Sat Liq) (K)		377
RWGS Pressure (MPa)	1.0		Cp H2 (kJ/kg-K)		14.53
			Cp CO2 (kJ/kg-K)		1.056

	kg/day	kg/hr	kg/s	mol/s	liter/s (STP)
Required CO2 Feed	2,572,001	107,167	29.8	677	15,155
Required H2 Feed	116,909	4,871	1.35	677	15,155
CO Product	1,636,728	68,197	18.9	677	15,155
H2O Product	1,052,182	43,841	12.2	677	15,155

Required Thermal Input to Sustain Reaction		Required Thermal Input to Heat Feed to RWGS Operating Temp	
Endothermic Input (kJ/mol)	38.9		
Power Input (MWth)	**26.3**	**CO2/H2 RWGS Heat Requirement (MWth)**	**20.5**

Mixing of Recycle Gases (S-CO2)

Gas Mixer prior to FT MCR

H2 Process Streams	Flow rate (kg/s)	Temp (K)	Enthalpy (kJ/kg)
Elect to Mixer (in)	3.20	373	5,014.70
ATR to Mixer (in)	1.19	613	8,499.20
Mixer to FT MCRs (out)	4.38	523	7,190.50
CO Process Steams			
RWGS to Mixer (in)	18.94	740	907.97
ATR to Mixer (in)	11.08	613	773.47
Mixer to FT MCRs (out)	30.02	523	678.16
Mixing Pressure (MPa)	1.00		
Thermal Power in (MWth)	51.88		
Thermal Power out (MWth)	51.88		
Difference	0%		

Required ATR CO/H2 Heat Rejection (MWth)	**-10.2**

D - Synfuel via Alkaline Electrolysis, RWGS, and LTFT with Recycle via Autothermal Reforming

ATR Heating (S-CO2)

ATR H2O Feed Heating from S-CO2

Assumed Min ΔT (K)	15
H2O Flow Rate (kg/s)	3.56
Cpf H2O (kJ/kg-K)	4.2686
Initial H2O Temp (K)	310.00
Cp S-CO2 (kJ/kg-K)	1.25
S-CO2 Initial Temp (K)	943.00
Tsat @ 0.3 MPa (K)	406.67
Cp(g) (kJ/kg-K)	2.263
H(fg) (kJ/kg)	2,163.5
Final Steam Temp (K)	928.0
Power Required (MWth)	**13.4**

O2 Heating / HC Heating

	O2 Heating		HC Heating	
mass flow rate (kg/s)	3.16	mass flow rate (kg/s)	4.08
Pressure (MPa)	0.3	Pressure (MPa)	0.3
Avg Cp (kJ/kg-K)	1.00	Avg Cp (kJ/kg-K)	3.12
Initial Temp (K)	373	Initial Temp (K)	310
Final Temp (K)	928.0	Final Temp (K)	928
Power (MWth)	**1.76**	**Power (MWth)**	**7.86**

ATR RHX

ΔT (K)	5.00

Process Stream	Flow Rate (kg/s)	Inlet Temp (K)	Inlet Enthalpy (kJ/kg)	Outlet Temp (K)	Outlet Enthalpy (kJ/kg)
H2 (ATR out)	1.19	973	13,792	964	13,658
CO (ATR out)	11.08	973	1,154	964	1,145
H2O (ATR in)	3.56	928	3,826	959	3,896
Power in (MWth)	0.26				
Power out (MWth)	0.25				
Difference	-6%				

Heater Power Necessary to Heatup to 973 K

	Inlet Temp (K)	Enthalpy_in (kJ/kg)	Outlet Temp (K)	nthalpy_out (kJ/kg)
Steam	959	3896.1	973	3927.9
HC	928.00	-	973	-
O2	928	872.68	973	872.68
Power In (MWth)	0.143	**Power In (MWe)**	**0.150**	

D - Synfuel via Alkaline Electrolysis, RWGS, and LTFT with Recycle via Autothermal Reforming

Compression Energy

Compressor Efficiency   0.9

Processes	CO2 (RWGS)	H2 (Mix & RWGS)	H2 (ATR-Mix)	CO (ATR-Mix)	H2 (Mix-FT)	CO (Mix-FT)	O2 (ATR)
$\dot{m}$ (kg/s)	29.77	4.45	1.19	11.08	4.38	30.02	3.16
T_1 (K)	318	373	613	613	523	523	373
P_1 (Mpa)	0.116	0.101	0.3	0.3	1.00	1.00	0.101325
P_2 (Mpa)	1.0	1.0	1.0	1.0	3.0	3.0	0.3
r_p	8.60	9.87	3.33	3.33	3.00	3.00	2.96
c_p (kJ/kg-K)	0.90	14.47	14.54	1.10	14.54	1.10	0.94
c_v (kJ/kg-K)	0.69	10.34	10.41	0.805	10.41	0.805	0.67
γ	1.31	1.40	1.40	1.37	1.40	1.37	1.39
K	0.24	0.29	0.28	0.27	0.28	0.27	0.28
Power (MWe)	6.23	24.6	4.79	3.16	13.6	6.57	0.43

D - Synfuel via Alkaline Electrolysis, RWGS, and LTFT with Recycle via Autothermal Reforming

Overall Alkaline Electrolysis Energy Requirements

Power Input (MWth) (S-CO2)	
RWGS Endothermic Heat Input	26.3
RWGS RXN/Feed Heating	20.5
ATR Feed Heating	23.0
HC Refining Heating	8.59
Total (MWth)	**78.4**

Electric Power (MWe) (S-CO2)	
CO2 Capture & Desalination	21.6
Alkaline Electrolysis	789
Compression (non refining)	59.4
Compression (refining)	4.85
ATR Heaters	0.15
Total (MWe)	**875**

Power Output (MWth) (S-CO2)	
ATR Heat Rejection	-10.2
LTFT Heat Rejection	-177
Fractionalization Process	-61.7
Refining Heat Rejection	-12.9
Total (MWth)	**-262**

Recuperated Power (MWth) (S-CO2)	
ATR Feed Heating	0.25
Total (MWth)	**0.25**

Power Input (MWth) (PWR)	
RWGS RXN/Feed Heating	7.7
ATR Feed Heating	6.9
HC Refining Heating	6.22
Total (MWth)	**20.9**
% Change from S-CO2 Case	-73.4%

Electric Power (MWe) (PWR)	
CO2 Capture & Desalination	21.6
Alkaline Electrolysis	789
Compression (non refining)	59.4
Compression (refining)	4.85
RWGS Electric Heaters	40.6
ATR Electric Heaters	4.61
Refining Electric Heaters	2.49
Total (MWe)	**922**
% Change from S-CO2 Case	5.44%

Power Output (MWth) (PWR)	
ATR Heat Rejection	-8.0
LTFT Heat Rejection	-177
Fractionalization Process	-61.7
Refining Heat Rejection	-12.9
Total (MWth)	**-259**
% Change from S-CO2 Case	-1%

Recuperated Power (MWth) (PWR)	
ATR Feed Heating	2.52
Total (MWth)	**2.52**
% Change from S-CO2 Case	913%

D - Synfuel via Alkaline Electrolysis, RWGS, and LTFT with Recycle via Autothermal Reforming

RWGS (PWR)

# Stages for 100% Conversion	5		CO2:CO Conversion Ratio	1.0
Catalyst	Cu/Alumina		H2O Product Pressure	0.118325
RWGS Temperature (K)	740		H20 Temp (Sat Liq) (K)	377
RWGS Pressure (MPa)	1.0		Cp H2 (kJ/kg-K)	14.53
			Cp CO2 (kJ/kg-K)	1.056

	kg/day	kg/hr	kg/s	mol/s	liter/s (STP)
Required CO2 Feed	2,572,001	107,167	29.8	677	15,155
Required H2 Feed	116,909	4,871	1.35	677	15,155
CO Product	1,636,728	68,197	18.9	677	15,155
H2O Product	1,052,182	43,841	12.2	677	15,155

CO2 Heating from Steam

Assumed Min ΔT (K)	15
CO2 Feed Flow Rate (kg/s)	29.77
Cp CO2 Feed (kJ/kg-K)	1.155
Initial CO2 Temp (K)	318
Cp Steam (kJ/kg-K)	5.31
Steam Initial Temp (K)	558
Final CO2 Feed Temp (K)	543
Power (MWth)	**7.7**

Required Thermal Input to Sustain Reaction

Endothermic Input (kJ/mol)	38.9
Power Input (MWth)	**26.3**

Electric Heat to Sustain RWGS

CO2 Feed Flow Rate (kg/s)	29.77
CO2 Feed Temp (K)	543
Enthaply Inlet (kJ/kg)	737.1
RWGS Temp (K)	740
RWGS Enthalpy (kJ/kg)	954.4
Power to RWGS Temp (MWth)	12.2
Power for Reaction (MWth)	26.3
Total Heater Power (MWe)	**40.6**

D - Synfuel via Alkaline Electrolysis, RWGS, and LTFT with Recycle via Autothermal Reforming

Mixing of Recycle Gases (PWR)

Gas Mixer prior to FT MCR

H2 Process Streams	Flow rate (kg/s)	Temp (K)	Enthalpy (kJ/kg)
Elect to Mixer (in)	3.20	373	5,014.70
ATR to Mixer (in)	1.19	613	8,499.20
Mixer to FT MCRs (out)	4.38	523	7,190.50
CO Process Steams			
RWGS to Mixer (in)	18.94	740	907.97
ATR to Mixer (in)	11.08	613	773.47
Mixer to FT MCRs (out)	30.02	523	678.16
Mixing Pressure (MPa)	1.00		
Thermal Power in (MWth)	51.88		
Thermal Power out (MWth)	51.88		
Difference	0%		

Required ATR CO/H2 Heat Rejection (MWth)	**-7.97**

ATR Heating (PWR)

ATR H2O Feed Heating from Steam

Assumed Min ΔT (K)	15
H2O Flow Rate (kg/s)	1.19
Cpf H2O (kJ/kg-K)	4.2686
Initial H2O Temp (K)	310.00
Cp Steam (kJ/kg-K)	5.31
Steam Initial Temp (K)	558.00
Tsat @ 0.3 MPa (K)	406.67
Cp(g) (kJ/kg-K)	2.263
H(fg) (kJ/kg)	2,163.5
Final Steam Temp (K)	543.0
Power Required (MWth)	**3.4**

O2 Heating / HC Heating

	O2 Heating		HC Heating	
mass flow rate (kg/s)		3.16	mass flow rate (kg/s)	4.08
Pressure (MPa)		0.3	Pressure (MPa)	0.3
Avg Cp (kJ/kg-K)		1.00	Avg Cp (kJ/kg-K)	3.12
Initial Temp (K)		373	Initial Temp (K)	310
Final Temp (K)		543	Final Temp (K)	543
Power (MWth)		**0.54**	**Power (MWth)**	**2.96**

ATR RHX

ΔT (K)	5.00				
Process Stream	Flow Rate (kg/s)	Inlet Temp (K)	Inlet Enthalpy (kJ/kg)	Outlet Temp (K)	Outlet Enthalpy (kJ/kg)
H2 (ATR out)	1.19	973	13,792	887	12,513
CO (ATR out)	11.08	973	1,154	887	1,063
H2O (ATR in)	3.56	543	3,008	882	3,724
Power in (MWth)	2.52				
Power out (MWth)	2.55				
Difference	1%				

Heater Power Necessary to Heatup to 973 K

	Inlet Temp (K)	Enthalpy_in (kJ/kg)	Outlet Temp (K)	Enthalpy_out (kJ/kg)
Steam	882	3723.6	973	3927.9
HC	543	-	973	-
O2	543	503.32	973	872.68
Power In (MWth)	4.382	**Power In (MWe)**	**4.61**	

D - Synfuel via HTCE, HTSE, and LTFT with Recycle via Autothermal Reforming

Co-Electrolysis and High Temperature Steam Electrolysis

	kg/hr	kg/s	mol/s	liter/s (STP)
H2 Production Required for LTFT	15,439	4.29	2,144	48,032
H2 Production Required for Refining	340	0.09	47	1,059
H2 Produced from ATR	4,272	1.19	593	13,292
CO Production Required for LTFT	108,072	30.0	1,072	24,016
CO Produced from ATR	39,875	11.1	396	8,861
Total Required H2 Production	**11,507**	**3.20**	**1,598**	**35,800**
Total Required CO Production	**68,197**	**18.94**	**677**	**15,155**
HTCE O2 Generated	117,034	32.51	1,016	22,757
HTCE Steam Required	88,078	24.47	1,359	
Total Amount of CO2 Required	107,651	29.90	680	15,223

Performance Characteristics of SOECs for HTCE

Cell Inlet Temperature (K)	1,073	H2 Outlet Fraction	0.668260	H2 Generated via HTCE (kg/s)	3.0277
Cell Outlet Temperature (K)	1,084	H2O Outlet Fraction	0.001740	HTCE H2O Remaining (kg/s)	0.07
Pressure (MPa)	3.00	CO2 Outlet Fraction	0.0013525	CO Generated (kg/s)	20.8465
Cell Area (cm^2)	225.00	CO Outlet Fraction	0.32865	CO2 Remaining (kg/s)	0.13
ASR (ohm-cm^2)	0.25	Cell Voltage (volts)	1.3614	O2 Generated via HTCE (kg/s)	32.51
i (Amps/cm^2)	1.00	Cell Power (watts)	306.3152	H2/CO wt% to total gas	99.1456%
CO2/Steam Flow Rate (mol/s)	0.0013			Inlet H2/CO Ratio	2.33
H2 Inlet Fraction	0.070			**Outlet H2/CO Ratio**	**2.03**
H2O Inlet Fraction	0.600				
CO2 Inlet Fraction	0.30	# Cells for HTCE	1,742,605	CO for Recycle (kg/s)	1.9029
CO Inlet Fraction	0.03			H2 For Recycle (kg/s)	0.2764
O2 Out Flow Rate (mol/s)	0	**Power (MWe)**	**534**		

D - Synfuel via HTCE, HTSE, and LTFT with Recycle via Autothermal Reforming

Co-Electrolysis and High Temperature Steam Electrolysis (cont)

Performance Characteristics of SOECs for HTSE

Cell Inlet Temperature (K)	1073	H2 Outlet Fraction	0.94691	H2 Demand via HTSE (mol/s)	223
Cell Outlet Temperature (K)	1,106	H2O Outlet Fraction	0.053092	H2 Generated via HTSE (kg/s)	0.4698
Pressure (MPa)	3.0	Cell Voltage (volts)	1.3011	H2 Recyled back to HTSE (kg/s)	0.0248
Cell Area (cm^2)	225	Cell Power (watts)	292.7486		
ASR (ohm-cm^2)	0.25			Non-recycle HTSE H2 (kg/s)	0.45
i (Amps/cm^2)	1.0			Non-recycle HTCE H2 (kg/s)	2.7514
Steam Flow Rate (mol/s)	0.0013			Total Non-recycle H2 (kg/s)	3.1964
H2 Inlet Fraction	0.05	# Cells for HTSE	190,841	Downstream H2 Demand (kg/s)	3.1964
H2O Inlet Fraction	0.95				
O2 Out Flow Rate (mol/s)	0.00058299	**Power (MWe)**	**55.9**	O2 Generated via HTSE (kg/s)	3.56

HTCE & HTSE Process Stream Breakdown

H2 Generated from HTCE (kg/s)	3.03	HTCEin_recycle H2 (kg/s)	0.276	HTCEout_remain H2 (kg/s)	2.75
H2O Remaining From HTCE (kg/s)	0.07	HTCEin_recycle H2O (kg/s)	0.006	HTCEout_remain H2O (kg/s)	0.06
CO Generated From HTCE (kg/s)	20.8	HTCEin_recycle CO (kg/s)	1.903	HTCEout_remain CO (kg/s)	18.94
CO2 Remaining from HTCE (kg/s)	0.13	HTCEin_recycle CO2 (kg/s)	0.012	HTCEout_remain CO2 (kg/s)	0.12
HTCEout,total Syngas Product (kg/s)	**24.1**	**HTCEin_recycle,total (kg/s)**	**2.20**	**HTCEout_remain (kg/s)**	**21.9**
HTCEout H2/CO Molar Fraction	**2.03**			**HTCEout_remain H2 & CO wt%**	**99.1456%**
H2 Generated from HTSE (kg/s)	0.47	HTSEin_recycle H2 (kg/s)	0.025	HTSEout_remain H2 (kg/s)	0.45
H2O Remaining from HTSE (kg/s)	0.24	HTSEin_recycle H2O (kg/s)	0.013	HTSEout_remain H2O (kg/s)	0.24
HTSEout,total Product (kg/s)	0.71				
HTSE H2 Product for Refining (kg/s)	0.09	H2 Membrane H2O Reject (kg/s)	0.24	O2 Generated via HTSE (kg/s)	3.56
HTSE H2 Product for LTFT (kg/s)	0.350	Required HTSE Steam Feed (kg/s)	4.24	O2 Required for ATR (kg/s)	3.16
		DI H2O Feed for HTSE (kg/s)	4.01	Waste HTSE O2 OVBD (kg/s)	0.40
		DI H2O Feed for HTCE (kg/s)	24.5	Waste HTCE O2 OVBD (kg/s)	32.51
		Total DI H2O Feed (kg/s)	28.5	CO2 Feed for HTCE (kg/s)	29.9
				# Air Capture Units	**2,584**
				Power Required (MWe)	**20.4**

D - Synfuel via HTCE, HTSE, and LTFT with Recycle via Autothermal Reforming

Heat Transfer for HTCE Process (S-CO2)

Assumed S-CO2 Temp (K)	943	S-CO2 Cp (kJ/kg-K)	1.25

CO2 Heating from S-CO2		H2O Feed Heating from S-CO2		H2O Feed Heating from HTCEout	
Assumed Min ΔT (K)	15.0	Assumed Min ΔT (K)	15.0	Assumed Min ΔT (K)	10.5
CO2 Feed Flow Rate (kg/s)	29.9	H2O Flow Rate (kg/s)	24.5	H2O Feed Flow Rate (kg/s)	24.5
Cp CO2 Feed (kJ/kg-K)	1.16	Cpf H2O (kJ/kg-K)	4.4164	Cp H2O Feed (kJ/kg-K)	2.33
Initial CO2 Temp (K)	318	Initial H2O Temp (K)	300	Initial H2O Temp (K)	928
Cp S-CO2 (kJ/kg-K)	1.25	Cp S-CO2 (kJ/kg-K)	1.25	HTCEout Flow Rate (kg/s)	21.9
S-CO2 Initial Temp (K)	943	S-CO2 Initial Temp (K)	943	Cp HTCEout (kJ/kg-K)	2.80
Final CO2 Feed Temp (K)	928	Tsat @ 3MPa (K)	507	Intial HTCEout Temp (K)	1,084
Power (MWth)	**21.1**	Cp(g) (kJ/kg-K)	3.421	Final HTCEout Temp (K)	949
		H(fg) (kJ/kg)	1,794.9	Final H2O Feed Temp (K)	1,073
		Final Steam Temp (K)	928	**Recuperated Power (MWth)**	**8.27**
CO2 Heating from HTCE O2		**Power Required (MWth)**	**102**		
Assumed Min ΔT (K)	6.4				
CO2 Feed Flow Rate (kg/s)	29.9				
Cp CO2 Feed (kJ/kg-K)	1.23				
Initial CO2 Temp (K)	928				
HTCE O2 Flow Rate (kg/s)	32.5				
Cp Waste O2 (kJ/kg-K)	1.10				
Intial O2 Temp (K)	1,084				
Final O2 Temp (K)	934				
Final CO2 Feed Temp (K)	1,073				
Recuperated Power (MWth)	**5.33**				

Heat Transfer for HTSE Process (S-CO2)

H2O Feed Heating from S-CO2		H2O Feed Heating from HTSEout		H2O Feed Heating from HTSE O2	
Assumed Min ΔT (K)	15.0	Assumed Min ΔT (K)	5.2	Assumed Min ΔT (K)	2.0
H2O Flow Rate (kg/s)	4.24	H2O Feed Flow Rate (kg/s)	4.24	H2O Feed Flow Rate (kg/s)	4.24
Cpf H2O (kJ/kg-K)	4.4164	Cp H2O Feed (kJ/kg-K)	2.33	Cp H2O Feed (kJ/kg-K)	2.33
Initial H2O Temp (K)	300	Initial H2O Temp (K)	928	Initial H2O Temp (K)	1,053
Cp S-CO2 (kJ/kg-K)	1.25	HTSEout Flow Rate (kg/s)	0.682	O2 Flow Rate (kg/s)	3.56
S-CO2 Initial Temp (K)	943	Cp HTSEout (kJ/kg-K)	10.51	Cp O2 (kJ/kg-K)	1.10
Tsat @ 3MPa (K)	507	Intial HTSEout Temp (K)	1,106	Intial O2 Temp (K)	1,106
Cp(g) (kJ/kg-K)	3.421	Final HTSEout Temp (K)	933	Final O2 Temp (K)	1,055
H(fg) (kJ/kg)	1,795	Final H2O Feed Temp (K)	1,053	Final H2O Feed Temp (K)	1,073
Final Steam Temp (K)	928.0	**Recuperated Power (MWth)**	**1.24**	**Recuperated Power (MWth)**	**0.20**
Power Required (MWth)	**17.6**				

D - Synfuel via HTCE, HTSE, and LTFT with Recycle via Autothermal Reforming

HTCE, HTSE and ATR Heat Rejection (S-CO2)

Heat Rejected From HTCE FT Feed		Heat Rejected From HTSE H2 LTFT/Refining Feed			
HTCE_out Rate (kg/s)	21.9	HTSE H2 Feed Rate (kg/s)	0.682		
Initial HTCEout Temp (K)	949	Cp HTSE H2 (kJ/kg-K)	10.5		
Final HTCEout Temp (K)	473	Initial HTSE H2 Temp (K)	933		
Cp HTCEout (kJ/kg-K)	2.70	Final HTSE H2 Temp (K)	463		
Power Rejected (MWth)	**-28.1**	**Power Rejected (MWth)**	**-3.37**	**Required ATR H2/CO Heat Rejection (MWth)**	**-9.68**

Gas Mixer prior to LTFT

H2 Process Streams	Flow rate (kg/s)	Temp (K)	Enthalpy (kJ/kg)
HTCE to Mixer (in)	2.75	473	6478.9
HTSE to Mixer (in)	0.350	463	6333.6
ATR to Mixer (in)	1.19	637	8865.0
Mixer to LTFT (out)	4.29	523	7205.6
CO Process Steams			
HTCE to Mixer (in)	18.944	473	623.6
ATR to Mixer (in)	11.08	637	800.5
Mixer to LTFT (out)	30.02	523	677.6
Mixing Pressure (MPa)	3.00		
Thermal Power in (MWth)	51.25		
Thermal Power out (MWth)	51.24		
Difference	0%		

Note: The power contributions from small amounts of CO2 and H2O in HTCE mix are neglected.
Increasing cooling water flow to HTCEout cooler can ensure proper LTFT inlet temperature

ATR RHX

ΔT (K)	31.00				
Process Stream	**Flow Rate (kg/s)**	**Inlet Temp (K)**	**Inlet Enthalpy (kJ/kg)**	**Outlet Temp (K)**	**Outlet Enthalpy (kJ/kg)**
H2 (ATR out)	1.19	973.00	13,792	970.00	13,747
CO (ATR out)	11.08	973.00	1,154	970.00	1,151
H2O (ATR in)	3.56	928.00	3,826	939.00	3,851
Power in (MWth)	0.09				
Power out (MWth)	0.09				
Difference	0%				

ATR H2O Feed Heating from S-CO2			HC Heating from S-CO2	
Assumed Min ΔT (K)	15		Assumed Min ΔT (K)	15
H2O Flow Rate (kg/s)	3.56		HC Flow Rate (kg/s)	4.08
Cpf H2O (kJ/kg-K)	4.2686		Cp HC (kJ/kg-K)	3.12
Initial H2O Temp (K)	310		Initial HC Temp (K)	310
Cp S-CO2 (kJ/kg-K)	1.25		Cp S-CO2 (kJ/kg-K)	1.25
S-CO2 Initial Temp (K)	943		S-CO2 Initial Temp (K)	943
Tsat @ 0.3 MPa (K)	406.67		Final CO2 Feed Temp (K)	928
Cp(g) (kJ/kg-K)	2.263		**Power (MWth)**	**7.86**
H(fg) (kJ/kg)	2,163			
Final Steam Temp (K)	928			
Power Required (MWth)	**13.37**			

Process Stream	Flow Rate (kg/s)	Inlet Temp (K)	Enthalpy_in (kJ/kg)	Outlet Temp (K)	Enthalpy_out (kJ/kg)
Steam	3.6	928	3826.1	948	3871.2
HC	4.08	928	-	948	-
O2	3.16	1,055	872.68	948	872.68
Power In (MWth)	25.84				
Power Out (MWth)	26.21				

Heater Power Necessary to Heatup to 973 K

	Inlet Temp (K)	Enthalpy_in (kJ/kg)	Outlet Temp (K)	Enthalpy_out (kJ/kg)
Steam	948	3871.2	973	3927.9
HC	948	-	973	-
O2	948	872.68	973	872.68
Power In (MWth)	0.457	**Power In (MWe)**	**0.481**	

Compression Energy

Assumed Efficiency   0.9

Processes	CO2 (HTCE)	H2-Refining	H2 (ATR-Mix)	CO (ATR-Mix)
flow rate (kg/s)	29.90	0.09	1.19	11.08
T_1 (K)	318.00	463.00	637.00	637.00
P_1 (Mpa)	0.116	0.101	0.300	0.300
P_2 (Mpa)	3.00	5.00	3.00	3.00
r_p	25.79	49.50	10.00	10.0
$c_{p \, (kJ/kg\text{-}K)}$	0.967	14.66	14.65	1.10
$c_{v \, (kJ/kg\text{-}K)}$	0.707	10.54	10.52	0.81
γ	1.37	1.39	1.39	1.37
K	0.27	0.28	0.28	0.27
Power (MWe)	**14.3**	**1.42**	**11.2**	**7.37**
m^3/hr	54,804	3,813		30,903

Note: All pump work for compression of liquid phase fluids neglected

Overall HTCE Energy Requirements

Power Input (MWth) (S-CO2)	
HTCE Feed Heating	123
HTSE Feed Heating	17.6
ATR Feed Heating	21.2
HC Refining Heating	8.59
Total (MWth)	**170**
Change from Alk. Electrolysis	117%

Electric Power (MWe) (S-CO2)	
CO2 Capture & Desalination	21.7
HTCE	534
HTSE	55.9
ATR Heaters	0.481
Compression (non refining)	34.3
Compression (refining)	4.85
Total (MWe)	**651**
Change from Alkalkine Electrolys	-25.6%

Power Output (MWth) (S-CO2)	
HTCE Product Heat Rejection	-28.1
HTSE Product Heat Rejection	-3.37
ATR/Recycle Heat Rejection	-9.7
LTFT Heat Rejection	-177
Fractionalization Process	-61.7
Refining Heat Rejection	-12.9
Total (MWth)	**-261**
% Change from Alk Electrol	-0.21%

Recuperated Power (MWth) (S-CO2)	
H2O Heating from HTCEout	8.27
CO2 Heating from HTCE O2	5.33
H2O Heating from HTSEout	1.24
H2O Heating from HTSE O2	0.20
H2O Heating from ATRout	0.09
Total (MWth)	**15.1**

Power Input (MWth) (PWR)		Power Output (MWth) (PWR)		Electric Power (MWe) (PWR)		Recuperated Power (MWth) (PWR)	
HTCE Feed Heating	77.1	HTCE Product Heat Rejection	-6.6	CO2 Capture & Desalination	21.7	H2O Heating from HTCEout	30.6
HTSE Feed Heating	12.0	HTSE Product Heat Rejection	-0.61	HTCE	534	CO2 Heating from HTCE O2	19.14
ATR Feed Heating	13.23	ATR/Recycle Heat Rejection	-7.24	HTSE	55.9	H2O Heating from HTSEout	4.73
HC Refining Heating	6.22	LTFT Heat Rejection	-177	ATR Heaters	5.380	H2O Heating from HTSE O2	22.14
Total (MWth)	**109**	Fractionalization Process	-61.7	HTSE Heaters	0.771	H2O Heating from ATRout	2.52
		Refining Heat Rejection	-12.9	Refining Heaters	2.49	**Total (MWth)**	**79.1**
% Change from S-CO2	-36.2%	**Total (MWth)**	**-266**	Compression (non refining)	34.3		
				Compression (refining)	4.85	% Change from S-CO2	423%
		% Change from S-CO2	2%	**Total (MWe)**	**659**		
				% Change from S-CO2	1.25%		

D - Synfuel via HTCE, HTSE, and LTFT with Recycle via Autothermal Reforming

Heat Transfer for HTCE Process (PWR)

Assumed Steam Temp (K)	558	Steam Cp (kJ/kg-K)	5.31

CO2 Heating from Steam		H2O Feed Heating from Steam		H2O Feed Heating from HTCEout	
Assumed Min ΔT (K)	15	Assumed Min ΔT (K)	15	Assumed Min ΔT (K)	5
CO2 Feed Flow Rate (kg/s)	29.90	H2O Flow Rate (kg/s)	24.5	H2O Feed Flow Rate (kg/s)	24.5
Cp CO2 Feed (kJ/kg-K)	1.155	Cpf H2O (kJ/kg-K)	4.4164	Cp H2O Feed (kJ/kg-K)	2.33
Initial CO2 Temp (K)	318	Initial H2O Temp (K)	300	Initial H2O Temp (K)	543
Cp Steam (kJ/kg-K)	5.31	Cp Steam (kJ/kg-K)	5.31	HTCEout Flow Rate (kg/s)	21.9
Steam Initial Temp (K)	558	Steam Initial Temp (K)	558	Cp HTCEout (kJ/kg-K)	2.8
Final CO2 Feed Temp (K)	543	Tsat @ 3MPa (K)	507	Intial HTCEout Temp (K)	1,084
Power (MWth)	**7.77**	Cp(g) (kJ/kg-K)	3.421	Final HTCEout Temp (K)	585
		H(fg) (kJ/kg)	1794.9	Final H2O Feed Temp (K)	1,079
CO2 Heating from HTCE O2		Final Steam Temp (K)	543	**Recuperated Power (MWth)**	**30.6**
Assumed Min ΔT (K)	5.1	**Power (MWth)**	**69.3**		
CO2 Feed Flow Rate (kg/s)	29.90				
Cp CO2 Feed (kJ/kg-K)	1.23				
Initial CO2 Temp (K)	543				
HTCE O2 Flow Rate (kg/s)	32.51				
Cp Waste O2 (kJ/kg-K)	1.1				
Intial O2 Temp (K)	1,084				
Final O2 Temp (K)	548				
Final CO2 Feed Temp (K)	1,064				
Recuperated Power (MWth)	**19.1**				

Process Stream	Flow Rate (kg/s)	T in (K)	Enthalpy_in (kJ/kg)	Tout (K)	Enthalpy_out (kJ/kg)
Steam	24.5	1,079	4160.8	1073	4146.6
CO2	29.90	1,064	1342.9	1073	1355.5
Power In (MWth)	141.956				
Power Out (MWth)	141.985				
Difference	0%				

D - Synfuel via HTCE, HTSE, and LTFT with Recycle via Autothermal Reforming

Heat Transfer for HTSE Process (PWR)

H2O Feed Heating from Steam		H2O Feed Heating from HTSEout		H2O Feed Heating from HTSE O2	
Assumed Min ΔT (K)	15.0	Assumed Min ΔT (K)	5.1	Assumed Min ΔT (K)	4.9
H2O Flow Rate (kg/s)	4.24	H2O Feed Flow Rate (kg/s)	4.24	H2O Feed Flow Rate (kg/s)	4.24
Cpf H2O (kJ/kg-K)	4.4164	Cp H2O Feed (kJ/kg-K)	2.33	Cp H2O Feed (kJ/kg-K)	2.33
Initial H2O Temp (K)	300	Initial H2O Temp (K)	543	Initial H2O Temp (K)	947
Cp Steam (kJ/kg-K)	5.31	HTSEout Flow Rate (kg/s)	0.68	O2 Flow Rate (kg/s)	3.56
Steam Initial Temp (K)	558	Cp HTSEout (kJ/kg-K)	10.51	Cp O2 (kJ/kg-K)	1.1
Tsat @ 3MPa (K)	507	Intial HTSEout Temp (K)	1,106	Intial O2 Temp (K)	1,106
Cp(g) (kJ/kg-K)	3.421	Final HTSEout Temp (K)	548	Final O2 Temp (K)	952
H(fg) (kJ/kg)	1,795	Final H2O Feed Temp (K)	947	Final H2O Feed Temp (K)	1,008
Final Steam Temp (K)	543	**Recuperated Power (MWth)**	**4.00**	**Recuperated Power (MWth)**	**0.60**
Power Required (MWth)	**12.0**				

Process Stream	T in (K)	Enthalpy_in (KJ/kg)	Tout (K)	Enthalpy_out (kJ/kg)
Steam	1,008	3,993	1,012	4,003
HTSE_H2O recycle	1,106	4,211	1,012	4,003
HTSE_H2 recycle	1,106	15,804	1,012	14,400
Power In (MWth)	17.386			
Power Out (MWth)	17.388			

Heater Power Necessary to Heatup to 1,073 K (MWth)

Process Stream	T in (K)	Enthalpy_in (KJ/kg)	Tout (K)	Enthalpy_out (kJ/kg)
Steam	1,012	4,003	1,073	4,147
HTSE_H2O recycle	1,012	4,003	1,073	4,147
HTSE_H2 recycle	1,012	14,400	1,073	15,319
Power In (MWth)	0.732	**Power in (MWe)**	**0.771**	

HTCE, HTSE and ATR Heat Rejection (PWR)

Heat Rejected From HTCE FT Feed		Heat Rejected From HTSE H2 LTFT/Refining Feed	
HTCE_out Rate (kg/s)	21.9	HTSE H2 Feed Rate (kg/s)	0.682
Initial HTCEout Temp (K)	585	Cp HTSE H2 (kJ/kg-K)	10.5
Final HTCEout Temp (K)	473	Initial HTSE H2 Temp (K)	548
Cp HTCEout (kJ/kg-K)	2.70	Final HTSE H2 Temp (K)	463
Power Rejected (MWth)	**-6.61**	**Power Rejected (MWth)**	**-0.61**

Required ATR H2/CO Heat Rejection (MWth)	**-7.24**

Gas Mixer prior to LTFT

H2 Process Streams	Flow rate (kg/s)	Temp (K)	Enthalpy (kJ/kg)
HTCE to Mixer (in)	2.75	473	6478.9
HTSE to Mixer (in)	0.350	463	6333.6
ATR to Mixer (in)	1.19	637	8865.0
Mixer to LTFT (out)	4.29	523	7205.6
CO Process Steams			
HTCE to Mixer (in)	18.944	473	623.6
ATR to Mixer (in)	11.08	637	800.5
Mixer to LTFT (out)	30.02	523	677.6
Mixing Pressure (MPa)	3.00		
Thermal Power in (MWth)	51.25		
Thermal Power out (MWth)	51.24		
Difference	0%		

Note: The power contributions from small amounts of CO2 and H2O in HTCE mix are neglected.
Increasing cooling water flow to HTCEout cooler can ensure proper LTFT inlet temperature

ATR RHX

ΔT (K)	7.00				
Process Stream	Flow Rate (kg/s)	Inlet Temp (K)	Inlet Enthalpy (kJ/kg)	Outlet Temp (K)	Outlet Enthalpy (kJ/kg)
H2 (ATR out)	1.19	973.00	13,792	887.00	12,513
CO (ATR out)	11.08	973.00	1,154	887.00	1,063
H2O (ATR in)	3.56	543.00	3,008	880.00	3,719
Power in (MWth)	2.52				
Power out (MWth)	2.53				
Difference	0%				

1st and 2nd Stage Heating Prior to ATR (PWR)

ATR H2O Feed Heating from Steam		HC Heating from Steam	
Assumed Min ΔT (K)	15	Assumed Min ΔT (K)	15
H2O Flow Rate (kg/s)	3.56	HC Flow Rate (kg/s)	4.08
Cpf H2O (kJ/kg-K)	4.2686	Cp HC (kJ/kg-K)	3.12
Initial H2O Temp (K)	310	Initial HC Temp (K)	310
Cp Steam (kJ/kg-K)	5.31	Cp Steam (kJ/kg-K)	5.31
Steam Initial Temp (K)	558	Steam Initial Temp (K)	558
Tsat @ 0.3 MPa (K)	406.67	Final CO2 Feed Temp (K)	543
Cp(g) (kJ/kg-K)	2.263	**Power (MWth)**	**2.96**
H(fg) (kJ/kg)	2,163		
Final Steam Temp (K)	543		
Power Required (MWth)	**10.3**		

Process Stream	Flow Rate (kg/s)	Inlet Temp (K)	Enthalpy_in (kJ/kg)	Outlet Temp (K)	Enthalpy_out (kJ/kg)
Steam	3.56	880	3719.2	722	3377.9
HC	4.08	543	-	722	-
O2	3.16	952	872.68	722	684.6
Power In (MWth)	21.54				
Power Out (MWth)	21.55				

Heater Power Necessary to Heatup to 973 K

	Inlet Temp (K)	Enthalpy_in (kJ/kg)	Outlet Temp (K)	Enthalpy_out (kJ/kg)
Steam	722	3377.9	973	3927.9
HC	722	-	973	-
O2	722	684.6	973	872.68
Power In (MWth)	5.111	**Power In (MWe)**	**5.38**	

D - Synfuel via Methanol Synthesis and Olefin Oligomerization

Olefin Oligomerization

Inlet Temp (K)	500		Assumed Olefin Feed Distribution		JP-5 Oligomerization Weight Fraction (~C9-C16)			0.5
Pressure (MPa)	5.52		Methane (CH2)	0.75%	Oligomerization Recycle Weight Fraction (~C5-C8)			0.5
ΔT across Stage	30		Ethylene (C2H4)	12.03%	* Recycle fraction consits mainly of C5-C8 HCs (gasoline).			
Catalyst	ZSM-5/SiO2/Al2O3		Propylene (C3H6)	24.06%				
# Stages	3		Butylene (C4H8)	16.54%				
			Pentene (C5H10)	12.03%	**Assuming SS, w/ recycle of unused HCs, the olefin feed flow			
			Hextene (C6H12)	34.59%	will directly make up for JP-5 product HCs.			

	kg/day	kg/hr	kg/s	mol/s
Required JP-5 Production	126,311	5,263	9.43	71.5
Oligomerization Recycle	126,311	5,263	9.43	
CH2 Feed	6,128	255	0.07	5.07
C2H4 Feed	98,046	4,085	1.13	40.5
C3H6 Feed	196,091	8,170	2.27	54.0
C4H8 Feed	134,813	5,617	1.56	27.9
C5H10 Feed	98,046	4,085	1.13	16.2
C6H12 Feed	281,881	11,745	3.26	38.8
Total Olefin Feed	815,003	33,958	9.43	

Methanol to Olefins

Catalyst Used:	ZSM-5			
Temp (K)	673	ΔH (kJ/mol), exothermic		-45.90
Pressure (MPa)	0.14	**Heat Removal Requirement (MWth)**		**-30.93**

	kg/day	kg/hr	kg/s	mol/s
Methanol Feed Required	1,862,865	77,619	21.6	673.8
H2O Product	1,047,861	43,661	12.1	673.8

D - Synfuel via Methanol Synthesis and Olefin Oligomerization

Methanol Synthesis via CAMERE

Stage 1 (RWGS)

Inlet Temp (K)	773
Pressure (MPa)	1.01325
Catalyst:	Cu/ZnO/Al2O3 (6:3:1)

Stage 2 (Methanol Synthesis)

Inlet temp (K)	523
Pressure (MPa)	3.03975
Catalyst:	Cu/ZnO/ZrO2/Ga2O3 (5:3:1:1)

CAMERE Material Balance (mol/h) / Material Balance of CAMERE Process (all quantities are molar fractions)

Process	CO	CO2	H2	H2O	CH3OH	CO	CO2	H2	H2O	CH3OH	sum
Feed	0.00000	2.30050	7.76265	0.00000	0.00000	0.00000	0.22861	0.77139	0.00000	0.00000	1.00000
Mix1_out	0.93386	2.89242	11.99615	0.00530	0.00000	0.05900	0.18274	0.75792	0.00033	0.00000	1.00000
Rx1_out	2.43036	1.48823	10.57890	1.41247	0.00000	0.15276	0.09354	0.66492	0.08878	0.00000	1.00000
Water_out	0.00000	0.00116	0.00000	1.39923	0.00000	0.00000	0.00083	0.00000	0.99917	0.00000	1.00000
Separator_out	2.34036	1.48707	10.57890	0.01324	0.00000	0.16230	0.10313	0.73365	0.00092	0.00000	1.00000
Syngas	1.40422	0.89224	6.34735	0.00794	0.00000	0.16230	0.10313	0.73365	0.00092	0.00000	1.00000
Split Stream	0.93614	0.59483	4.23156	0.00530	0.00000	0.16230	0.10313	0.73365	0.00092	0.00000	1.00000
Mlx_out	2.82928	1.63572	13.57670	0.00880	0.00000	0.15674	0.09062	0.75215	0.00049	0.00000	1.00000
Rx_out	2.04515	1.09456	10.36040	0.55029	1.34243	0.13286	0.07111	0.67307	0.03575	0.08721	1.00000
Sep2-liq	0.00057	0.02554	0.00168	0.54907	1.31980	0.00030	0.01347	0.00089	0.28949	0.69585	1.00000
Sep2-vap	2.04458	1.06902	10.35870	0.00123	0.02263	0.15149	0.07921	0.76753	0.00009	0.00168	1.00000
Tee-out2	0.61337	0.32071	3.10762	0.00037	0.00679	0.15149	0.07921	0.76753	0.00009	0.00168	1.00000
Tee-out1	1.43120	0.74831	6.25110	0.00085	0.01584	0.16943	0.08859	0.74001	0.00010	0.00188	1.00000
H2O	0.00000	0.00000	0.00000	0.54905	0.09599	0.00000	0.00000	0.00000	0.85119	0.14881	1.00000
Methanol	0.00057	0.02554	0.00168	0.00001	1.22381	0.00046	0.02041	0.00134	0.00001	0.97779	1.00000

Molar Ratio: H2 Feed_in / Methanol Product_out	6.34	ΔH (kJ/mol-CO), exothermic	-128.11
Molar Ratio: CO2 Feed_in / Methanol Product_out	1.88	ΔH (kJ/mol-CO2), exothermic	-86.99

	kg/day	kg/hr	kg/s	mol/s
Required Methanol Feed	1,862,865	77,619	21.6	674
Required H2 Feed	738,512	30,771	8.55	4,274
Required CO2 Feed	4,814,955	200,623	55.7	1,267

Alkaline electrolysis power required (Mwe)	**1,482**	# Electrolyzers	711
HTSE Power Required (MWe)	**1,068**	# HTSE Cells	3,665,400

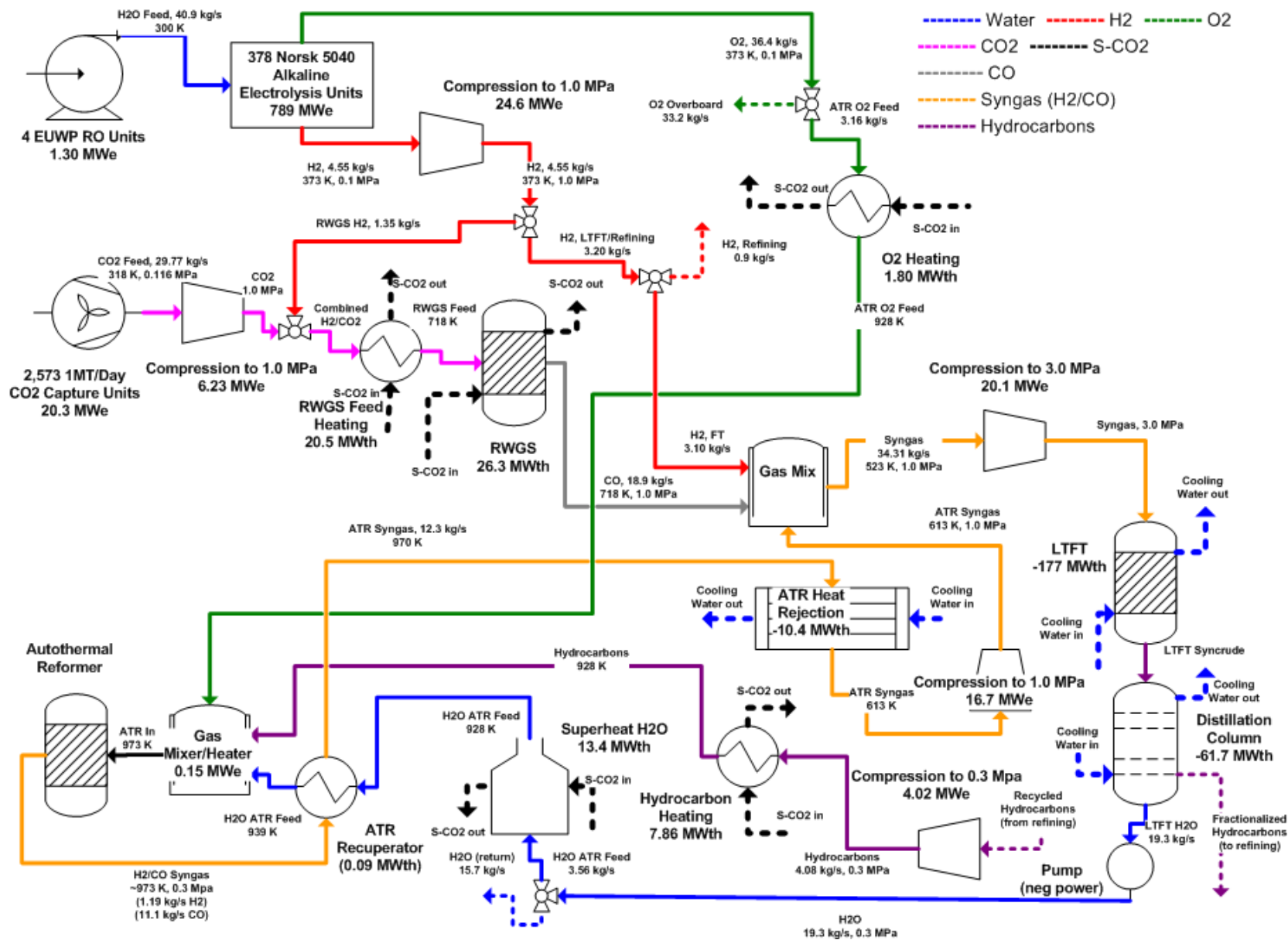|	
CO2 Air Capture Power Required (Mwe)	**38.0**
# Air Capture Units	4,815

Heat Removal Requirement (MWth)	**-74.05**

(This Page Intentionally Blank)
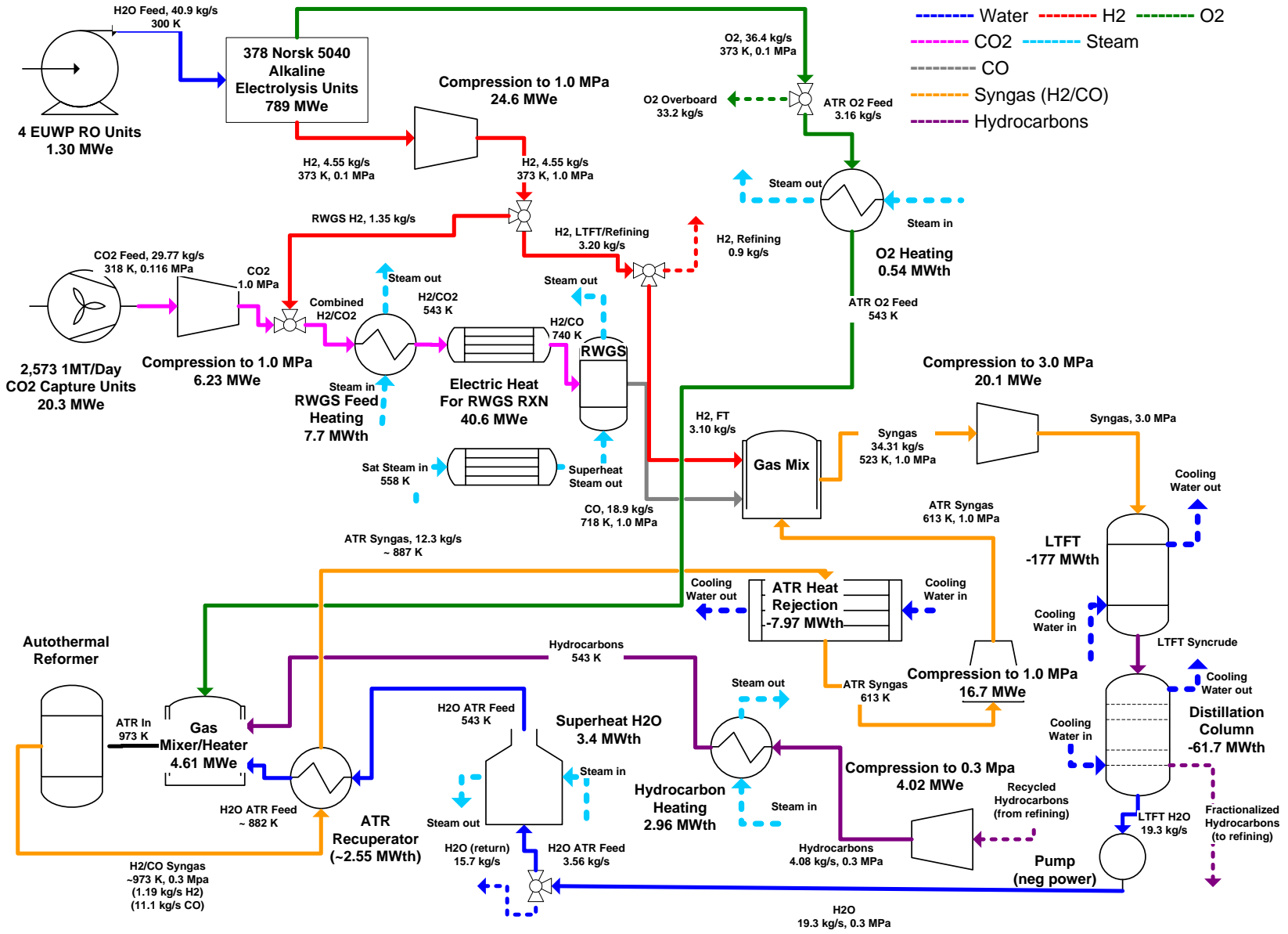
Appendix E - Liquid Fuels Production Flowsheets

This appendix contains system flowsheets describing mass and energy transfers through various liquid fuel production schemes.
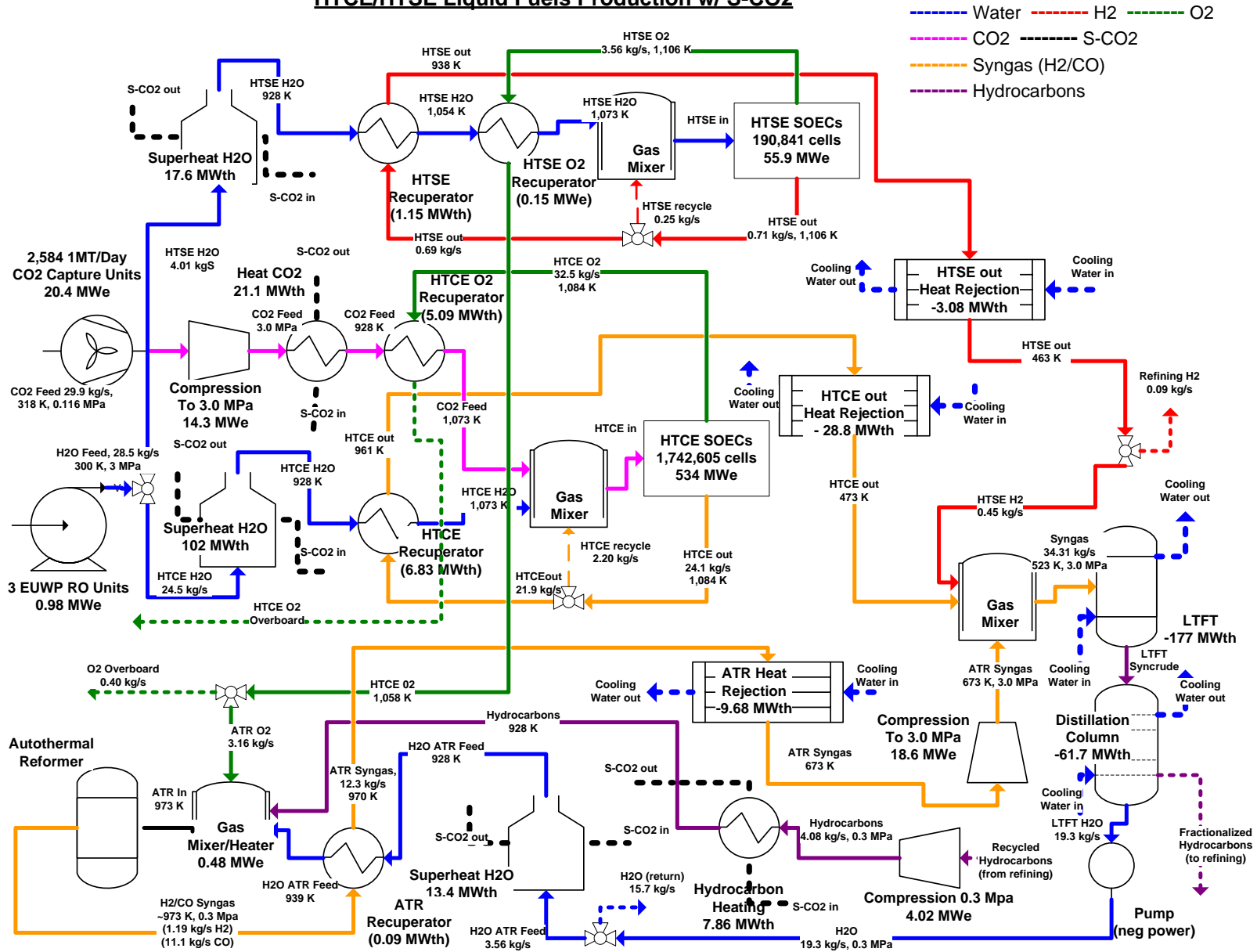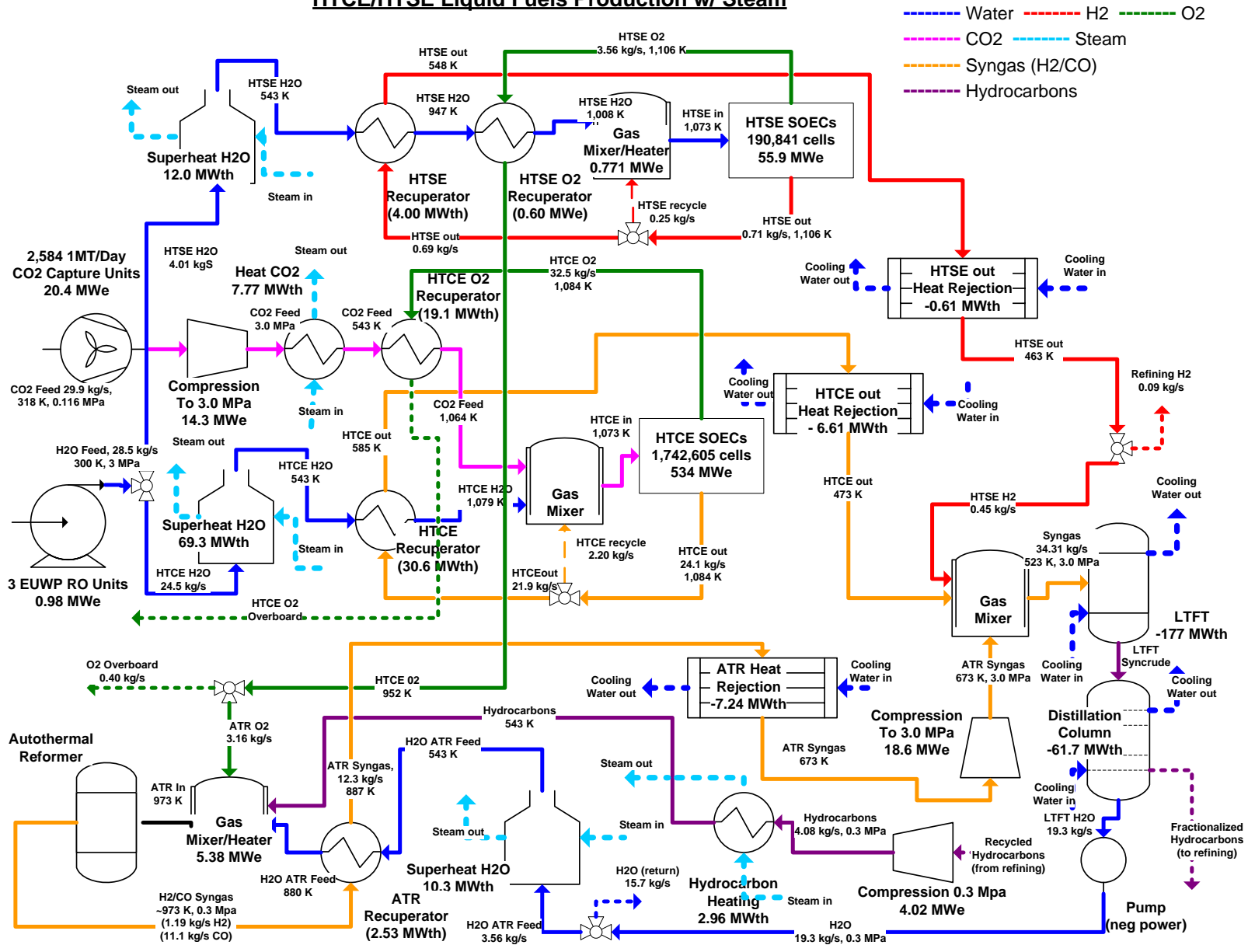
Alkaline Electrolysis Liquid Fuels Production w/ S-CO2

Alkaline Electrolysis Liquid Fuels Production w/ Steam

Legend:
- Water
- H2
- O2
- CO2
- Steam
- CO
- Syngas (H2/CO)
- Hydrocarbons

4 EUWP RO Units 1.30 MWe

H2O Feed, 40.9 kg/s, 300 K

378 Norsk 5040 Alkaline Electrolysis Units 789 MWe

Compression to 1.0 MPa 24.6 MWe

O2, 36.4 kg/s, 373 K, 0.1 MPa

O2 Overboard 33.2 kg/s

ATR O2 Feed 3.16 kg/s

H2, 4.55 kg/s, 373 K, 0.1 MPa

H2, 4.55 kg/s, 373 K, 1.0 MPa

RWGS H2, 1.35 kg/s

H2, LTFT/Refining 3.20 kg/s

H2, Refining 0.9 kg/s

Steam out

Steam in

O2 Heating 0.54 MWth

CO2 Feed, 29.77 kg/s, 318 K, 0.116 MPa

CO2 1.0 MPa

Combined H2/CO2

Steam out

H2/CO2 543 K

Steam out

H2/CO 740 K

RWGS

ATR O2 Feed 543 K

2,573 1MT/Day CO2 Capture Units 20.3 MWe

Compression to 1.0 MPa 6.23 MWe

Steam in

RWGS Feed Heating 7.7 MWth

Electric Heat For RWGS RXN 40.6 MWe

Compression to 3.0 MPa 20.1 MWe

Sat Steam in 558 K

Superheat Steam out

H2, FT 3.10 kg/s

Gas Mix

Syngas 34.31 kg/s, 523 K, 1.0 MPa

Syngas, 3.0 MPa

Cooling Water out

CO, 18.9 kg/s, 718 K, 1.0 MPa

ATR Syngas 613 K, 1.0 MPa

LTFT -177 MWth

ATR Syngas, 12.3 kg/s, ~ 887 K

Cooling Water in

Cooling Water in

LTFT Syncrude

Autothermal Reformer

ATR In 973 K

Gas Mixer/Heater 4.61 MWe

Hydrocarbons 543 K

ATR Heat Rejection -7.97 MWth

Cooling Water in

Cooling Water out

Compression to 1.0 MPa 16.7 MWe

ATR Syngas 613 K

Distillation Column -61.7 MWth

Steam out

Superheat H2O 3.4 MWth

H2O ATR Feed 543 K

H2O ATR Feed ~ 882 K

ATR Recuperator (~2.55 MWth)

Steam in

Steam out

H2O (return) 15.7 kg/s

H2O ATR Feed 3.56 kg/s

Hydrocarbon Heating 2.96 MWth

Steam in

Compression to 0.3 Mpa 4.02 MWe

Recycled Hydrocarbons (from refining)

Cooling Water in

Cooling Water out

H2/CO Syngas ~973 K, 0.3 Mpa (1.19 kg/s H2) (11.1 kg/s CO)

Hydrocarbons 4.08 kg/s, 0.3 MPa

Pump (neg power)

LTFT H2O 19.3 kg/s

Fractionalized Hydrocarbons (to refining)

H2O 19.3 kg/s, 0.3 MPa

297

HTCE/HTSE Liquid Fuels Production w/ S-CO2

Legend:
- Water
- H2
- O2
- CO2
- S-CO2
- Syngas (H2/CO)
- Hydrocarbons

HTCE/HTSE Liquid Fuels Production w/ Steam

Legend:
- Water
- H2
- O2
- CO2
- Steam
- Syngas (H2/CO)
- Hydrocarbons

Refining Fischer-Tropsch Syncrude to Jet Fuel (Kerosene)

300
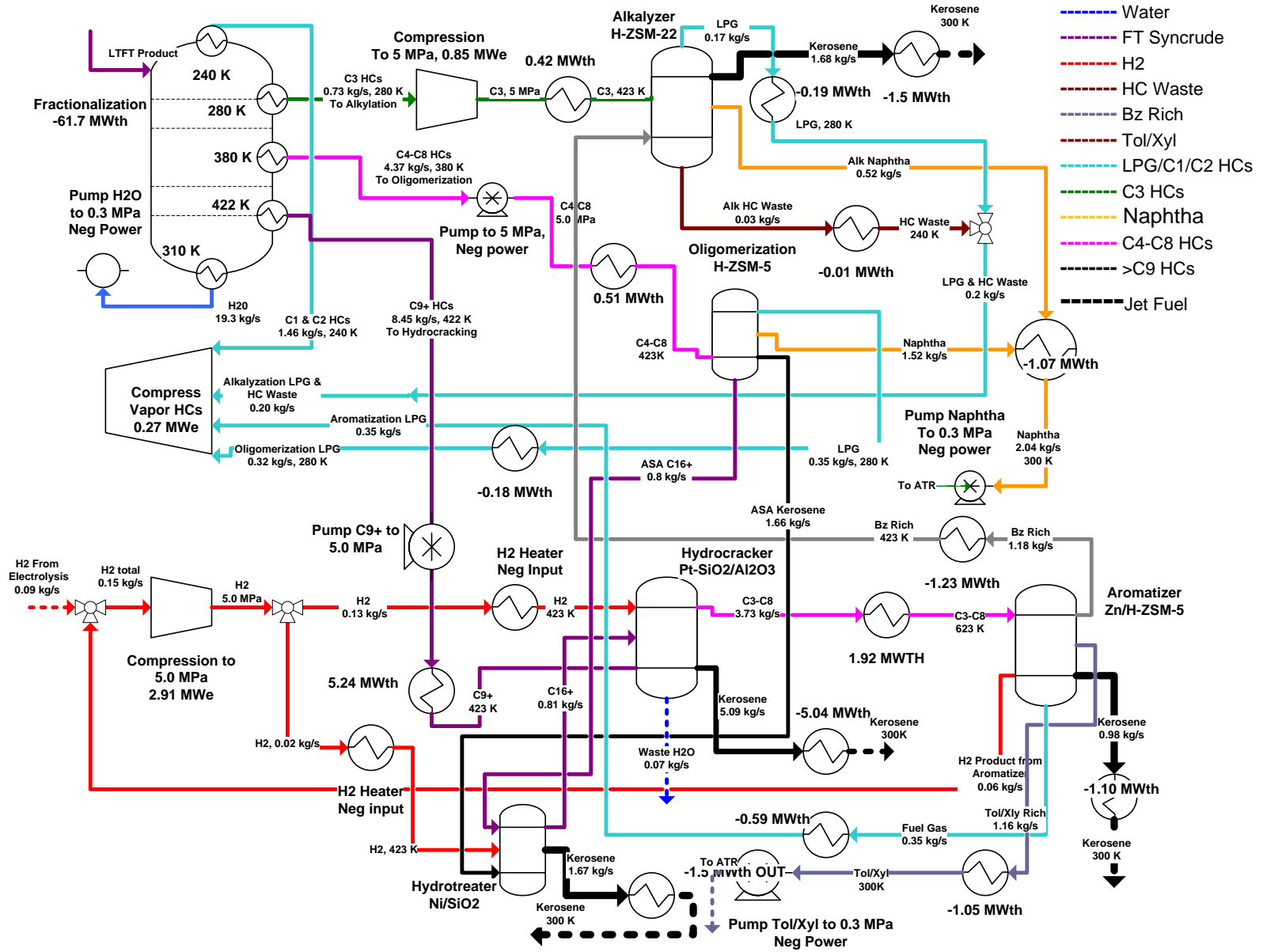
Appendix F - Power Cycle Calculations
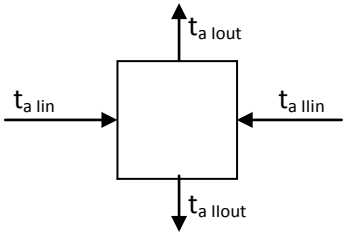
Simple Brayton Cycle

The PCS model uses fundamental thermodynamic principles and conservation laws (refer to chapter 3), and it evaluates the properties at each point of the cycle in order to determine the important parameters measuring cycle performance (thermal efficiency, net work, compressor work, etc.). The following parameters are fixed:

- Cycle net power $\left(\dot{W}_{net} \right)$
- Turbine inlet pressure (p_4)
- Turbine inlet temperature (t_4)
- Compressor inlet temperature (t_1)
- Component efficiencies (compressor, heat exchanger, turbine)

The cycle is optimized by varying the turbine pressure ratio ($rT=p_4/p_5$) between 1.1-5.0.

The calculations are performed for a steady-state condition, neglecting frictional losses, and assuming that component efficiencies are known. Reference [1] provided the applicable thermodynamic properties. The computational algorithm is as follows (refer to figure below for state point locations):

Cycle State Points		
Point 4	P_4 is constant; t_4 is constant	
Point 5	Enthalpy h_5 computed from turbine efficiency: $$\eta_T = \frac{h_4 - h_5}{h_4 - h_{5,ideal}}$$	(F-1)
	P_5 computed from pressure ratio: $$p_5 = \frac{p_4}{rT}$$	(F-2)
Point 1	T_1 is constant; $p_1=p_5$	
Point 2	H_2 computed from compressor efficiency: $$\eta_C = \frac{h_{2,ideal} - h_1}{h_2 - h_1}$$ And $P_2=P_4$	(F-3)

Point 6	H_6 is computed from HX efficiency: $$\eta_{HX} = \frac{h_5 - h_6}{h_5 - h_{6,ideal}}$$ And $P_6 = P_5$	(F-4)
Point 3	$$h_3 = h_2 + q_{HX}$$	(F-5)
	$$q_{HX} = h_5 - h_6$$	(F-6)
	And $P_3 = P_2$	
Point 7	H_7 is computed from energy balance at flow junction prior to cooler: $$h_7 = \left(\frac{h_6 \dot{m}_y + h_x \dot{m}_x}{\dot{m}_z}\right)$$ And $P_7 = P_6$	(F-7)
	$$h_{x=} \left(\frac{h_a \dot{m}_a + h_b \dot{m}_b + \cdots + h_5 \dot{m}_{r_5}}{\dot{m}_x}\right)$$	(F-8)
	$$\dot{m}_x = \dot{m}_a + \dot{m}_b + \cdots + \dot{m}_{r_5}$$	(F-9)
	$$\dot{m}_a = \frac{\dot{Q}_a}{h_4 - h_{a\,lout}} ; \;\; \dot{m}_b = \frac{\dot{Q}_b}{h_4 - h_{b\,lout}} \dots etc$$	(F-10)
	$$t_{a\,lout} = t_{a\,llin} + \Delta T$$ Where index a_{lout} refers to outlet temperature at primary side of heat exchanger "a" Where index a_{llin} refers to inlet temperature at secondary side of heat exchanger "a" $T_{a\,llin}$, $T_{a\,llout}$, and $\dot{Q}_a$ are known from electrolysis/refinery temperature specification. ΔT assumed at 15 ^{o}C	(F-11)
	$\dot{m}_y$ computed from net power as follows: $$\dot{W}_{net} = \dot{W}_T - \dot{W}_C \text{ and}$$ $$\dot{m}_z = \dot{m}_x + \dot{m}_y$$ $$\therefore m_y = \frac{[W_{net} + m_x(h_2 - h_1)]}{(h_4 - h_5 - h_2 + h_1)}$$	(F-12)

Cycle Performance		
Heat Rejected	$\dot{Q}_{out} = \dot{m}_z(h_7 - h_1)$	(F-13)
Heat Input	$\dot{Q}_{in} = \dot{m}_z(h_4 - h_3)$	(F-14)
Turbine Work	$\dot{W}_T = \dot{m}_y(h_4 - h_5)$	(F-15)
Compressor Work	$\dot{W}_C = \dot{m}_z(h_2 - h_1)$	(F-16)
Cycle Thermal Efficiency	$\eta_{TH} = \dfrac{\dot{W}_T - \dot{W}_C}{\dot{Q}_{in}}$	(F-17)

Table F-1 - Brayton Cycle Computational Algorithm

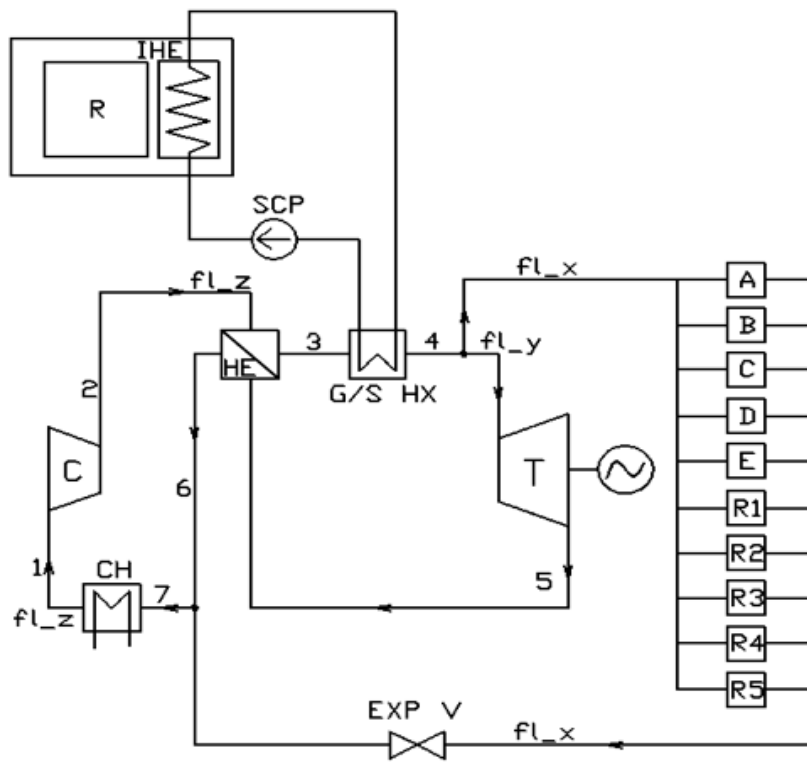The computations were performed using reference [2] with gracious assistance by Martin Kulhanek.

Figure F-1 - Simple Brayton PCS

Alkaline Electrolysis and HTCE/HTSE Liquid Fuels Production Options	
R	Reactor (AHTR)
IHE	Intermediate Heat Exchanger (IHE)
SCP	Salt Coolant Pump
G/S HX	Salt-to Gas HX
T	Turbine
C	Compressor
HE	Recuperative Heat Exchanger
CH	Chiller
fl_i	Flow Rate
EXP V	Expansion Valve

Alkaline Electrolysis Option Only		HTCE/HTSE Option Only	
A	RWGS Reaction	A	HTCE (CO_2)
B	ATR (H_2O)	B	HTCE (H_2O)
C	ATR (O_2)	C	HTSE (H_2O)
D	ATR (Hydrocarbons)	D	ATR (H_2O)
E	N/A	E	ATR (Hydrocarbons)
R1	Alkylation	R1	Alkylation
R2	Hydrocracking	R2	Hydrocracking
R3	Aromatization	R3	Aromatization
R4	Oligomerization	R4	Oligomerization
R5	Hydrotreating	R5	Hydrotreating

Table F-2 - Brayton Cycle Legend

Recompression Cycle

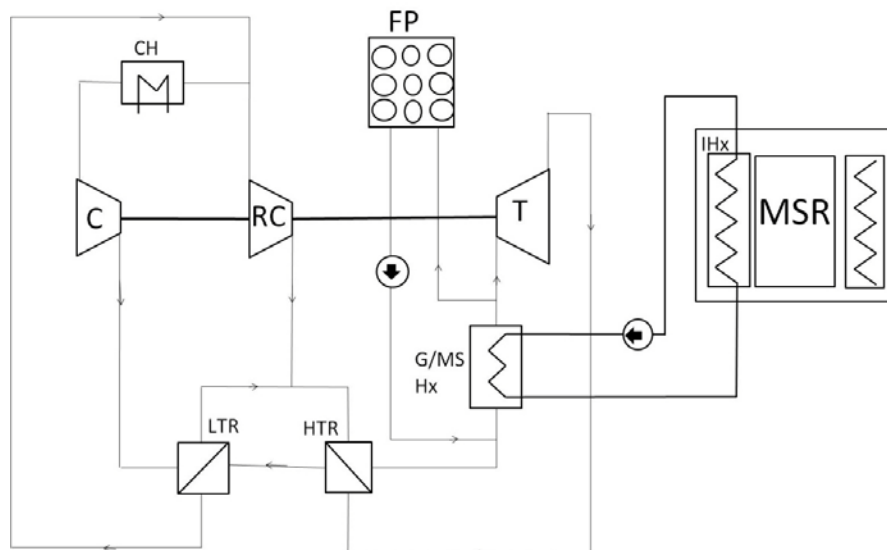Figure F-2 shows the S-CO_2 used in the analysis:

Figure F-2 - S-CO2 Recompression Cycle

The nomenclature is similar to the simple Brayton cycle, except that MSR is "molten salt reactor", "IHX" is the salt-to-salt intermediate heat exchanger, and "G/MS Hx" is the gas/molten salt heat exchanger. "FP" denotes all of the fuel plant heat loads, and "LTR" and "HTR" denote low and high temperature recuperator, respectively. The cycle thermodynamics are easier to explain in relation to a temperature vs. entropy diagram, shown in Figure F-3:
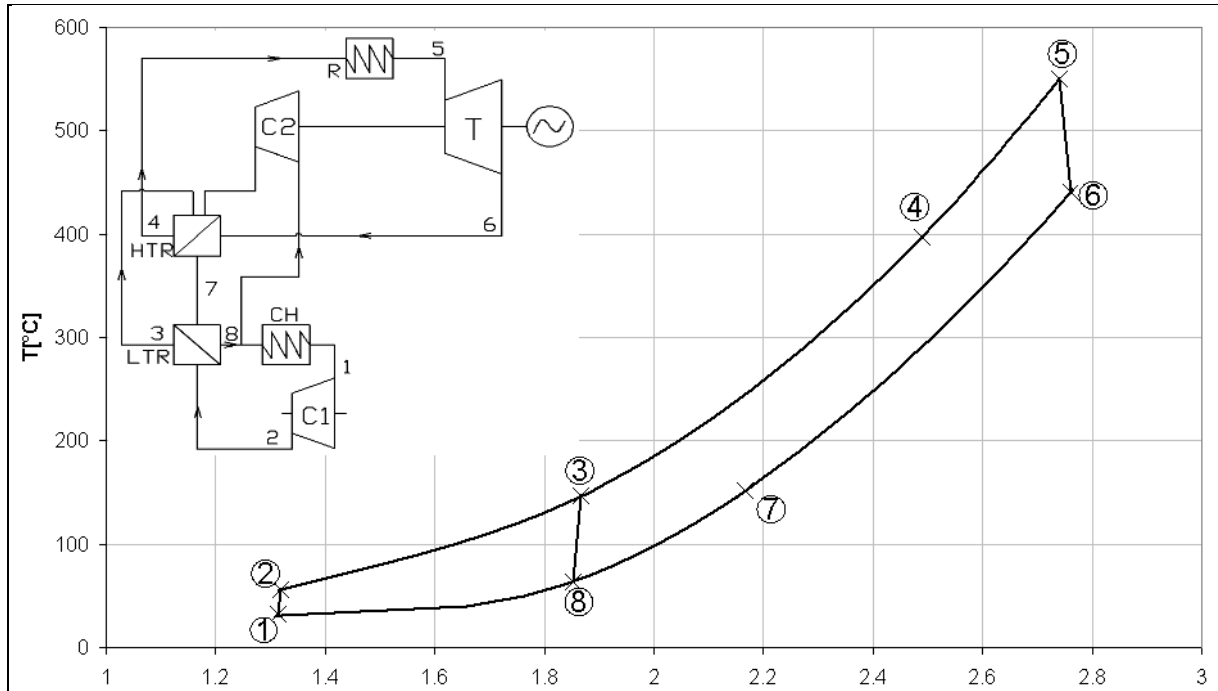

Figure F-3 - Recompression Cycle T-S Diagram

Except for a small portion of the fluid that is diverted to the fuel plant (m_{fp}), flow m_T of the working fluid expands in the turbine (state 6), and continues through the high temperature recuperator where a large part of available heat is regenerated (state 7). A remainder of available heat is regenerated in the low temperature recuperator (state 8). Subsequently, the full flow is split into flows m_1 and m_2, and part m_1 is chilled to the main compressor inlet temperature 32°C (state 1) and further compressed in the main compressor (state 2). After pre-heating in the low temperature recuperator (state 3), the m_1 part is combined again with the m_2 part, which has been compressed in the re-compressor to the same pressure level. The full turbine flow m_T is re-heated in the high temperature recuperator (state 4), and then recombined with m_{fp} before the full flow m is heated in the reactor to required turbine and fuel plant inlet temperature, 670°C (state 5). The mathematical model below details the computation algorithm used by reference [2], again with gracious assistance by Martin Kulhanek.

Recompression Cycle Mathematical Model

Variables:

Pressure ratio - $ra = P_2/P_1$

Main compressor outlet pressure – P_2

Constants:

Main compressor inlet temperature – $T_1 = 32°C$

Turbine inlet temperature – $T_5 = 670°C$

Compressor efficiency – $\eta_c = 0.89$

Turbine efficiency – $\eta_t = 0.90$

Recuperator efficiency – $\eta_r = 0.95$

Mass flow rate – $m = 1\ kg/s$

Since no pressure losses, the following pressures are equal:

$$P_2 = P_3 = P_4 = P_5$$
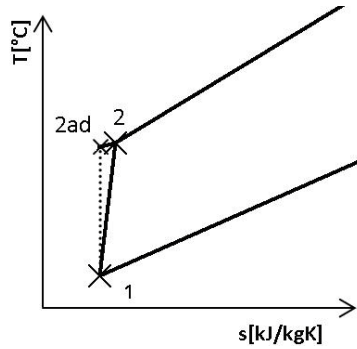
$$P_1 = P_6 = P_7 = P_8$$

Computation of cycle states:

- State 1: The pressure P_1 is computed from known variables ra, P_2:

$$p_1 = \frac{p_2}{ra}$$

(F-18)

T_1 is a constant. Two state properties are known, thus from CO_2 thermodynamic tables (reference [3]) h_1, s_1, d_1 can be determined.

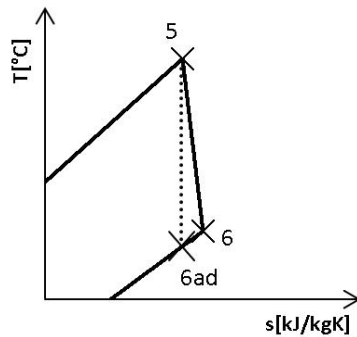- State 2: The enthalpy h_2 is computed from compressor efficiency which is defined as:

$$\eta c = \frac{h_{2ad} - h_1}{h_2 - h_1}$$

(F-19)

The pressure P_2 is a known variable. Two state properties are known, thus from CO_2 thermodynamic tables T_2, s_2, d_2 and can be determined

- State 5: $P_5 = P_2$ (no pressure losses) and temperature is a known constant, T_5. Two state properties are known, thus from CO_2 thermodynamic tables h_5, s_5, d_5 can be determined.

- State 6: The enthalpy h_6 is computed from turbine efficiency which is defined as:

$$\eta t = \frac{h_5 - h_6}{h_5 - h_{6ad}}$$

(F-20)

The pressure P_6 is computed from the pressure ratio:

$$p_6 = \frac{p_5}{ra}$$

(F-21)

and from CO_2 thermodynamic tables T_6, s_6, d_6 can be determined.

- State 8: The enthalpy h_8 is computed from recuperator efficiency which is defined as:

$$\eta r = \frac{h_6 - h_8}{h_6 - h_{8id}}$$ (F-22)

Where: The enthalpy h_{8id} corresponds to ideal recuperation when $T_{8id} = T_2$. Since there are no pressure losses, $P_{8id} = P_8 = P_1$. Two state properties are known, thus from CO_2 thermodynamic tables T_8, s_8, d_8 can be determined.

- State 3: The enthalpy h_3 is computed from compressor efficiency which is defined as:

$$\eta c = \frac{h_{3ad} - h_8}{h_3 - h_8}$$ (F-23)

$P_3 = P_2$. Two state properties are known, thus from CO_2 thermodynamic tables T_3, s_3, d_3 can be determined.

- State 7: The enthalpy h_7 is computed from recuperator efficiency which is defined as:

$$\eta r = \frac{h_6 - h_7}{h_6 - h_{7id}}$$ (F-24)
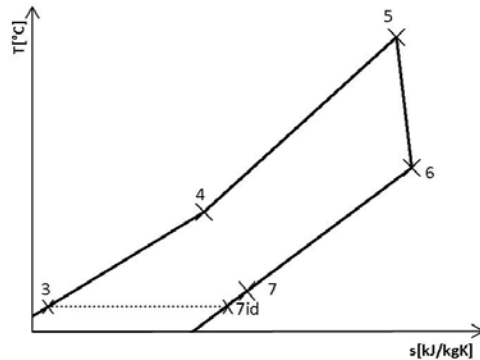
Where: h_{7id} corresponds to ideal recuperation when $T_{7id} = T_3$. $P_{7id} = P_7 = P_6$. Two state properties are known, thus from CO_2 thermodynamic tables T_7, s_7, d_7 can be determined.

- State 4: In the high temperature recuperator the heat transferred from one side to another side is considered to be equal (i.e. no thermal losses). Hence the enthalpy h_4 can be easily computed:

$$h_4 = h_3 + q_{HTR,}$$

(F-25)

where: $q_{HTR} = h_6 - h_7$

$P_4 = P_3$ and from CO_2 thermodynamic tables T_4, s_4, d_4 can be determined.

All cycle states are known, before the performance analysis a parameter - flow ratio has to be computed from a heat balance in the low temperature recuperator:

$$\dot{m}_1 \cdot (h_3 - h_2) = \dot{m} \cdot (h_7 - h_8) \quad \rightarrow \quad rm = \frac{\dot{m}_1}{\dot{m}} = \frac{h_7 - h_8}{h_3 - h_2}$$

(F-26)

Main compressor work:

$$W_{C1} = rm \, (h_2 - h_1)$$

(F-27)

Re-compressor work:

$$W_{C2} = (1 - rm) \, (h_3 - h_8)$$

(F-28)

Turbine work:

$$W_T = h_5 - h_6$$

(F-29)

Cycle thermal efficiency:

$$\eta = \frac{WT - (WC1 + WC2)}{(h_5 - h_4) - Qfp}$$

(F-30)

Where Q_{fp} is the thermal power consumed by the fuel production plant

Rankine Cycle Results

As stated in chapter 4, the Rankine cycle calculations follow the procedure established in reference [4], subject to the enumerated assumptions. A complete breakdown of the Rankine cycle results is as follows:

Rankine PCS for Liquid Fuels Production

Assumptions

eta_turb	0.90	eta_pump	0.90	T_cond (K)	303	X_steam	1.0
Subcooling (K)	10.0	Steam Temp (K)	558	Density_scl (kg/m^3)	998	X_heat load out	0.0
P_stm (MPa)	6.8993	P_scl (MPa)	0.0023177	**Steady State**			

Alkaline Electrolysis

Loads

Turbine Power (MWe)	921	Alkylation (MWth)	0.42
RWGS Heat (MWth)	7.70	Hydrocracking (MWth)	3.63
ATR H2O Heat (MWth)	3.40	Aromatization (MWth)	1.33
ATR HC Heat (MWth)	2.96	Oligomerization (MWth)	0.51
ATR O2 Heat (MWth)	0.54	Hydrotreating (MWth)	0.35

Turb

h_stm (kJ/kg)	2,774
s_stm (kJ/kg-K)	5.822
h_cond,i (kJ/kg)	1,758
turb flow rate (kg/s)	1,007

Cond

h_cond,r (kJ/kg)	1,859
h_scl (kJ/kg)	83.286
Heat_out (MWth)	1,788

Pump

Pump power,i (MWe)	6.96
Pump power,r (MWe)	7.73
h_1 (kJ/kg)	90.96

Thermal Loads

h_satliq (6.9 MPa) (KJ/kg)	1,262.5
RWGS stm (kg/s)	5.09
ATR H2O stm (kg/s)	2.25
ATR HC stm (kg/s)	1.96
ATR O2 stm (kg/s)	0.36
Alkylation stm (kg/s)	0.28
Hydrocracking stm (kg/s)	2.40
Aromatization stm (kg/s)	0.88
Oligomerization stm (kg/s)	0.34
Hydrotreating stm (kg/s)	0.23
Total Aux Stm (kg/s)	13.8

S/G

S/G flow rate (kg/s)	1,021
h_s/g in	106.8
Heat_in (MWth)	**2,722**
Cycle Efficiency	**33.6%**

Rankine PCS for Liquid Fuels Production

HTCE/HTSE

Loads

Turbine Power (MWe)	658	Alkylation (MWth)	0.42
HTCE CO2 Heat (MWth)	7.80	Hydrocracking (MWth)	3.63
HTCE H2O Heat (MWth)	69.3	Aromatization (MWth)	1.33
HTSE H2O Heat (MWth)	12.0	Oligomerization (MWth)	0.51
ATR H2O Heat (MWth)	10.27	Hydrotreating (MWth)	0.35
ATR HC Heat (MWth)	2.96		

Turb

h_stm (kJ/kg)	2,774
s_stm (kJ/kg-K)	5.822
h_cond,i (kJ/kg)	1,758
turb flow rate (kg/s)	736

Cond

h_cond,r (kJ/kg)	1,879
h_scl (kJ/kg)	83.286
Heat_out (MWth)	1,321

Pump

Pump power,i (MWe)	5.08
Pump power,r (MWe)	5.65
h_1 (kJ/kg)	90.96

Thermal Loads

h_satliq (6.9 MPa) (KJ/kg)	1262.5
HTCE CO2 stm (kg/s)	5.16
HTCE H2O stm (kg/s)	45.85
HTSE H2O stm (kg/s)	7.94
ATR H2O stm (kg/s)	6.80
ATR HC stm (kg/s)	1.96
Alkylation stm (kg/s)	0.28
Hydrocracking stm (kg/s)	2.40
Aromatization stm (kg/s)	0.88
Oligomerization stm (kg/s)	0.34
Hydrotreating stm (kg/s)	0.23
Total Aux Stm (kg/s)	71.83

S/G

S/G flow rate (kg/s)	807.5
h_s/g in	195.2
Heat_in (MWth)	**2,082**
% Change from Alkaline	-23.5%
Cycle Efficiency	**31.3%**
% Change from Alkaline	-6.63%

Appendix F References

[1] Linstrom, P., and Mallard, W., 2010, "NIST Chemistry WebBook, NIST Standard Reference Database Number 69," National Institute of Standards and Technology, Gaithersburg, MD, pp. N/A.

[2] Dostal, V., Legault, D., and Hejzlar, P., 2006, "CYCLES," **2**.

[3] Lemmon, E., Huber, M., and McLinden, M., 2007, "Reference Fluid Thermodynamic and Transport Properties (REFPROP) (NIST Standard Reference Database 23)," **8**.

[4] Todreas, N., and Kazimi, M., 1989, "Nuclear Systems 1: Thermal Hydraulic Fundamentals,"Taylor and Francis Group, New York, NY, pp. 192-208, Chap. 6.